DOCUMENT NO. 67SD4380

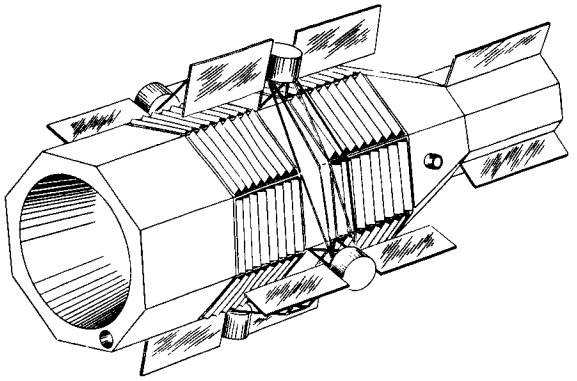

FEASIBILITY STUDY OF HIGH PRECISION TRIAXIAL ATTITUDE CONTROL FOR SPACECRAFT

FINAL REPORT

SEPTEMBER 1967

PREPARED FOR

NATIONAL AERONAUTICS AND SPACE ADMINISTRATION
ELECTRONICS RESEARCH CENTER
CAMBRIDGE, MASS.

UNDER CONTRACT NAS-12-95

F.E. XYDIS
STUDY PROGRAM MANAGER

GENERAL ELECTRIC
SPACECRAFT DEPARTMENT
A Department of the Missile and Space Division
Valley Forge Space Technology Center
P.O. Box 8555 • Philadelphia, Penna. 19101

TABLE OF CONTENTS

TABLE OF CONTENTS (Cont'd)

TABLE OF CONTENTS (Cont'd)

TABLE OF CONTENTS (Cont'd)

TABLE OF CONTENTS (Cont'd)

TABLE OF CONTENTS (Cont'd)

LIST OF ILLUSTRATIONS

LIST OF ILLUSTRATIONS (Cont'd)

LIST OF TABLES

SECTION 1

INTRODUCTION

SECTION 1

INTRODUCTION

NASA's recognition of the need to determine the feasibility of achieving precision triaxial control and stabilization (in the range of 10^{-4} to 10^{-6} degrees of arc) prompted the initiation of this study contract early in 1966. It was time phased into four items of work over a period of 18 months, culminating with the final report presented here. The first two items of work were completed in October of 1966 and the results were contained in a midterm interim report distributed the following month. The final report presented here contains a complete summary of all four items of the contract work statement.

The work completed prior to midterm established, with the concurrence of the Electronics Research Center Technical Director, a specific mission for study and formulated the technical feasibility of system concepts compatible with the mission selected and amenable to the precision required of the spacecraft control and stabilization system. Further, the scope of work during that period, as covered by the first two items of the contract, included:

a. Delineation of mission objectives and pertinent parameters such as target size, target illumination, spacecraft orbit, spacecraft mass and inertias, and derivation of pointing requirements.

b. Derivation of approaches applicable to the formulation of system concepts from which the technical feasibility of these concepts could be assessed. These derivations were based on analysis, sound engineering judgment and consideration of R&D effort that has a high probability of success.

c. Examination of critical components and subsystems such as fine error sensors, torquing subsystems and control logic suitable for use in the control system formulated.

d. Tradeoffs necessary for the selection of the most promising attitude reference and control systems, compatible with mission requirements, for system synthesis and analysis to be accomplished during the latter half of the contract.

Early study of a variety of potential missions requiring pointing accuracies in the range of 10^{-4} to 10^{-6} degrees of arc, that are considered practical for the 1975 to 1980 time period,

narrowed the choice of missions to that of laser communications between Earth and a spacecraft in the vicinity of one of the nearby planets or an astronomical telescope. The selection, with the concurrence of the ERC Technical Director, of an interplanetary laser communications mission required the addition of certain study items to the contract inherent in this type of mission. These included:

a. Point ahead required by the transport lag of the laser beam over interplanetary distances.

b. Station switching required on Earth and in the spacecraft because of Earth rotation to maintain essentially continuous communication.

c. The tradeoff between torquing the entire spacecraft to maintain the proper pointing direction of the spacecraft laser and torquing only an element in the laser optical system.

Consistent with the time period of 1975 to 1980 to be covered by the study, and with the concurrence of ERC, only unmanned spacecraft are considered applicable. Analysis showed the frequency of disturbance torques for the postulated mission to be very low (much lower than 1 Hz). This fact, together with the relatively modest size and mass and high rigidity of the postulated spacecraft (RTG power supply instead of a solar array), indicates a relatively high first structural bending mode frequency and no significant coupling of the structural and attitude control dynamics. For this reason it was agreed prior to the midterm that control analyses should assume the spacecraft to be a rigid body.

The work completed during the later half of the study utilized the tradeoffs and system concepts formulated earlier, to derive, with the concurrence of the Electronics Research Center Technical Director, a spacecraft control system capable of meeting the mission and system requirements and included the formulation of a mathematical model to determine the feasibility of achieving stabilization and control with accuracies better than 10^{-5} degrees of arc. System analysis and synthesis were performed to evaluate the control system so defined. Further, the scope of work during this period covered by Items 3 and 4 of the contract included:

a. An examination of thermal and structural considerations insofar as these parameters affected control performance.

b. An error analysis to determine the apportionment of errors to:

- Spacecraft control to the attitude reference.
- Internal alignment of spacecraft attitude reference control axes and point ahead axes via alignment of the associated equipment.
- Servoed optics control of the spacecraft laser beam relative to the spacecraft "point ahead" axes.

c. Analyses, utilizing angular momentum as a state variable, to derive equations from basic physical laws to describe the operation of control moment gyros, favored by actuator tradeoff studies, and derivation of mathematical models of several methods of applying them for spacecraft fine pointing attitude control.

d. Control system tradeoffs to insure a design that is technically feasible with a high probability of success and compatible with derived system requirements.

e. Establishment of spacecraft control subsystem specifications.

The report format employed summarizes the results of this Space Vehicle Precision Triaxial Control Feasibility Study in Section 2, which is followed by sections devoted to comprehensive discussions of Mission Analysis, Formulation of System Concepts and Control Requirements, Control System Definition and Mathematical Model Development, Control System Performance Verification, and Appendixes.

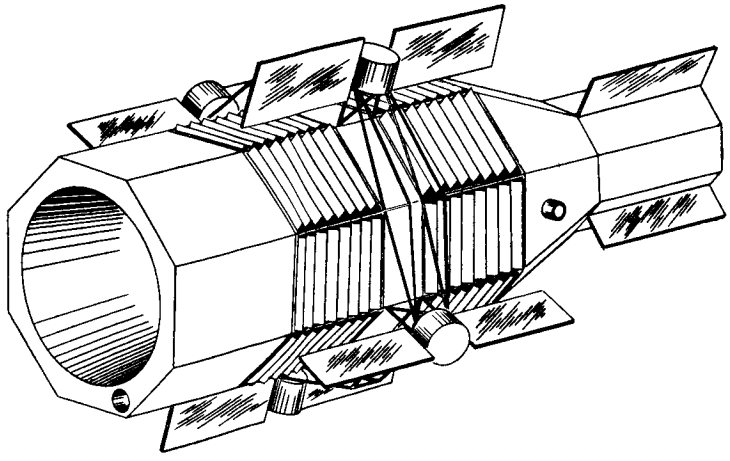

Figure 1-1. In-Orbit View of Spacecraft

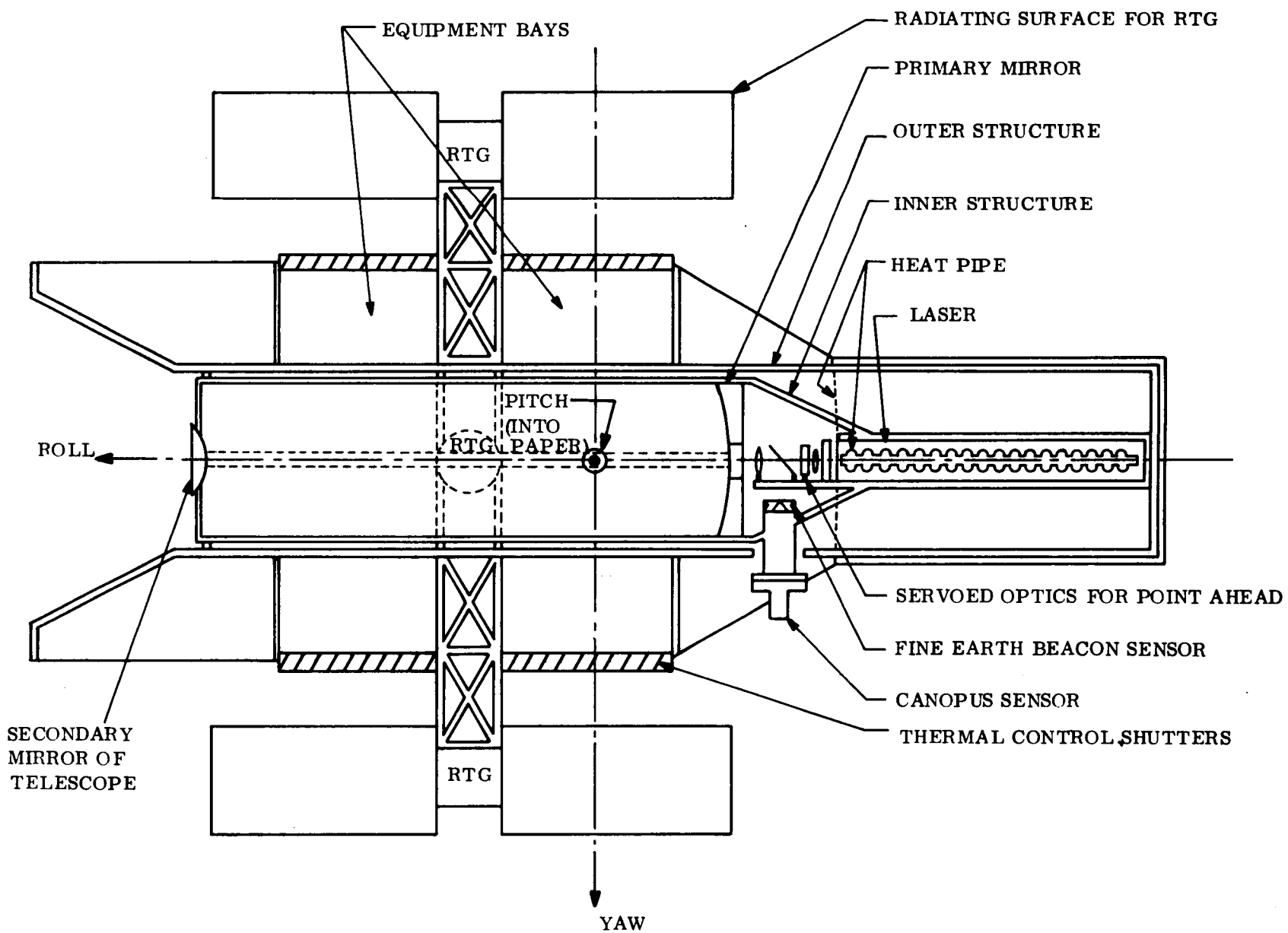

Figure 1-2. Cutaway Sketch of Spacecraft

SECTION 2

SUMMARY

SECTION 2

SUMMARY

2.1 MISSION SELECTION

The objective of this study has been to determine the feasibility of achieving precision triaxial attitude control and stabilization for spacecraft of the 1975 to 1980 era. The range of pointing accuracy or pointing stability under consideration is 10^{-4} to 10^{-6} degree (0.3 to 0.003 arc second). From the outset, the ERC Technical Director agreed that the course of the required study would be significantly influenced by the type of mission chosen for investigation. The attitude control problems and sequences are far different, for example, for a mission whose goal is laser communication and that of an astronomical telescope. For this reason, item 1(a) of the Statement of Work provided for analyses to define a specific mission, appropriate system parameters, and spacecraft characteristics.

Some reflection on the various possible missions that could effectively utilize a pointing precision of 10^{-4} to 10^{-6} degree quickly reduces the possibilities to those spacecraft employing optical imaging or transmissions systems. Specifically, we can contemplate no mission requiring a precision of point in excess of 10^{-4} degree except for those employing astronomical telescopes or laser communication telescopes. For both these general mission classes, a pointing precision of the order of 10^{-4} to 10^{-6} degree can effectively be used in two axes. For the third axis (rotation about the line-of-sight), control accuracies in the range of 10^{-2} to 10^{-3} degree is adequate. Consideration of these missions resulted in the selection of high data rate real time laser communication from a Mars orbiting spacecraft, which utilizes an Earth laser beacon reference, as the framework for detailed study of spacecraft precision triaxial control. The rationale for this selection is summarized in Sections 2.1.1 and 2.1.2.

2.1.1 ASTRONOMICAL TELESCOPE

For an astronomical observatory mission it can be assumed that a large diffraction limited telescope is employed in which stability of pointing for extended periods is required. The most stringent three axis pointing requirement for such a mission is probably associated with

astrometric photography. Here, image motion at the film plate should be maintained to less than one-tenth the full diameter of the Airy disc of the telescope objective in order not to compromise its angular resolution or to significantly increase exposure time for faint objects. This criteria requires a control precision of the order of 10^{-6} degrees of arc for a diffraction limited objective having a diameter, D_r, of the order of 270 inches, operating at a wave length of 5000 angstroms, where the full diameter of the Airy disc, 2θ, for a diffraction limited circular objective is given by the familiar relation:

$$2\theta = \frac{2.4\lambda}{D_r} \text{ radians} \qquad (2\text{-}1)$$

Only as it becomes possible to produce and maintain diffraction limited operation for shorter wavelength sources can control of this precision for reduced objective size be envisioned. Realistically, one should associate 10^{-6} degree pointing with an aperture size of 300 to 400 inches, and 10^{-5} degree with an aperture of 30 to 60 inches, depending on the minimum wavelength for which diffraction limited operation is possible.

Although it has not been demonstrated, it is reasonable to expect that present optical technology can produce a 40 to 50 inch telescope system that will be diffraction limited in the near ultraviolet (3500 angstroms). As for very large sizes (300 to 400 inches), no such astronomical telescope has been built, and a development program of many years duration would undoubtedly be necessary to determine the most practical method of fabricating and maintaining such a diffraction limited telescope.

A previous study demonstrated the feasibility of astronomical telescope pointing stability of the order of 10^{-5} degree for a 120-inch aperture telescope of the 1975 to 1980 time era. This work was accomplished (by the General Electric Co. in conjunction with the Boeing Co.) as part of the Manned Orbital Telescope Study directed by NASA's Langley Research Center, and is reported in Boeing Document D2-84042-1, dated October, 1965. The salient results of that study show that for a telescope physically decoupled from a companion manned orbiting station (i.e., manned disturbance torques are avoided), the required attitude control system is currently near-fringe technology, and that no inventions would be necessary for implementation.

Based on these considerations, and the desire of the ERC Technical Director to explore possible laser communication missions, the astronomical telescope mission was not considered in further detail.

2.1.2 LASER COMMUNICATIONS

The general class of missions involving spacecraft communications was examined and several mission variations identified as candidates for the 1975 to 1980 time period. They were:

a. Interplanetary spacecraft to earth-based transmitter/receiver.
b. Satellite in near earth space to Earth.
c. Satellite to satellite in near earth space.

These three missions were considered in some detail, with particular emphasis on the first. Preliminary analysis was performed to size the spacecraft, its optical system, laser power, transmitted beamwidth, information data rate, etc., for a variety of interplanetary fly-bys and orbiters from Mars to Pluto. Typically, we have considered the desired information rates to be on the order of 10^5 to 10^7 bps.

Laser communication between earth and an interplanetary spacecraft logically breaks down into two missions with significantly different problems, depending on distance from earth. For planets from Jupiter and beyond, the very long transmission/reception time lag introduces a difficult earth beacon acquisition problem. Further, the close angular proximity of the sun and earth as viewed from the spacecraft poses a formidable problem of solar interference with the source being tracked by the spacecraft receiver. From Jupiter, the sun is never more than 11 degrees from the Earth, and from Pluto, less than 2 degrees. Table 2-1 summarizes the round trip transport time and the sun/earth angles for the outer planets.

Because of the distinct difference in the Mars mission, as compared to the deep space planet mission, a separate study would be indicated for each. The Mars mission was selected for

Table 2-1. Summary of Time and Angles

Planet	Typical Range (km)	Estimated Microwave Information Rate 1975/80 (bps)	Round Trip Transport Time Lag (hours)	Approximate Maximum Angle Between Sun & Earth (degrees)
Mars	2×10^8	4×10^6	20 min	45
Jupiter	3×10^8	2.5×10^5	1.3	11
Saturn	16×10^8	6×10^4	2.6	6
Uranus	30×10^8	1.5×10^4	5	3
Neptune	46×10^8	6×10^3	7.6	2
Pluto	60×10^8	4×10^3	10	1.5

detailed study since it will logically be flown before the deep space probe. As initially conceived, two variations of a Mars orbiting spacecraft that maintains real time communication with Earth were considered:

a. The spacecraft continuously tracks a laser beacon located on earth. Several earth-based beacons (and associated receiving equipment) are necessitated to accommodate the rotation of the Earth and to assure a high probability of no local cloud cover. The spacecraft laser beamwidth is assumed to be 0.2 arc second and a daytime information rate of 10^6 bps is provided.

b. The spacecraft continuously tracks the geometrical center of the Earth, and a computation is made to determine the instantaneous location of one of the preselected earth-based receivers. No laser beacon on earth is provided. The spacecraft laser beamwidth must be increased to approximately 2 arc seconds to accommodate the greater uncertainty in earth receiver location. Daytime information rates of 10^5 bps can be achieved at some increase in laser power over that of the beacon tracking mode.

Each of these two operating modes was examined in some detail. The Earth tracking mode was eliminated from further study because it was determined that the attitude control problem is not a significant extension of state-of-the-art and hence poses no significant problems that would warrant study under the present contract. Secondly, the relatively low information

rate (10^5 bps day time) is less than an order of magnitude over those planned for Voyager, and confidence is high that this information rate can be achieved by microwave techniques by the early 1970 time period. On this basis, and with the concurrence of ERC, the mission selected for detailed study of the attitude control and stabilization was limited to that of the 0.2 arc second transmitted beamwidth system employing a cooperative earth laser beacon.

One conclusion that has been reached is that there appears to be an optimum in the spacecraft laser transmitter beamwidth (for this mission, and for the assumed system parameters) on the order of 0.3 to 0.1 arc seconds. This implies a pointing accuracy on the order of 10^{-5} degree (0.03 arc second). The reason for the optimization is that for beamwidths much larger than a few tenths of a second, the laser system becomes grossly inferior to microwave (S-Band) techniques using any (or all) reasonable criteria such as cost, weight, data rate, complexity, development time, atmospheric effects and interference from the sun. On the other hand, beamwidths much smaller than a few tenths arc seconds require inordinately large spacecraft optics (larger than Mount Palomar for 0.02 arc second beamwidth) in order to form the beam. For large optical systems (> 1-meter), it is generally more advantageous to increase laser data rates by increasing transmitted power rather than increasing telescope aperture since a linear relation exists between weight increase and power increase, whereas the weight of the spacecraft will increase with the 5/2 power of telescope aperture. A second very important disadvantage of increasing aperture significantly is the resulting greater precision required in the point ahead required to lead the earth-based receiving antenna. For an 0.02 arc second beamwidth, the point ahead precision must be on the order of 0.002 seconds, or one part in 35,000 of the total point ahead angle. This then becomes an incredibly complex problem.

Since optical communications is in its infancy, a very significant amount of development in the areas of lasers, modulators, optical filters, and receiver techniques are required to bring this mission to fruition. Further, the cost of erecting numerous Palomer size earth-based receiving telescopes must be a major factor in systems planning, as is appropriate site location.

2.2 SYSTEM PARAMETERS AND ASSUMPTIONS

Maximum emphasis on the study of high precision attitude control was facilitated by certain assumptions related to technical capabilities and advances in related fields as required. In generating sets of system parameters for the various missions, the assumptions which have been used are as consistent with projected progress as the time available to investigate these fields has allowed.

2.2.1 ASSUMPTIONS

The assumptions listed below were the principal ones used as part of the basis for this study:

a. The launch time of interest is the 1975 to 1980 era.

b. Only the Mars orbiter-to-Earth based station laser communication mission will be considered during the control and stabilization portion of the study.

c. The spacecraft orbit about Mars is such as to prevent occulation of the Earth by Mars for the 6-month orbiting mission life.

d. The spacecraft is unmanned.

e. The spacecraft weight will not be restricted by the payload capabilities of existing launch vehicles, except that the Saturn V capability will not be exceeded.

f. The maintaining of very narrow (0.2 arc second) laser beamwidths is possible in the time period of interest. (This will not be investigated as part of the study.)

g. The orbiting of a 30 to 40-inch aperture diffraction-limited optical system is possible in the time period of interest.

h. The assumed power levels and efficiencies are achievable.

i. Laser modulation techniques and narrow band interference filters consistent with the required channel capacities (data rates) will be developed.

j. Multiple ground based telescopes of 200-inch aperture will be installed as receiving antennae.

k. A low data rate (100 bps) microwave communication link exists between the earth and the spacecraft.

2.2.2 SYSTEM PARAMETERS

Tables 2-2, 2-3, and 2-4 present derived system parameters and spacecraft characteristics for the two Mars mission variations, i.e., utilization of a cooperative Earth beacon attitude reference for spacecraft control and for tracking the Earth. The tabulations furnish the detailed data to support the selection of the narrow Mars orbiting spacecraft laser beamwidth system employing a cooperative Earth laser beacon, as the mission framework for this study.

2.3 SYSTEM CONCEPTS

The interdependence of the formulation of system concepts and spacecraft control requirements, compatible with the selected Mars orbiting spacecraft laser communications mission, required that they be performed in parallel. For ease in presentation, the statement of the control requirements will follow the summary of selected system concepts presented here.

2.3.1 THE SPACECRAFT ATTITUDE REFERENCE SYSTEMS

The apparent direction of the laser pulses from the earth-based beacon and two orthogonal axes normal to this line is the obvious selection of a triad to serve as a spacecraft attitude control coordinate reference frame. The attitude reference system selected utilizes earth-based laser beacons as a spacecraft pitch and yaw reference. The third axis reference selected is the line normal to the beacon-spacecraft reference (spacecraft roll axis) that lies in the plane including the apparent position of the beacon, the spacecraft and the star Canopus. This necessitates an additional inertial reference during occultation of Canopus for the Mars orbital mission assumed. In the implementation proposed, a gyro reference is used for this purpose.

2.3.2 THE SPACECRAFT AND SPACECRAFT LASER CONTROL CONCEPT

The control concept proposed for pointing a 0.2 arc second laser beam to an Earth station from a Mars orbiter, for high data rate laser communications, features a spacecraft attitude control subsystem and a servoed optics subsystem that use a common fixed primary optic as shown in Figure 2-1. Stabilization of the spacecraft to the attitude reference furnished by the apparent position of an earth-based laser beacon and the star Canopus is accomplished by the attitude control subsystem. Pointing of the laser beam relative to the position of the

Table 2-2. Mars Orbiter Laser Communication System Parameters (Spacecraft to Earth Link)

System Parameter	Beacon Tracking	Earth Tracking
Data rate (daytime)	$>10^6$ bps	$>10^5$ bps
Spacecraft laser beamwidth (half power)	0.2 arc-sec	2.0 arc-sec
Spacecraft primary telescope aperture (diffraction-limited)	30-inch	6-inch
Spacecraft laser transmitted power (cw)	10 watt	25 watt
Spacecraft laser efficiency	0.5%	0.5%
Spacecraft laser input power	2000 watt	5000 watt
Spacecraft power supply capability	300 lb/kwe	300 lb/kwe
Spacecraft power supply weight	600 lb	1500 lb
Approximate laser beam pointing accuracy	$\pm$0.05 arc-sec	$\pm$0.5 arc-sec
Spacecraft laser/modulator weight	200 lb	300 lb
Spacecraft optical system weight	600 lb	200 lb
Spacecraft sunshield weight	100 lb	Negligible
Spacecraft sunshield length (for 10^4 attenuation)	12 ft	2.5 ft
Spacecraft optical communication system (total weight)	1500 lb	2000 lb
Ground station required	6 to 12 telescopes of 200-inch diameter receiving aperture.	
Ground station receiver/ (S/N Ratio Daytime)	5	5
Ground station receiver field-of-view (Tracking)	$(10 \text{ arc-sec})^2$	$(10 \text{ arc-sec})^2$

Table 2-3. System Parameters Assumed for Study (Earth to Spacecraft Link)

System Parameter	Beacon Tracking
Up link	
Ground station laser beamwidth (half power)	4 arc-sec
Ground station laser power (pulsed)	340 mw
Ground station laser (PRF)	20 to 30/sec
Ground station laser pulsewidth	0.1μ sec
Ground station laser power (average)	680 watt
Ground station laser transmitting (and receiving) aperture	200 inches
Earth radiance at spacecraft ($\pm$30%)	$1.8 \times 10^{-11} \frac{w}{cm^2}$
Spacecraft receiving aperature (diameter)	30 inch
Spacecraft receiver S/N ratio	60
Spacecraft receiver bandwidth	10 MHz
Spacecraft receiver field-of-view	
• Total	(1.5 min^2)
• Instantaneous	(1.5 min^2)

Table 2-4. Estimated Spacecraft Weight Breakdown

Equipment	Beacon Tracking (pounds)	Earth Tracking (pounds)
Optical communication subsystem (w/power supply)	1500	2000
Structure (excluding telescope)	500	500
Stabilization and control subsystem	300	300
Command control and data processing	300	300
Experiments	300	300
RF communications	100	100
Miscellaneous (thermal control, balance, weights, etc.)	1000	1000
Mars orbiter subtotal	4000	4500
Midcourse propulsion system w/fuel	800	900
Orbit insertion propulsion system w/fuel	3500	4000
Estimated total launch weight (Excluding shroud, LV adapter, etc.)	8300	9400

Note: GE-MSD Voyager design characteristics used as guidelines. The purpose of this breakdown is solely to provide a rough estimate of total spacecraft weight.

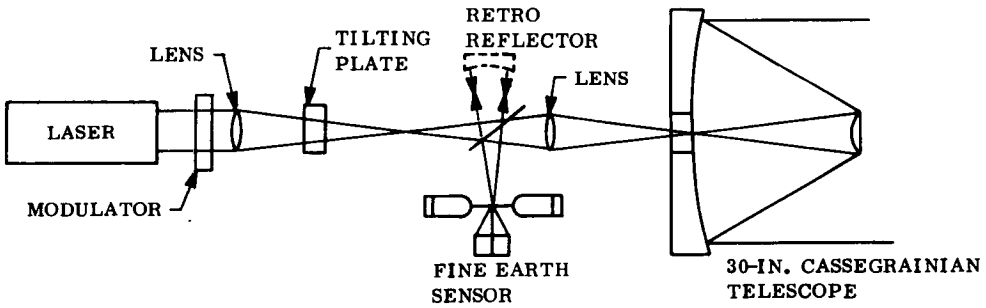

OPTICAL SCHEMATIC

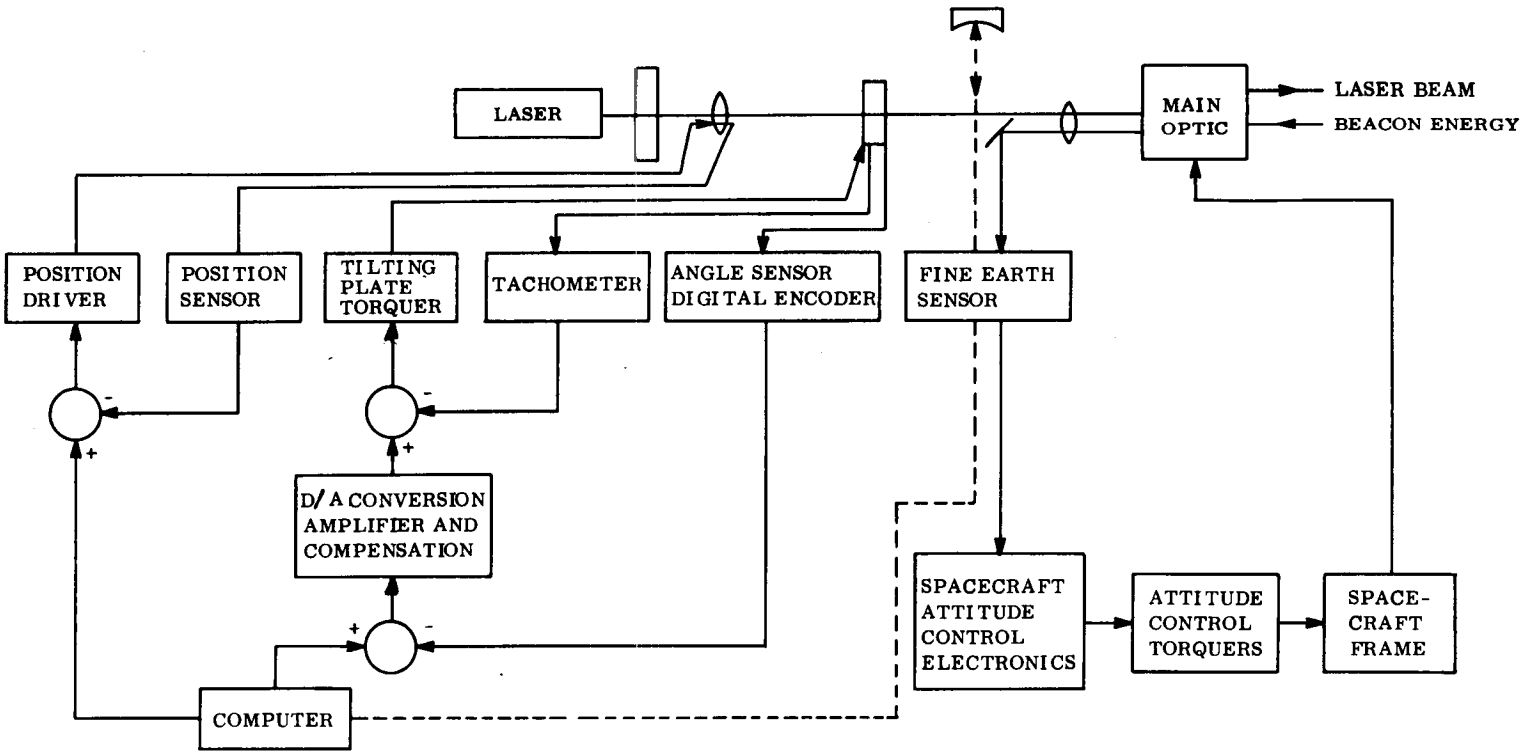

Figure 2-1. Mars Orbiting Spacecraft Attitude Control and Laser Beam Pointing Concept

primary optic is controlled by servoed optics in response to commands stored in the spacecraft computer. The combined control functions can be accomplished well within half the laser beam width, leaving the remainder of the pointing allowance for computation of the laser beam pointing commands.

The concept selected is considered the best engineering compromise with regard to all spacecraft subsystems in that:

a. It employs only a single primary optic, for reception of beacon radiation and transmission of laser radiation, with provision for self alignment of the laser beam pointing servoed optics subsystem to the pitch and yaw attitude reference furnished by the attitude control subsystem Fine Earth Beacon Sensor.

b. It minimizes light transmission losses in the spacecraft laser path, which is reflected in minimum heat dissipation aboard the spacecraft. The very low efficiency in producing laser radiation from the primary power source supports minimizing power requirements making possible the solution of the spacecraft thermal control problem and the effects of thermal gradients on alignment of spacecraft optics and control components.

c. It employs a reliable attitude control system which meets requirements and minimizes complexity. Alternate concepts employing additional servos and optical systems to ease the requirements imposed on the basic attitude control torquing subsystem offer needless additional complexity.

2.3.3 POINT AHEAD

The spacecraft attitude reference system selected is characterized by angular motions that are a function of the independent motions of the spacecraft and ground station relative to inertial space. The relative motion between the Mars orbiter and the earth-based station, which serves both as a pitch and yaw attitude reference for the spacecraft and a receiver of its laser communications, requires that the laser beam transmitted from the spacecraft be angularly offset in pitch and yaw.

Early conceptual studies defined a fixed primary optic abroad the spacecraft to serve both as a receiver of beacon radiation from the ground and a transmitter of the spacecraft laser beam. In this configuration the spacecraft pitch and yaw attitude is established as a reference

for laser transmission to the ground station by the alignment of the axis of the fixed primary optic (roll axis) to the apparent direction of incoming radiation from the Earth beacon. The roll attitude reference is achieved by rotation about this axis until the spacecraft star sensor (having a degree of freedom in the spacecraft roll-yaw plane) is aligned to Canopus.

The required angular offset or "point ahead" of the laser beam in pitch and yaw, relative to the axis of the primary optic, may be determined by consideration of the phenomenon familiarly known as the Bradley aberration*, which is a function of the relative velocity (RV) between the two systems and the constancy of the velocity of light (C). The classical special case in which this relative velocity vector is constant, examined in terms of the mission studied here, is a useful introduction to the point ahead concept. To determine the yaw and pitch angular offsets of the axis of the spacecraft primary optic relative to the spacecraft ground station vector, consideration of this ideal case involves the components of this constant relative velocity in the plane of the ground station, spacecraft, and Canopus and its normal plane through the ground station-spacecraft vector.

Under these conditions, the apparent direction of the ground beacon radiation reaching the spacecraft at any given time relative to the spacecraft-ground station vector is delineated in the diagram and mathematical relations given in Figure 2-2. In addition, the yaw and pitch angular offsets of the transmitted spacecraft laser beam relative to the spacecraft-ground station vector are noted in Figure 2-2. The total point ahead of the spacecraft laser beam relative to the axis of its fixed optic, about the yaw and pitch axes, is computed from the algebraic summation of the respective yaw and pitch angular offsets determined from:

a. The computed yaw and pitch angular offsets of the spacecraft roll axis relative to the spacecraft-ground station vector (the apparent direction of the ground station beacon) at any given time.

b. The computation of the required spacecraft laser beam angular offsets relative to the spacecraft-ground station vector necessary to accommodate the ground station velocity relative to the spacecraft.

*LIGHT by R. W. Ditchburn

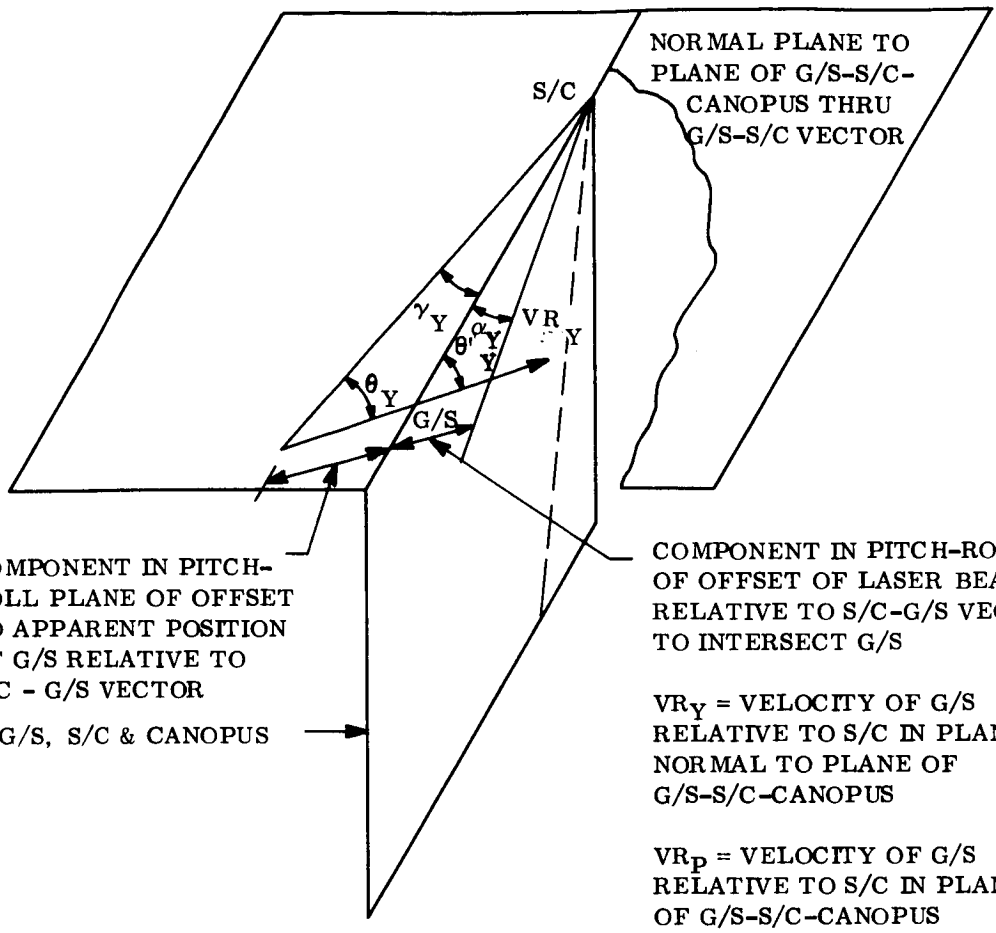

$$\theta_Y = \theta'_Y - \gamma_Y$$

$$\cos\theta = \cos(\theta' - \gamma_Y) = \cos\theta'_Y \cos\gamma + \sin\theta' \sin\gamma_Y = \frac{\cos\theta'_Y + \frac{VR_Y}{C}}{1 + \frac{VR_Y}{C}\cos\theta'_Y} \quad *$$

FOR VALUES OF γ_Y = 45 SEC MAX COS γ_Y = 1 WITH NEGLIGIBLE ERROR

$$\sin\gamma_Y = \frac{VR_Y \sin\theta'_Y}{C + VR_Y \cos\theta'_Y}$$

SIMILARLY:

$$\sin\gamma_P = \frac{VR_P \sin\theta'_P}{CVR_P \cos\theta'_P} \qquad \frac{\sin\alpha_Y}{VR_Y \Delta T} = \frac{\sin\theta'_Y}{C\Delta_t}$$

$$\sin\alpha_Y = \frac{VR_Y \sin\theta'_Y}{C}$$

SIMILARLY:

$$\sin\alpha_P = \frac{VR_P}{C} \sin\theta'_P$$

* LIGHT, CHAPTER 11, RELATIVISTIC OPTICS, BY R.W. DITCHBURN

Figure 2-2. Point Ahead

The mission under consideration in this study is more complex than the ideal case in that the velocity of the ground station relative to the spacecraft is not constant. The component values of the ground station velocity at a given time (in the plane of the ground station, spacecraft and Canopus and its normal plane through the ground station-spacecraft vector) must be determined from its change in position and the transmission time of the received light. The component value of ground station velocity determined in this manner, combined with the corresponding component values of spacecraft velocity, determine the velocity of the ground station relative to the spacecraft. Yaw and pitch point ahead may then be computed as in the ideal case. A detailed discussion of the point ahead concept rationale for the selected mission, including third axis effects, is given in Section 4.4.

2.3.4 ACQUISITION OF THE EARTH-BASED RECEIVER WITH THE SPACECRAFT LASER BEAM

It is probably too optimistic to hope that the point ahead function associated with the transmission of a narrow laser beam (0.2 arc seconds) from a Mars orbiter to an Earth receiver can be accomplished within the required precision, on the first try, using precomputed point ahead information. The uncertainty in initial point ahead computations alone has been estimated to be of the order of 0.5 arc seconds, based on best projected tracking data of the Mars orbiter from Earth, and the ephemeris uncertainties in the position of the Earth station with respect to Mars. Although the combined errors in attitude control of the spacecraft to its reference and errors in the pointing of the laser beam in response to its point ahead commands will be shown to be an order of magnitude smaller than initial errors in point ahead computation, it is evident that an operating mode is required to acquire the Earth receiver with the spacecraft laser beam.

Two concepts have been formulated to accomplish acquisition, both of which feature a potential for improving the point ahead computation:

a. A conical scan technique employing a slow circular rotation of the spacecraft laser beam about the computed point ahead direction, in which the radius of the circle of the laser beam centerline is equal to one half the uncertainty in the computer point ahead angle to assure illumination of the ground station.

b. The use of auxiliary ground receivers to detect the center of the spacecraft laser radiation reaching the Earth in relation to the main optical receiver for laser communications.

Errors in computation of the spacecraft laser beam point ahead, initially the major source of error, can be reduced through optimization of the mathematical model employed to determine point ahead commands through stochastic processes using known errors achieved from known commands. Such a process is a possible subject for a significant study beyond the scope of this contract.

A detailed definition of both acquisition concepts summarized here is given in Section 4.7.

2.4 SPACECRAFT CONTROL REQUIREMENTS/ERROR ALLOCATION

The basic control requirements derived for spacecraft system performance of the selected laser communications mission, from injection into Mars orbit to acquisition of the Earth beacon-Canopus reference and laser beam pointing to the Earth receiver, are presented here.

Detailed error analyses of the fine pointing mode were based on the obvious ground rule that the Earth-based receiver should be centered within the 0.2 arc second half power points of the spacecraft laser beam. The four main functions contributing to laser beam pointing error, i.e., spacecraft stabilization, laser and servoed optics, alignment stability, and point ahead computation were considered as independent errors and combined by root sum square.

The control requirements in the various operating modes is summarized in Table 2-5.

2.5 SPACECRAFT CONTROL DESCRIPTION AND OPERATIONAL SEQUENCE

The system proposed to provide spacecraft control during the interplanetary trajectory to Mars, the acquisition of and stabilization to the Earth beacon-Canopus reference after injection into Mars orbit, and the pointing of the laser beam to Earth receivers for high data rate communications, is shown in block diagram form. (See Figure 2-3.) The spacecraft control functions required prior to stabilization of the Mars orbiter in its Earth pointing mode have essentially been accomplished by Mariner spacecraft or will be accomplished in the near future by Voyager spacecraft. However, a brief description of the proposed control system and its operation during this phase of the mission is included for

Table 2-5. Mars Orbiting Spacecraft Attitude Control Functional Requirements (Fine Pointing to Earth-Based Beacon)

Coarse Pointing	
Acquire and Stabilize to Coarse Earth and Canopus Reference	
Pitch and Yaw	± 3.5 min
Roll	± 7.0 min
Pitch, Yaw, and Roll Rates	± 0.005 deg/sec
Intermediate Pointing	
Stabilize to Intermediate Earth and Fine Canopus Reference	
Pitch and Yaw	± 5 arc-sec
Roll	± 15 arc-sec
Pitch, Yaw, and Roll Rates	± 10 arc-sec/sec
Fine Pointing	
Acquire and Stabilize to Earth Beacon Reference and Fine Canopus Reference	
Pitch	± 0.035 arc-sec
Yaw	± 0.032 arc-sec
Roll	± 7.0 arc-sec
Laser Pointing Relative to Spacecraft Attitude Reference	
Pitch	± 0.023 arc-sec
Yaw	± 0.023 arc-sec
Computation of Point Ahead	
Pitch and Yaw	± 0.05 arc-sec
Slew Spacecraft During Station Switching (15 arc sec max) and stabilize to new beacon	
Reacquire Earth and Canopus in Event of Major Disturbance	
Acquire Sun and Canopus	
Commanded turns for acquisition of Earch	

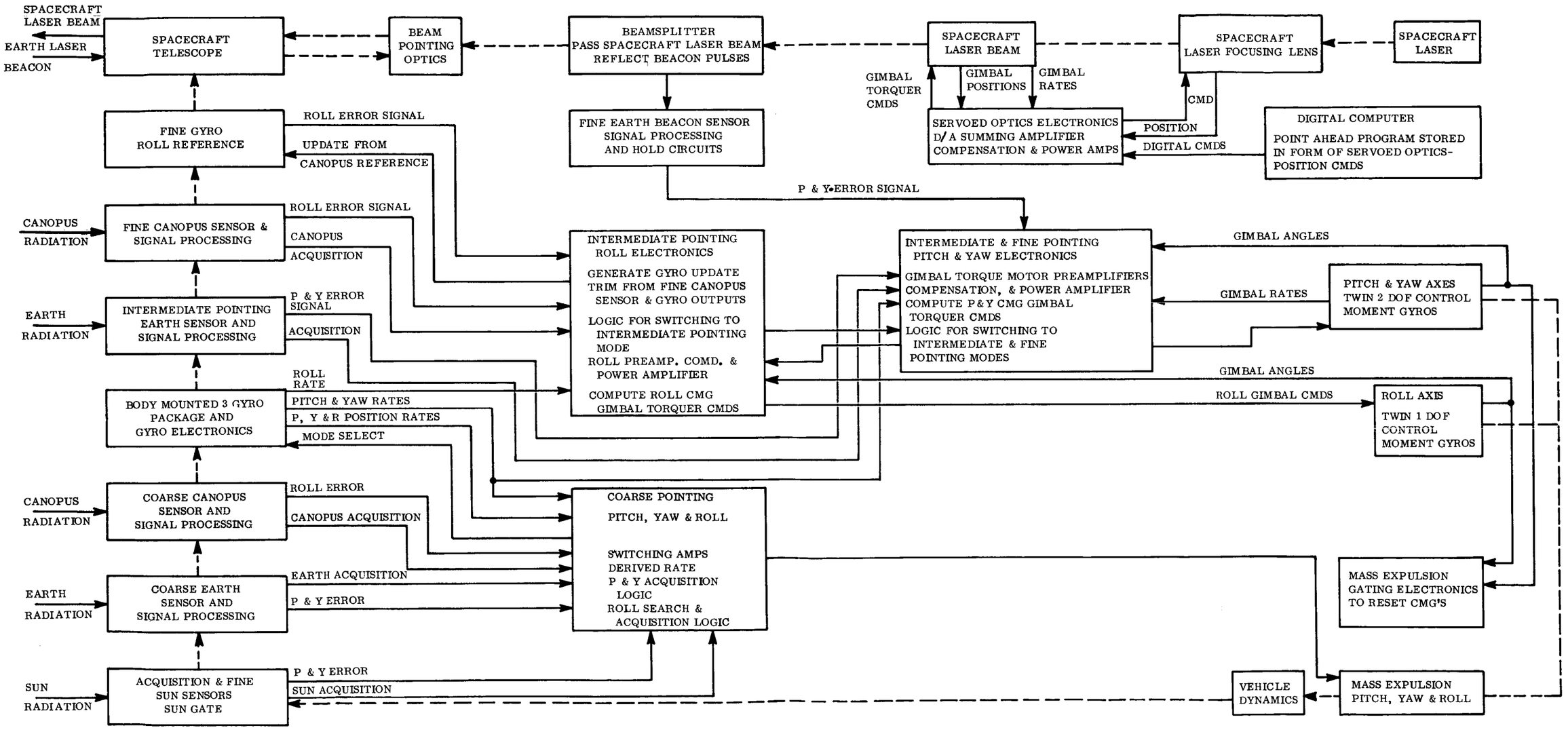

Figure 2-3. Spacecraft Control System Block Diagram for Laser Communications From Mars Orbit

completeness in the paragraph that follows. A summary of the spacecraft control formulated for the acquisition of the Earth-based beacon and pointing of its laser follow in Paragraphs 2.5.2 and 2.5.3. Definition of the spacecraft control to perform the latter function has received the major emphasis during the study in keeping with the objectives of the work statement. A detailed block diagram of the spacecraft attitude control system derived for acquisition of the fine pointing mode and stabilization to the attitude reference during pointing of the laser beam to Earth is shown in Figure 2-4.

2.5.1 LAUNCH TO EARTH ACQUISITION IN MARS ORBIT

After spacecraft launch and injection into its interplanetary trajectory to Mars, the conventional Sun-Canopus orientation is proposed to minimize solar pressure disturbance torques and to simplify thermal control. Initial spacecraft orientation of its roll axis to the Sun and removal of angular rates of separation are obtained through ON-OFF control of mass expulsion actuators in response to pitch and yaw attitude error signals from 4π steradian sun sensors and spacecraft angular rate signals from a triad of body mounted gyros. After the reduction of spacecraft angular rates to less than 0.05 degrees/second, a programmed roll search and acquisition of Canopus is commanded,employing roll search and acquisition logic similar to that perfected for the latest Mariner spacecraft. Acquisition of the Sun-Canopus reference is completed upon receipt of a Canopus star presence signal, which switches the attitude error in the roll channel from roll search to roll attitude error sensed by the Coarse Canopus Sensor.

As in Mariner-Voyager missions this orientation is maintained throughout the trip to Mars, except when trajectory corrections or injection into Mars orbit is performed. Transfer of the spacecraft roll axis pointing from the Sun to an arbitrary position in inertial space may be achieved by torquing the spacecraft about two axes in response to programmed turns commanded by the spacecraft computer and implemented in an inertial reference mode. Appropriate gyros in the position plus rate mode are sequentially torqued in this phase to alter the inertial roll reference in space to the required orientation for midcourse corrections. Return to the Sun-Canopus orientation after ΔV corrections may be accomplished through commanded turns in the inertial reference mode or by repeating the initial acquisition mode sequence.

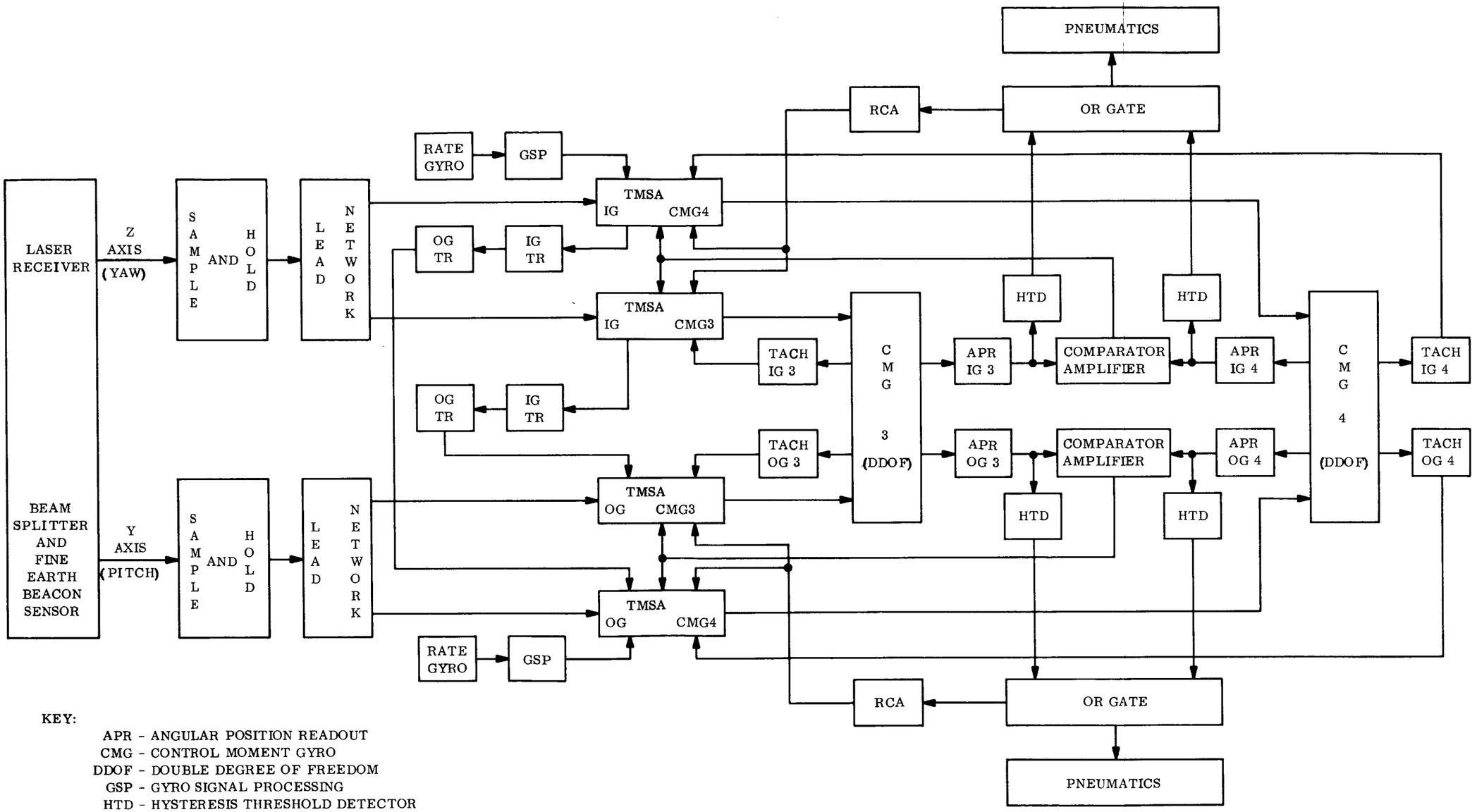

KEY:

APR - ANGULAR POSITION READOUT
CMG - CONTROL MOMENT GYRO
DDOF - DOUBLE DEGREE OF FREEDOM
GSP - GYRO SIGNAL PROCESSING
HTD - HYSTERESIS THRESHOLD DETECTOR
IG - INNER GIMBAL
OG - OUTER GIMBAL
RCA - RESET COMPENSATION AMPLIFIER
TMSA - TORQUE MOTOR SUMMING AMPLIFIER
TR - TANGENT RESOLVER

Figure 2-4. Mars Orbiting Spacecraft Fine Pointing Attitude Control Mode Block Diagram

The unmanned spacecraft is assumed to be oriented to the Sun and Canopus after the injection maneuver that places it in an orbit about Mars nearly normal to the ecliptic plane. Transfer of spacecraft roll axis pointing from the Sun to the Earth as a reference is accomplished in the inertial mode, as are orientation changes described for ΔV corrections. Based on Mariner performance such a maneuver can be performed to an accuracy of better than one degree. The field of view of the Coarse Earth Sensor aligned to the spacecraft roll axis is ± 2.5 degrees. Reacquisition of Canopus may be necessary after this maneuver, although the two spacecraft rotations required to alter the roll axis from the Sun to the Earth may be accomplished while maintaining Canopus within the field of view of the Coarse Canopus Tracker. If acquisition of Earth is lost at any time, due to some unexpected large scale disturbance or correctable malfunction, reacquisition may be accomplished by returning to the Sun-Canopus reference by the methods previously described.

2.5.2 ACQUISITION OF THE EARTH-BASED BEACON

Automatic acquisition of the Earth-based laser beacon may be achieved after stabilization of the spacecraft to the Earth and Canopus. Several sensors are proposed to cover the wide dynamic range associated with the desired wide field of view and high resolution as shown in Figure 2-3. Spacecraft torques will be provided by mass expulsion actuators until attitude errors and rates are reduced well within the capture capability of control moment gyro momentum storage actuators.

After the spacecraft pitch and yaw pointing errors are reduced well within the linear range of an Intermediate Earth Sensor, roll pointing error is reduced well within the linear range of the Fine Canopus Sensor and spacecraft rates are less than 0.005 degrees per second about all spacecraft axes, as discerned by analog logic, spacecraft attitude control is switched to the Intermediate Pointing Control Mode. In this control mode control torques are provided by control moment gyros in response to attitude errors sensed by the Intermediate Earth Sensor and Fine Canopus Sensor.

For the mission selected, an Earth-based laser beacon, located at the site of each laser receiver, illuminates the spacecraft with a narrow pulsed beam (5 arc sec) to serve as a point source reference. Since the spacecraft position will be known within one arc second total solid angle, this beam width will be sufficient to illuminate the vehicle. When the center of the Earth is tracked to an accuracy of approximately 5 arc seconds by the Intermediate Earth Sensor (well within the field of view of the Fine Earth Beacon Sensor) and spacecraft angular rates are within 10 arc seconds per second, and upon receipt of a beacon acquisition signal by the analog logic, in addition to the prescribed attitude and rate signals above, the attitude control pitch and yaw reference will be switched to the Fine Earth Beacon Sensor. Because the linear range of the Fine Earth Beacon Sensor is so small (0.4 arc seconds), the sensor will probably begin operation in saturation. However, loop stabilization is obtained during the acquisition of the fine pointing mode through the use of rate information from spacecraft body mounted gyros. When operation within the linear range of the Fine Earth Beacon Sensor is achieved, derived rate information from a lead network will be used to replace gyro rate signals.

2.5.3 ACQUISITION OF THE EARTH-BASED RECEIVER WITH THE SPACECRAFT LASER BEAM

To begin the primary function of the mission it remains for the Spacecraft laser to acquire the Earth-based receiver. Pointing the spacecraft laser beam to the Earth receiver is accomplished by a two axis servoed optics subsystem. The beam angular offset for point ahead in pitch and yaw, relative to the optical axis of the fixed telescope, is commanded from a stored program in the spacecraft digital computer. The mechanization proposed to provide the angular deflection of the spacecraft laser beam consists of a two degree of freedom "tilting plate" and corrective lens. The tilting plate, being a refractive optic, has the desirable characteristic that a small lateral deflection can be obtained for a relatively large angular rotation. This feature is used to advantage to obtain the high resolution required for point ahead. Defocusing is an undesirable by-product of tilting plate action, and must be compensated for by a corrective lens. Thus, to accomplish the point ahead the computer commands two tilting plate servo loops and the corrective lens position.

Analysis of the computation involved in the prediction of the point ahead angles indicates uncertainties in this prediction of the order of 0.5 seconds which is in excess of the 0.2 arc second narrow laser beamwidth and dictates the need for an acquisition mode. A conical scan technique has been formulated to accomplish this acquisition in which the same servoed optics used for point ahead is placed under the command of the digital computer for scanning purposes. In this technique, the spacecraft laser beam center line is slowly rotated through a circular path with a radius, relative to the predicted point ahead, equal to one-half the uncertainty in the predicted point ahead. Thus, more than the entire area of uncertainty will be covered during the scan if both the laser beamwidth and the total solid angle defined by the path of the beam center line are equal to the angular uncertainty in the point ahead.

As the spacecraft laser beam is rotated through the scan pattern, the signal intensity of the Earth receiver will vary unless the station is at the center of the circle of scan. From the time correspondence between the received signal intensity and the angular position of the beam in the scan, the correct point ahead angle can be determined. Improvement in the mathematical model for point ahead computation by several such acquisition sequences spaced several hours apart should enable the development of a point ahead program to be stored in the spacecraft digital computer that will maintain acquisition of the Earth receiver for an extended period. Periodic update of this program will probably be required by programmed scanning to improve the accuracy of the mathematical model used for computation of point ahead.

Once an acceptable model for point ahead computation is achieved, 24 hour point ahead programs may be stored in the spacecraft digital computer.

Laser communication may commence upon correct point ahead of the laser beam in response to commands to both servo loops of the tilting plate and corrective lens.

Station switching is achieved by simultaneous switch-off of one Earth-based laser beacon and turn-on of another. The new beacon reference appears as a step change in attitude error of up to 10 arc seconds to the attitude control Fine Earth Beacon Sensor and slewing to the new attitude reference is accomplished automatically.

The programmed point ahead angles must take station switching into account, so that the switching of the spacecraft point ahead programs, stored in its digital computer, are synchronized with the switching of ground stations.

2.6 SPACECRAFT CONTROL SYSTEM MATHEMATICAL MODEL

The reduction of a physical system to a mathematical model is the cornerstone of any system analysis and synthesis effort. There are numerous equivalent models that may be generated for any system. In modeling the precision attitude control system under investigation it was found to be advantageous to emphasize that attitude control is realized by exchanging stored angular momentem between the control actuators (four control moment gyros) and the structure of the spacecraft. This approach simplifies the mathematical description of the most complex portion of the control system, the control moment gyros.

A complete set on nonlinear differential equations defining the operation of the control moment gyros is derived in Appendix C. These equations are linearized in Appendix D and many useful transfer functions, which indicate the peculiar characteristics of these control actuators, have been developed. In summarizing the work of these Appendices and also Sections 5.3 and 5.4, three single axis linearized math models are presented to illustrate in simplest terms the operation of the precision attitude control system.

2.6.1 THE X-AXIS LINEARIZED MATH MODEL

This model appears in Figure 2-5 in a signal flow graph format. The figure indicates that the effect of an external torque T_x is to change the X-axis angular momentum H_x. Any deviation in attitude, O_x, is sensed and processed through the compensation network to drive the torque motors of the twin single degree of freedom control moment gyros. The model of the first control moment gyro results from representing its gimbal angle as a perturbation, $a_{(1)}$, about a nominal gimbal angle A. Likewise since the second control moment gyro is torqued in an opposite direction, its gimbal angle is represented as a perturbation, $a_{(2)}$, about is nominal angle of -A. The angular momentum h_x, stored by the two gyros is then a superposition of the momentum stored by each gyro resolved along the X-axis. In the math model, $dh_x(1)$ and $dh_x(2)$ indicate the perturbations in stored angular momenta from the nominal $h_x0(1)$

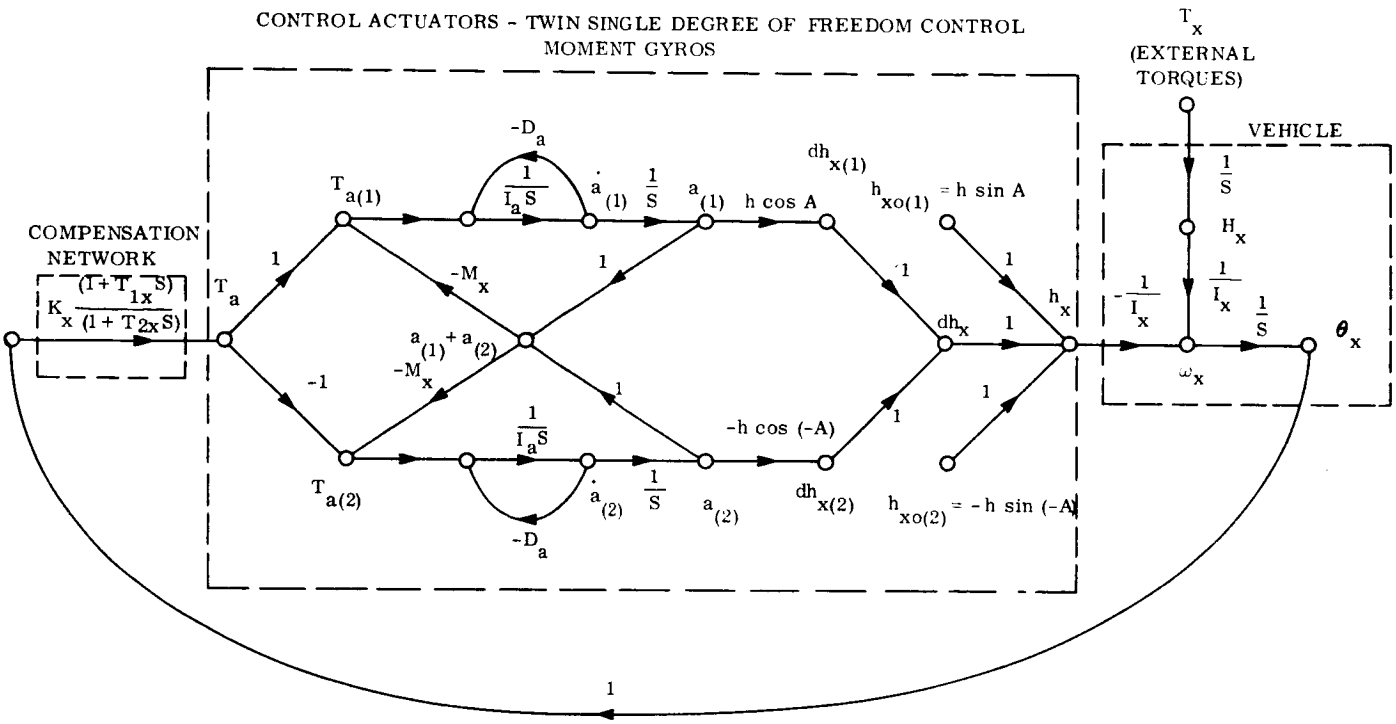

Figure 2-5. X-Axis Linearized Math Model

and $h_{x0}(2)$ due to the perturbations in gimbal angles $a_{(1)}$ and $a_{(2)}$ from the nominal A and -A. Note that to hold the system motionless, all the momentum (H_x) must be stored by the gyros (h_x). The constraint loops which keep the gimbal angles of the twin gyros equal in magnitude but opposite in sign are also shown.

Nonlinearities not appearing include gimbal friction, sensor and torque motor characteristics considerably removed from null, and the pneumatic reset logic (unloading) that becomes operative when a gimbal angle exceeds sixty degrees.

2.6.2 THE Y-AXIS LINEARIZED MATH MODEL

This model appears in Figure 2-6. It is very similar to the X-axis model. The only significant difference is that to obtain the large amount of viscous gimbal damping required to have the twin double degree of freedom control moment gyros operate in the highly damped mode necessitates the use of electronic feedback of gimbal rate through the torque motors.

Y-axis nonlinearities not shown again include gimbal friction, sensor and torque motor amplifier saturations, and pneumatic reset logic. In addition the Y and Z axes must consider the sample and hold circuitry receiving the pulsed laser beacon. They also have rate gyro information driving the torque motors through a deadzone characteristic in order to speed up acquisition and station switching and to incorporate a large safety factor into the system acquisition capability.

2.6.3 THE Z-AXIS LINEARIZED MATH MODEL

This model appears in Figure 2-7. The only significant difference in Z-axis control from Y-axis control is that inner gimbal motion must be compensated for by decoupling in the control law. This is shown as the processing of inner gimbal information through the tangent functions.

An important point emphasized by all of these models is that the control system characteristics are gimbal angle dependent.

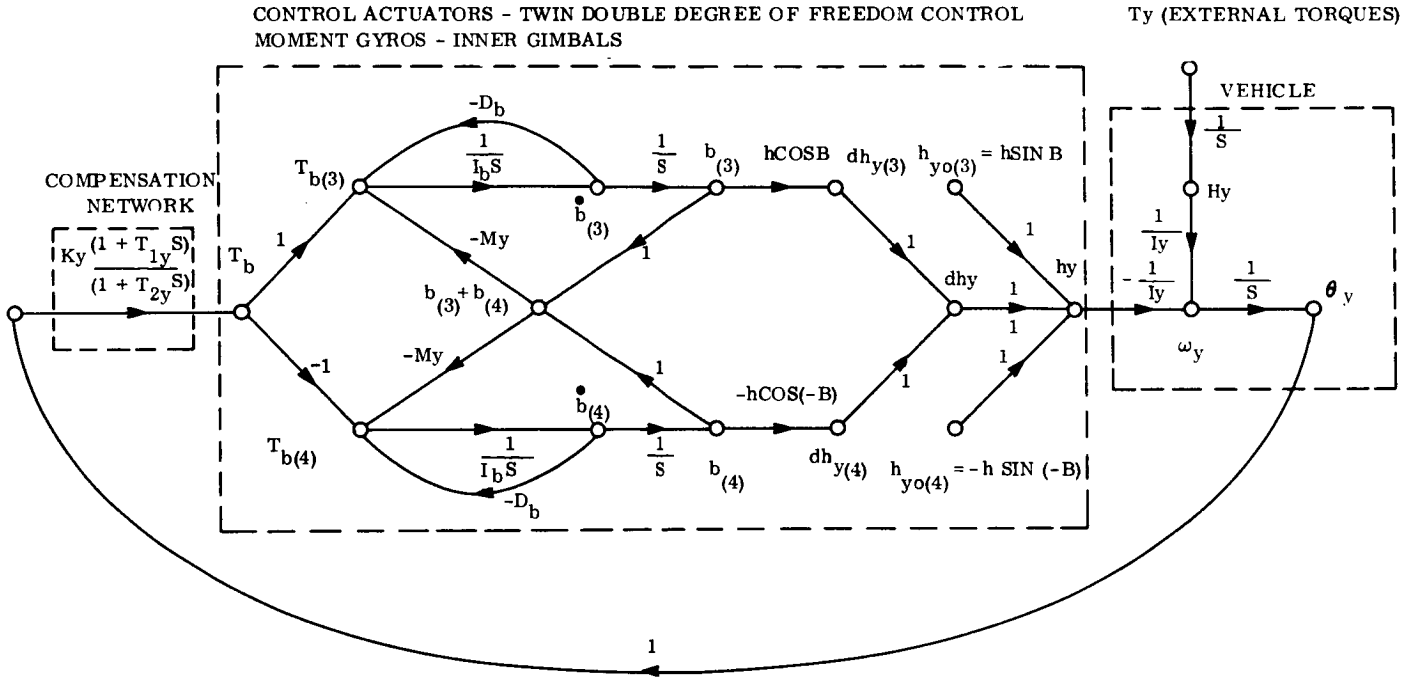

Figure 2-6. Y-Axis Linearized Math Model

2.7 SPACECRAFT CONTROL SYSTEM PERFORMANCE

Control laws have been identified in Section 5.4 that meet the system requirements. They were chosen considering accuracy, stability, acquisition capability, and gimbal angle constraints. In evaluating the performance of the control system, two modes of operation may be examined separately. During the attitude hold portion of fine pointing, the system nonlinearities are classified as slow; that is, the system remains linear over a time interval which is long compared to the response time of the system. The transfer function concept is valid and system performance is adequately described in terms of poles and zeros which wander slowly about the complex plane. However, during fine acquisition of the pitch and yaw axes to the earth reference beacon, fast nonlinearities, such as saturation in the sensor and torque motor summing amplifiers are encountered, which modify the characteristics of the system rapidly compared to the response time. In this case the transfer function concept loses its significance and the analog computer was used to evaluate system performance.

2.7.1 SPACECRAFT X-AXIS CONTROL SYSTEM PERFORMANCE

The accuracy of the X-axis control system is limited by gimbal starting friction (stiction) rather than the peak disturbance torque encountered. The maximum error occurs just as the torque motor overcomes the gimbal stiction. The magnitude of the error is (neglecting noise effects)

$$O_x\,(\max) = \frac{f_s}{k_x} = \frac{3.6 \times 10^{-4}\ \text{ft-lb}}{5 \times 10^{-4}\ \text{ft-lb/arc second}} = 0.72\ \text{arc second} \qquad (2\text{-}2)$$

This number is about one-quarter of the amount alloted by the error analysis listed in Section 4.2.2.

2.7.2 SPACECRAFT Y-AXIS CONTROL SYSTEM PERFORMANCE

The accuracy of the Y-axis control system is limited by the peak disturbance torque rather than gimbal friction. The reason this is just the opposite from the X-axis may be explained by examining the steady state error resulting from a constant external disturbance torque.

For the Y-axis this is

$$O_y = \frac{1}{k_y} \left(\frac{T_y D_b}{2h \cos B} + f_r \right) \qquad (2\text{-}3)$$

The equivalent expression for the X-axis is

$$O_x = \frac{1}{k_x} \left(\frac{T_x D_a}{2h \cos A} + f_r \right) \qquad (2\text{-}4)$$

Since the peak disturbance torque values, T_x and T_y, and the gimbal running friction, f_r, are very close in magnitude, the disturbance torque term dominates the Y-axis error because the ratio D_b/h is about 50, which is attained through use of a gimbal rate sensor which increases the damping. The gimbal friction dominates the X-axis error because the ratio D_a/h is 0.005 and the gimbal angle magnitude does not exceed 60 degrees.

Substituting the appropriate numbers into Equation 2-3 yields a maximum Y-axis error (neglecting noise effects) of

$$O_y \text{ (max)} = 0.0016 \text{ arc second} \qquad (2\text{-}5)$$

at a full gimbal excursion of 60 degrees. This number is about an order of magnitude better than the allotment in Section 4.2.2.

The analog computer simulation indicated that with the largest initial conditions specified in the requirements the fine acquisition and station switching could be completed even without the rate gyro information in roughly one minute. The use of the rate gyros provides a large design safety factor while simultaneously reducing the settling times.

2.7.3 SPACECRAFT Z-AXIS CONTROL SYSTEM PERFORMANCE

The Z-axis performance is very similar to the Y-axis. The only difference in the accuracy number is that now both inner and outer gimbal angles must be considered. The steady state error resulting from a constant disturbance torque T_z is

$$O_z = \frac{1}{k_z} \left(\frac{T_z D_c}{2h \cos B \cos C} + f_r \right) \qquad (2\text{-}6)$$

Due to the large value of D_c the disturbance torque term again dominates. With both gimbal angles at sixty degrees the maximum magnitude of the Z-axis error (neglecting noise effects) is

$$O_z \text{ (max)} = 0.0032 \text{ arc second} \qquad (2\text{-}7)$$

which is still well below the allotment.

The analog simulation dramatically indicates the need for the decoupling of the Z-axis from the Y-axis and that once this is implemented that the Z-axis acquisition and station switching performance is comparable to that of the Y-axis.

2.8 CRITICAL SPACECRAFT CONTROL SUBSYSTEM PROBLEM AREAS

The integration, alignment, and verification of performance of the control system sensors with their associated primary optics and servoed optics is viewed as the salient critical area requiring effort in the near future. An inseparable part of this problem is the effect of thermal gradients due to the dissipation of large amounts of heat in close proximity.

A significant problem area associated with accurately pointing the narrow beam spacecraft laser to illuminate the ground station within the half power points of the beam has been identified with the requirement to accurately compute the point ahead angles of the spacecraft laser beam relative to its altitude reference. Since this information must be generated to accuracies of the order of 10^{-5} degrees of arc, it is envisioned that an accurate computer model of the changing spatial position of the spacecraft and ground station is required. A detailed study of this stochastic control process and methods to improve the model to insure solutions within the required accuracies require a detailed analytical study.

Finally an early evaluation of the physical nonlinearities in the Fine Earth Beacon Sensor and Control Moment Gyro actuators is deemed advisable through a combined physical and computer simulation. It is envisioned that physical hardware combined with a computer simulation of the spacecraft structure and associated disturbances would furnish an effective method of evaluating the control system proposed.

2.9 CONCLUSIONS

The objective of this study has been to establish the feasibility and to formulate a practical concept of a spacecraft control system capable of successful performance of precision spacecraft triaxial control for a selected mission envisioned for the 1975 to 1980 time period. The mission selected, involving high data rate laser communications from a Mars orbiter, has established requirements for spacecraft attitude control to Earth beacon and Canopus attitude references to an accuracy of 10^{-5} degrees of arc. An additional requirement has been established to control the pointing of the transmitted laser beam relative to the spacecraft reference to an accuracy of 10^{-5} degrees of arc.

The study has demonstrated the feasibility of accomplishing both spacecraft control requirements with essentially state-of-the-art control system hardware within the assumptions that certain associated systems are available in the time period of interest. These include a spacecraft 30-inch aperture diffraction limited optical system, the assumed spacecraft laser system and radioisotope thermionic power generator, and the assumed ground receiver and beacon.

SECTION 3

MISSION ANALYSIS

SECTION 3

MISSION ANALYSIS

3.1 INTRODUCTION

The objective of this study is to determine the feasibility of a triaxial attitude control system capable of orienting a spacecraft with a precision of 10^{-4} to 10^{-6} degrees of arc. Studies of attitude control for spacecraft invariably require that certain characteristics of the spacecraft, of the energy source to be tracked, and of mission-dominant characteristics be specified. Some of these characteristics are:

a. Frequency and amplitude of disturbing torques to spacecraft
b. Spacecraft inertias
c. Spacecraft structural bending moments
d. Spacecraft mass
e. Radiance characteristics of source to be tracked
f. Angular diameter of source
g. Angular rate of source in the appropriate coordinate system
h. Absolute tracking accuracy vs. stability of point
i. Proximity of optical noise sources: the sun, Earth, stars, planets and moons

In a practical sense, the spacecraft mission(s) must be defined in order to permit selection of the above and other parameters of the problem. This is Item 1(a) of the Work Statement.

At the request of the ERC Technical Director, we have limited our analyses to the general category of spacecraft communicating with Earth via an optical link. There are many variations of this type mission, and we have considered the following, each of which is discussed in the following pages.

a. Deep Space Probe (Jupiter to Pluto), with fixed and variable spacecraft transmitter beamwidth

b. Mars orbiter, with and without a cooperative Earth laser beacon

c. Global optical communication system in Earth orbit (synchronous altitude)

Laser communication from a Mars orbiter employing a cooperative Earth laser beam was selected as the mission for this study, based on the analyses of this section and the conclusions of Paragraph 3.8.

3.2 INFORMATION RATES

There is considerable discussion in the literature of the potential for high data rate communication by optical means with a spacecraft over interplanetary ranges (References 1 through 9). The limitations of present communications equipment was pointedly brought to light during the 1965 Mariner probe to Mars, where data rates of 8-1/3 bps necessitated many hours to transmit a single TV frame of information.

Most discussion of ideal or desired data rates consider about 5×10^7 bps to 10^8 bps as an upper bound, based on the bandwidth requirement for real time high resolution pictorial information. This seems entirely safe as an upper limit. Perkin-Elmer (Reference 3) indicates that bonafide requirements for information rates exceeding 10^6 bps will be rare. Certainly the bandwidth requirements for sensors other than image forming devices do not approach the 10^8 bps figure within three orders of magnitude, and even four orders or greater would be more realistic for any practical situation.

The cost that one is forced to pay for such a high "ideal" data rate of 10^8 bps may be quite high; hence, it is appropriate to also consider how low a data rate one could employ and still obtain most or all the desired information from an interplanetary probe. Consider the pictorial information rate (TV system or equivalent) since this is the dominant sensor requiring high rates. Any system operating in real time would have a high percentage of redundant information that need not be transmitted. Data processing techniques could be employed on board the spacecraft to reduce the transmittal of redundant information at some increase in overall complexity. Alternately, one may operate the sensory system in near real time rather than real time to reduce redundant information and data rates. (A reduction in frame rate from 30 to 3 fps would reduce the information rate by the same order of magnitude.) For anything other than a planetary impact, this would probably be entirely

satisfactory. Even for an impact mission, e.g., Ranger, it may be satisfactory. The highest frame rate used on Ranger was 5 fps for the P cameras, and the video bandwidth requirement was 2×10^5 Hz for this relatively low resolution (300 horizontal lines) system.

For a planetary fly-by or orbital mission, rather than impact, there exists the alternative of operating the sensory system in real time or near real time, and storing the information on board for subsequent transmittal at a much lower rate. This technique is planned for Voyager where data will be received at a rate of 200 Kbps and transmitted at a rate of 15 Kbps (Reference 10). The penalty paid for this alternative is the additional storage capacity.

For a given mission, a comparison would be necessary at the systems level to determine the relative cost/weight/reliability tradeoff of using either or both the data compression and data storage techniques, vs. the option of operating in real time. If non-real time transmission rates are preferable (as in the case for Ranger, Mariner, and Voyager), the desired or ideal information rates may drop by two or three orders of magnitude from the real time case, i.e., to 10^5 to 10^6 bps. These rates would adequately handle high resolution TV data, and would also be more than adequate to handle any reasonable assortment of scientific and engineering nonimaging sensors. For comparison purposes, Voyager contemplates average information rates of less than 100 bps for all non-imaging scientific and engineering sensors (Reference 10).

3.3 OPTICAL COMMUNICATIONS

The communications system aboard the spacecraft consists of an optical telescope, a laser transmitter with its modulator and prime power supply, and a fine pointing sensor required to locate and track a laser beacon on or near the earth. We will consider the telescope on the probe to be a Cassegrain configuration.

The Earth terminal elements of the communication system consist of essentially the same elements, though the parameters are significantly different.

A single telescope on the spacecraft will serve as both the transmit and receive antennas, with different wavelengths being used for each function. It is a practical necessity to use only one telescope (in addition to the weight that is conserved) since it would be virtually impossible to boresight two separate antennas to the required accuracy, and maintain this alignment for extended periods.

The aperture of the telescope on the probe should ideally be as large as possible (for example, three meters or greater) for both the transmitting and receiving functions, but unfortunately this may not be practical due to weight and optical technology considerations. Whatever its size, the telescope should be diffraction-limited. If it is not, a larger telescope must be carried to obtain the equivalent performance of a smaller diffraction-limited telescope for both the receive and transmit function. This would be blatantly wasteful.

Large diffraction-limited telescopes have never been orbited, and no firm plans exist today (in the form of a program) to do so. None of the OAO telescopes (up to 38-inch aperture) are diffraction-limited (Reference 11), and it would be during the early 1970's at the earliest before it is known whether diffraction-limited performance can reasonably be maintained in the space environment for a telescope as large as 40 inches in aperture.*

It would seem prudent from this standpoint to restrict our thinking to a telescope of perhaps 30 to 40 inches in size. From a weight standpoint, this size telescope seems reasonable also. A 30-inch telescope of reasonable f/number would weigh on the order of 1000 pounds (optics, mounts, automatic alignment equipment and structure, but excluding the laser system and all other subsystems). A 60-inch telescope would weigh perhaps 5000 pounds. If the aperture is significantly increased, a new class booster beyond Saturn V would have to be considered for a deep space probe. The aperture can be a parameter (over the 30- to

*It must be recognized that we are in the infancy of the science of optical communications, compared with the more advanced microwave communications. Major advances are required not only in optics, but in laser development, modulation techniques, and optical receiving techniques as well.

60-inch range) for later calculations, but 40 inches is tentatively selected (arbitrarily) for present purposes as the largest aperture that should be considered for the laser communication system. This telescope would weigh about 2000 pounds.

The characteristics of the optical communication system to be determined in this analysis will generally be found to exceed the present state of the art by a wide margin. This simply reflects the fact that a practical technology in this field has not yet developed. High average power (watts) lasers must be developed that are rugged and reliable, and operate with an order of magnitude increase in efficiency over present devices. Significant development effort is required to improve modulation techniques and detector quantum efficiency. Narrow band optical filters must be developed, and methods must be developed to maintain the figure of a large-aperture, diffraction-limited telescope in the space environment. Finally, methods must be developed to generate large quantities of electrical power (kilowatts) in an efficient manner.

These developments are not specifically related to attitude control technology, but influence the required precision of control for an optical communications mission. We assume (with some optimism) that the necessary technical developments are feasible, and will be made over the next decade to be consistent with an assumed launch period of 1975 to 1980.

3.4 SIGNAL-TO-NOISE RATIO IN THE PHOTOMULTIPLIER DETECTOR

Before proceeding to a discussion of the merits of any given mission, we wish to define the noise characteristics of the received laser signal, since this is basic to a determination of information rates and in establishing how well an attitude control system can ultimately point. We will consider noise in a photomultiplier since this type detector (or variations of it) are used almost exclusively in the visible and ultraviolet regions of the spectrum when optimum performance is required.

Consider a detection circuit consisting of a photomultiplier and a load resistor in the anode circuit to develop the signal voltage. It is assumed that the noise generated in the preamplifier following the detection circuit is an insignificant quantity in comparison with detector noise.

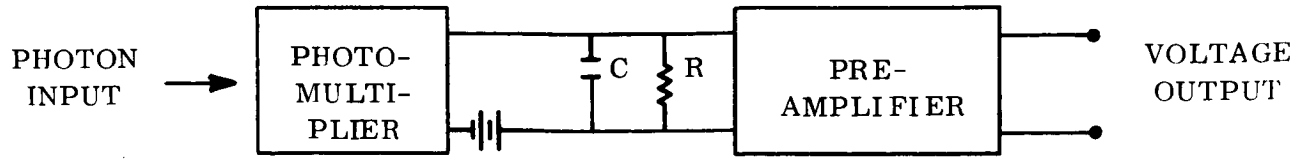

The noise component of the current generated by the photomultiplier has several sources:

a. The random generation of signal photoelectrons due to the arrival of signal photons.

b. The random arrival and presence of background noise photons, i.e., photons generated by a source other than that desired.

c. The thermal or otherwise spurious emission of electrons from the photocathode in the absence of input photons.

The average signal voltage developed across R from the source being observed is

$$V_s = I_s GR = \eta \bar{N}_s eGR \qquad (3\text{-}1)$$

where

V_s = average signal voltage (volts)

I_s = the photocathode current (amperes)

$I_s G$ = the anode current (amperes)

R = the anode load resistor (ohms)

η = the quantum efficiency of the photoelectric surface at the laser wavelength, λ (dimensionless)

$\bar{N}_s$ = the average rate of arrival of signal photons (photons per second at wavelength λ)

G = current amplification of photomultiplier (dimensionless)

e = electronic charge = 1.6×10^{-19} coulombs

The rms value of the total noise voltage generated by the photomultiplier current in the load is (Reference 12):

$$V_n = I_n R = \left[2e \, (I_s + I_b + I_d) \, G^2 \, H \Delta f \, R^2 \right]^{1/2} \qquad (3\text{-}2)$$

and the noise spectrum is white (shot noise). Here,

V_n = rms noise voltage (volts)

I_n = rms anode noise current (amperes)

I_b = photocathode current produced by background radiation (amperes)

I_d = photocathode dark current (amperes)

H = multiplier noise figure introduced because the collection efficiency at the first dynode is not unity, i.e., not all cathode photoelectrons reach the first dynode. Typically, H has a value between 1.1 and 1.5, and is dimensionless.

Δf = the electrical bandpass of the detector/filter/preamp (Hz)

An additional source of white noise is the thermal fluctuation of charge density along the resistor, R (Johnson noise). A pure resistance produces an rms voltage (Reference 12):

$$V'_n = (4kTR\,\Delta f)^{1/2} \tag{3-3}$$

where

k = Boltzman constant, 1.374×10^{-23} joules/^{o}K

T = Temperature of R (^{o}K)

The total rms noise voltage is $(V_n^2 + V'^2_n)^{1/2}$, or

$$V_t = V_n \left[1 + \frac{V'_n}{V_n}^2 \right]^{1/2} \tag{3-4}$$

The ratio V'_n/V_n can be shown to be far less than unity at $T = 300^{o}$K or less for any reasonable value of the parameters. For example, with an anode current on the order of 10^{-8} ampere, current amplification of 10^{7}, and R of one megohm, V_t differs from V_n by less than 0.1 percent. Only if R is made much smaller than one megohm would it be necessary to consider Johnson noise. The signal-to-noise voltage ratio at the input to the preamp is

$$\left(\frac{S}{N}\right) = \frac{V_s}{V_n} = \left[\frac{I_s\,GR}{2e\,(I_s + I_b + I_d)\,H\,\Delta f R^2} \right]^{1/2} \tag{3-5}$$

or

$$\left(\frac{S}{N}\right) = \left[\frac{I_s}{2e\,(I_s + I_b + I_d)\,H\,\Delta f} \right]^{1/2} \tag{3-6}$$

in terms of the photocathode currents.

Since $I = \eta \bar{N} e$, we can rewrite the above expression in terms of the average input arrival rate of photons:

$$\left(\frac{S}{N}\right) = \left[\frac{\eta \bar{N}_s}{2H \Delta f \left(1 + \frac{N_b + N_d}{N_s}\right)}\right]^{1/2} \tag{3-7}$$

Here, $\bar{N}_d$ must be interpreted as the equivalent photon arrival rate to produce the required number of dark current photoelectrons. Unless one is dealing with a laser source at a single wavelength, the quantities η, $\bar{N}_s$, and $\bar{N}_b$ must be related as a function of wavelength.

For the case where $\bar{N}_b$ and $\bar{N}_d$ are much less than $\bar{N}_s$, i.e., a quantum noise limited system where signal photons far outnumber noise photons,

$$\left(\frac{S}{N}\right) = \left(\frac{\eta \bar{N}_s}{2H \Delta f}\right)^{1/2} \tag{3-8}$$

From the ratio of the two preceding equations, we obtain the useful relationship,

$$\left(\frac{S}{N}\right)_{\text{with noise}} = \left(\frac{\bar{N}_s}{\bar{N}_s + \bar{N}_b + \bar{N}_d}\right)^{1/2} \left(\frac{S}{N}\right)_{\text{without noise}} \tag{3-9}$$

A final equivalent expression for sensor S/N can be written in terms of the anode current. Since anode current is simply G times the cathode current, we have

$$\left(\frac{S}{N}\right) = \left[\frac{I'_s}{2e\, GH \Delta f \left(1 + \frac{I'_b}{I'_s} + \frac{I'_d}{I'_s}\right)}\right]^{1/2} \tag{3-10}$$

where the primes on the currents are used to designate anode current. Figure 3-1 shows a plot of signal-to-noise ratio vs. incoming photon arrival rate. The quantity $\left|\eta/2H\ \Delta f\right|^{1/2}$ is plotted as a parameter. H is assigned a value 1.25. In the region of 3500 Å, the average value of η for high performance photomultipliers of today is on the order of 0.1, and Δf will typically be a few cycles per second. This leads to a typical value of the parameter of about 0.1. Contrary to the very low signal-to-noise ratios typical for communications work, a signal-to-noise ratio of perhaps 50 to 500 is usually required in a star tracker sensor to reduce the noise input to the control system to a suitable level. For an ideal optical communication system, information rate and photon arrival rate should be synonymous, i.e., each arriving photon denotes some intelligence. In a practical system, where all photons cannot be detected, and where signal-to-noise ratios in excess of unity are desirable, a significantly greater number of photons per bit of information is required. Since

$$\frac{\bar{N}_s}{\Delta f} = \left(\frac{S}{N}\right)^2 \frac{2H}{\eta} \tag{3-11}$$

we obtain $\bar{N}_s/\Delta f = 32$ photons/bit for a signal-to-noise ratio of 2 (H = 1.2, and $\eta = 0.3$). This quantum efficiency assumes an improvement of two or three times over present values, a gain considered reasonable by the time period of interest (1975-1980). This photon-to-bit equivalence will be used in subsequent work for the photon-noise-limited environment.

The cathode dark current of a representative photomultiplier (RCA 7625, S-20 photocathode) is on the order of 2.2×10^{-15} ampere at 25°C, and more than an order of magnitude lower at -70°C. The higher figure corresponds to a cathode emission of 1.4×10^4 electrons per second, which in turn corresponds to about 10^5 photons per second equivalent noise input (4×10^{-14} watt at 5000 Å).

For information rates greater than about 10^5 bps, it is apparent that photomultiplier dark current will not limit the performance of the system. At rates of 10^7 bps, the ratio $\bar{N}_s/\bar{N}_d$ is seen to exceed 3000.

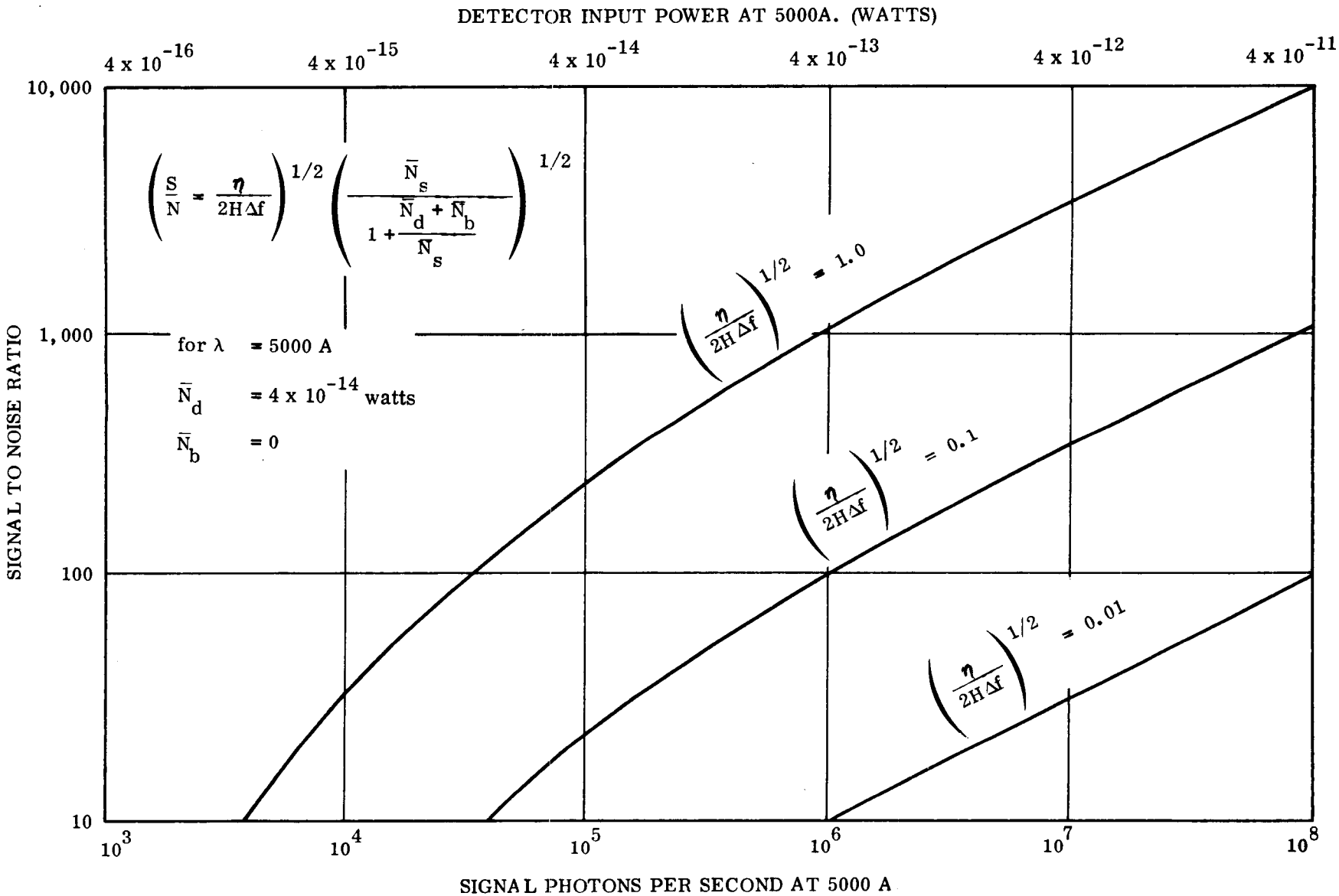

Figure 3-1. Signal-to-Noise Ratio for a Photomultiplier Detector vs. Input Radiant Power

3.5 DEEP SPACE PROBE

The characteristics of the required optical communication subsystem aboard the probe are considered first. The category of deep space probe includes any vehicle operating at or beyond the orbit of Jupiter. From these ranges the apparent angular size of the Earth varies from about 3.3 arc seconds (Jupiter) to less than 0.5 arc seconds (Pluto).

As a first approximation, let us consider a scheme where we illuminate the entire Earth disc (as viewed from the probe) with the laser transmitter, but do not have any significant "spill-over." This infers a variable transmitter beamwidth with distance from the Earth, i.e.,

$$\theta_t R = \text{constant} = \text{Earth Diameter.} \tag{3-12}$$

where θ_t is the half-power laser beamwidth and R is the range to Earth. The advantage of this mode of operation lies in the fact that any and all receiving stations on Earth may receive the probe transmission. With a more narrow beamwidth, the probe must point to the vicinity of one particular Earth receiver.

The worst case attitude pointing requirement occurs at the Pluto range and is approximately 0.1 arc second . This follows from the fact that nothing significant is gained by pointing the telescope with an accuracy better than 1/5 to 1/4 the angular diameter of the beam.

Let us assume the probe carries an optical system with a diameter of about 40 inches, i.e., the maximum practical size for the 1975/80 time period. This telescope would weigh about 2000 pounds. To a first approximation, the total weight of the laser system (transmitter, modulator, receiver, and power supply) should approximately equal the weight of the telescope. This is based on the fact that we should maximize the received irradiance at the Earth terminal for a given total weight of the telescope and laser system weight of about 2000 pounds to go with the 40-inch telescope weight of 2000 pounds, for if we choose some significantly different weight for the laser, it is probable that we can change the size of the telescope and the laser system and yield the same irradiance at the Earth for lower total weight in the probe.

Based on a total communication system weight of 4000 to 5000 pounds, it would appear the weight of the entire probe would be on the order of 10,000 to 12,000 pounds. This is a reasonable figure for a Saturn V booster. Previous studies by GE and others indicate the Saturn V capability will launch a 12,000 to 15,000 pound payload to the orbit of Jupiter with a time of flight of about one and one-half years. To reach the orbits of the outer planets, with the same payload, a Jupiter fly-by would be required that would perturb the probe's trajectory in the direction to achieve this goal. Without the encounter, the maximum launch weight to the orbit of Saturn would be under 10,000 pounds, and far less for the remaining planets.

The 2000 pounds of weight allocated to the laser portion of the system will be made up primarily (perhaps 90 percent) of prime power supply. Assuming the availability of thermionic radioisotope power supplies in the time period of interest with a weight efficiency of 3 kilowatts electrical output per kilopound weight * leads to 6 kw average electrical power generation. For a diffraction-limited gas laser operating in the visible region with an efficiency of 0.5 percent, an average laser power of about 30 watts is obtained.

With the variable beamwidth mode of operation that has been selected, the data rate obtainable on Earth is independent of range since $(\theta_t R)$ is constant, The power delivered to the detector of the Earth-based receiving antenna (assuming inverse-square attenuation) is

$$P_R = \frac{k_1 k_2 k_3 k_4 P_t D_R^2}{2 (\theta_t R)^2} \qquad (3\text{-}13)$$

where

k_1 = transmissivity of probe telescope optics ≈ 0.4

*Based on studies by the Advanced Nuclear Systems Operation, General Electric Company Missile and Space Division

k_2 = transmissivity of earth atmosphere ≈ 0.6

k_3 = transmissivity of receiving telescope optics ≈ 0.4

k_4 = transmissivity of narrow band optical filter in receiving telescope ≈ 0.4

$\theta_t R = 1.3 \times 10^9$ cm = diameter of earth

P_t = average power transmitted by laser = 30 watts

D_R = diameter of receiving aperture on earth = 500 cm (Equivalent to the 200-inch Hale Telescope at Mt. Palomar)

Using these quantities,

$$P_R = 1.12 \times 10^{-20} P_t D_R^2 \approx 10^{-13} \text{ watt}$$

At 5000 Å, this power is equivalent to a photon arrival rate of 2.5×10^5 per second. Now, the information rate can be obtained from a knowledge of the photon arrival rate and the receiving system characteristics as derived in Paragraph 3.4. Using our predicted equivalence of 32 photons per bit, an information rate of about 7800 bits per second is obtained for this mission, with no margins (for a photon-noise-limited system). This will be very near the performance to be expected for nighttime operation, i.e., when the receiving antenna is located on the dark side of the Earth.

Unfortunately, nighttime operation is possible only about six months out of the year for the planets of Jupiter and beyond, so the expected reduction in data rate for daytime reception on Earth should be ascertained. The daytime sky spectral radiance is assumed to be about 2.5×10^{-7} watt/cm^2 ster. Å, for angles significantly away from the sun. Assuming a one angstrom bandpass filter is achievable for use in the receiving telescope, the noise power delivered to the receiver is

$$P_R = 1/4 \pi k_3 k_4 D_R^2 R_S \frac{\alpha^2}{4} \text{ for small } \alpha\text{'s} \qquad (3\text{-}14)$$

where R_S is the spectral radiance of the daylight sky and α is the total cone angle of the field of view of the receiving telescope. For $D_R = 500$ cm, and using the 1 Å filter

$$P_R = 1.9 \times 10^{-3} \alpha^2$$

Let us determine the telescope field of view, α, for which the sky background will be equivalent to the signal power. This will occur for

$$P'_R = P_R = 1.9 \times 10^{-3} \alpha^2 = 10^{-13} \text{ watt} \qquad (3\text{-}15)$$

or

$$\alpha = 0.72 \times 10^{-5} \text{ radian} = 1.4 \text{ arc sec} \qquad (3\text{-}16)$$

For this field of view our "no noise" information rate is reduced by a factor of 0.707 (see Paragraph 3.4) to 5500 bps. If the receiver field of view is opened up to a more reasonable value, the situation becomes virtually hopeless. With a field of view of even 14 arc second cone angle, for example, the information rate will drop below 1000 bps.

Several conclusions can now be reached regarding this mode of operation:

a. Information rates are grossly inadequate for near real time pictorial information from any of the planets considered.

b. Serious constraints on launch window are imposed to avoid planetary encounter that would require daytime viewing from Earth.

c. This mode of operation is vastly inferior to that achievable with microwave transmission.

d. Laser transmitter beamwidths on the order of 0.1 to 0.2 arc second are required to achieve information rates of 10^6 bps from Jupiter and Saturn.

e. One to two orders of magnitude increase in laser efficiency are desirable to boost data rates and minimize the problem of dissipating heat generated in the large spacecraft-borne laser power supply.

3.5.1 POINTING REFERENCE FOR DEEP SPACE PROBE

Even though it appears that the mode of operation selected will provide information rates which are too low to be of practical value, consider appropriate tracking references for the spacecraft that will allow orienting the spacecraft laser to point to the Earth. The references that might be used are:

a, Offset guidance using the sun.

b. Direct tracking of the sunlit Earth.

c. Direct tracking of a cooperative laser beacon on Earth.

In any deep-space mission, the sun appears close to the Earth as seen from the spacecraft. At Saturn, for example, the maximum separation is about six degrees, and varies sinusoidally throughout the Earth year for trajectories in or near the ecliptic plane. If the spacecraft tracking system employs the illuminated Earth or an Earth-based laser as its fine pointing source, solar radiations must be greatly attenuated to provide a usable signal-to-noise ratio. At these small sun angles, sun shields which provide the required attenuation may be impractically long. Furthermore, for an Earth-based laser beacon, transmitted power required for satisfactory tracking by the spacecraft in the high solar optical noise environment may be impractically high. Therefore, a possible alternative is to use the sun as a tracking source and offset-point to the Earth. The aspects of a mission based on this concept are explored briefly in the following paragraphs. An unmanned spacecraft is assumed throughout.

It is assumed initially that the half-power beamwidth of the spacecraft laser is sized to equal the Earth's apparent diameter, as seen at the spacecraft. At the distance of Saturn (approximately 10^9 miles), the Earth's angular diameter is about 2 arc sec. If the received power, density at any point on the Earth's illuminated hemisphere is to be maintained above 50 percent of the beam-center level, the maximum total pointing error must be limited to about 0.5 arc sec. This pointing error includes the sun tracking error, the sun-to-Earth offset error (through a changing angle), the error in third-axis control about the spacecraft-sun line, and the spacecraft transmitter/tracker alignment error.

To minimize the sun tracking error, a high optical system gain is desirable. For example, at the distance of Saturn, the sun's angular diameter is about 180 arc seconds. If the sun's image nearly fills the field of view of a 2000 x 2000 element image dissector, the detector accuracy is about 0.1 arc second, and the total spacecraft stability is optimistically assumed to be 0.3 arc second.

Offset pointing could be achieved through a combination of electronic and mechanical offsets. In a star tracking system, for example, the detector null of an image dissector can be offset nearly to the edge of the field of view. If this electronic offset is insufficient, the total offset can be increased by mechanically or optically offsetting the image dissector itself in fixed, precisely known increments. Thus, a large offset range can be covered with high accuracy. However, it was seen in the previous paragraph that, to achieve even the minimum acceptable pointing stability, the sun's image must fill a 2000 x 2000 element detector, leaving essentially no electronic offset capability if a simple high-resolution image dissector is used as the spacecraft detector.

If the total absolute offset pointing accuracy of 0.5 arc second is to be achieved, the actual offset angle error must be limited to about 0.2 arc second. While this is certainly a challenge, it may be possible through either optical, mechanical, or electronic techniques. An example of an electronic offset technique which would be capable of offsetting accurately through large angles is to fabricate an array of solid state image dissectors. One-inch square detectors containing 1000 x 1000 elements are being developed, and a 20 x 20 dissector array could provide offsets of $\pm$2.5 degrees.

A final and most important consideration in offset pointing is that it really need not be done 'bpen-loop". If the offset can be varied from the ground through a fixed search pattern, the variation in signal received at even one Earth receiving station is sufficient to determine the location of the beam centerline, relative to the Earth. Ground commands can then be sent to "center" the beam on the Earth. This technique could be used periodically to "trim out" offset of alignment errors due to incorrect driving rate of the offset angle, thermal deformation, structural stress relief, or even improper ground calibration. These adaptive corrections should not be required too frequently, particularly near encounter, since the spacecraft will

have had many months to "stabilize." The final pointing stability is then dependent almost entirely upon the sun (pitch and yaw) and star (roll) tracking stabilities.

3.5.2 TRACKING THE EARTH FOR FINE POINTING

If the Earth itself could be tracked with sufficient accuracy, a narrow laser beam on a deep space probe could be pointed at specific Earth stations by offsetting from the Earth's geometric center.

There are three major problems in high-precision tracking of the Earth:

a. The Earth's stellar magnitude varies widely as a function of the probe-Earth-sun angle during the period of continuous communications.

b. The angular separation of the Earth and the sun as seen at the probe is always small (less than 6 degrees at Saturn).

c. The Earth is always seen in a gibbous, quarter, or crescent phase, thus requiring some sensor signal processing technique for accurately locating the geometric center.

A brief investigation of Item a., above, has shown the illumination at a distance from a diffusely reflecting sphere which receives collimated illumination to be

$$E_R = \frac{a E_o r^2}{4R^2} \left[(\cos\gamma)^3 + \frac{\sin\gamma}{2} (\pi + 2\gamma + \sin 2\gamma) \right. \qquad (3\text{-}17)$$

where

a is the albedo (reflectivity) of the sphere

E_o is the power density (illumination) in the source beam

r is the radius of the sphere

R is the observer's distance from the sphere

γ is the angle at the source between the sphere and the observer less 90 degrees

When the sphere is the Earth, the source is the sun, and the observer is at the orbit of Saturn,

$$E_R = 2.7 \times 10^{-13} \quad f(\gamma) \text{ watts/cm}^2 \qquad (3\text{-}18)$$

where $f(\gamma)$ is the trigometric function in the first equation. Figure 3-2 depicts the geometry of the situation and shows values of stellar magnitude correlated with levels of illumination resulting from the above expression. The relation between γ (the earth phase angle) and the earth-probe-sun angle is also shown. Thus if the latter is to be limited to the region of 3 to 6 degrees, γ may vary from +60 to -60 degrees, and the earth's stellar magnitude may vary from +1.2 to +5.6 (a power variation of about 40). It is shown in the following paragraph that for the deep space probe tracking an Earth-based laser a "one bounce"* sun shield is required if the probe detector is to operate internal noise-limited. Figure 3-3 describes the length of sun shield required for various probe receiving apertures as a function of sun-probe-Earth angle (and therefore as a function of time available for continuous high data rate transmission).

Figure 3-4 shows the Earth as seen from Saturn at the start of the 120-day communication window when $\gamma = -60$ degrees. It is clear that only a few percent of the probe-facing hemisphere is illuminated; furthermore, the illumination is very non-uniform over the crescent, thus making the determination of the S/N ratio for detector elements in various regions of the image very difficult. This specific problem is related to the difficulty of determining where the edge of the Earth is on the detector, which is directly related to the accuracy with which the Earth's center can be located.

Preliminary investigations into the use of both image dissector and image orthicon detectors have indicated that a probe receiving aperture considerably in excess of the 40 inch maximum previously described would be required to achieve a S/N ratio sufficiently high for the required detector accuracy.

*Sunlight must be reflected once from the inner wall of the shield, where it is attenuated via a black coating, before reaching the primary mirror.

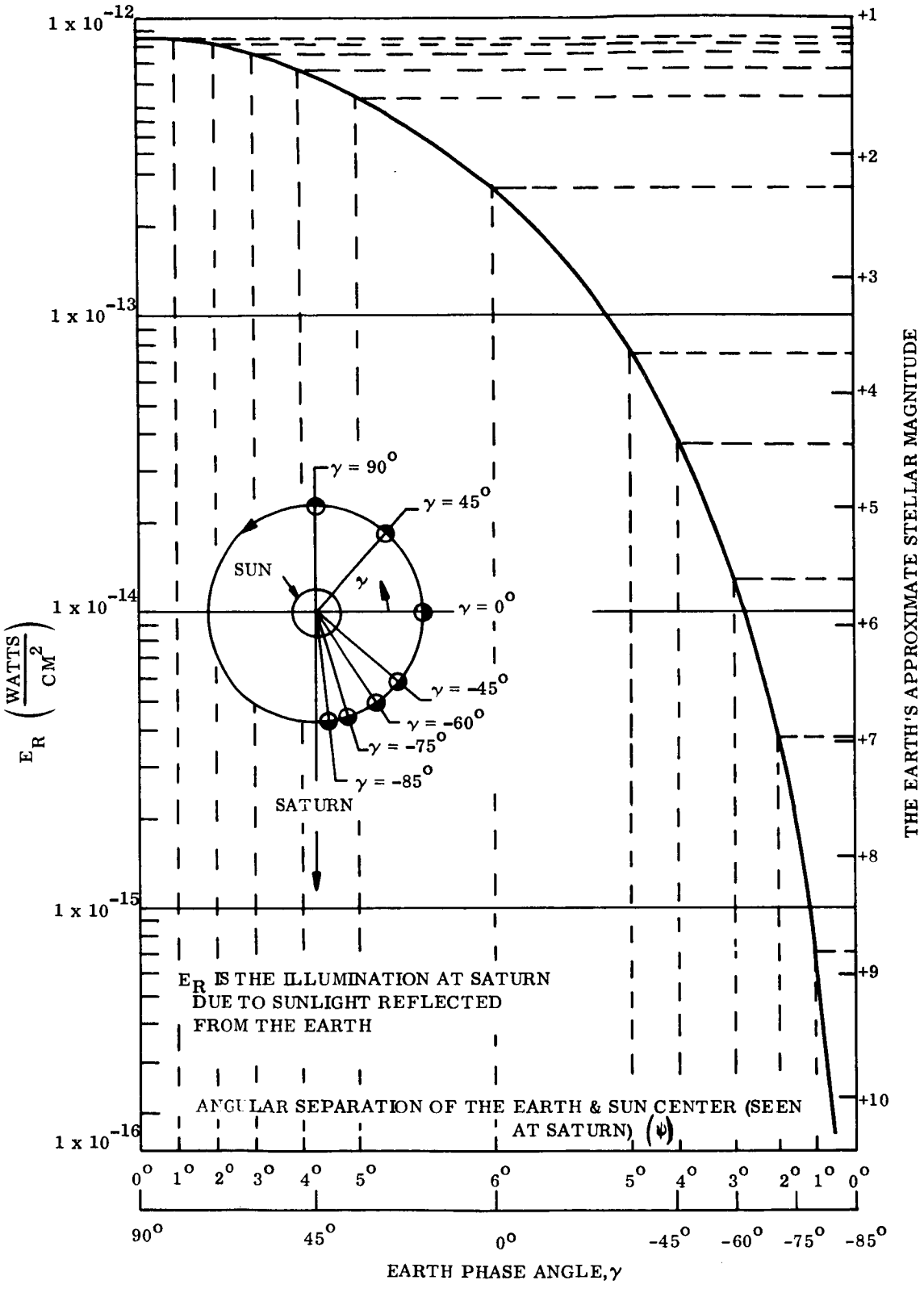

Figure 3-2. Variation in Earth's Magnitude with Phase

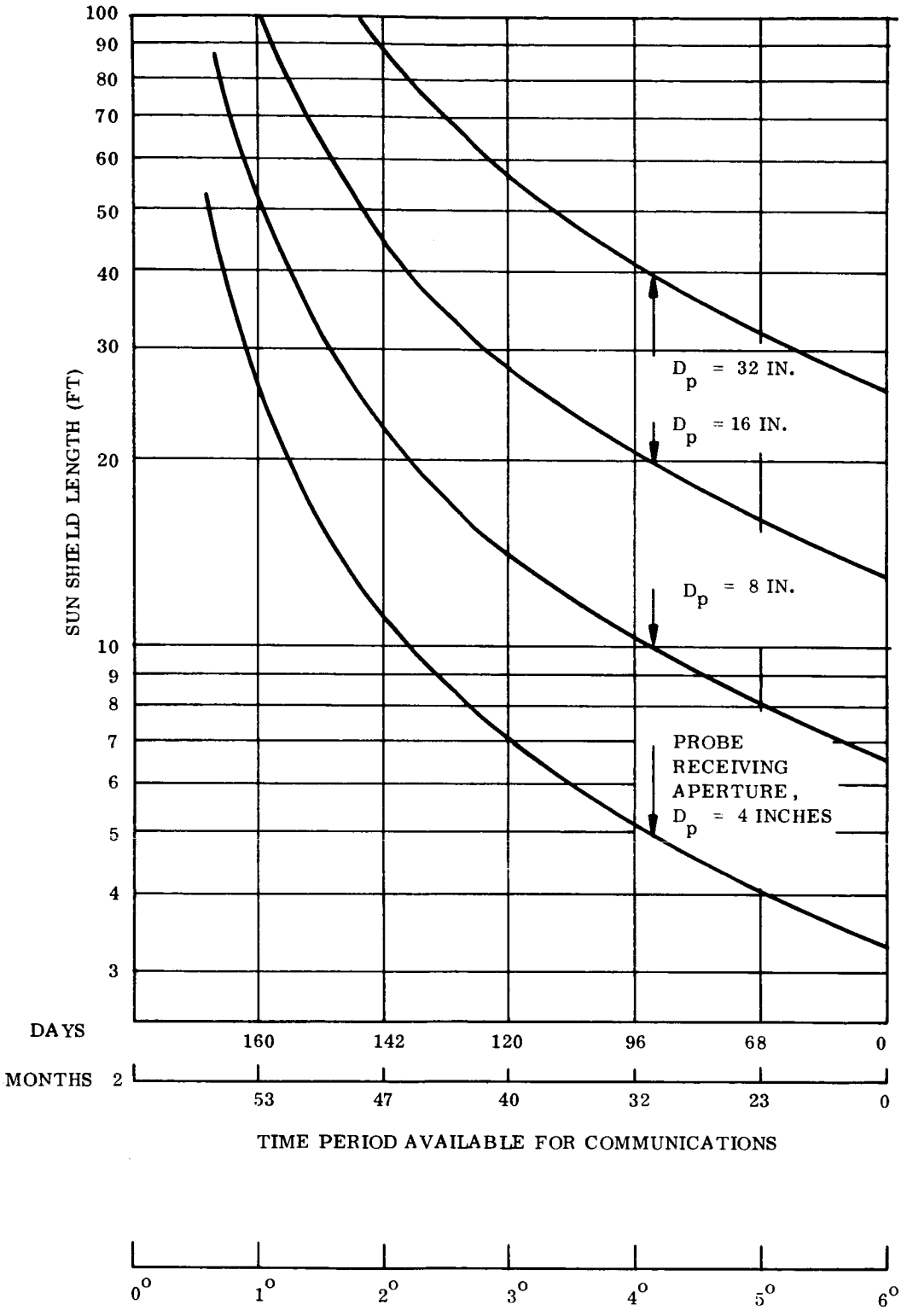

Figure 3-3. Sun Shield Lengths

FOR $\gamma = -60^{\circ}$

$60^{\circ} < \theta < 90^{\circ}$

EARTH'S STELLAR MAGNITUDE AT THIS POSITION IS MINIMUM (+5.6)

AVERAGE ILLUMINATION IS 1.35×10^{-14} W/CM^2 AT SATURN

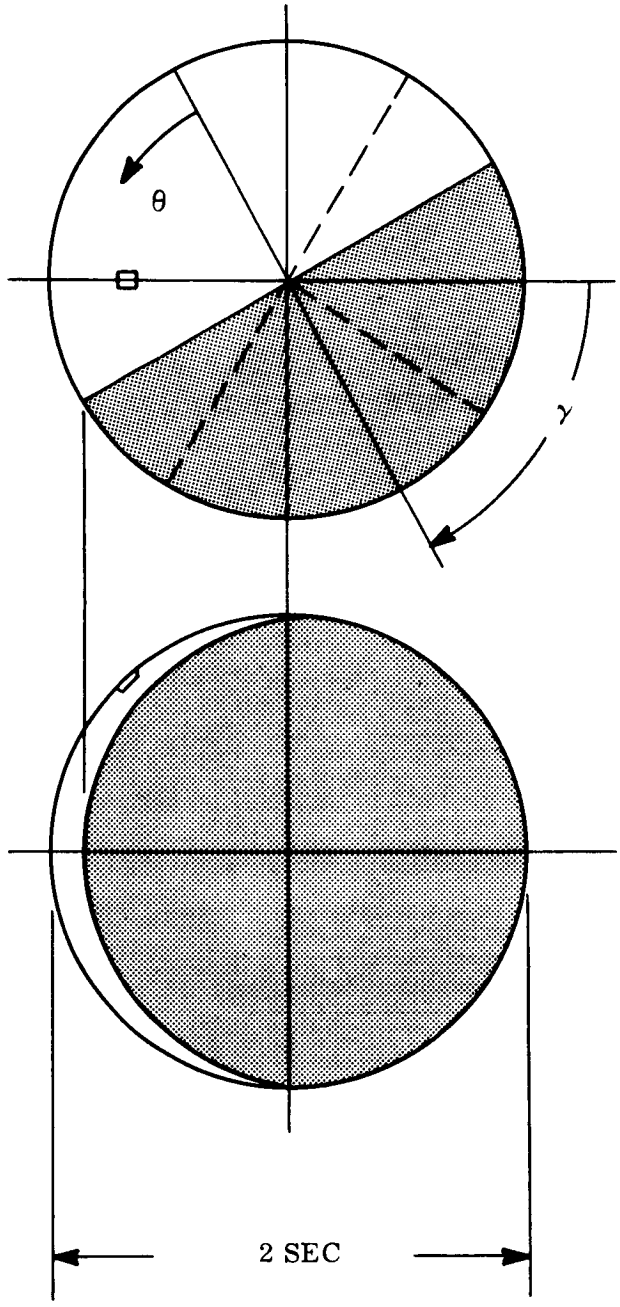

Figure 3-4. The Crescent Earth as Seen from Saturn

3.5.3 TRACKING AN EARTH-BASED COOPERATIVE LASER BEACON

In this mode, the Earth-based laser serves only as a beacon for fine pointing of the probe, and not as a primary communications link. Let us assume the desired pointing accuracy to be about 0.03 arc sec (10^{-5} degree) in order to accommodate a narrow laser beam-width. To assure a sufficient S/N ratio for tracking the Earth-based beacon against the sunlit Earth, an image dissecting image orthicon is chosen as the probe fine pointing sensor. The sensor's active surface is assumed to be one inch square and to contain 10^6 resolution elements. If the probe field of view is limited to $(6 \text{ arc-sec})^2$, each element will be $(0.006 \text{ sec})^2$. The optical system focal length is found from

$$\text{F. L.} = \frac{\text{Detector size}}{\text{Field of View}} \tag{3-19}$$

$$= \frac{1 \text{ inch}}{6 \text{ arc sec}}$$

$$= 33,000 \text{ inches}$$

If the probe primary mirror is assumed to be 40 inches in diameter, consistent with the diffraction-limited beamwidth of about 0.1 arc sec and the anticipated capability to orbit large diffraction-limited optics in the 1980 period, the system focal ratio is about f/1000. The linear dimension of each resolution element (0.006 arc second) is consistent with the required pointing accuracy (0.03 arc-second).

3.5.4 PROBE DETECTOR SIGNAL/NOISE CONSIDERATIONS

3.5.4.1 Earth Noise

The spectral irradiance from the Earth at Saturn is

$$E_e = B_e \alpha^2 \text{ watts/cm}^2 \text{ per element} \tag{3-20}$$

where B_e = the Earth's brightness $= 1.7 \times 10^{-6}$ w/cm^2 . ster . $\mathring{A}$

α = the angular size of the source (in this case, a single square resolution element since the instantaneous field of view sees only a small part of the Earth at a time)

$= 0.006$ arc-sec $= 3 \times 10^{-8}$ radians

$E_e = 1.53 \times 10^{-21}$ watts/cm^2 . Å

The Earth power per element transmitted by a 1Å filter is

$$P_e = E_e \cdot A_p \, k_1 \, k_4 \qquad (3\text{-}21)$$

where: A_p = probe mirror area

k_1, k_4 = transmissivities previously defined

$= 6 \times 10^{-18}$ watts per element (max.)

The earth power level is well below the internal tube noise (NEP) of the orthicon (about 10^{-15} watts per element) for the frame rates required in this application.

3.5.4.2 Sun Noise

In any deep space mission, laser communication with the Earth is complicated by the angular proximity of the sun to the probe-Earth line of sight. At Saturn, for example, the maximum Earth-probe-sun angle is only six degrees. Thus there is a tradeoff to be made between the minimum practical Earth-probe-sun angle (which governs the duration of the encounter 'window') and the maximum practical sun shield length. For the mission being examined, the sun noise power per detector element is determined as follows:

If the sun were allowed to directly illuminate the probe primary mirror, the power density would be approximately

$$E_s = 1.4 \times 10^{-3} \text{ watts/cm}^2 \text{ at Saturn} \qquad (3\text{-}22)$$

For a 40-inch (100-cm) mirror the total power delivered to the 1Å narrow-band filter is

$$P_I = E_s \cdot A_R \cdot k_1 \qquad (3\text{-}23)$$

$= 4.4$ watts

If the filter wavelength is 6000 Å, the sun power which passes through the filter to the detector is

$$P_D = P_I \cdot k_4 \cdot 1.3 \times 10^{-4} / \text{Å} \tag{3-24}$$

For a 1Å filter,

$$P_D = 2.6 \times 10^{-4} \text{ watts} \tag{3-25}$$

This sun power input to the detector assumed that the sun's image is within the field of view of the probe receiver. Certainly this will not be the case. Thus the only sunlight reaching the detector will be that which is diffusely reflected by the mirror or from surface flaws on the surface of the mirror. Furthermore, the receiver field of view is restricted to about (6 arc seconds)^2 in fine pointing. It is therefore assumed that only 0.1 percent of the total sun power falling on the primary mirror actually reaches the detector, or

$$P_D = 2.6 \times 10^{-7} \text{ watts} \tag{3-26}$$

The attenuation of 10^3 is considered quite conservative (the actual reduction is probably greater) since solar impingement tests of the OAO star-tracker showed that an attenuation of about 10^8 was achieved when sunlight was first reflected from a blackened wall of the telescope, and then scattered by the mirror surface. Since it is assumed that the sun power is evenly distributed over the entire detector, the power received by each element is

$$P_{DE} = \frac{P_D}{10^6 \text{ elements}} \tag{3-27}$$

Thus $P_{DE} = 2.6 \times 10^{-13}$ watts per element.

This is about two orders of magnitude above the internal noise (NEP) of the orthicon (about 10^{-15} watts/element). Thus, if sunlight is allowed to fall directly on the primary mirror, the detector is sun-noise limited and the Earth laser beacon must be sized on this basis.

If a "one-bounce" sunshield is used (one in which the sunlight can only reach the primary through a reflection from the inside wall of a long hollow tube), the sun power level will be reduced by 10^4 or 10^5, thus making the detector limited by internal noise. However, the sun shield becomes extremely long for the 40-inch primary mirror when operating only a few degrees from the sun. If the minimum period of continuous communications is set at 120 days, the Earth-probe-sun angle varies from 3 to 6 degrees. For operation at the beginning and end of this "window" (3 degrees), the sunshield length must be about 80 feet. (See Figure 3-3.) While it is conceivable that a lightweight, rigid, telescoping shield such as this could be developed, it is certainly not now state of the art. In addition, such an appendage would place unusual restrictions on the operation of the control system. However, the shield could be "softly" coupled to the spacecraft and would not be responsive to the higher frequency motions of the vehicle or servoed optics which might be used for fine pointing. Since the tube centerline would point at the sun, no significant solar disturbance torques would be produced. However, during planetary encounter, particularly for Jupiter or Saturn, the gravity gradient torques will be very significant, and may be the major problem in stabilizing the entire spacecraft with the required accuracy.

3.5.4.3 Earth Laser Beacon

Since the detector noise level is considered to be about 10^{-15} watts/element, the Earth-based laser should deliver about 10^{-14} watts/element to the detector for a S/N ratio of 10, which is considered minimum for the required pointing accuracy.

The size of the laser image's central disk (half-power) on the detector is found from

$$d = F.L. \times \theta_t \qquad (3\text{-}28)$$

where F. L. = Probe mirror focal length
= 33,000 inches
θ_t = Mirror diffraction limit (half-power)
= 0.1 arc sec = 0.5×10^{-6} rad
= 0.017 inch

The area of the spot (half-power points) is 3×10^{-4} in.^{2}. Since the area of each detector element is 10^{-6} in.^{2} the number of elements illuminated at or above the half-power level is

$$N = \frac{A \text{ spot}}{10^6} = 300 \text{ elements} \tag{3-29}$$

If it is assumed that all elements are equally illuminated, then the total earth beacon power delivered to the detector must be

$$P_B = (300)(10^{-14}) = 3 \times 10^{-12} \text{ watts} \tag{3-30}$$

The total power which must be supplied to the probe mirror is

$$P_{BR} = \frac{3 \times 10^{-12}}{k_1 k_4} = 1.9 \times 10^{-11} \text{ watts} \tag{3-31}$$

It is assumed that atmospheric effects will limit the Earth beacon half-power beamwidth, θ_B, to a minimum of about 2 arc seconds. The beacon power required to deliver 1.9×10^{-11} watts to the probe primary mirror is then given by the expression

$$P_{BT} = \frac{2\theta_B^2 R^2 P_{BR}}{K_2 K_3 D_P^2} \tag{3-32}$$

where P_{BT} is the beacon transmitted power

D_P is the probe mirror diameter = 40 in (100 cm)

R is the range (Saturn-Earth) $\approx 10^9$ miles $= 1.6 \times 10^{14}$ cm

K_2, K_3 are as previously defined

Then $P_{BT} = 20,000$ watts transmitted. (3-33)

If the laser efficiency is assumed to be 0.5 percent, the prime power supply for the Earth-based beacon must provide four million watts. Since the beacon beamwidth was made an

absolute minimum, the probe receiver aperture a practical maximum and since the range is set by the mission, there is no way to substantially reduce this enormous requirement for beacon transmitter power. Based on the current progress of laser technology it is a near certainty that such power will not be practically achieved even through a laser array, in the 1980 time period. Since we have employed an orthicon detector in this application, and the orthicon is an integrating device, only average received power is significant, not peak power. This means no advantage can be obtained by using pulsed laser techniques.

Considering the deep space probe in total, we now find that not only are low data rates typical, but the problems associated with accurately tracking the Earth or a laser beacon on the earth are fantastically difficult. The interference of the sun is a major contributing factor in this difficulty.

3.6 MARS ORBITER

Optical communication between Mars and Earth will inherently yield a more promising situation than the deep space probe because of the much smaller range and the more favorable location of the sun with respect to the earth as viewed from Mars. We now wish to examine the system parameters associated with a Mars orbiter maintaining a laser communication link with Earth.

An examination of the radiometric equations presented in the previous paragraph quickly shows that data rates on the order of 10^6 bps from Mars will only be obtainable for transmitter antenna beamwidths on the order of an arc secor less with reasonable laser power. We will examine two configurations for this mission, i.e., an orbiter that produces a beamwidth of two arc seconds, and another that will produce a beamwidth of 0.2 arc seconds. In the former case, the beamwidth should be sufficiently large to avoid the necessity of a cooperative laser beacon on earth, i.e., the earth itself can be tracked and the location of the ground receivers computed on a continuous basis. For the narrow beam configuration, a cooperative beacon on earth is required to accurately locate the receivers.

Except as otherwise noted, the ground rules for both configurations are identical.

We will assume the Mars probe is launched on a trajectory requiring about nine months to reach the planet. We further assume the probe orbit is suitable to the extent that several months of operation is possible prior to

a. The probe being occulted by Mars as viewed from Earth.

b. The angle between the Sun and Earth (as viewed from Mars) becoming less than 15 degrees, or, the angle between Mars and the Sun (as viewed from Earth) becoming less than about the same angle.

The first of these constraints is necessary to avoid a dual reacquisition of laser beams probe once per probe orbital period, and the second is necessary to minimize the solar impingement problem at the probe and the very bright sky problem as viewed from the earth. A restriction of angles as small as 15 degrees will impose very severe penalties, and an increase of this angle to 20 or more degrees would be desirable.

The Earth, as viewed from Mars, subtends an angle of 9 to 35 seconds of arc, depending on the range. This is much too large an angle for the probe antenna beamwidth if on-board laser power is to be reasonable. It will thus be necessary to communicate with specific receiving stations located on earth. These same stations will also provide the high-power beacon beam which is required for highly precise tracking by the probe. In order to maintain 24 hour per day communications coverage with a rotating earth and to allow for local adverse weather conditions, a number of ground stations will be required, (possibly six to nine). This necessitates the capability to switch ground stations as viewed from the probe.

With an operational period extending over several months, it will not always be possible for the Earth terminal receiver to be on the dark side of the Earth. This means that the receiving antenna on Earth must often look into the daylight sky to see the probe, and that the probe must be able to locate the Earth beacon in the presence of sunlight reflected from Earth. The system parameters must be selected based on these worst case conditions.

The desired data rates correspond to near-real time TV, i.e., on the order of 10^5 to 10^7 bps depending on TV resolution and on the number of frames per second. The primary influence of data rate on the mission is that high data rates can be achieved through very narrow probe antenna beamwidth (hence tightening pointing accuracy and point ahead requirements), or by increasing laser power in the probe (hence increasing the weight of the probe).

3.6.1 THE DATA LINK FROM MARS TO EARTH

The primary data link consists of the spacecraft transmitting system and the Earth-based receiver. The requirements of the spacecraft transmitting system are determined by a process which begins with an examination of the S/N ratio at the Earth-based receiver detector.

If this detector is a photomultiplier, a reasonable choice for this application, the signal-to-noise voltage ratio has been shown (Paragraph 3.4) to be

$$\frac{S}{N} = \left[\frac{\eta \bar{N}_s}{2 H \Delta f \left(1 + \frac{\bar{N}_b + \bar{N}_d}{\bar{N}_s}\right)} \right]^{1/2} \qquad (3\text{-}34)$$

where η is the detector quantum efficiency

$\bar{N}_s$ is the average number of signal photons received per second

$\bar{N}_b$ is the average number of background photons received per second

H is the photomultiplier noise factor

Δf is the bandwidth of the receiving channel

$\bar{N}_d$ is the photon rate equivalent of dark current

For high data rates, $\bar{N}_s$ is assumed initially to be considerably larger than $(\bar{N}_b + \bar{N}_d)$. (Later in the discussion the effects of raising $\bar{N}_b$ will be examined.)

H is assumed to be 1.2 (a typical value) and η is taken as 0.15. This value is based on the assumption that a helium-neon gas laser, operating at 6328 Å, is used, and that the quantum efficiencies of typical detectors, which are about 0.05 at this wavelength, will improve by a factor of three.

Thus

$$\frac{S}{N} = \left(\frac{\eta N_s}{2.4 \Delta f}\right)^{1/2} \tag{3-35}$$

If the system can operate with a S/N ratio of 2,

$$\overline{N}_s = 64 \Delta f \text{ photons/second} \tag{3-36}$$

For an information rate, B, equal to the channel bandwidth, Δf, the photon arrival rate at the detector required for 10^6 bits per second is

$$\overline{N}_s = 64 \times 10^6 \text{ photons/second} \tag{3-37}$$

which is equivalent to 2.6×10^{-11} watts at an operating wavelength of 6328 Ångstroms, as shown from Equation 3-65.

The expression which relates key system parameters to the signal power delivered to the earth receiver detector is

$$P_{SR} = \frac{K_1 K_2 K_3 K_4 P_t D_R^2}{2 R^2 \theta_t^2} \tag{3-38}$$

where K_1 = transmissivity of the transmitting optics (≈ 0.4)

K_2 = transmissivity of the receiving optics (≈ 0.4)

K_3 = transmissivity of the narrow-band optical filter in the receiver (≈ 0.4)

K_4 = transmissivity of the earth's atmosphere (≈ 0.6)

P_t = transmitter power radiated

D_R = receiver antenna aperture

R = transmitter-to-receiver range $\approx 10^8$ miles for Mars-to-Earth = 1.6×10^{13} cm

θ_t = transmitter half-power beamwidth

For the narrow beamwidth system, let $\theta_t = 0.2$ arc-sec and $P_t = 10$ watt. Then with a 200-inch (508 cm) receiving aperture on earth, P_{SR} is approximately 12×10^{-11} watt. At 6328 Å, this is equivalent to a data rate of 4.6×10^6 bps for a photon noise-limited environment. For the wide beamwidth case ($\theta_t = 2$ arc-sec), 25 watts of spacecraft laser power is assumed. This will then yield a data rate of about 1.2×10^5 bps. Figure 3-5 is a plot of data rate versus laser power for a variety of transmitter beamwidths.

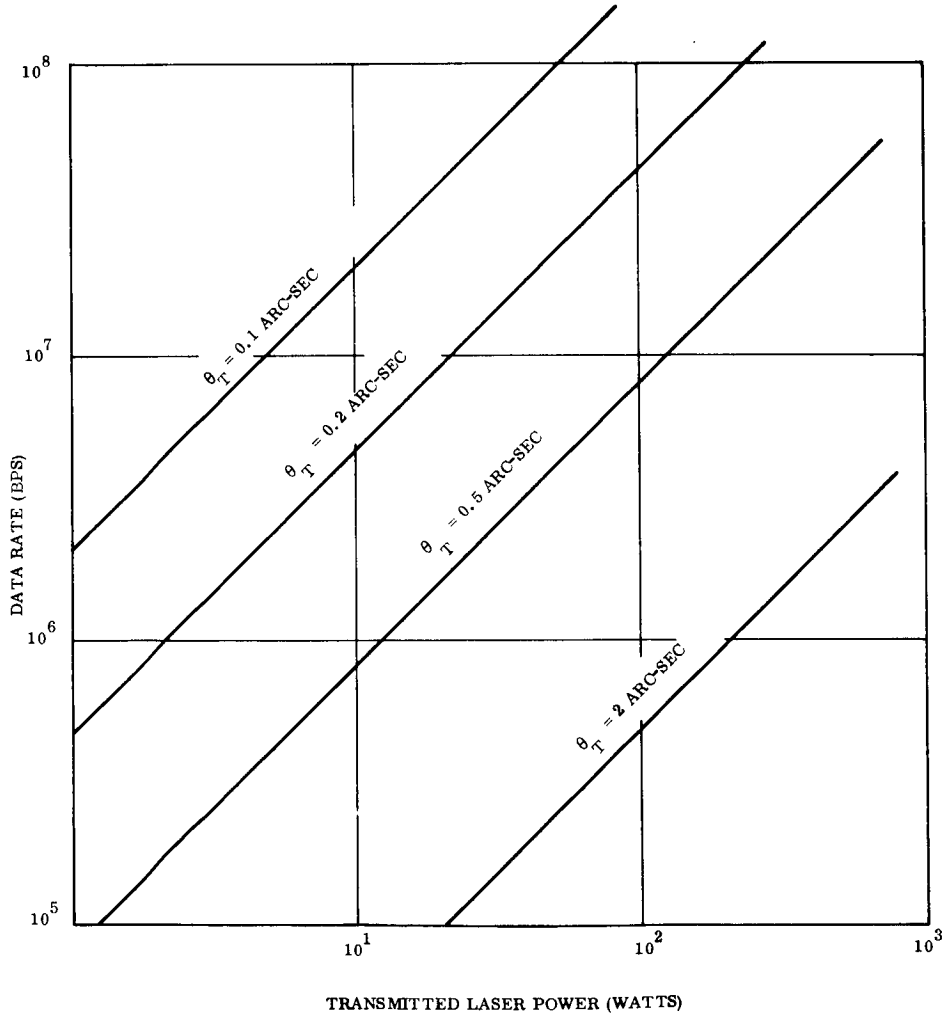

Figure 3-5. Typical Data Rate vs Laser Power for a Mars to Earth Communication Link

The influence of the external and internal noise on data rate must now be determined:

3.6.1.1 Sky Light

The radiance of the daytime sky is the primary source of background noise in the Earth receiver. The sky noise power at the detector is given by

$$P_{SLR} = K_2 K_4 \pi B_E A_R \sin^2 \left(\frac{\alpha}{2}\right) \qquad (3\text{-}39)$$

$$= \frac{K_2 K_4 \pi^2 B_E D_R^2 \alpha^2}{16} \text{ for small values of } \alpha.$$

where: K_2, K_4, D_R are as previously defined

B_E = the average radiance of the day sky in a one Angstrom bandpass $\approx 2.5 \times 10^{-7}$ watts/cm^2 steradian

α = the receiver field of view (one dimension) in arc-sec

Thus: $P_{SLR} = 1.5 \times 10^{-13} \alpha^2$ watts

The signal power was shown previously to be 4.5×10^{-11} watts for the narrow beamwidth case. This is equivalent to the sky noise in a receiver field of view, α, of 20 arc-seconds cone angle, or about one-half arc-minute square. This is a reasonable field of view, considering the fact that the Earth receiver will be tracking the spacecraft laser to maintain system "lock."

3.6.1.2 Detector Noise (Dark Current)

The noise equivalent power (NEP) in photomultiplier detectors of the quality used in high precision tracking systems is of the order of 10^{-14} watts. Since this is at least three orders of magnitude below the signal or sky noise power levels, it is insignificant, and need not be considered further.

3.6.1.3 Direct or Scattering Sunlight

With typical Mars-Earth-Sun geometry for a six month orbiter (spacecraft) lifetime, Mars never appears closer than 30 degrees to the sun as seen from the earth receiver. Thus direct sunlight can be prevented from falling directly on the 200-inch earth receiving mirror by a 350-inch sun shield or its equivalent.

Experience with large reflecting telescopes, as evidenced by the design of the Hale telescope at Mt. Palomar, has shown that thermal disturbances of the optical image are less severe with open, frame-like supports for the components than with the closed tubes seen in smaller instruments. Thus the observatory dome with its moving slit forms the primary light shield. For a 200-inch instrument, the slit will certainly exclude direct solar illumination of the mirror, and it is assumed that care will be used to minimize the possibilities of wholesale scattering or reflection from the structure.

These considerations, coupled with the losses due to the narrow field of view and 1 Å receiving filter, will assure that direct or scattered sunlight within the instrument will not be a significant source of earth receiver noise.

3.6.1.4 Data Rate in the Noise Environment

If the S/N ratio at the detector is to be maintained at 2 as previously described, it can be shown that by manipulation of Equations 3-8 and 3-9 and by assuming that $B = \Delta f$ (the channel bandwidth), the data rate, B, is reduced by noise power, P_N, according to the relation

$$B' = B \left[\frac{P_s}{P_s + P_n} \right]^{1/2} \qquad (3\text{-}40)$$

where P_s is the signal power, and B' is the reduced data rate.

Thus, for $P_s = P_n$ as indicated previously, the data rate in the presence of noise,

$$B' = (0.50)^{1/2} B \qquad (3\text{-}41)$$

$$= 0.7\, B$$

Since the "no-noise" data rate was about 5×10^6 bits/second, the actual data rate in the expected noise environment is about 3×10^6 bits/second.

3.6.1.5 The Spacecraft Laser as a Tracking Beacon

Once acquisition has been achieved, the earth station must track the spacecraft data beam with fairly high precision (≈ 1 arc second) in order to continuously illuminate the spacecraft with the Earth-based laser beacon. Since the electrical bandwidth of the tracking channel need not exceed the order of 10 Hz, an examination of the basic S/N ratio expressions presented at the beginning of this paragraph shows that the tracking S/N ratio will be of the order of several hundred, which is certainly satisfactory for this tracking accuracy requirement with either a photomultiplier or image tube detector.

3.6.2 THE TRACKING LINK FROM EARTH TO MARS

The primary purpose of the uplink is to provide the spacecraft with a tracking reference for precise pointing of the 0.2 arc second data beam. In addition, this link may also be used to send commands and other operational data to the spacecraft at a low data rate. However, for this analysis only a beacon function including a very low frequency (20 to 30 Hz) "signature" modulation is considered for the earth-based transmitter.

For high precision pointing, a high S/N ratio is required at the tracking system detector.

As shown before, the expression for S/N ratio in a photomultiplier detector (where the shot noise in the tube itself is dominant) is

$$\frac{S}{N} = \left[\frac{\eta \overline{N}_s}{2.4\, \Delta f}\right]^{1/2} \qquad (3\text{-}42)$$

or

$$\overline{N}_s = \frac{2.4\,\Delta f}{\eta} \left(\frac{S}{N}\right)^2 \qquad (3\text{-}43)$$

Since previous analyses have shown that a high radiated power will be required from the earth beacon, it is expected that a pulsed laser will be used. A pulse repetition rate (PRR) of about 20 pps appears to be consistent both with laser technology and the attitude reference requirements of the spacecraft. A Fourier analysis of such a pulse train has shown that the electrical bandwidth of the spacecraft tracking detector should be of the order of 10 MHz for typical pulse durations of 100 nanoseconds.

The S/N ratio required to track the earth beacon is found from

$$\theta_N = \left(\frac{1.2\,\lambda}{D_R}\right) \left(\frac{S}{N}\right)^{-1} = \theta_{DL} \left(\frac{S}{N}\right)^{-1} \qquad (3\text{-}44)$$

where θ_N is the noise equivalent angle of the sensor (θ_N) can be considered as a 1σ error) λ is the beacon wavelength, DR is the probe mirror diameter and θ_{DL} is the diffraction limit of the mirror probe. Experience with the Manned Orbital Telescope sensor study (Reference 13) and the fine error sensor for the OAO Princeton Experiment (Reference 14) indicates that the noise equivalent angle, θ_N, should be about 10 percent of the maximum allowable pointing error. For the 0.04 arc second maximum error allowed for the 0.2 arc-second data beam, θ_N should be about 0.004 arc-second, thus

$$\frac{S}{N} = (0.2 \text{ arc-second}) \quad \frac{1}{0.004 \text{ arc-second}} \qquad (3\text{-}45)$$

(Subsequent iterations based upon attitude control system parameters indicate an S/N of 60 and a θ_N of 0.0033 to be more appropriate, but the above values are certainly good enough for this analysis.)

Detector peak quantum efficiencies range from 20 percent in flight-qualified S-20 photomultipliers to 50 percent or more in developmental silicon avalanche devices at wavelengths of about 4000 and 7000 Angstroms, respectively. For maximum transfer of energy,

the detector spectral response must be well matched to the laser output. The most advanced high power pulsed laser by far is the ruby, operating at 6943 Angstroms. At this wavelength, the response and quantum efficiency of an S-20 photomuliplier are only 20 percent of peak value (see Figure 3-6), although the transmissivity of the earth's atmosphere (which the beam must traverse) is relatively high ($\approx$ 40 to 50 percent). A frequency doubler on a ruby laser provides an output at 3472 Angstroms, where the quantum efficiency of an S-17 photomultiplier approaches 30 percent. However the frequency doubling process is only about 15 percent efficient, and the transmissivity of the earth's atmosphere is down to about 5 percent at 3500 Angstroms. Thus the silicon avalanche detector, whose response peaks are near the ruby laser wavelength holds great promise. Therefore in summary, at 6943 Angstroms, the quantum efficiencies of the S-20 photomulitplier (today) and the silicon avalanche detector (goal) are about 5 percent and 50 percent, respectively. Without choosing either, it will be assumed that a quantum efficiency of 10 percent can be achieved.

The required photon arrival rate is then from Equation 3-43 with

$$\Delta f = 10^7 \text{ Hz} \quad \eta = 0.10, \text{ and } S/N = 50,$$
$$\overline{N}_s = 6 \times 10^{11} \text{ photons/second.} \tag{3-46}$$

or

$$P_{SR} = 2.5 \times 10^{-7} \text{ watt} \tag{3-47}$$

is the required signal power at the spacecraft detector in the absence of background noise for an operating wavelength of 6943 Angstroms.

3.6.2.1 Signal Power

The expression for the power required from the earth beacon is

$$P_t = \frac{2 (\theta_t R)^2 P_{SR}}{K_1 K_2 K_3 K_4 D_R^2} \tag{3-48}$$

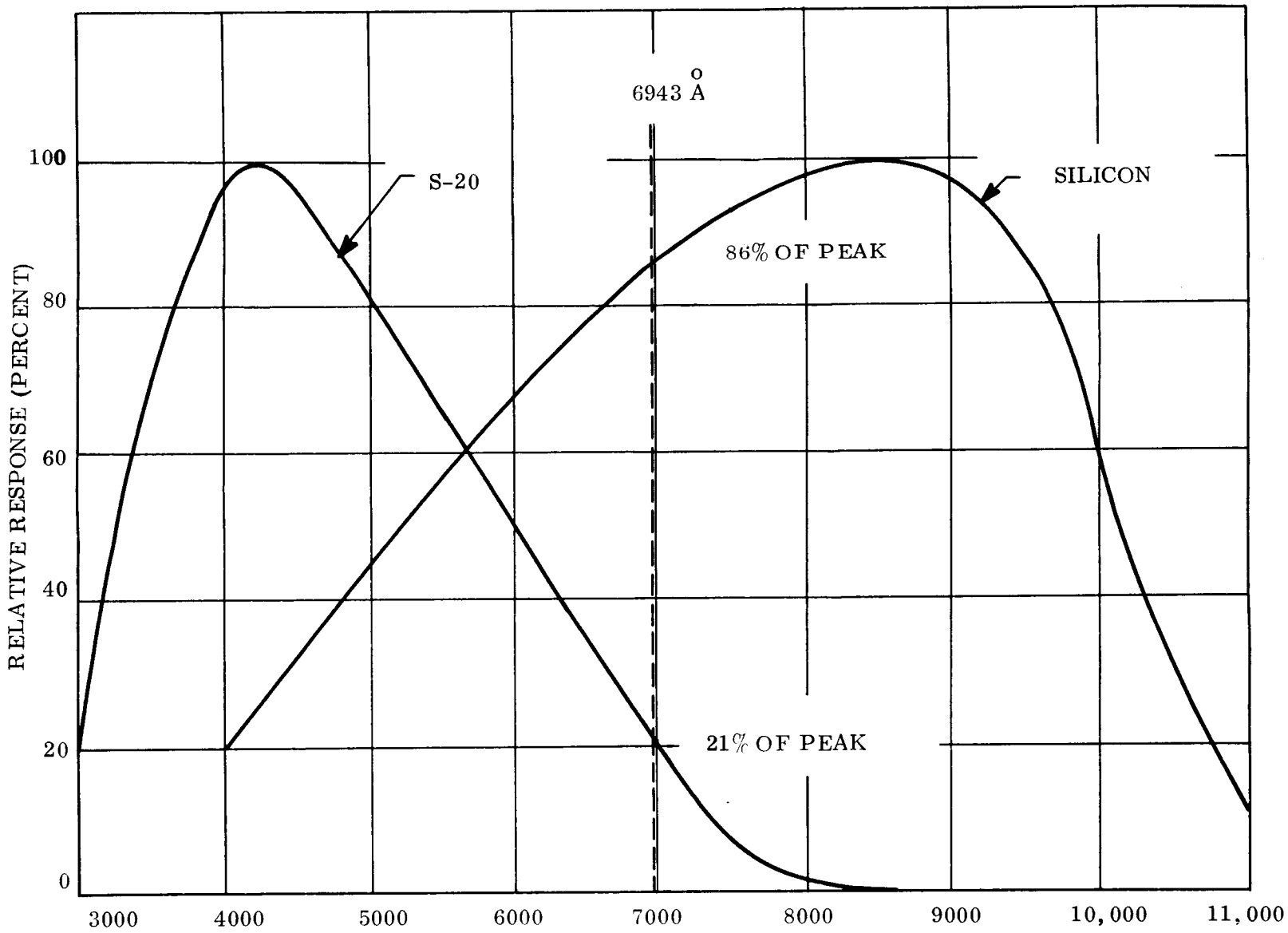

Figure 3-6. Detector Responses

where K_1 through K_4 are as previously defined but, in this case, θ_t is the beacon beam-width and D_R is the spacecraft receiving aperture. To produce a value P_{SR} of 2.5×10^{-7} watts with θ_t = 5 arc-seconds and D_R = 30 inches (as required to form the 0.2 arc-second data beam, assuming dual use of the prime optic).

$$P_t = 340 \text{ Megawatts (peak pulse power)} \tag{3-49}$$

It is understood that peak powers of this level and higher have been achieved, but not at the rate of 20 pulses per second. Although this power level is probably three to ten times that currently available at the required pulse rate, it does not seem unreasonable in light of advances being made in the laser field. (Relatively small ruby lasers are currently producing 10 megawatt pulses at 20 pps.)

3.6.2.2 Noise Power

We now examine the influence of various noise sources on the signal-to-noise ratio at the spacecraft.

3.6.2.2.1 Earth-Reflected Sunlight (Earthlight)

During a typical (Voyager 1971 type) six-month lifetime of the Mars orbiter, the earth appears to be from about 50 percent to about 95 percent illuminated as seen from Mars. It is reasonable to assume that the full earth (whole angular diameter varies from 19 to 8 arc seconds) will be within the field-of-view of the fine pointing sensor. Thus earthlight will always be a source of noise in the spacecraft receiver. Analyses have shown the earth irradiance at Mars to be about 1.8×10^{-11} watts/cm^2. Due to the compensating effects of a reduction of the earth's angular diameter and an increase in the percentage of illuminated earth visible from Mars during the six-month orbiter lifetime, this value of the earth's radiance is relatively constant ($\pm$ 30 percent).

Due to the narrow band (assumed to be 1Å) filter in the spacecraft receiving system to improve noise discrimination, the earthlight is greatly attenuated at the detector. It can be shown that the transmissivity of the filter for this broad-band reflected sunlight is

$$K_3 = 1.3 \times 10^{-4} / \text{Å} \tag{3-50}$$

in the region near 6943 Å, the beacon operating wavelength. Thus the earth noise power at the spacecraft detector is

$$P_{EN} = K_2 K_3 A_R I_E \tag{3-51}$$
$$= 4 \times 10^{-12} \text{ watts}$$

This is far below the signal power (P_{SR}) of 2.5×10^{-7} watts and its direct effect can be ignored.

3.6.2.2.2 Direct Sunlight

The Sun's radiance at the orbit of Mars is about 6×10^{-2} watts/cm^2. Since the sun is at least 20 percent from the Mars-Earth line-of-sight for a typical mission, it is assumed that a sunshield is used to prevent sunlight from falling directly on the 30-inch primary mirror in the spacecraft. The length of such a shield would be about 90 inches. Experience with the OAO startracker indicated that this type of sunshield produces an attenuation of about 10^8. Further attenuation is produced by the narrow field of view of the spacecraft receiver, whose solid angle (about 30 arc seconds square) is about 4×10^3 times smaller than the OAO startracker instantaneous FOV (about 1.0×0.3 degrees). Thus the sun power delivered to the spacecraft detector is

$$P_{SUN} \approx \frac{K_2 K_3^1 A_R I_{SUN} (10^{-8})}{4 \times 10^3} \tag{3-52}$$
$$\approx 3.4 \times 10^{-15} \text{ watts}$$

Thus even if the attenuation factors are optimistic by two orders of magnitude the sun power is still less than the earth noise by a factor of ten; therefore, sunlight scattered within the spacecraft receiver is not considered further in this analysis.

3.6.2.2.3 Other Noise Sources

Occasionally, other noise sources such as stars, planets, or the Earth's moon will enter the field of view of the spacecraft fine pointing sensor. Since none of these bodies provide significantly greater irradiance at Mars than the Earth, they will have no adverse effect on spacecraft pointing. The situation relative to the two natural satellites of Mars can only be analyzed for specific orbital parameters of the spacecraft. It is conceivable, however, that the Mars-Earth communication link could be temporarily interrupted by the presence of these satellites in the spacecraft sensor field of view.

Although the reflected earthlight power delivered to the spacecraft detector is about five orders of magnitude below the beacon signal power, it can affect the accuracy of the fine pointing loop through two separate phenomena:

a. Increased photomultiplier shot noise (over "no background" case) decreases S/N ratio.

b. A pointing bias is introduced since the fine pointing sensor most likely to be used is a four photomultiplier/beamsplitter device which normally tracks the center of illumination of an image.

3.6.2.2.4 Increased Shot Noise

The dc current in a photomultiplier produced by the laser beacon signal during a pulse is

$$I_B = G \cdot P_{SR} \tag{3-53}$$

where G is the radiant sensitivity of the tube.

For a typical S-20 photomultiplier, 6×10^4 amps/watt at 7000 Angstroms is a reasonable value for G.

Thus $I_B = 15 \times 10^{-3}$ amps. (3-54)

The shot noise due to this current is given by

$$i_{NB}^2 = 2\,e\,\omega\,H\,I_B\,\Delta f \qquad (3\text{-}55)$$

where: e is the electronic charge = 1.6×10^{-19} coulomb

ω is the multiplier gain

H is an empirical constant = 1.2

Δf is the detector channel bandwidth

Thus $i_{NB} = 2.4 \times 10^{-4}$ amps (3-56)

The "no background" S/N ratio is then

$$\frac{S}{N} = \frac{I_B}{i_{NB}} = 60 \qquad (3\text{-}57)$$

This checks reasonably well with the value of 50 which was chosen initially.

The dc current due to the earthlight, P_{EN}, is

$$I_{EN} = G \cdot P_{EN} \qquad (3\text{-}58)$$

The shot noise is given by

$$i_{NE}^2 = 2\,e\,\omega\,H\,I_{EN}\,\Delta f$$

Thus

$$i_{NE} = 7.2 \times 10^{-7} \text{ amps} \qquad (3\text{-}59)$$

It can be seen by comparison with the shot noise due to the beacon signal, i_{NB}, that the effect of earth shot noise is negligible in this type detector.

3.6.2.2.5 Pointing Bias Due to Illumination Centroid Tracking

An unfortunate characteristic of very high precision quadrant comparison sensors which employ photomultipliers is that they track the center of illumination of the received image. If the background noise is evenly distributed over a field of view containing the tracking source image, the sensor null axis is not displaced from the source image's center. In the mission being considered, however, the beacon appears to traverse the earth's partially illuminated disk due to the earth's rotation; therefore, the sensor null axis is "drawn" toward the center of illumination of the Earth, the offset depending upon the relative strengths of the inputs received from the beacon and the Earth. The system responds as if a second point source in which the Earth's radiant energy is concentrated is in a field of view, and the center of illumination is found by the same method used to locate the "center of moments" in a parallel-force mechanical system.

From an examination of the Earth's image and the potential locations of ground stations, it can be seen that the maximum separation of a beacon from the center of the Earth's illuminated portion is about 10 arc-seconds. Thus assuming that the pointing bias is small, and using the relative power levels received from the beacon and the earth (2.5×10^{-7} and 4×10^{-12} watts, respectively), the following relation may be written:

$$(\epsilon_p \text{ max})\ (2.5 \times 10^{-7}) = (10 \text{ arc-sec})\ (4. \times 10^{-12}) \qquad (3\text{-}60)$$

Thus:

$$\epsilon_p \text{ max} = 0.00016 \text{ arc-seconds}$$

Since this is considerably smaller than the minimum desirable sensed error of 0.004 arc-seconds, this effect is also negligible. Further, the detector channel bandpass will be cut off sharply below the 20 Hz fundamental of the pulse repetition rate to exclude low-frequency noise, including the Earth.

3.6.3 TRACKING THE EARTH IN THE ABSENCE OF A COOPERATIVE LASER BEACON

For the narrow beamwidth laser system (0.2 arc-sec), the pointing accuracy required of the spacecraft laser is sufficiently critical (0.04 arc-sec) to preclude the possibility of pointing to specific earth receivers without laser beacons. Such may not be the case for the wide beamwidth (2 arc-sec) system provided an earth sensor which can achieve the required accuracy is employed.

For typical missions, the Earth appears only partially illuminated as seen from Mars. Since the spacecraft laser will be pointed at individual Earth-based receiving stations whose positions change relative to the earth's image due to diurnal rotation, some stable point on or near the earth's image must be used as a reference from which the transmitting axis can be offset. This point might be the geometric center of the Earth; the point of intersection of two orthogonal tangents (from which the location of the Earth's center can be determined through knowledge of the image size); or the center of illumination of the earth's image.

The last of these has been rejected as a reference because, in the spectral region of the potentially useful detectors (essentially visible), the Earth's radiance is very nonuniform from point to point due to differences in reflectivity of water and land masses and varies considerably with time as a function of weather conditions (cloud cover and snow fields) and seasonal changes. Furthermore, the photometric characteristics of the Earth's terminator as seen from space are not well known, thus introducing an uncertainty in the apparent "phase" of the Earth. Attempting to provide the spacecraft with continuous data on the location of the Earth's center of illumination with respect to its geometric (circular) center through a knowledge of the instantaneous radiance of every region on the Earth's surface would be a hopelessly complex task.

The most positive means of providing a reference point for pointing of the spacecraft laser is to sense the outer (nonterminator) edge of the earth's image. Means are available for implementing this approach although there does not now exist a sensor that will provide the required accuracy. A discussion of the required sensor characteristics is given in Section 6.

Another possible method of achieving the required pointing accuracy without the need to provide a laser beacon on Earth would be to use the star field as a reference. This approach has been considered, but was found to have many disadvantages.

The primary considerations in evaluating this last technique are these:

a. The required precision of tracking the guide stars.

b. The required precision of third-axis control.

c. The required precision of offset pointing the spacecraft laser from the star tracking axis.

d. The required frequency of switching to a new guide star.

If it is assumed that the beamwidth of the spacecraft laser is two arc-seconds, the two-axis pointing accuracy of the spacecraft should be about 0.4 to 0.5 arc-second. This maximum error includes both the star tracking error and the offset pointing error. The star tracking error is largely a function of the tracker aperture and the brightness of the guide stars being tracked. The offset error includes the error in establishing the required r due to imperfect third-axis control, both of which tend to increase linearly with the required offset.

The maximum allowable error, B, for control of the third-axis is given by

$$B = \frac{E}{R \text{ Tan } X} \qquad (3\text{-}61)$$

where: E is the allowable beam centerline linear deviation from the ground station, measured on the Earth's surface,

R is the range

X is the offset pointing angle

For an Earth-Mars link with a two arc second laser beam, R is on the order of 10^8 miles and E should be limited to about 200 miles (0.4 arc-second). Thus

$$B = \frac{10^6}{\text{Tan } X} \qquad (3\text{-}62)$$

A few examples show the X-B relationship

X, the offset	B, the third axis maximum error
1 arc-min	20 arc-minutes
1 degree	22 arc-seconds
6 degrees	4.0 arc-second
30 degrees	0.6 arc-second

The magnitude of a typical offset angle will depend upon the separation of stars along the Earth's apparent path (as seen from Mars) which are bright enough to assure tracking with sufficient accuracy. Available data (Reference 13) indicates that for a 36-inch diameter tracking aperture, a tracking system bandwidth of five Hz and a pointing accuracy of 0.2 arc second, a star magnitude of about +9 is required. It has also been shown (Reference 15) that, for a near-unity probability of finding a star of this magnitude within a given area of sky, that area must be on the order of one square degree. Thus the offsets may approach one degree, requiring 20 arc-second accuracy for roll control. Furthermore, the offset accuracy required is about 0.2 arc-second in 3600 arc-seconds, or one part in 18,000. This will undoubtedly be difficult to achieve.

The frequency of switching guide stars depends on the rate of rotation of the Mars-Earth line of sight in inertial space, and the maximum allowable offset. An examination of Voyager trajectory plots reveals that the LOS rotation rate is about 0.7 degree/day for a typical six-month Mars orbit lifetime. Thus, if the maximum offset is limited to about one degree to minimize the roll axis requirement, a new guide star must be acquired about every 16 hours. This will require either a temporary suspension of communications or a rather elaborate dual acquisition and tracking system, neither of which are desirable.

Finally, this approach requires accurate ephemeral data on the Earth's apparent motion against the stellar background as seen from an object in a high inclination orbit about Mars, and requires a programmed image motion compensation on the order of two arc-seconds per minute of time.

The possibility of using the Sun as a primary reference and offsetting the spacecraft optical axis from the sun line by a precise amount has also been considered. This method for accurately pointing the two-arc-second spacecraft laser beam with an accuracy of 0.4 to 0.5 arc second is rejected for four major reasons:

a. Tracking the Sun's geometric center to within one part in 3,000 is not considered reasonable within the time frame considered by this study. Further, it is probable that fundamental limitations may arise due to the instability of the solar surface.

b. For a typical six-month Mars orbit lifetime, the offset angle (Sun-Mars-Earth) varies from 15 to 40 degrees. Offset accuracies of about one part in one million would be required to maintain illumination of a single ground station. It is unlikely that such precision can be maintained at any time in the foreseeable future.

c. For a 40 degree offset from the Sun, third axis errors must be limited to about 0.2 arc-second, a requirement which would require a rather large, sophisticated tracking system (on the same order as the primary optical system) to achieve, and would impose unreasonable constraints on spacecraft structural/thermal design.

d. Image motion compensation would have to be inserted on a continuous basis due to the changing direction of the Mars-Sun line introduced by the parallax of the Mars orbit and the relative motion of the Mars-Earth line due to their revolution about the sun.

It is apparent from the above that another method of obtaining a fine pointing reference is required in the case of the two-arc-second spacecraft laser. The method which is recommended, if this system were implemented, is to track the Earth. A planet tracker has been under development which determines the geometric center of a planet via tracking of the planet edge (planet/space boundary). Some modifications of this tracker are required, which are delineated in a comparison of the existing and desired specifications in Appendix A. A detailed discussion of the selection of an appropriate Earth sensor for the two arc second laser beamwidth mission can be found in Section 5.2.1.3.

A selection of spacecraft parameters was performed for the two-arc-second mission in a manner analogous to that for the 0.2 arc-second spacecraft laser mission. The pertinent parameters of this mission, which were dropped early in the study, are summarized in the next section.

3.6.4 SPACECRAFT COMMUNICATION SYSTEM PARAMETERS

The narrow and wide beamwidth systems will require telescopes of approximately 30-inch and 6-inch diameters, respectively, in order to form the beam. Diffraction limited lasers are required in either case. For an assumed gas laser efficiency of 0.5%, the required prime power will be 2 KW and 5 KW to provide the required 10 W and 25 W laser output for the two configurations.

Reasonable assumptions for the weight of modulators, sun shields, structure, etc., have been made, in arriving at total spacecraft weight of 4000 to 4500 pounds. To this payload weight must be added another 3000 to 5000 pounds for the engine and fuel to inject the payload in the Mars orbit. This results in an Earth launch weight of 8000 to 10,000 pounds, that is, a weight well within the capability of Saturn V, but far in excess of that of any other present-day booster.

Tables 3-1 and 3-2 summarize the spacecraft and Earth-based system parameters. For the narrow beamwidth laser system, one may want to consider telescope apertures larger than 30 inches to reduce the required on board laser power and weight and to reduce the amount of required power for the ground beacon. For example, aperture sizes of 40 to 60 inches may seem reasonable. In the present case, increasing the aperture to 40 inches or more does not seem warranted on several counts. First, the required laser power (10 watts) for the 30-inch aperture is not excessive, and is within projected 1970 state of the art for the argon ion laser. Second, the telescope weight will increase approximately as the 5/2 power of its diameter, whereas the reduction in laser power and weight will go down only linearly with increasing telescope aperture. Thus an overall weight increase would result. Third, the length and diameter of the required sunshield increase linearly with telescope aperture so that a further weight penalty is imposed. Finally, the required pointing accuracy of the telescope varies inversely with telescope diameter; hence, an additional weight and complexity factor associated with attitude control is introduced by increasing the aperture.

Considering all these factors, it seems that an aperture of about 30 inches is the largest that should be employed. If high efficiency laser technology should develop significantly over the next few years, it may be desirable to reduce the telescope aperture even further, to perhaps 10 to 15 inches.

It is seen from Table 3-2 that the laser transmitter aperture is listed as 200 inches. This, of course, is the receiving "antenna" of the earth station which is tracking the spacecraft laser for the high data rate downlink. For this receiving function, the 200-inch mirror system need not be diffraction-limited. However, this large aperture (nondiffraction-limited) is required to collimate the output beam of the pulsed ruby beacon laser from its characteristic natural beamwidth of about one milliradian or 200 arc seconds down to the desired value of five arc-seconds.

3.7 GLOBAL LASER COMMUNICATION NETWORK

In considering various missions as potential applications for high precision attitude control of spacecraft, a global communication network employing laser data links is of considerable interest. The investigation of such a system includes the aspects of precise pointing of very narrow beams for both space-to-space and space-to-earth applications. In this paragraph a representative communication network is described and analyzed with emphasis on the attitude control and transmitter/receiver requirements.

The most precise pointing required for this potential mission has been determined to be on the order of 10^{-4} degrees. Since the attitude control requirements are determined to be current state-of-the-art, we have not pursued the mission beyond this initial analysis.

3.7.1 REQUIREMENTS

The network considered is sized to permit high data rate communications (10^7 bits/second) between any two points on the Earth's surface, and to limit the ground area illuminated by the laser beam main lobe to a circle one mile in diameter. The system will accommodate one or two commercial-grade TV channels and will provide the ultimate in secure, rapid global data transmission. For operation in bad weather, a backup RF system can be

Table 3-1. Mars Orbiter Parameters

	Beacon Tracking	Earth Tracking
Total weight	8400 lb	9300 lb
Data rate (daytime)	10^6 bps	10^5 bps
Laser beamwidth (half power)	0.2 arc-sec	2.0 arc-sec
Primary telescope aperture	30 inch	6 inch
Transmitted power	10 w	25 w
Prime power input (e = 0.5%)	2000 w	5000 w
Power supply wt (300 lb/kw	600 lb	1500 lb
Spacecraft pointing error (3σ)	0.05 arc-sec	0.5 arc-sec
Communication system weight (Including prime power supply)	1500 lb	2000 lb

Table 3-2. Ground Station Parameters for Mars Orbiter

	Beacon Tracking	Earth Tracking
Laser beamwidth (half power)	5 arc-sec	---
Laser power (pulsed)	340 mw (peak)	---
Laser power average	680 w	---
Laser pulse rate	20/sec	---
Laser pulse width	10^{-7} sec	---
Laser transmitter and receiver aperture	200 inch	---
Earth radiance at spacecraft	---	$1.8 \times 10^{-11} \frac{W}{CM^2}$
Spacecraft receiver S/N ratio	60	5
Spacecraft receiver bandwidth	10 MHz	10 Hz
Spacecraft receiver field of view	4 $(\text{arc-min})^2$	3$(\text{arc-min})^2$

provided with a sacrifice in security. However, choice of ground stations in areas of generally fair weather should minimize the backup requirement.

3.7.2 DESCRIPTION

The system consists of three satellite relays in synchronous equatorial orbit, and any number of ground stations. Spacing the satellites 120 degrees apart provides maximum earth coverage without excessive atmospheric effects at low-elevation lines-of-sight. The orbital geometry is depicted in Figure 3-7. Each spacecraft will include four tracking/transmitting/receiving subsystems (two for space-to-space links and two for space-to-earth links), plus additional attitude control equipment.

Such a system could be placed in operation as follows:

a. Spacecraft No. 1 placed in synchronous orbit above ground point No. 1.

b. Stabilize one axis to the local vertical with earth sensors.

c. Stabilize about this axis with star trackers using a near-polar guide star. The tracker axis generates a cone about the desired position of the spacecraft "polar" axis during the daily revolution). The beam of Spacecraft No. 1 is pointed at the expected orbital position of Spacecraft No. 2.

d. Repeat 1, 2 and 3 for Spacecraft No. 2.
(After initial stabilization, adjust orbital position as required.)

e. Activate beacon of Spacecraft No. 1. (This beacon will appear in the field of view of the Spacecraft No. 2 tracker.)

f. Spacecraft No. 2 relinquishes the Earth reference and nulls on the Spacecraft No. 1 beacon, maintaining star tracker lock for third-axis control.

g. Beacon on Spacecraft No. 2 is activated.

h. Spacecraft No. 1 tracker relinquishes Earth tracking and nulls on beacon of Spacecraft No. 2, maintaining star track.

By a similar process, spacecraft No. 3 is launched, stabilized and placed in contact with the two orbiting spacecraft. Of the two optical systems on each spacecraft for space-to-

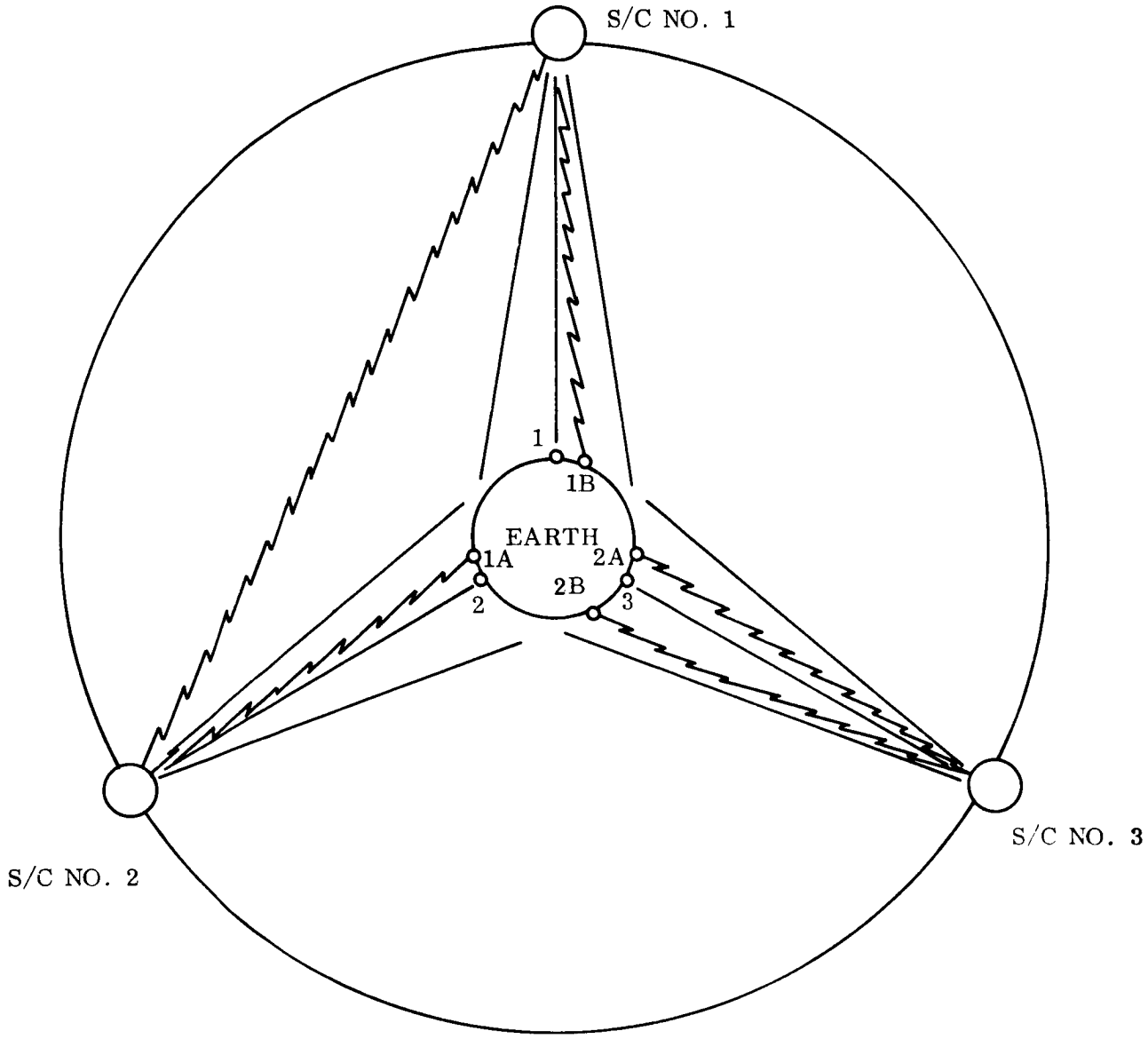

SPACECRAFT ORBIT IS SYNCHRONOUS, EQUATORIAL.
LINK 1A - 1B ILLUSTRATES LONG RANGE CAPABILITY.
LINK 2A - 2B ILLUSTRATES SHORT RANGE CAPABILITY.

Figure 3-7. Laser Global Communication Network

space links, one may be fixed to the vehicle. However, to allow for completion of the acquisition process and high precision tracking in the presence of spacecraft "drifting" during station keeping, some means must be provided for steering the other system. In "closing the loop," the first two spacecraft can relinquish star tracking and null on the beacons of spacecraft No. 3 for third axis reference. Thus, the final condition of the system is that of complete self-reference.

The earth-space link must now be provided. It is assumed that the three spacecraft will be RF-tracked from the ground to provide continuous position data for station keeping. Thus their positions will be well known, and it should be possible to slew any network ground station tracker axis to the spacecraft in view within several hundredths of a degree. Since the spacecraft-ground station geometry will always be well known, the spacecraft can be commanded over a low-power RF link to slew open-loop to the position of the ground station. The ground beacon is then activated, providing a reference for nulling of the spacecraft tracker. The spacecraft beacon, aligned with the tracker, is then activated and the ground station tracker is nulled. Thus, the initial earth-space acquisition has been completed, and the transmitter beamwidths and receiver fields of view may be drastically reduced (by 2 or 3 orders of magnitude) for the high data rate mode.

The receiving ground station must now be notified that communication with it is desired. This can easily be done by relaying an RF command through the spacecraft(s) to the receiving ground station, directing it to point at the spacecraft and to activate its beacon. The spacecraft's earth-looking system will then null on the ground beacon and complete the acquisition as described above. If the two ground stations are both within the "field of coverage" of the same relay spacecraft, two independently steerable earth-looking systems must be provided. Otherwise, the "interrogating" command will be relayed through two spacecraft during acquisition of the second ground station. The transmitter beamwidth and receiver fields of view can again be reduced for this link, and the entire system is ready for high-speed two-way data transmission.

3.7.3 SPACECRAFT CHARACTERISTICS

From the foregoing operational procedure, the general characteristics of the relay spacecrafts may be summarized as follows:

a. Four optical systems, each including the capability for beacon, tracking, transmitting and receiving functions. (For each optical system, the axes of operation for these four functions are ideally coincident.)

   1. The optical axis of one space-to-space system can be fixed to the vehicle. The other, however, and both earth-looking systems must be steerable. One very promising means for providing beam steering without gimballing the entire system is to use a pair of independently controlled wedges in front of the main receiving/transmitting aperture.

   2. Since some satisfactory means can surely be devised for diplexing the receiving and transmitting equipment, four separate lasers and receivers should not be necessary for each spacecraft. For example, a single laser could, through the use of beamsplitters, provide beacon radiation in several directions simultaneously. This area, however, requires further investigation.

b. Earth sensors and momentum devices capable of erecting one spacecraft axis to the local vertical for initial stabilization.

c. Star tracker and momentum devices capable of providing for spacecraft control about the vertical axis during the initial closing of the loop.

d. A computer for handling coordinate transformations, resolutions of errors, and other functions associated with the attitude control subsystem.

e. A relatively unsophisticated RF communication system (for earth-to-space links only).

f. Prime power, thermal control and other normal "housekeeping" functions.

The remainder of this discussion is devoted to the sizing of transmitter beamwidths, receiver apertures and fields of view, laser power, and pointing accuracy requirements.

3.7.4 ANALYSIS OF SYSTEM PARAMETERS

The basic geometry of the system is shown in Figure 3-7. The more important characteristics are as follows:

a. Spacecraft to spacecraft range:

3.4×10^4 nautical miles (6×10^9 cm)

b. Spacecraft to earth range:

2.0×10^4 nautical miles (3.5×10^9 cm)

c. Data rate = 10^7 bps.

d. Earth subtended angle at the spacecraft = 17^o.

3.7.4.1 Spacecraft to Spacecraft Link

3.7.4.1.1 Acquisition

Before data transmission can take place the spacecraft must acquire one another in this process, the beacon of one spacecraft must illuminate and be detected by the tracker/receiver of another. (The beacon may actually be the primary laser operating in a wide-beam mode.) Illumination of the second spacecraft can be ensured if the beacon beamwidth is made sufficiently large. However, the irradiance for a fixed laser power decreases as the square of the beamwidth and some reasonable compromise must be sought. The obvious arrangement is to employ a wide beam for acquisition and a narrow one for data transmission.

The acquisition beamwidth is determined primarily by the uncertainty in initial stabilization of one spacecraft, and in the orbital position of the other. Current data indicate that to allow for these variations, beacon beamwidths of 1/2 to 1 degree are reasonable. Similarly, receiver fields of view should be essentially the same for acquisition (1/2 to 1 degree).

Since it will be useful throughout the discussion to relate irradiance, transmitted power, transmitter beamwidth, and receiver aperture with data rate, Figure 3-8 has been prepared. Figure 3-8 was generated as follows:

For a laser transmitter of power P_t, operating through an optical system of efficiency K_1, and transmitted with beamwidth θ_t, the average irradiance at a range R is

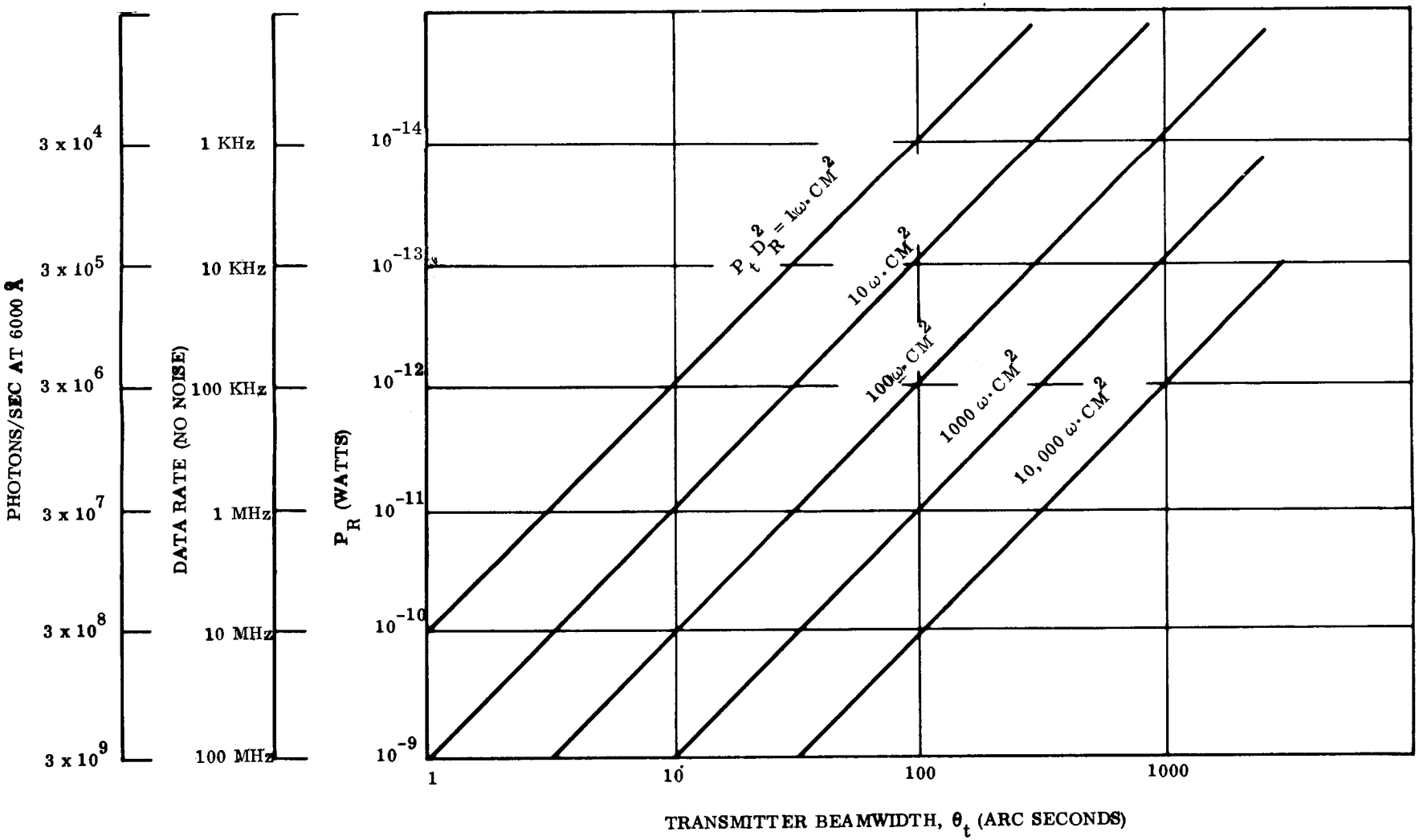

Figure 3-8. Maximum Information Rate

$$I = \frac{4K_1 P_t}{\pi (\theta_t R)^2} \text{ watts/cm}^2 \tag{3-63}$$

If the energy is intercepted by a receiving system of diameter D_R and efficiency K_2, the available receiver power is

$$P_R = K_2 I A_R = \frac{K_1 K_2}{R^2} \frac{P_t D_R^2}{\theta_t^2} \text{ watts} \tag{3-64}$$

Figure 3-8 is a plot of Pr versus θ_t for various values of ($Pt \cdot D_r^2$) at $R^2 = 3.6 \times 10^{19}$ cm^2 and $K_1 K_2 = 0.1$. The power at the receiver is also expressed in photons/second ($\overline{N}_s$) at 6000Å from the conversion:

$$\overline{N}_S = \frac{P_R \lambda}{h c} \tag{3-65}$$

where λ is the wavelength, h is Planck's constant and c is the speed of light.

For the case where the receiver is quantum noise limited (no background), the signal-to-noise ratio is

$$\frac{S}{N} = \left[\frac{\overline{N}_S}{2 \Delta f \cdot H}\right]^{1/2} \tag{3-66}$$

where η is the quantum efficiency of the detector and Δf is the detector bandwidth, and H is a detector constant approximately equal to 1.2. The spectral characteristics of the S-17 and S-20 surfaces make them attractive for these applications, and a representative value of η is 0.10 at 5000 Å. Assuming an improvement to 30 percent can be expected by the time of interest (1975 to 1980) a signal-to-noise ratio of 2 could be obtained for $N_S/\Delta f$ = 32, or 32 photons/data bit.

3.7.4.1.2 Data Transmission and Tracking

Figure 3-8 shows the maximum information rate that can be obtained for the conditions specified. For example, 10^7 bps can be achieved with a 3 to 5 arc-second transmitter beamwidth and ($P_t \cdot D_r^2$) of about 10 to 20 watts $\cdot$ cm^2. This could be provided with a 0.1 watt laser and a 10 cm (about 4-inches) diameter receiver aperture. The figures, however, are valid only in the absence of external noise. When the effects of the stars, the sun, the moon and the earth's albedo are included, this signal-to-noise ratio will be reduced as described in Section 3.4.

Figure 3-8 can also be used to size the tracking loop parameters. Analysis during the Manned Orbiting Telescope (MOT) Study (Reference 13) indicated that the noise error voltage of the fine pointing sensor should be about one-tenth of the required pointing accuracy. The sensor noise error voltage was shown to be

$$\text{NEV} = (\text{Total sensor linear range}) \left(\frac{S}{N}\right)^{-1} \tag{3-67}$$

Thus for pointing accuracies on the order of one-half arc second, which is consistent with a 3 to 5 second beamwidth, and for a linear range of ± 30 arc-seconds, the signal-to-noise ratio should be about 1200, which is very high. Now, from Section 3.4,

$$\frac{\overline{N_S}}{\Delta f} = \left(\frac{S}{N}\right)^2 \frac{2H}{\eta} = 1.2 \times 10^7 \text{ photons/sec/Hz} \tag{3-68}$$

For a 3 Hz sensor bandwidth, $\overline{N_S} = 3.6 \times 10^7$ photons/sec. It can be seen from Figure 3-8 that this value is an order of magnitude less than that required for transmission of a 10 mc data rate. Thus, the choice of ($P_t \cdot D_r^2$) must be based on the data rate requirement, rather than on the requirements of the fine pointing sensor.

The tracking/transmitting equipment must operate in two basic modes, acquisition and pointing. During acquisition, the transmitter functions as a beacon, providing a beamwidth on the order of one degree. The tracker field of view will initially be large to ensure assure sensing the beacon. In nulling on the beacon, the system switches to the pointing mode.

For high data rate transmission, the transmitter beamwidth will be only 3 to 5 arc-seconds, pointed to about one-half arc-second accuracy. It has been shown above that the margin in signal-to-noise ratio is more than adequate. Between data transmissions, contact is maintained by operating the laser at a reduced power level and accepting somewhat less precise pointing.

From the foregoing discussion, a set of system parameters which meet the stated requirements might be selected as follows:

Data Rate	10^7 bps
Transmitter Beamwidth	
- Beacon mode	1^o
- Fine Pointing mode	3 to 5 arc-sec
$P_t D_r^2$	10 to 20 watt · cm^2
Transmitter Power (Fine Pointing mode)	0.1 watt
Receiving Aperture, D_r	10 cm
Fine Pointing Precision	0.5 arc-second ($\approx 10^{-4}$ degrees)
Fine Pointing Sensor Noise	0.05 arc-second

A diffraction-limited argon laser with primary output lines at 4880 and 5145 Å is assumed; current data indicates that powers considerably in excess of 0.1 watt are available. Anticipating an increase in efficiency from the present 0.1 to 0.5 percent in the period of interest, the input power required is only 20 watts. The average power will be still less, depending on the duty cycle.

3.7.4.1.3 Noise Considerations

Actual data rates and pointing precision of the system are greatly affected by noise. The major noise sources in the free-space links are the sun, the moon, the stars and planets, and Earthshine.

3.7.4.1.3.1 Earthshine. Since the Earth is at least 20 degrees from the spacecraft-to-spacecraft lines of sight, it can be assumed with reasonable certainty that adequate shielding and baffling will limit the effect of Earthshine to a negligible fraction of input signal power. The only possible problem area is during acquisition, where signal power is low and receiving fields of view are large. This is an area which sould be analyzed further if a more detailed study of a global laser communications system is performed.

3.7.4.1.3.2 Starlight (including the planets). The background star field energy is given[3] as about 10^{-13} watts per cm^2 per deg^2. In the 300 Å bandwidth that encompasses both argon lines, the value is about $3 = 10^{-15}$ $watt/cm^2 \cdot degree^2$, or about 10^{-12} watts to the detector for a 1/2 x 1/2 degree field of view. This is about two orders of magnitude less than signal power for the parameters selected in the narrow-beam mode. In the acquisition mode, however, problems could be encountered. The situation can be improved by

a. Reducing receiver field of view below 1/2 x 1/2 degree

b. Reducing receiver aperture and increasing transmitter power holding $P_t D_r^2 = 900$ W · cm^2 at constant value.

c. Operating with only one of the two laser frequencies and using a narrow band optical filter.

d. Developing a narrow-band filter with high transmission only at the two wavelengths of interest.

The number of choices is sufficiently broad to predict no serious problem from background starlight.

When a single bright star or planet enters the receiver field of view, the situation is more acute. The worst case situation would be Venus* (visual magnitude -4.3) that would provide 5×10^{-14} w/cm^2 · Å irradiance, or about 10^{-12} watts to the detector after considering optical losses. With a 1 Å optical filter at the two laser wavelengths, the noise power is about one-tenth of the signal power. Operation during this time might be impaired somewhat by a reduction in data rate. Since the event will occur at most very infrequently and would last only a few minutes for expected fields of view, it is a tolerable situation. It does indicate, however, that either one argon line or the complex dual transmission filter must be used.

3.7.4.1.3.3 The Sun. The effects of incident solar radiation pose the most serious problems in the continuous operation of the laser network. When directly in the detector field of view (if this were permitted), about 10^{-2} watts would be received through a 1 Å filter. The seriousness of the sun problem varies throughout the year, since the angle between the Earth-sun line and the orbital plane changes sinusoidally, completing one cycle each year. When the sun is at or near the line of nodes (line formed by the intersection of the ecliptic and the equatorial orbital planes), the sun will approach very closely the axis of one spacecraft tracker/receiver every four hours as the relays rotate with the Earth. This situation is not significantly improved by choosing a nonequatorial orbit plane. The problem can be overcome by periodically (during each day) altering the "data route" between the three satellites, such that if the sunlight interferes with direct transmission from 1 to 2, the alternate route of 1 to 2 to 3 (the "long way") is chosen.

However, the network geometry dictates that not only will the spacecraft-to-spacecraft links suffer from the sun problem, but also the Earth-to-space links. There appears to be no simple way to eliminate this problem except by operating the system when the satellites are well separated from the sun as seen from the ground stations. This may prevent high data rate operation for several hours at a time because the sky brightness often is quite high in the vicinity of the sun, particularly in the presence of haze or overcast.

*All other stars or planets would be an order of magnitude fainter. Whether it is possible for Venus to enter the field of view has not been determined.

3.7.4.1.3.4 The Moon. The maximum visual magnitude of the moon is -12.7, or about eight magnitudes brighter than Venus. This represents an increase in irradiance over Venus of about 1.5×10^3, or an absolute irradiance of 10^{-10} watts/cm^2 · Å. For the 10 cm diameter receiving aperture and a 1 Å filter, the received power is on the order of 10^{-8} watts, which is a factor of 100 greater than the signal power for the 10 MHz data rate. Thus, passage of the moon through a receiver field of view will reduce the data rate by a factor of 10 to 10^6 bits/sec (from Equation 3-40). This difficulty with the moon will occur twice each month rather than twice each year, as with the sun. The judicious choice of timing for acquisition activities should avoid interference from the moon during this critical phase where signal powers are low and receiver fields of view large.

One very important noise discrimination technique which has not been investigated is that of modulation. Providing lasers with characteristic modulations should considerably ease the noise problems described. This area should be investigated further if a subsequent, more detailed, global laser communications study is performed.

3.7.4.2 Earth-to-Satellite and Satellite-to-Earth Links

These links of the communication system must have the same information rate capability as the spacecraft-to-spacecraft links. The principal differences between these links and the free space links are as follows:

a. The spacecraft-to-Earth range is 3.5×10^9 cm versus 6×10^9 cm for the free space links.

b. Atmospheric effects (absorption, local weather, and sky brightness) are major considerations.

c. The brightness of the Earth (reflected sunshine) is very significant.

3.7.4.2.1 The Uplink

Consider first the uplink (Earth-to-spacecraft). The beamwidth of the ground transmitter is limited by various atmospheric effects to a minimum of 2 or 3 arc seconds. This beamwidth is more narrow than the initial uncertainty in satellite position, or in the variability of atmospheric refractive index during the course of a day. Since we are not greatly

constrained concerning available ground transmitter power, we elect to broaden the beamwidth to about 10 arc seconds to reduce the tracking problem. This presupposes the ability to point to the spacecraft open-loop to within a few arc seconds.

Signal power at the receiver in the spacecraft is:

$$P_R = \frac{k_1 k_2 k_3 P_t D_R^2}{(\theta_t R)^2} \text{ watts} \qquad (3\text{-}69)$$

The quantity $k_1 k_2$ as before is the overall transmission of the two optical systems and is assumed to be 0.1. k_3 is the transmission of the atmosphere and is assumed to be 0.6 minimum. With the value of θ_t and R as specified, we have

$$P_R = 2 \times 10^{-12} P_t D_R^2 \text{ watts} \qquad (3\text{-}70)$$

Figure 3-9 is a plot of this function with D_R as a parameter.

3.7.4.2.1.1 Earthshine. We must now compare the signal power levels with those of noise power from the illuminated Earth. The spectral radiance of the Earth at 5000 $\mathring{A}$ is about 1.7×10^{-6} w/cm^2 ster. $\mathring{A}$. This will produce a power at the spacecraft receiving detector of

$$P'_R = \frac{\pi B_e}{4} \left(\frac{\alpha}{2}\right)^2 D_R^2 K_2 K_3$$

$$= 2.3 \times 10^{-7} \left(\frac{\alpha}{2}\right)^2 D_R^2 \frac{\text{watts}}{\mathring{A}} \qquad (3\text{-}71)$$

where: α^2 is the receiver field of view

B_e is the earth radiance

To ease the problem of acquiring and tracking the ground-based laser against the Earth background, an imaging-type detector with 1000 x 1000 resolution elements is chosen for

the spacecraft receiver. Because only the noise detected by a single element is compared with the signal, the signal-to-noise ratio for the element containing the laser image is greatly increased.

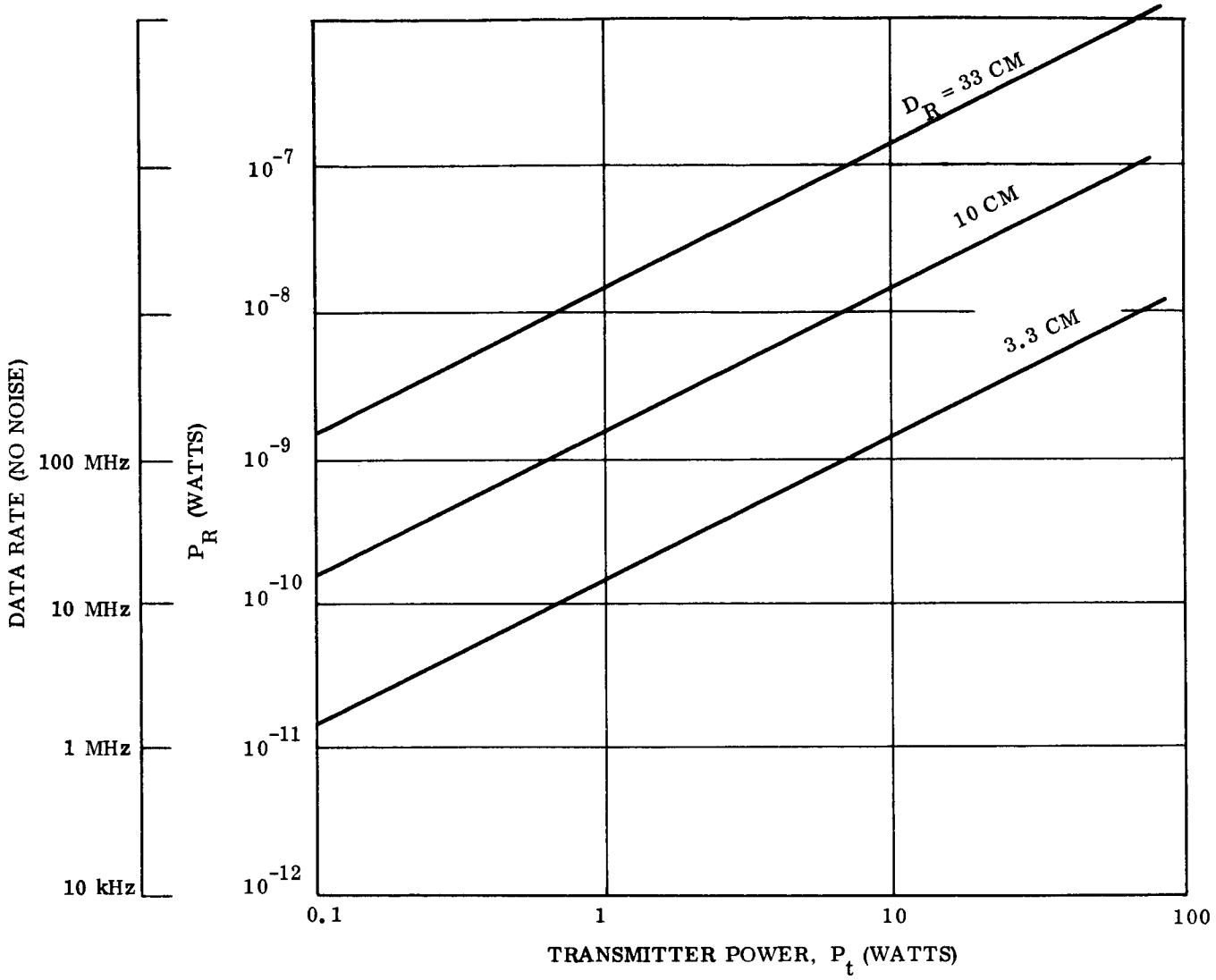

Figure 3-9. Graphical Representation of P_R with D_R as a Parameter

For acquisition, the spacecraft optical system gain is chosen to provide a receiver/tracker field-of-view of about 1 degree. Thus, each resolution element is approximately 4 arc-second square. From the expression (3-71) for received power, P_R, due to Earthshine.

$$P_R = 2.5 \times 10^{-15} \text{ watts} \qquad (3\text{-}72)$$

for a 1 Å filter and a spacecraft receiver aperture of 10 cm. It is clear from Figure 3-9 that this noise is negligible when compared with the signal power at 10 mc.

For fine pointing in the high data rate mode, the spacecraft receiver/tracker optical gain is increased so that each resolution element subtends an angle of about 0.4 arc-second. The total field-of-view is 400 arc-seconds or about 6-1/2 arc-min. This is consistent with the required pointing accuracy of ± 1 arc-second. The average noise power per element is thus about 2.2×10^{-17} watts. Considering the nonuniformity of the Earth's radiance and the fact that the peak radiance may be as much as 100 times the average, the noise power is still only about 2.2×10^{-15} watts. Thus, the signal-to-noise ratio is far in excess (three-to-four orders of magnitude) of that required.

3.7.4.2.1.2 Sunshine. The sun may,in certain system orientations, come to within a few degrees of a receiving telescope axis near sunset or sunrise as viewed from the spacecraft. The sun will provide about 10^{-3} watts/angstrom to the detector on axis for a 10 cm receiving aperture. A sun shield design would be necessary to provide an attenuation of 10^{-7} to 10^{-9} (depending on system parameters) in order not to seriously degrade information rate. If the receiving aperture is kept small (under 10 cm), a sunshield length of perhaps 100 cm will provide this attenuation down to 5 to 6 degrees of the sun axis.

3.7.4.2.2 The Downlink

The spacecraft-to-Earth link is now considered. To limit the area on the Earth which is illuminated by the laser's main lobe to a diameter of one mile, the transmitter beamwidth should be about 5 arc-seconds, pointed with a precision of ± 1 arc-second. For a spacecraft laser power of 0.1 watt, receiver signal power will be about 10^{-9} watts for a 33 cm diameter receiving aperture.

The receiver noise power consists primarily of day sky glow. Assuming an average radiance of 5×10^{-7} w/cm^2 ster. Å, the noise power in a 200 x 200 second field-of-view for the 33-cm diameter receiver and a 1 Å filter is

$$P_N \cong 10^{-10} \text{ watts} \qquad (3\text{-}73)$$

This provides a signal-to-noise ratio of about 2, which is adequate for acquisition. The 3-minute (plus) field-of-view is probably greater than necessary since the spacecraft position may be known to much greater accuracy. If so, the field may be reduced with a corresponding increase in signal-to-noise ratio.

For fine pointing, a 20 x 20 arc second field-of-view provides a signal-to-noise ratio of about 200 which is more than adequate.

The sky brightness becomes much greater than the previously indicated value as one looks nearer to the sun. Additionally, the amount of scattered light within the telescope goes up drastically. The length of sun-shade used, as well as the brightness of the sky near the sun (data that is not available at this time), will determine the smallest angle between spacecraft and sun lines-of-sight for which high data rates can be maintained. An estimation at this time is that it would be at most 10 degrees, and possibly as small as 5 degrees. If it is possible to narrow the receiver field of view or reduce the transmitter beamwidth below 10 seconds, operation even closer to the sun may be possible.

Based on these discussions, it appears that the Earth-spacecraft link can maintain high data rates for all cases except when the sun comes to within perhaps 5 degrees of either telescope axis. Based on the foregoing analysis, we tentatively select the key functional parameters of a global laser communication system as follows:

	Spacecraft	Ground Station
Objective aperture	10 cm	33 cm
Transmitter power (average)	0.1 watt	1 watt
Information rate	10^7 bps	10^7 bps
Transmitter beamwidth	5 arc-sec	10 arc-sec
Pointing precision	±1 arc-sec	±1 to 2 arc-sec

This preliminary analysis of a global laser communication network indicates the general feasibility of such a system with moderate state-of-the-art improvements required in key subsystems. The most precise pointing required for this mission is on the order of 10^{-4} degrees. Data rates in excess of 10^{8} bps could realistically be provided with a small increase in aperture size and a boost in transmitter power.

3.8 MISSION SELECTION

The most precise pointing required for a global communication network employing laser data links has been determined to be of the order of 10^{-4} degrees of arc. Since the attitude control requirements are determined to be state of the art, this mission was not pursued beyond the initial analysis given in Section 3.7.

The analyses summarized in Sections 3.1 through 3.6 were performed for a variety of planetary fly-by and orbiter missions from Mars to Pluto, considering information rates of the order of 10^{5} to 10^{7} bps and diffraction-limited optics of 40 inches maximum diameter. The inherent very long transmission/reception time lag for laser communication between Earth and planets beyond Mars introduce a difficult Earth acquisition problem. Further, the close angular proximity of the sun and the Earth as viewed from the spacecraft at these ranges poses a formidable problem of solar interference with the source being tracked by the spacecraft receiver. In contrast, these problem areas are considerably less severe for laser communications from a Mars orbiter, and the amount of development in the area of diffraction-limited optics and lasers is more reasonable. Further, since the Mars mission will logically be flown before the deep space probe, it was selected as the mission for detailed study.

It was concluded (with the concurrence of ERC) from studies of the two candidate modes for laser communications to Earth from a Mars orbiter that the mode employing a cooperative Earth beacon should be the selected mission to serve as the basis for the precision triaxial attitude control study. The Earth-tracking mode was eliminated because it has been determined that the attitude control problem is essentially state of the art and hence poses no significant problem that would warrant study under this contract. Secondly, the

relatively low information rate (10^5 bps for daytime communication) is less than an order of magnitude improvement over those planned for Voyager and is essentially microwave state of the art for the early 1970 time period.

3.9 REFERENCES

1. "Laser Potential in Deep-Space Link Grows," Aviation Week, January 31, 1966, page 71.

2. Moss, E.B., "Some Aspects of the Pointing Problem for Optical Communication in Space," Journal of Spacecraft, Vol. 2, No. 5.

3. Determination of Optical Technology Experiments for a Satellite, Perkin-Elmer Co., Engineering Report 7846, November, 1964.

4. Study of Laser Pointing Problems, Kollsman Instrument Co., Report Number KIC-RD-000162-2, December, 1964.

5. Optical Space Communications System Study, General Electric Company, Final Report on Contract NAS W-540, March, 1964.

6. Deep Space Optical Communications System Study, Hughes Aircraft Co., Report No. NASA CR-73, July, 1964.

7. Gubin, S., et al.,"Lasers vs. Microwaves in Space Communications," Journal of Spacecraft and Rockets, 3, 818 (1966).

8. Marsten, R.B., et al.,Performance of Communication Systems, etc. ibid. 828.

9. Moss, E.B., Aids to Acquisition in Optical Communication, ibid. 834.

10. Voyager Spacecraft System Report, Phase 1A Task B Preliminary Design, prepared for the Jet Propulsion Laboratory under Contract 951112 by the General Electric Co., Missile and Space Division, Document No. DIN 65SD4514, 31 January, 1966.

11. Ziemer, R.R., and Kuperian, J.E. Jr., The Mission of the Orbiting Astronomical Observatory, NASA Goddard Space Flight Center Document X-600-62-219, December 27, 1962.

12. Astronomical Techniques, W.A. Hiltner, Editor, University of Chicago Press, 1962.

13. A Fine Pointing Sensor Study for the Manned Orbital Telescope, prepared for the Boeing Company by the General Electric Company, Missile and Space Division, Document No. 65SD4418, 30 August 1965.

14. Gundersen, N.A., "Fine Guidance Sensor for High-Precision Control of OAO," Journal of Spacecraft, Sylvania Electronic Systems, Waltham, Mass., Vol. 1, No. 1, January 1964.

15. University of Michigan, Second Interim Report, Investigation of Optical Spectral Regions for Space Communications, May-July 1962.

SECTION 4

FORMULATION OF CONTROL REQUIREMENTS AND SYSTEM CONCEPTS

SECTION 4

FORMULATION OF CONTROL REQUIREMENTS AND SYSTEM CONCEPTS

4.1 INTRODUCTION

In Paragraph 3.8, the mission framework for the precision triaxial attitude control study was established to be a spacecraft in Mars' orbit which tracks a cooperative Earth laser beacon and employs an optical system to collimate a laser beam to 0.2 arc-second for high data rate communications. The next step is to derive the interdependent spacecraft control requirements and control concepts to accomplish this mission. As a preface to this and to the control system analysis and simulation reported in Sections 5 and 6, it is necessary to determine approximate values of vehicle and orbital parameters. For this purpose it is assumed that the same attention would be given to the design of the Mars Orbiter for this mission as regards mass distribution, to maintain low differences and products of inertia, as has been accomplished on spacecraft such as the Orbiting Astronomical Observatory.

For the estimated spacecraft weight of the order of 8300 pounds and for a spacecraft average diameter of the order of 15 feet, the spacecraft principal moments of inertia would be on the order of 5000 slug-ft^2. The spacecraft inertias are somewhat higher than for the selected configuration (Appendix B) due to the higher spacecraft diameter, but this is consistent with the conservative nature of the control system design. The differences in the principal moments of inertia are assumed to be less than 300 slug-ft and the products of inertia less than 50 slug-ft^2, both of which are somewhat high.

The spacecraft orbit about Mars, based on Voyager flight mechanics analysis, is taken to be on the order of 1000 km periapsis and 10,000 km apoapsis with an inclination near normal to the ecliptic plane such that occultation of the spacecraft by Mars during a six-month mission would be avoided. Considering these orbit parameters the external disturbance torques on the spacecraft are determined to be:

a. Gravity gradient disturbance torques based on the spacecraft and orbit parameters are computed to be as high as 2.2×10^{-4} ft-lb about each axis. (See Appendix C.)

b. Solar pressure torques are computed to be on the order of 1.6×10^{-5} ft-lb based on the pessimistic assumptions that the vehicle has a reflectivity of 100 percent, and the offset of the center of pressure from the center of mass is 0.5 foot and the surface area is that of a 20 foot diameter sphere. (See Appendix C.)

c. Consideration of all available information as to micrometeorite size and frequency in Martian orbit indicates little difference from near-Earth conditions. In a conversation with W. Merle Alexander, who had responsibility for the micrometeorite experiment on Mariner IV, the following data was ascertained.

   1. The vast majority of meteorites in the solar system are cometary rather than arising from the asteroid belt. This indicates little difference between near-Earth and near-Mars considerations.

   2. Mars is considerably removed from the high particle density regions of the asteroid belt.

   3. Near-Earth densities of micrometeorites are greater than in space between Earth and Mars by virtue of the Earth's gravitational attraction. Mars has one-tenth the mass of Earth and a lesser gravitational pull, so one would expect lower densities in Mars orbit.

   4. The Mariner IV micrometeorite experiment was only a threshold detector and counter. Information gained from Mars flyby and beyond showed no difference between near-Mars and deep space.

It was thereby concluded that consideration should be given to micrometeorite impacts in Mars orbit but it should not override other design considerations.

4.2 SPACECRAFT CONTROL REQUIREMENTS

Control requirements for the spacecraft following injection into Mars orbit are summarized in Table 2-5. The derivation of the precision triaxial control requirements are emphasized here in keeping with the objectives of the study, and the attitude control requirements preceding the acquisition of the fine pointing mode are treated briefly.

4.2.1 COARSE AND INTERMEDIATE MODE ATTITUDE CONTROL

The wide dynamic range required for the attitude control system to acquire the Earth and Canopus references together with the requirement to stabilize the spacecraft to its

attitude reference to a very small part of an arc-second determined the need for several control modes. By allowing a liberal field of view for the Earth and Canopus sensors in the coarse pointing mode, reliable acquisition of these references is assured. However, associated with this desirable feature is the limited resolution obtainable from electro-optical sensors conventionally used for this purpose. The "Intermediate Pointing" control mode adopted can be acquired after the spacecraft has been stabilized to within the coarse mode specification limits and permits the spacecraft to be stabilized to the Earth and Canopus with the accuracy required for capture by the fine pointing mode. Use of three different sensors and their associated control modes is required to reduce the pitch and yaw attitude errors to on the order of 10^{-5} degrees. Two different sensors are required to reduce the roll error to on the order of 10^{-3} degrees of arc.

4.2.2 SPACECRAFT ATTITUDE CONTROL ERROR ANALYSIS SUMMARY

The mission under study, involving laser communication from a Mars Orbiter to Earth while tracking a laser beacon at the Earth station, requires the Earth station receiver to be illuminated within the half-power points of the spacecraft laser beam. System concepts for precise pointing of the narrow-beam spacecraft laser to the Earth station have been formulated and are presented in the paragraphs that follow. An analysis of the beam-pointing accuracy considering these system concepts may be conveniently accomplished by considering the performance contribution of the necessary functions toward overall system operation:

a. Stabilization of the spacecraft to the selected attitude reference. Pointing of the spacecraft optical axis to the apparent direction of received radiation from the Earth beacon reference through spacecraft pitch and yaw attitude control is involved as well as third axis (roll) control about the optical axis using the star Canopus as a reference.

b. Computation of the time-varying point-ahead angles for command of the spacecraft laser beam relative to the spacecraft pitch and yaw axes to permit interception by the beam of the Earth-based receiver.

c. Command and execution of the laser beam-pointing function relative to spacecraft pitch and yaw reference axes in response to commands from a stored program in the spacecraft digital computer.

d. The stability of the alignment of the spacecraft laser and its beam-steering servoed optics subsystem relative to the spacecraft attitude reference in pitch and yaw.

The 0.2 arc-second half-power beamwidth of the spacecraft laser, defined by mission analysis, determines the $\pm$ 0.1 arc-second total allowable tolerance of the spacecraft laser beam pointing that may be distributed among the functions above.

The major contribution to pointing error is the uncertainty in the computation of the point ahead angle. It is envisioned that the computation of point-ahead angles can be improved as the mission progresses as a result of actual data obtained after establishing the laser communication link by the acquisition techniques. Error contributions from sources that are a function of the magnitude of the point-ahead angle take on a maximum value toward the end of the six-month mission. This compensating effect will result in slightly better laser beam-pointing performance than derived here using maximum errors from each function.

Considering the four main functions contributing to the laser beam-pointing error itemized above as independent error sources, the errors about each axis may be combined by root-sum-square. Using the maximum values derived from the analysis that follows and listed for each function in Table 4-1, we have:

$$\text{Pointing Error (Each Axis)} = \sqrt{\left(\begin{matrix}\text{S/C}\\ \text{Stab.}\\ \text{Error}\end{matrix}\right)^2 + \left(\begin{matrix}\text{Laser \&}\\ \text{Servoed Optics}\\ \text{Error}\end{matrix}\right)^2 + \left(\begin{matrix}\text{Align-}\\ \text{ment}\\ \text{Error}\end{matrix}\right)^2 + \left(\begin{matrix}\text{Point}\\ \text{Ahead}\\ \text{Comp.}\\ \text{Error}\end{matrix}\right)^2} \qquad (4\text{-}1)$$

$$\text{Pitch Error} = \sqrt{(0.035)^2 + (0.023)^2 + (0.025)^2 + (0.050)^2} \qquad (4\text{-}2)$$

$$= 0.0695 \text{ arc-second}$$

$$\text{Yaw Error} = \sqrt{(0.032)^2 + (0.023)^2 + (0.025)^2 + (0.050)^2} \qquad (4\text{-}3)$$

$$= 0.0683 \text{ arc-second}$$

$$\text{Beam Pointing Error} = \sqrt{(0.0695)^2 + (0.0683)^2} = 0.097 \text{ arc-second} \qquad (4\text{-}4)$$

$$\cong 0.1 \text{ arc-second}$$

Table 4-1. Laser Beam Pointing Error Summary

	Pitch (Arc-Seconds)	Yaw (Arc-Seconds)
Spacecraft Stabilization		
Sensor Noise Equivalent	0.020	0.020
Attitude Control	0.010	0.010
Roll Axis Cross-Coupling	0.005	0.002
	0.035	0.032
Laser and Servoed Optics		
Point Ahead Command	0.010	0.010
Servoed Optics	0.007	0.007
Zero Calibration	0.003	0.003
Cross-Coupling Calibration	0.003	0.003
	0.023	0.023
Alignment Stability	0.025	0.025
Computation of Point-Ahead	0.050	0.050

4.2.3 ANALYSIS OF STABILIZATION AND CONTROL ERRORS IN ORIENTATION OF SPACECRAFT RELATIVE TO ATTITUDE REFERENCE

The pitch and yaw orientation of the spacecraft that produces a null at the fine pointing sensor tracking the Earth-based beacon within its field of view, and the vehicle roll

orientation that produces a null at the fine Canopus sensor when viewing that star is the inertial orientation used as an attitude reference for pointing the spacecraft laser. Spacecraft stabilization derived from:

a. Fine pointing sensor errors due to sensor noise which results in uncertainty in the sensor pitch and yaw error signal. The 3σ noise equivalent error for a single photomultiplier detector considering a signal-to-noise ratio of 60 is

$$3\,\frac{\text{diameter of Airy disc}}{\text{S/N}} = \frac{3\ (0.2\ \text{arc-sec})}{60} = 0.010\ \text{arc-second.}$$

Since the sensor employs four photomultipliers, the sensor 3σ noise equivalent error is given by:

$$\sqrt{4(0.010)^2} = 0.020\ \text{arc-second.}$$

b. Pitch and yaw axis attitude control error including standoff error resulting from storage of momentum from external disturbance torques. A maximum value of 0.01 arc-second is considered reasonable for errors from this source.

c. Cross-coupling of roll axis errors into pitch and yaw as defined by the product or roll error and point-ahead angle. This error is a maximum near the end of the six-month mission where the point-ahead angle is at maximum but occurs when the error in the computation of the point-ahead angle is at minimum. The initial alignment of the fine Canopus sensor and backup gyro (mechanical and electrical null offset) must be such that null about the roll axis is obtained when the apparent position of Canopus is anywhere within 3 arc-seconds of the normal to the pitch axis as determined by the fine pointing sensor and within 16 degrees of the negative yaw axis, as determined by the fine pointing sensor. An additional 7 arc-seconds misalignment need be allocated for distortion due to launch and long term thermal effects. Roll sensor noise equivalent error is specified as less than 1 arc-second and spacecraft roll controller error less than 3 arc-seconds, including standoff error at maximum controller momentum storage condition. The total maximum combined roll error is less than 14 arc-seconds. Since a roll error results in a pitch error when cross coupled through a yaw point-ahead angle, the pitch error resulting from the 14 arc-second maximum roll error and the 75 arc-second maximum yaw point-ahead angle is $\frac{75 \times 14}{2 \times 10^5} = 0.005$ arc-seconds. Similarly, the yaw error resulting from the 14 arc-second maximum roll error and the 30 arc-second maximum pitch component of the point-ahead angle is $\frac{30 \times 14}{2 \times 10^5} = 0.002$ arc-seconds.

In summary then, the total allowable 3 σ spacecraft error about the yaw axes relative to the apparent sensed radiation from the Earth-based beacon, as determined by the fine pointing sensor, is specified to be 0.032 arc-second. The total allowable 3 σ spacecraft

error about the spacecraft pitch axis relative to the apparent sensed radiation from the Earth-based beacon as determined by the fine pointing sensor is specified to be 0.035 arc-second.

4.2.4 ERROR ANALYSIS OF SERVOED OPTIC SUBSYSTEM FOR LASER BEAM POINTING RELATIVE TO SPACECRAFT ATTITUDE REFERENCE

The spacecraft optical design philosophy designates the main optic as both a receiver of radiation from the Earth beacon and a transmitter to collimate the spacecraft laser output to the required beamwidth. The interference-type beam splitter in the recommended design provides high reflectivity at the beacon wavelength to illuminate the fine pointing sensor and a high transmissivity at the spacecraft laser beamwidth for laser communications. Servoed optics are provided, in the form of a two degree-of-freedom tilting plate, for introduction of the required point-ahead in the pitch and yaw axes relative to the pitch and yaw attitude reference established by the fine pointing sensor. Thus, small deformations in the main optic, within field of view limitations, affect the incoming beacon radiation and outgoing laser beam equally. The spacecraft attitude control provides the vehicle torques to null the fine error sensor in pitch and yaw and the point ahead is executed relative to that reference. The proposed design features a self-alignment operating mode to calibrate the laser and its beam-steering servoed optics subsystem at the zero point-ahead position.

Sources of error to be considered in the command and execution of laser beam-pointing relative to the attitude reference are:

a. The error in commanded point-ahead angle determined by the rate of change of the point-ahead angle and rate of command update. By design, the tilting plate angle command is updated every six seconds about both the pitch and yaw axis to limit the point-ahead error to 0.01 arc-second from this source at the maximum rate-of-change of point ahead angle. Its value could be made smaller by increasing the command update rate of the spacecraft digital computer, but this would entail a corresponding increase in computer storage capacity. The other limiting factor to be considered for command update rate is governed by the tilting plate servo loop response; however, responses in the range of 10 to 100 Hz are attainable. Therefore, this is not a limiting factor. Based upon the

update rate of once every six seconds, the 3 σ error in the commanded point ahead angle is 0.01 arc-seconds in pitch and yaw.

b. The error in positioning the tilting plate to the command angle. Errors in each serve loop for positioning the tilting plate in response to the commanded input from the spacecraft digital computer are derived from gimbal axis pickoff errors, quantization at the servo input summing junction and dynamic and steady-state servo errors. Maximum errors allocated are $\pm$ 10 arc-seconds to the pickoff, $\pm$ 5 arc-seconds for quantization of the computed point-ahead angular command stored in the spacecraft digital computer and $\pm$ 3 arc-seconds for servo loop operation including drifts in the electronics, torquer threshold and hysteresis. Aside from the torquer threshold the remaining errors may be considered independent and combined in root-sum-square fashion. Considering the torquer threshold error equal to 2 arc-seconds we have an error in each servo loop for positioning the tilting plate in response to a computed command of $\pm (2 + \sqrt{10^2 + 5^2 + 3^2}) = \pm 14$ arc-seconds. Applying the maximum tilting plate mechanism scale factor of 0.01 arc-second point-ahead per 28 arc-second tilting plate angle, the 3σ error in yaw and pitch axis point-ahead for a 14 arc-second tilting plate angular error is (0.01) 14/28 = 0.005 arc-second. For a worst case analysis (adding 2, 10, 5, and 3 instead of root-sum-squaring them), the maximum tilting plate servo positioning error in pitch and yaw is (0.01) 20/28 = 0.007 arc-second.

c. The error in the calibration of the tilting plate zero point-ahead position is a function of the mechanization used for in-flight alignment of the spacecraft laser beam relative to the fine error sensor null. By providing a separate servo loop utilizing a gimbal axis pickoff with a high gain for limited linear range about the zero spacecraft laser point-ahead angle, precise positioning of the tilting plate may be obtained in response to error signals from the fine error sensor. Telemetered outputs from the gimbal axis digital pickoff during the in-flight alignment mode can be used to determine the relationship of the digital readout of the tilting plate gimbal axes relative to the zero point-ahead position. A completely autonomous on-board servo subsystem could be provided, if desired, to take out any angular excursions of the prescribed digital pickoff position relative to the zero point-ahead position. The angular error remaining after calibration is estimated to be a maximum of 0.003 arc-second based on low sensor noise when sensing spacecraft laser illumination.

d. Calibration cross-coupling error in the determination of the angular error between the pitch and yaw reference axes determined by the fine pointing sensor and the tilting plate pitch and yaw axes. This is maximum at maximum tilting plate angles. Misalignments between the pitch and yaw axes as determined by the gimbals of the tilting plate and the fine error sensor may be determined by commanding angular rotations about the pitch tilting plate axis and detecting and telemetering the output in the tilting plate yaw axis and vice versa. Any

distortion may be accounted for in deriving the point-ahead angles to be stored in the spacecraft computer. The angular error remaining after calibration is estimated to be a maximum of 0.003 arc-second based on low sensor noise when sensing spacecraft laser illumination.

The total maximum error in the command and execution of the pitch and yaw laser beam-pointing relative to the attitude reference is 0.01 + 0.007 + 0.003 + 0.003 = 0.023. It should be noted that the maximum error in the servo positioning of the tilting plate occurs at the maximum tilting plate angles (where the tilting plate scale factor — 0.01 arc-second beam deflection/28 arc-second tilting plate rotation— is maximum) and the maximum residual error after calibration due to misalignment of the servoed optics relative to the fine error sensor also occurs at maximum tilting plate angles. It should be further noted that the maximum tilting plate angles occur well into the mission when computation of point-ahead angles will have been considerably improved by virtue of data obtained after spacecraft laser acquisition of the ground station.

4.2.5 ANALYSIS OF STABILITY OF CALIBRATED ALIGNMENT OF SPACECRAFT LASER AND ITS BEAM STEERING SERVOED OPTICS SUBSYSTEM

As previously stated, the proposed design features a self-alignment operating mode to calibrate the laser and its beam-steering servoed optics subsystem at the zero point ahead position. The short term stability of this calibration, i.e., changes that occur before subsequent calibration, need to be examined as an error source. An increase in the angular misalignment between the zero pitch and yaw angles, as determined by the fine pointing sensor and its associated electronics, and the zero point-ahead direction of the laser, as determined by the laser and its beam-steering servoed optics, results in a corresponding error in the point-ahead of the laser beam. Based on thermal design considerations (Appendix B) requiring temperature control of the order of $0.1^{\circ}F$, a maximum value of 0.025 arc-second is permitted to accrue between calibrations.

Computation of Point Ahead Angle. A total of 0.050 arc-second has been allocated to the computation of the point-ahead angle about the pitch and yaw axes. This figure assumed that a computer program will be used that utilizes adaptive and stochastic techniques, and that the point-ahead angle will be updated whenever the 0.050 arc-second error is

approached. Use of the conical scan technique or auxiliary receivers (discussed in Paragraph 4.7) is proposed to maintain the point-ahead error within the specified value.

4.3 ATTITUDE REFERENCE CONCEPTS

The apparent direction of the Earth-based laser beacon and two orthogonal axes normal to this line is the obvious selection for the spacecraft coordinate reference. Since offset pointing from any celestial reference other than Earth requires knowledge of the Earth's position relative to that reference, the associated errors inherent in any such method would make it inferior. Utilization of the "point" source reference of a laser beacon rather than the Earth's center provides better than an order of magnitude improvement in pointing the spacecraft, based on the capability of electro-optical sensors. Having established the apparent direction of the Earth beacon-spacecraft line as a reference for pitch and yaw control of the spacecraft it remains to select a third axis (roll) reference.

The basic tradeoff between the two leading candidate concepts, the star Canopus with a gyro back-up during occultation of Canopus, and a two star reference such as Canopus and Vega, appears to be the ability to achieve the required gyro performance versus the required gimbal positioning accuracy of star sensors. Projected moderate improvements by the 1975-1980 period favor the Canopus-gyro reference system.

4.3.1 ALTERNATIVES IN ESTABLISHING A THIRD REFERENCE AXIS

Due to the fine pointing accuracy required, a third axis reference based upon sensing the position of either the Sun, Mars, one of the other planets or one or more of the fixed stars has been investigated:

a. The use of the Sun was rejected because of the relatively small angle between it and the Earth as viewed from Mars during a portion of the mission and the varying nature of this angle, and because both the Earth and the Sun cannot be viewed from the Mars orbit for a six-month period without an occultation by Mars during a portion of some orbit.

b. Mars was rejected because of the complexity of constant realignment of the

reference axis as the probe orbits the planet and because of the difficulties introduced by the eccentricity (1000 x 10000 km) of the probe orbit.

c. The use of one of the other planets was deemed undesirable because of the problems of discrimination from nearby stars and the accuracy of realignment required as the planet moved along its orbit during the six months of the mission.

d. The use of a fixed star, Canopus in particular, as a reference presents the following advantages:

1. The star represents a point source, eliminating the problem of finding its center.

2. The technology of star sensors is well advanced.

3. Canopus is the second brightest star in the sky, and has no close neighbors of comparable magnitude.

4. The line-of-sight from Mars to Canopus is approximately normal to the ecliptic plane and thus to the Earth-Mars line of sight, which will tend to minimize sensor cross-coupling in the derivation of the third axis error signal. However, since the spacecraft orbit about Mars must be approximately normal to the ecliptic plane to avoid loss of laser communications due to occultation of the Earth by Mars, any star sufficiently close to the normal to the Earth-Mars line to provide a good third axis reference is occulted by Mars, once per probe orbit. Therefore, an alternate third axis reference must be provided during this period of occultation of Canopus. Two possible methods of providing such a reference are:

- The use of a second star as a reference during the period of occultation of Canopus.

- The use of a gyro reference during occultation.

4.3.2 TWO-STAR THIRD AXIS REFERENCE

Since it is desirable to have guide stars near the ecliptic poles to minimize sensor cross-coupling in the derivation of the third axis error signal, the best star to be used in conjunction with Canopus is Vega. Vega is approximately 27 degrees from the north ecliptic pole, while Canopus is only 14 degrees from the south ecliptic pole. As is the case with Canopus, there are no stars of comparable magnitude near Vega in the celestial

sphere. Furthermore, Vega is the fifth brightest star in the sky. Several alternatives in implementation of the two star reference system are examined below:

a. A reference concept based upon slewing one star sensor alternately to the position of Canopus and Vega may be ruled out because of the loss of reference during the slewing of the sensor.

b. The use of two star sensors gimballed separately possesses the disadvantage that two degrees-of-freedom are required of each sensor to accommodate the apparent motion of Canopus and Vega during the mission, with an attendant introduction of error by four mechanical gimbals.

c. Another reference concept was derived that would employ two star sensors fixed to a common spacecraft-mounted platform such that the lines of sight of the sensors matched the angular separation of Canopus and Vega on the celestial sphere. The platform would have its attitude fixed in inertial space, by virtue of being locked to celestial references by spacecraft control torques applied in response to third axis attitude errors sensed by the star sensors. Considering the plane of the platform to be oriented to a fixed attitude in inertial space between the ecliptic and Mars orbit plane, two degrees-of-freedom would be required between the platform and the spacecraft to permit the spacecraft fixed primary optic to track the apparent direction of the Earth beacon. One degree-of-freedom normal to the platform would be provided to accommodate the component of angular movement of the Earth-Mars line of sight in the plane of the platform as Earth and Mars move along their orbits during the six-month mission. A second degree-of-freedom in the plane of the platform and orthogonal to the axis of the fixed spacecraft primary optic would provide a rotation normal to the apparent direction of the Earth beacon from the Mars Orbiter and accommodate the angle between the spacecraft-Earth beacon line (roughly the Mars-Earth vector) and the plane of the platform.

   In this scheme, a difficulty arises because each star sensor would have to provide an output arising from deviation of star position from the null in each of two dimensions. Due to rotation of the star sensor platform about the first axis described above, the vehicle roll about the Earth-Mars line of sight would produce different components of error in the two measuring directions of the star sensors at different times during the mission. Rather than using some means of resolving the two star sensor outputs, only one output could be used at any one time with an appropriate gain factor inserted in the control loop that was varied as the mission progressed. Since rotation of the star platform about the first axis would be very slow, it would be months between switches from one star sensor output to the second output of the same sensor. Implementation of the above two-star sensor configuration would involve switching from one

star sensor to the second, twice per probe orbit of Mars. However, such switching would introduce transients in the third axis control loop arising from any inconsistencies in the outputs of the two sensors due to inaccuracies in derivation of the control error signal. The maximum magnitude of such a transient would be twice the tolerance of an individual sensor. Since both stars are visible to the probe for periods of at least 15 minutes, it is possible to use the output of both sensors during this time. Through the use of some signal processing technique such as least-squared error when both signals were available, the transients would be introduced twice as often - when the first sensor was turned on and again when the second was turned off - but the total error introduced at any one time would be halved. To minimize the errors introduced by the star sensors, the outputs of the sensors could be passed through a low pass filter to remove any high frequency components of the sensor outputs, since the frequencies of motion are known to be very low. A possible configuration is shown in Figure 4-1.

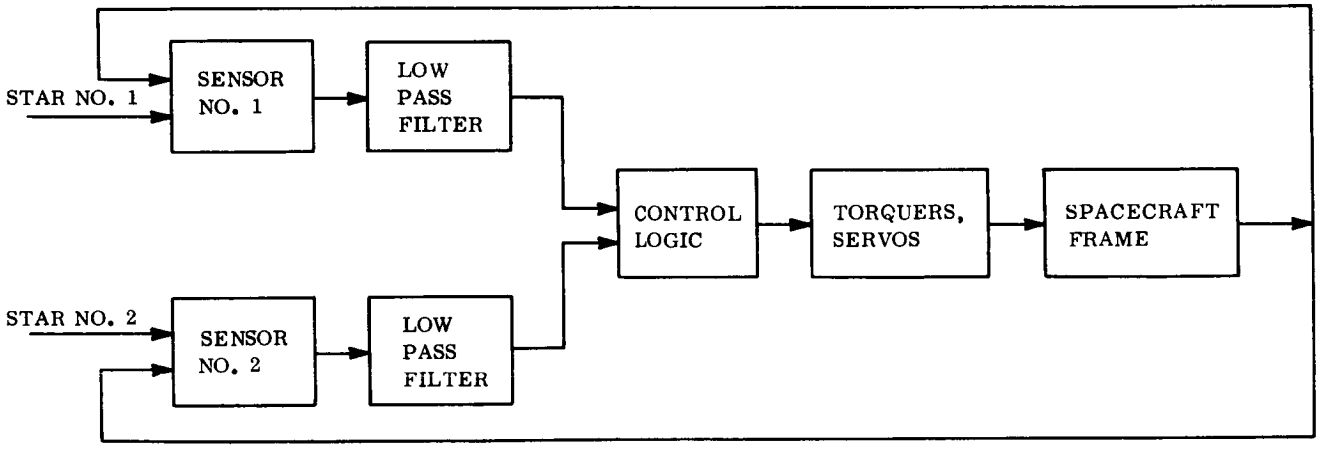

Figure 4-1. Possible Configuration for Low Pass Filter

4.3.3 SINGLE-STAR SENSOR AND GYRO REFERENCE

As stated previously, a reference system that delineates two axes normal to the Earth-spacecraft line and employs the line of sight to Canopus as a reference for the third axis, must provide a back-up during occultation of Canopus by Mars. One method of implementation would be to simply use the output of a gyro whenever the star sensor output was not available. In this concept, the star sensor output would be used to update the gyro whenever available. A figure of merit for this type of system would be the gyro drift rate. With the best gyros available today, the floated rate integrating gyros,

drift rates as low as 15 arc-seconds per hour can be maintained with frequent update, as in this system. Since the maximum period of occultation is on the order of 2 hours, gyro drift could introduce errors as large as 30 arc-seconds, a factor of four too large. However, the use of gas bearing gyros, electrostatic gyros or laser gyros and the realization of the resultant lower drift rates are very probable for the 1975-1980 period. A variation of the above concept would be to use the gyro as the third axis reference, updating it with star sensor inputs whenever available as shown in Figure 4-2.

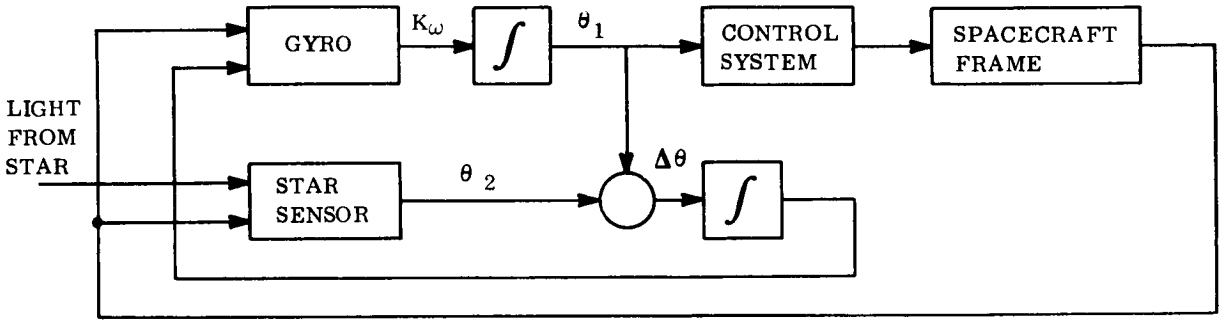

Figure 4-2. Variation Using Gyro as Third Axis Reference

This method has the advantage that switching from one reference to another would be avoided, with a reduction in hardware and an attendant increase in reliability.

During the mission, the apparent motion of Canopus is through an approximately circular path. A great simplicity in the design can be gained if the spacecraft is rolled about its optical axis so as to maintain constant alignment about the axis with respect to Canopus, as in the Mariner missions. Two aspects peculiar to this technique are:

a. The sensor must be gimballed about one axis, but the gimballing is done in the non-measuring direction, with the result that the errors introduced are only those of a cross coupling nature and are small.

b. Computation of the laser transmitter point-ahead angles relative to the two reference axes normal to the optical axis will have to take into account the slowly varying spacecraft motion about the optical axis during the six-month mission period.

4.3.4 CONCLUSIONS

The major sources of error for the two-star sensor configuration third axis reference are:

a. Mechanically gimballing the tracker platform about two axes. Present state of the art would indicate a 10 to 20 arc-second error would be introduced by each gimbal.

b. Star sensor errors of 2 to 3 arc-seconds.

c. Short term structural thermal deformation of unknown amplitude inducing misalignment of the sensor optical axis.

The major sources of error for the star sensor and gyro configuration are:

a. Gyro drift during Canopus occultation could cause third axis errors to grow to the order of 30 arc-seconds with state of the art hardware.

b. Error introduced by a star sensor that must be gimballed in the non-measuring direction on the order of 5 arc-seconds with hardware projected for the 1975-1980 mission period.

c. Short term structural thermal misalignment.

Based upon the above considerations and the good possibility of improvement in the performance of gyros by the 1975-1980 mission period, the Canopus Sensor and gyro configuration is selected as the third axis attitude reference.

4.4 POINT-AHEAD

Having established an Earth-based beacon as the pitch and yaw fine pointing attitude reference for the Mars Orbiter and the star Canopus as the roll reference, consideration must be given to the orientation of the spacecraft to these references and its laser beam pointing requirements. The selected control system concept for the spacecraft fine pointing mode (Section 4.5) defines a primary optic rigidly attached to the spacecraft

structure to serve as both a receiver of Earth beacon radiation and a transmitter of the spacecraft laser beam. In this configuration the spacecraft pitch and yaw attitude is established as a reference for laser communication to the ground station by alignment of the axis of the primary optic (the spacecraft roll axis) to the apparent direction of incoming radiation from the Earth beacon. The roll attitude reference is achieved by rotation about this axis until the spacecraft star sensor (having a degree of freedom in the spacecraft yaw-roll plane) is aligned to Canopus.

4.4.1 POINT-AHEAD COMPUTATION RATIONALE

Since there is relative motion between the Earth ground station - the reference for spacecraft pitch and yaw control and the receiver of its laser communications - and the Mars Orbiter, it is evident that the laser beam transmitted from the spacecraft must be angularly offset in pitch and yaw, relative to the spacecraft attitude established by tracking the Earth beacon and Canopus, in order to intercept the ground station (Refer to Figure 2-2). The total angular offset about the pitch axis of the spacecraft laser beam relative to the spacecraft roll axis is defined as the pitch point-ahead angle, and the yaw point-ahead angle is similarly defined.

The required time varying pitch and yaw point-ahead may be conveniently determined by separating the point-ahead computations, referred to a specific instant in time, into two parts. Defined in the framework of the selected control concept, they are:

a. Part 1 - The components of the angular offset of the axis of the primary optic between the apparent direction of incoming radiation from the ground beacon and the spacecraft-ground station vector in the plane of the ground station, spacecraft and Canopus and in its normal plane through the spacecraft-ground station vector.

b. Part 2 - The components of the angular offset of the transmitted spacecraft laser beam relative to the spacecraft-ground station vector, in the orthogonal planes indicated in Part 1, necessary to accommodate the ground station velocity relative to the spacecraft and to make possible the laser interception of the ground receiver.

It should be noted here that associated with the development of the spacecraft angular offset components as a function of ground station velocity relative to the spacecraft, as defined in Part 1, a small rotation about the optical axis is required to maintain spacecraft roll control to the star Canopus. This is illustrated in Figure 4-3 in conjunction with defining mathematical relations and computation of the maximum roll angle corresponding to worst-cause values of pertinent mission parameters. The result is that a maximum roll angle of the order of 9 arc-seconds occurs during the maximum angular offset of the optical axis relative to the spacecraft-ground station vector (on the order of 40 arc-seconds) and the maximum angular offset of the star Canopus from the normal to the spacecraft-ground station vector of 16 degrees. Employing this value of maximum roll angle in transforming optical axis offset components, defined in Parts 1 and 2, from the orthogonal reference planes indicated to the spacecraft yaw-roll plane and pitch-roll plane, where the respective laser beam pitch and yaw point ahead is implemented, produces no change in the value of angular offsets within the degree of precision required. Therefore the required angular offsets of the spacecraft laser beam computed in the plane of the spacecraft-ground station and Canopus, and its normal plane through the spacecraft-ground station vector, may be applied about the spacecraft pitch and yaw axes respectively.

4.4.2 POINT AHEAD COMPUTATION

The two-part definition of point-ahead, expressed previously, is illustrated in Figure 2-2 for an ideal case in which the ground station velocity is constant in both magnitude and direction during light transmission from the ground station to spacecraft and spacecraft to ground station. The relative velocity between the two systems that is of interest for computation of the angular offset of the spacecraft optical axis from the spacecraft-ground station vector is determined in the reference frame indicated. In that frame the relative velocity which results in an offset between the incoming radiation and the spacecraft ground station vector is determined from the vector summation of the spacecraft velocity at the specific time of interest, t_2, and the ground station velocity during the time of beacon light transmission which leaves Earth at an earlier time, t_1, and is received at the time t_2. In the same frame the relative velocity of interest (for computation

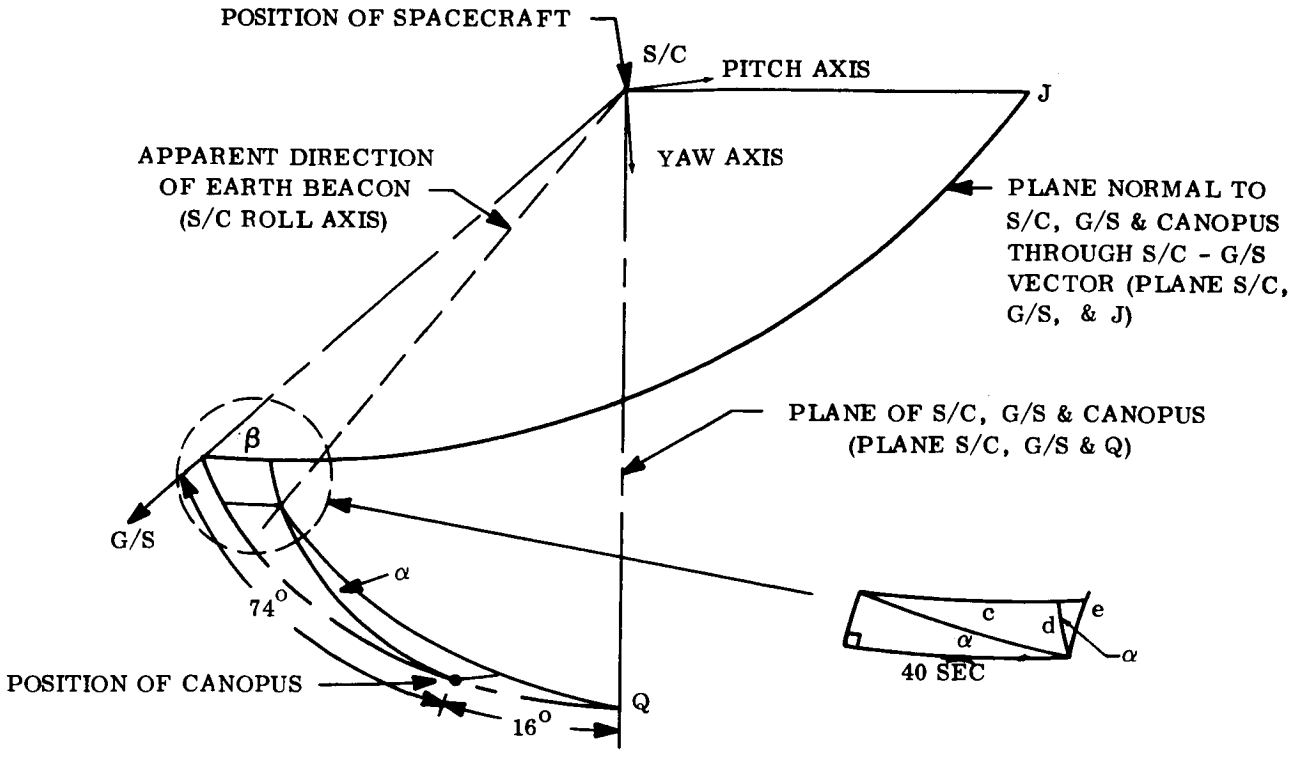

NOTES:

β = Max Angular Offset of Apparent Direction of Earth Beacon

β = 40 Arc-Seconds

G/S = Ground Station

S/C = Spacecraft

ANALYSIS:

Examining the case where Canopus is at the maximum angle from the normal to the S/C-G/S Vector (16^{o})

$$\cos b = \cos \beta$$

$$\cos 74^{o} \text{ z } \cos 40 \widehat{\text{sec}} \cos 74^{o}$$

$$\alpha = \sin^{-1}\left(\frac{16^{o}}{74^{o}} \sin 40 \widehat{\text{sec}}\right) = \sin^{-1}(0.22 \sin 40 \widehat{\text{sec}}) = 9 \widehat{\text{sec}}$$

Therefore, the angle between the frame in which the angular offset was computed and the spacecraft frame in which the point ahead will be applied, α, is 9 $\widehat{\text{sec}}$.

$$c = \tan^{-1}\left(\frac{\tan 40 \widehat{\text{sec}}}{\cos 9 \widehat{\text{sec}}}\right) \cong 40 \widehat{\text{sec}}$$

$$e = \tan^{-1} \frac{\tan d}{\cos 9 \widehat{\text{sec}}} \cong d$$

Therefore, the point ahead computed in the plane of the S/C, G/S & Canopus, and its normal plane through the S/C - G/S vector may be applied without error in the spacecraft yaw-roll and pitch-roll planes.

Figure 4-3. Representation and Analysis of the Roll Component of Point-Ahead

of the required laser beam angular offset relative to the spacecraft-ground station vector at time t_2) is determined from the vector summation of the spacecraft velocity at time t_2, the ground station velocity during a laser transmission originating at the spacecraft at time t_2, and received by the ground station at a later time t_3. As can be seen in Figure 2-2, the analysis is considerably simplified by the fact that the ground station velocity remains constant in the t_1 to t_3 interval.

The mission under consideration in this study is more complex than the ideal case in that the velocity vector of the ground station relative to inertial space is not constant. The ground station velocities for this realistic case, determined relative to the same reference frame as before, may be determined from the change in ground station position and the corresponding time of light transmission as shown in Figure 4-4. The ground station velocity of interest for computation of the angular offset of the spacecraft optical axis relative to the spacecraft-ground station vector at a specific time t_2, may be computed from its change in position during the time interval t_1 to t_2. This interval corresponds to the time interval for the beacon laser transmission from the Earth station to the spacecraft. Similarly the ground station velocity of interest, for computation of angular offset of the transmitted spacecraft laser beam relative to the spacecraft-ground station vector necessary for interception of the ground receiver, may be computed from its change in position during the time interval, t_2 to t_3. This interval corresponds to the transmission time to the ground station of the laser beam that originated at the spacecraft at t_2.

The vector summation of the spacecraft velocity and the computed value of ground station velocity during the interval(t_1 to t_2), determined in a suitable reference frame and transformed to the reference frame indicated in Figure 4-4, determines the relative velocity of interest for computation of the angular offset of the axes of the spacecraft primary optic from the spacecraft-ground station vector. These yaw and pitch angular offsets from the spacecraft-ground station vector, γ_y and γ_p, are a function of the relative velocity vector and may be determined from the expressions given in Figure 2-2.

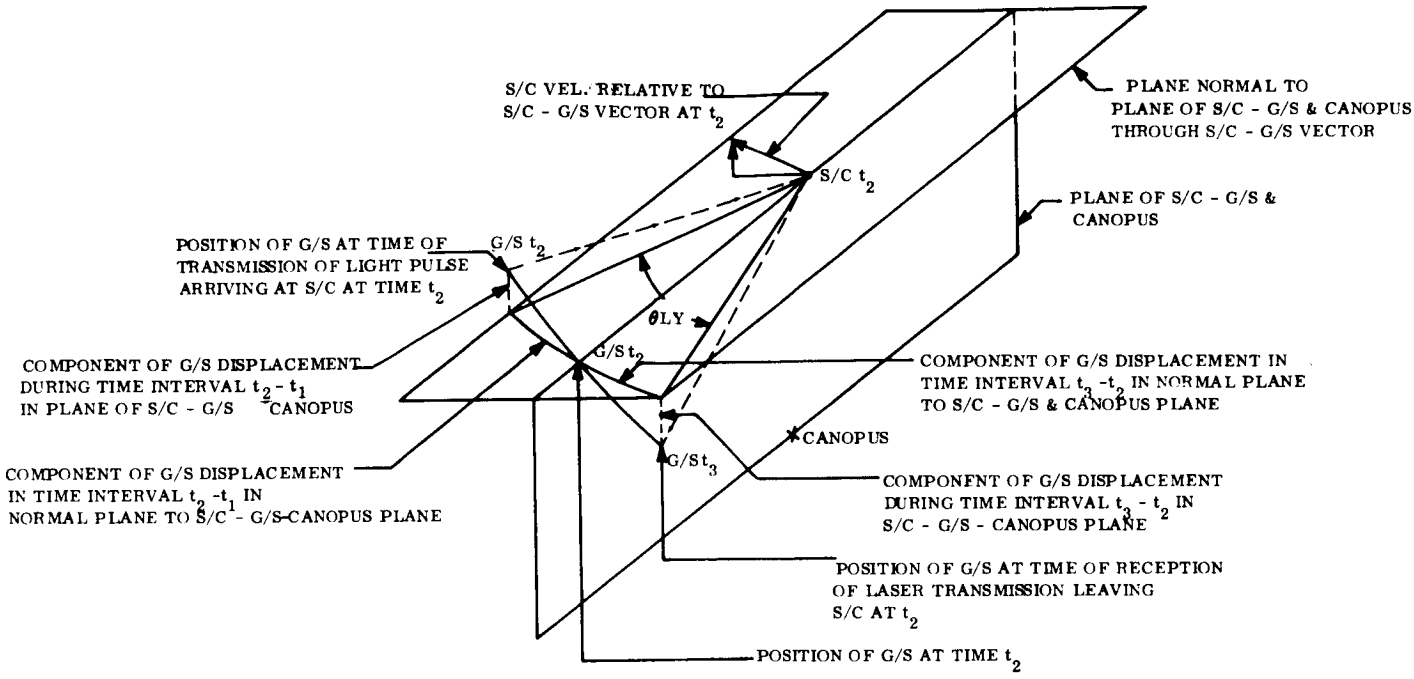

Figure 4-4. Change in Ground Station Position and Corresponding Time of Light Transmission

The vector summation of the spacecraft velocity and the computed value of ground station velocity during interval (t_2 to t_3), determined in a suitable reference frame and transformed into the reference frame of Figure 4-4, determines the relative velocity of interest for computation of the angular offset of the spacecraft laser to intercept the ground station. These yaw and pitch angular offsets from the spacecraft-ground station vector, α_y and α_p, are a function of the component of the relative velocity vector and may be determined from expressions given in Figure 2-2.

In summary, the point-ahead angles for the realistic case of variable ground station velocity are given by the following relations.

$$\sin \gamma_y = \frac{VR_y (t_2 - t_1) \sin \theta'_y (t_2 - t_1)}{c + VR_y (t_2 - t_1) \cos \theta'_y (t_2 - t_1)} \qquad (4\text{-}5)$$

$$\sin \gamma_p = \frac{VR_{p\,(t_2 - t_1)} \sin \theta'_{p\,(t_2 - t_1)}}{c + VR_{p\,(t_2 - t_1)} \cos \theta'_{p\,(t_2 - t_1)}} \tag{4-6}$$

$$\sin \alpha_y = \frac{VR_{y\,(t_3 - t_2)} \sin \theta'_{y\,(t_3 - t_2)}}{c} \tag{4-7}$$

$$\sin \alpha_p = \frac{VR_{p\,(t_3 - t_2)} \sin \theta'_{p\,(t_3 - t_2)}}{c} \tag{4-8}$$

$$\text{Point-Ahead Yaw} = \gamma_y + \alpha_y \tag{4-9}$$

$$\text{Point-Ahead Pitch} = \gamma_p + \alpha_p \tag{4-10}$$

where

$VR_{y\,(t_2 - t_1)}$ and $VR_{p\,(t_2 - t_1)}$ are the components of the relative velocity determined from the ground station position change during the time interval, t_1 to t_2, of beacon transmission to the spacecraft.

$VR_{y\,(t_3 - t_2)}$ and $VR_{p\,(t_3 - t_2)}$ are the components of the relative velocity determined from the ground station position change during the time interval t_2 to t_3, of spacecraft laser transmission to the ground station

$\theta'_{y\,(t_2 - t_1)}$, $\theta'_{p\,(t_2 - t_1)}$, $\theta'_{y\,(t_3 - t_2)}$ and $\theta'_{p\,(t_3 - t_2)}$ are the angles the computed relative velocity components make with the spacecraft ground station vector.

c is the velocity light.

An alternate method of determining point-ahead may be derived considering the angular offsets caused by the velocity of the ground station relative to the spacecraft-ground station vector separately from the angular offsets caused by the spacecraft velocity relative to the spacecraft-ground station. Referring to Figure 4-4 it may be seen that the angle θ_{Ly} describes the yaw point-ahead resulting from the change in position of the ground station in that plane during beacon light transmission to the spacecraft in time interval, t_1 to t_2 and spacecraft laser transmission to the ground station in time interval, t_2 to t_3,

when one considers the spacecraft velocity to be zero. The component of yaw point ahead due to spacecraft velocity relative to the spacecraft-ground station vector is given by the familiar expression $\frac{2V_{sy}}{c}$. The parameter V_{sy} represents the normal component of the spacecraft velocity relative to the spacecraft-ground station vector. Thus alternate expressions for point-ahead are given by the expressions

$$\text{Point-Ahead Yaw} = \frac{2V_{sy}}{c} + \theta_{Ly} \tag{4-11}$$

$$\text{Point-Ahead Pitch} = \frac{2V_{sp}}{c} + \theta_{Lp} \tag{4-12}$$

4.5 SYSTEM OPTICS FOR LASER COMMUNICATIONS

4.5.1 INTRODUCTION

The major functions of the optical system on-board a spacecraft which returns data to Earth over a narrow laser beam are the following:

a. To collimate the laser output to the required beamwidth.

b. To provide a sufficiently intense small image of the beacon for the fine pointing sensor.

c. To permit efficient use of the main optic both as a receiver and as a transmitter.

d. To offset the transmitting axis from the tracking axis over a relatively wide range with high precision for introduction of the "point-ahead" required by the transport lag.

e. If possible, to provide for "self-alignment" of the tracking and transmitting axes to minimize the pointing uncertainties at the time of initial acquisition.

f. If required, to decouple the high precision pointing functions from the spacecraft attitude control system through incorporation of a servoed optics subsystem.

4.5.2 SUMMARY

A preliminary optical design indicates that a 30-inch aperture Cassegrainian telescope with an overall focal ratio of f/25 operating as both a receiver and transmitter will provide the required system performance.

A tilting plate mechanization is proposed to provide the required spacecraft laser angular offset required for point-ahead, and on-board alignment of the laser optical axis to the telescope axis, as defined by the null of the fine Earth beacon sensor, is accomplished by sensing the spacecraft laser radiation by the fine Earth beacon sensor via use of a retractable reflector, as shown in Figure 2-1.

A second servoed optics mechanization was considered to achieve the required fine pointing of the optical axis with a less precise vehicle control loop for follow-up. This configuration was not recommended due to the additional complexity, high prime power and associated weight required due to transmission losses, and the fact that no significant improvement in response in fine pointing could be attained due to the limited pulse rate of the laser beacon reference.

4.5.3 COLLIMATING SPACECRAFT LASER BEAM

The 30-inch aperture Cassegrainian telescope will provide an output half-power beamwidth of 0.2 arc-seconds at the transmitter wavelength, provided that it operates diffraction limited. This requires that the laser output be focused to a point image whose diameter is equal to or smaller than the telescope's Airy disk; this condition is met if, for a one-inch diameter laser, the first focusing lens has a focal length shorter than 30 inches. Formation of the 0.2 arc-second beam also requires that aberrations of all intermediate optical components, including the transfer or focusing lenses and tilting plates, be corrected to a diffraction limited combination.

4.5.4 PROVIDING A SUFFICIENTLY INTENSE SMALL IMAGE OF BEACON FOR THE FINE POINTING SENSOR

It has been shown (See Section 3 of this report) that the 30-inch aperture will collect adequate energy from the beacon to assure satisfactory operation of the fine pointing sensor. The system overall focal length has been chosen on the basis of the relative sizes of the Airy disk (diffraction image of the beacon) and the radius of the tip of the beam-splitting pyramid in the fine pointing sensor. Past experience has shown such radii to be on the order of 0.0001 inch. The chosen focal length (750 inches) produces

an Airy disk of 0.0015-inch diameter. The overall focal ratio is f/25, with a f/4.16 primary mirror, a secondary magnification of 3X, and a transfer lens magnification of 2X.

4.5.5 USE OF MAIN OPTIC AS BOTH RECEIVER AND TRANSMITTER

In order to provide isolation between the incoming (Earth beacon) and outgoing (spacecraft laser) beams, the main optical system utilizes an interference coating-type beam splitter that is designed with a high reflectivity at the beacon wavelength (to illuminate the fine pointing sensor) and a high transmissivity at the spacecraft laser wavelength. An efficiency of 75 percent in performing each of these functions is within state of the art.

4.5.6 INTRODUCTION OF POINT-AHEAD ANGLE

The transmitted beam can be offset from the received (tracking) beam by passing it through some type of deflection device which varies the laser image position in the focal plane of the main telescope. The mission requires a maximum offset of 75 arc-seconds with a resolution of about 0.01 arc-second; this is about one part in 7500. As the system is presently configured, the maximum deflection in the focal plane of the telescope is therefore

$$d = (75 \text{ arc-sec})\,(5 \times 10^{-6} \text{ rad/arc-sec})\,(750 \text{ in.}) = 0.28 \text{ in.} = \pm 0.14 \text{ in.} \qquad (4\text{-}13)$$

Similarly, the resolution required for a 0.01 arc-second pointing error is

$$r = (0.01 \text{ arc-sec})\,(5 \times 10^{-6} \text{ rad/arc-sec})\,(750 \text{ in.}) = 37.5 \text{ microinches}$$

Several techniques could be used to provide the desired deflection:

a. Appendix B discusses in detail the tilting plate which operates by the principle of refraction. This technique has the advantage of producing small deflections of the laser beam for relatively large rotations of the tilting plate. The disadvantage of this technique is that the system is driven out of focus by the rotation of the tilting plate; this must be corrected for by movement of the lens between the tilting plate and the laser, which is used to focus the beam whether or not the tilting plate is present.

b. The lens near the laser can be translated to implement the point-ahead angle. However, the laser image deflection to lens translation is one-to-one under this technique, and achieving the desired resolution in beam deflection would be very difficult.

c. Still another approach is through an electro-optical deflector - a crystal which deviates a light beam through application of a high voltage electric field. However, this technique requires precise control of very high (multikilovolt) voltages.

Because the latter two techniques show little promise of achieving the high resolution required over a wide operating range, the tilting plate was chosen as the preferred design. The tilting plate must be rotated about two axes to achieve the two orthogonal components of the point ahead angle, and the corrective lens must be moved along the optical axis to maintain diffraction limited operation. A detailed discussion of the feasibility of the tilting plate-corrective lens combination is included in Appendix F of this report.

4.5.7 SELF-ALIGNMENT TECHNIQUE

The interference coating-type beamsplitter shown in Figure 2-1 will not transmit 100 percent of the laser radiation, but will reflect some fraction of it. In normal operation, this stray energy must be absorbed to avoid introduction of background noise into the fine error sensor. At the time of initial acquisition, however, the effects of misalignments that have accumulated as a result of launch stresses, thermal deformation, and component and structural aging can be minimized if the "zero point-ahead" position of the transmitted beam can be brought into coincidence with the null axis of the fine pointing sensor.

This can be achieved by directing the laser radiation reflected from the beam splitter to the fine error sensor by means of a concave spherical mirror. A shutter would be provided to enable this type of operation when desired, and filters or other attenuators would be used to provide a satisfactory image intensity at the sensor. In the presence of a null offset error, the sensor output will drive the point-ahead tilting plate to an angle that will null the laser's image at the sensor. This angle then becomes the "zero point-ahead" in the computation of the tilting plate angle and corrective lens position (both are non-linear functions of point-ahead angle).

4.5.8 SERVOED OPTICS FOR FINE POINTING

The fine pointing function can be separated from the spacecraft attitude control system by the use of a servoed optical element that is free to move with respect to the main telescope and through which both the transmitted and tracking beam pass. Devices of the type described above for "point ahead" are also useful for fine pointing, with the tilting plate again the most promising candidate. Though high resolution is still required, the total range of operation of the servoed optics control loop can be greatly reduced from that required of the spacecraft, probably to only a few arc-seconds.

The advantages of the use of servoed optics over control of the entire spacecraft for fine pointing include:

a. The spacecraft frame would not need to be controlled to the high accuracy imposed upon the attitude control system by the narrow (0.2 arc-second) laser beamwidth, but rather to slightly less than the range of operation of the servoed optics.

b. Because the tilting plate is a low inertia device (when compared to the inertia of the entire spacecraft), the servoed optics loop should be capable of a faster response. Since the major disturbance torques in Mars orbit (the gravity gradient and solar pressure torques) are slowly varying, the faster response would be of advantage only during station switching and in case of micrometeorite impact. However, all available information (see Section 4.1 of this report) indicates that the probability of a micrometeorite impact of sufficient force to require a response faster than that possible through control of the entire spacecraft for fine pointing is too small to be of concern. Furthermore, the spacecraft-to-Earth high data rate communications link will be lost for only a few seconds during station switching if the entire spacecraft is controlled for fine pointing. Therefore, the faster response capability of the servoed optics loop is of very questionable value.

The disadvantages of the use of servoed optics are:

a. The tilting plate used in the servoed optics technique is an additional element through which the spacecraft laser beam must pass, causing power losses on the order of 7 to 10 percent, via reflection at the glass-vacuum interfaces. This will lead to further problems:

1. Both the spacecraft laser and power supply must be increased in size and weight to provide the necessary effective radiated power.

2. The power losses are undesirable from a thermal point of view.

b. The complexity of the fine pointing function is increased:

1. Three extra control loops are added by the use of servoed optics - two loops for the two axes of tilting plate rotation and one for corrective lens position control.

2. While the tilting plate angle can be controlled by a simple closed loop servo, the corrective lens must be controlled to a complicated function of the tilting plate angle (actually the vector sum of the two tilting plate angles) because the divergence from diffraction limited operation cannot be measured on board the spacecraft. Therefore:

a) The computation requirements on board the spacecraft are increased.

b) The time lag between tilting plate movement and correction by the lens due to the time involved in making the corrective lens position computation and the response time of the corrective lens servo loop is of concern, since the telescope will be somewhat off diffraction limited operation during that time.

c. The faster response of the servoed optics is severely limited by the pulse repetition rate of the Earth beacon. The prf of 20 Hz will limit the frequency response of the servoed optics on the order of 2 Hz, while a frequency response of this order is attainable through control of the entire spacecraft for fine pointing.

Because the potential faster response of the servoed optics loop is not realizable in fine pointing and not significantly advantageous in station switching, and because of the additional complexity introduced by servoed optics, and also because of the associated power losses of the additional optical element, no net advantage of servoed optics over control of the entire spacecraft for fine pointing can be substantiated.

4.6 SPACECRAFT CONTROL SYSTEM CONCEPTS

The criterion employed in evaluating candidate control system concepts, formulated to perform the Mars Orbiter laser communications mission, was one of determining that concept which provided the best assurance of mission success. The mission performance

desired required examination of difficult design problems in several spacecraft system areas and consideration of their interaction in order to present a practical solution to the spacecraft control problem.

The unique requirements for precise but variable angular offset of a laser beam (to an accuracy of the order of 0.5×10^{-5} degrees of arc) relative to a reference system established aboard the spacecraft, which itself must be controlled within the same degree of accuracy to an Earth beacon moving in inertial space, demands the ultimate in alignment accuracy and control between the two functions. A design problem comparable in magnitude is the thermal control necessary to maintain thermal stability of the structure between the laser fine pointing attitude sensors and the laser beam control optics. It was these design problems that were dominant in the selection of the spacecraft control concept for detailed analysis and evaluation.

The spacecraft control system options considered were as follows:

a. Stabilize the spacecraft and fixed telescope to the attitude reference.

Pitch:	± 0.035 arc-sec.
Yaw:	± 0.032 arc-sec.
Roll:	±7 arc-sec.

Implement laser beam point-ahead relative to the attitude reference furnished by the spacecraft optical axis and fine pointing sensor.

Pitch:	± 0.023 arc-sec.
Yaw:	±0.023 arc-sec.

Slew spacecraft during station switching.

Yaw:	15 arc-sec. max.
Pitch:	1 arc-sec. max.

b. Stablize the spacecraft and fixed telescope to the attitude reference:

Pitch:	1 arc-sec.
Yaw:	1 arc-sec.
Roll:	15 arc-sec.

Stablize optical attitude reference axis to the attitude reference with servoed optics:

Pitch:	± 0.03 arc-sec.
Yaw:	± 0.03 arc-sec.
Roll:	± 7 arc-sec.

Implement laser beam point-ahead relative to the attitude reference established by the attitude reference servoed optics:

Pitch:	± 0.023 arc-sec.
Yaw:	± 0.023 arc-sec.

Slew spacecraft during station switching:

Yaw:	15 arc-sec. max.
Pitch:	1 arc-sec. max.

c. Stablize spacecraft and fixed telescope to the attitude reference:

Pitch:	± 0.03 arc-sec.
Yaw:	± 0.03 arc-sec.
Roll:	± 7 arc-sec.

Implement point-ahead with a gimballed telescope.

Pitch:	± 0.023 arc-sec.
Yaw:	± 0.023 arc-sec.

The third concept was rejected on the basis that two telescopes would be required with two degrees-of-freedem provided between them. The complex alignment problem between the two optical systems would be virtually impossible, and the additional telescope weight caused this concept to be rejected.

The first concept was favored over the second since spacecraft control to the accuracies required in an environment of extremely low external disturbance torques can be attained

with state-of-the-art hardware with the exception of a modest improvement in gyro performance. The spacecraft control system avoids the complexity of a servoed optics subsystem required by the third concept to maintain the attitude reference within limits. Since attitude control of the spacecraft to the Earth beacon and Canopus references can be achieved with the spacecraft attitude control system, additional complexity is unwarranted. This concept features the maximum optical transmission since it minimizes the number of optical elements in the light path. Associated with this feature is the very important fact that the laser power requirements are less, which is important because of the extremely difficult thermal control problem. Additional optical elements in the light path for servo control of the attitude reference would cause up to 15 percent transmission loss in the outgoing spacecraft laser beam requiring additional laser power of up to 300 watts to be dissipated. The complexity of the control of an attitude reference servoed optics control is discussed in detail in Section 4.5.8. The difficult nonlinear servo problem in the second concept,without any significant improvement in response, would seem to make it inferior to the selected concept.

Servoed optics may be used to best advantage in applications requiring fine pointing stabilization, of the order of precision required here, where impulse type disturbances are present and the response is not limited by the error sensing mechanism. A manned astronomical observatory is an example of such a mission. It should be noted, however, that even in such an application the response may be limited by sensor noise.

4.7 CONCEPTS FOR ACQUIRING EARTH-BASED RECEIVER WITH SPACECRAFT LASER BEAM

4.7.1 INTRODUCTION

In the Earth-Mars laser communications mission, the spacecraft laser will be pointed ahead with respect to the received illumination from the Earth beacon to illuminate the appropriate Earth-based receiver. However, due to the uncertainty in the position of the receiver on Earth relative to the spacecraft in orbit about Mars (on the order of 0.5 arc-second) and because of a slight deformation of that part of the spacecraft optical

system used to implement the point-ahead, it is probably too optimistic to hope that the spacecraft laser can illuminate the appropriate Earth-based receiver on the first try during acquisition using pre-computed point-ahead information. In addition, there may also be drifts associated with spacecraft control system and optical system paramenters during the six-month period of the mission. Their cumulative effect will deteriorate the essentially open loop pointing of the spacecraft laser transmitter.

Because of these considerations, it will be necessary to determine the spacecraft laser pointing error during acquisition and periodically throughout the mission so that the spacecraft laser pointing accuracy can then be improved. It will be assumed for illustration purposes that the uncertainty in pointing the spacecraft laser is a total solid angle of 4 arc-seconds. This number is chosen only for purposes of analysis, but it can be seen to be much greater than the component of error introduced by the uncertainty (approximately 0.5 arc-second) in relative positions of the Earth station and Mars orbiting probe.

4.7.2 CONICAL SCAN TECHNIQUE

In the conical scan technique, the spacecraft laser beam centerline is slowly rotated through a circular path as shown below. The radius of the circle of the laser beam centerline relative to the computed point-ahead direction is equal to one-half the uncertainty in the computed point-ahead angle.

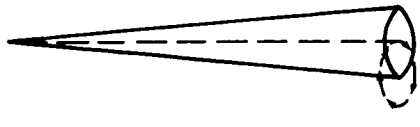

It can be seen that the entire area of uncertainty will be covered during the scan if both the laser beamwidth and the total solid angle defined by the path of the beam centerline are equal to one-half the angular uncertainty in pointing the spacecraft.

In the implementation, the scanning will actually be superimposed upon the movement of the beam centerline due to the relative motion of the Earth receiver and the spacecraft. As the spacecraft laser beam is rotated through the scan pattern, the signal intensity at the Earth receiver will vary unless the Earth station is located in the center of the circle of scan, because the spacecraft laser transmitted power varies with angle from the beam centerline as shown in Figure 4-5.

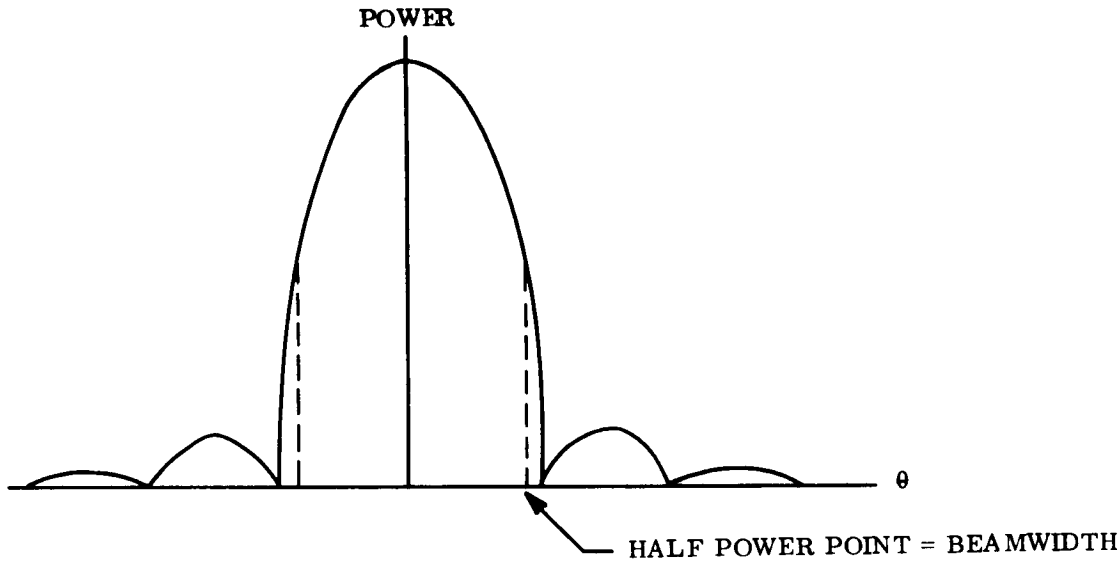

Figure 4-5. Spacecraft Laser Transmitted Power

Based upon the time correspondence between the variation in intensity of the received signal and information as to where the spacecraft laser is in its scan pattern, the receiving station position in the scan, and thus the error in pointing of the spacecraft laser, can be determined.

It remains only to show that this can be done with high accuracy. The signal power received at the Earth receiver detector when the detector is within the laser beamwidth half-power points is at least:

$$P_{sr} = \frac{K_1 K_2 K_3 K_4 P_t D_r^2}{2 R^2 \theta_t^2} \qquad (4\text{-}14)$$

where

K_1 = transmissivity of the transmitting optic (≈ 0.4)
K_2 = transmissivity of the receiving optics (≈ 0.4)
K_3 = transmissivity of the narrow band optical filter in the receiver (≈ 0.4)
K_4 = transmissivity of the Earth's atmosphere (≈ 0.6)
P_t = transmitter power radiated
D_r = receiver antenna aperture
R = transmitter-to-receiver range $\approx 10^8$ miles for Mars-to-Earth
θ_t = transmitter half-power beamwidth

For P_t = 10 watts, D_r = 200 inches, and θ_t = 2 arc seconds, $P_{sr} = 1.9 \times 10^{-12}$ watts. This corresponds to a photon arrival rate, $\bar{N}_s$, of 4.7×10^6 photons/second.

The signal-to-noise ratio at the Earth-based detector is given by:

$$\frac{S}{N} = \left[\frac{n \bar{N}_s}{2.4 \Delta f}\right]^{1/2} \qquad (4\text{-}15)$$

where

n = detector quantum efficiency (≈ 0.3)
$\bar{N}_s$ = photon arrival rate = 4.7×10^6 photons/second
Δf = electrical bandwidth of the receiving channel

A value of Δf of 30 Hz will be assumed, since the spacecraft laser can be modulated during scan so that the major part of the modulation is within that bandwidth. The resultant signal-to-noise ratio is approximately 90. Since such a signal-to-noise ratio

is more than adequate for the Earth receiver to determine accurately the variations in signal intensity, power considerations in no way limit the implementation of the conical scan.

The only remaining consideration in determining the feasibility of the conical scan is whether the scan can be implemented by the spacecraft optics. However, the conical scan is is no more than a two-dimensional variation of the point-ahead angle. Since the point ahead angle must be implemented with an accuracy of 0.02 arc-second, if the point-ahead angle can be implemented, the conical scan technique is deemed possible.

Therefore, there is no apparent reason why the conical scan cannot be implemented.

4.7.3 USE OF AUXILIARY GROUND RECEIVER

In this technique the spacecraft laser beamwidth is increased to the size of the area of uncertainty. Scattered about the intended receiving optic are smaller telescopes, as shown below. Such a configuration would be required at only one Earth station.

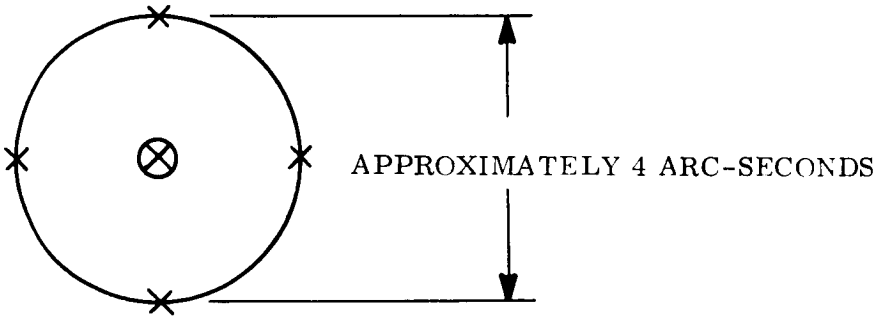

The center of the spacecraft laser beam will be somewhere within the pattern of receivers. Since the signal intensity decreases with increasing angle from the beam centerline, the signal intensity at each receiver can be measured, with the result that the center of illumination and thus the error in pointing the spacecraft laser can be determined.

The size of the auxiliary receivers must be determined to demonstrate the feasibility of this technique. As before, an electrical bandwidth of 30 Hz is assumed adequate. A signal-to-noise ratio of 10 will be assumed adequate to detect variations in intensity at the different receivers. Then, since

$$\frac{S}{N} = \left[\frac{n\,N_s}{2.4\Delta f}\right]^{1/2} \tag{4-16}$$

$$\bar{N}_s = \frac{2.4\Delta f}{n}\left(\frac{S}{N}\right)^2 \tag{4-17}$$

$$= 2.4 \times 10^4 \text{ photons/second} \tag{4-18}$$

This is equivalent to a received power of 9.75×10^{-15} watts at 5000 Angstroms.

$$P_{sr} = \frac{K_1 K_2 K_3 K_4 P_t D_r^2}{2 R^2 \theta_t^2} \tag{4-19}$$

results in

$$D_r = R\,\theta_t \sqrt{\frac{2P_{sr}}{K_1 K_2 K_3 K_4 P_t}} \tag{4-20}$$

$$= 28.2 \text{ inches} \tag{4-21}$$

Thus, an aperture of approximately 30 inches would be required for each of the auxiliary receivers.

4.7.4 CONCULSIONS

Both the conical scan and auxiliary receiver techniques of determining the spacecraft laser pointing error are feasible for reasonable pointing error. However if the uncertainty in pointing of the spacecraft laser is greater than ± 2 arc-seconds, the use of auxiliary receivers will not be practical due to the large apertures required for the auxiliary receivers.

The conical scan technique has the advantage that a minimum of additional hardware is required and better resolution is possible due to the use of the 200-inch receiving optic. An array of auxiliary receivers is advantageous in that the pointing error can be measured at least once per day (when the array is in the proper position) without the loss of high data rate transmission which occurs when the spacecraft laser goes into a scan mode.

SECTION 5

SPACECRAFT CONTROL SYSTEM DEFINITION AND MATHEMATICAL MODEL DEVELOPMENT

SECTION 5

SPACECRAFT CONTROL SYSTEM DEFINITION AND MATHEMATICAL MODEL DEVELOPMENT

5.1 SPACECRAFT CONTROL SYSTEM DESCRIPTION

The control system proposed for a Mars orbiting spacecraft capable of performance of high data rate laser communications to Earth station receivers while tracking a pulsed laser beacon located at the operational ground station is presented in this section of the report. The mission parameters, performance requirements, and system concepts formulated in Sections 3 and 4 and summarized in Section 2 are used as the basis for the spacecraft control system synthesized.

In accordance with the Precision Triaxial Attitude Control Study objectives, the detailed analyses and mathematical model development of the spacecraft control system has been limited to the Fine Pointing Mode and its acquisition, attitude hold during laser communications, and slewing between Earth stations as required by Earth rotation. These analyses are summarized in Sections 5.3 through 5.5, with references to supporting analyses and mathematical models reported in Appendixes D and E.

A discussion of the components associated with the control system is presented in Section 5.2.

The system proposed to perform spacecraft control functions from its injection into interplanetary trajectory until the completion of the laser communications mission from Mars orbit is delineated in block diagram form in Figure 2-3. As indicated in the block diagram and in Table 5-1, the system design philosophy adopted provides several control modes that:

a. Cover the wide dynamic range that is imposed on spacecraft control sensors and actuators by acquisition and fine-pointing requirements.

b. Are compatible with the attitude references selected for performance of the mission.

c. Permit spacecraft acquisition of and fine stabilization to the apparent direction of the Earth laser beacon and the star Canopus while point ahead of its laser transmission to the Earth receiver is accomplished with servoed optics.

Table 5-1. Spacecraft Attitude Control Modes

Control Mode	Attitude Reference	Function	Sensors		Torquers
Initial Acquisition	Sun and Canopus	Remove separation rates and attitude references	Pitch	Sun Sensors Gyro-rate mode	Mass Expulsion Actuators
		Roll axis to the Sun	Yaw	Sun Sensors Gyro-rate mode	
		Yaw axis in plane of the Sun, spacecraft, and Canopus	Roll	Coarse Canopus Trackers and gyro-rate mode	
Interplanetary Cruise	Sun and Canopus	Attitude Hold-Low power	Pitch	Sun Sensors	Mass Expulsion Actuators
		Roll axis to the Sun	Yaw	Sun Sensors	
		Yaw axis in plane of the Sun, spacecraft, and Canopus	Roll	Coarse Canopus Trackers Derived rate on all axes	
Inertial	Gyros	Provide the desired reference in space for a trajectory correction or injection into Mars orbit.	Pitch Yaw Roll	Gyro-position and rate mode Gyro-position and rate mode Gyro-position and rate mode	Mass Expulsion Actuators
Earth Acquisition	Earth and Canopus	Acquire the Earth reference	Pitch	Coarse Earth Sensor	Mass Expulsion Actuators
		Roll axis to Earth	Yaw	Coarse Earth Sensor	
		Yaw axis in plane of the Earth, spacecraft, and Canopus	Roll	Coarse Canopus Sensor and gyro	
Intermediate Pointing Mode	Earth and Canopus	Improve Pointing Accuracy to attitude references to permit capture of Fine Pointing Mode	Pitch Yaw Roll	Intermediate Earth Sensor Intermediate Earth Sensor Fine Canopus Sensor and gyro	Control Moment Gyros
Fine Pointing Mode	Earth-beacon and Canopus	Fine Pointing to Earth-beacon and Canopus to provide S/C reference for laser transmission to Earth station	Pitch Yaw Roll	Fine Earth Beacon Sensor Fine Earth Beacon Sensor Fine Canopus Sensor	Control Moment Gyros

The design concept chosen features a fixed primary optic operating as both a receiver of Earth beacon laser pulses and a transmitter of the spacecraft laser beam as described in Section 4.5. This chosen concept further defines the spacecraft roll axis as nominally coincident with the optical axis of the primary optic and the pitch and yaw axes orthogonal to it, as determined by the alignment of the Fine Earth Beacon Sensor to the primary optic. The alignment of all spacecraft control sensors and actuators to the appropriate axes so defined provides attitude control in all operating modes about these axes as summarized in Table 5-1. For ease in presentation, the control system will be considered in terms of its control modes in their normal operating sequence, the attitude reference employed during each mode, and the pertinent sensors and actuators operating during the mode.

5.1.1 CONTROL MODES DURING THE INTERPLANETARY TRIP TO MARS

The guidance and control of a spacecraft following separation from its transition stage that places it on an interplanetary trajectory to Mars until its injection into Mars orbit have essentially been accomplished by Mariner spacecraft or will be accomplished by Voyager spacecraft in the early 1970's. The technology is defined and the necessary hardware performance have been achieved. However, a brief treatment of the control system definition to perform this phase of the mission will be presented here for completeness and to identify equipment employed in this phase that may also be required during performance of control modes in Mars orbit.

After launch and spacecraft injection into its interplanetary trajectory to Mars, the unmanned spacecraft will be required to remove separation rates and acquire its celestial references for the cruise portion of the trip. The control definition proposed for this phase of the mission under study is the conventional one of acquisition of the Sun and Canopus. After separation, the control logic is automatically switched to the Initial Acquisition Control Mode. In this mode, "On-Off" control of the pitch and yaw mass expulsion actuators is achieved in response to attitude error signals from the 4π steradian field-of-view pitch and yaw sun sensors and signals from pitch and yaw body-mounted gyros operating in the rate mode. "On-Off" control of the roll mass expulsion actuators is achieved in response to rate signals from the roll rate gyros. Upon alignment of the roll axis to the Sun, within 1/4 degree, and reduction of initial rates below 0.05 degree per second, as detected by control Sun Gate position and rate logic, the spacecraft is automatically commanded to perform a roll search through introduction of a roll rate bias of the order of 0.1 degree per second in the roll channel. The acquisition of the star Canopus by the Coarse Canopus Tracker is completed upon receipt of a Canopus star presence signal by the roll search and acquisition logic, which removes the roll search signal and switches the Coarse Canopus roll error output signal to the roll mass expulsion switching amplifier. Initial acquisition is now complete, and the Cruise Control Mode is established when rates drop below 0.005 degree per second. In the Cruise Mode, gyros are switched off and control damping is supplied from derived rate in the control logic.

The Cruise Control mode employs Sun Sensors and the Coarse Canopus Tracker to sense attitude errors, mass expulsion actuators to provide "On-Off" control torques, and derived rate for control loop damping. This mode is maintained throughout the trip to Mars except for trajectory corrections or injection of the spacecraft into Mars orbit.

The inertial mode is used for positioning and holding the spacecraft to the proper inertial attitude during thrusting of the orbit correction and orbit injection rocket engine. In this mode the triad of body mounted gyros are switched to the position-plus-rate mode, and replace the Sun Sensors and Canopus Tracker as the spacecraft attitude reference sensors. The desired pointing of the roll axis in space for rocket engine thrusting is achieved through commanded program turns of the gyro attitude references which are followed up automatically by attitude control of the spacecraft to these references. That the rocket engine would be constrained to be mounted along the roll axis is a good assumption, since this mounting would provide the least difficulty to the primary optic, also aligned nominally to the roll axis. Upon completion of rocket engine thrusting, the spacecraft may be returned to its previous cruise attitude using the initial acquisition mode or performing the commanded turns in reverse order.

After injection into Mars orbit, the acquisition of the Earth by the Coarse Earth Sensor will be achieved in the Inertial Control Mode through proper commanded turns. Based on Mariner performance in which such maneuvers were performed with less than one degree of error, capture of the Earth by the Coarse Earth Sensor having a ± 2.5 degree field of view should be no problem. Reacquisition of Canopus after Earth acquisition should not be required since two spacecraft rotations may be used to alter the roll axis from the Sun to the Earth while maintaining Canopus in the field of view of the tracker. If acquisition of the Earth is lost at any time due to some large scale unexpected disturbance, reacquisition may be accomplished by returning to the Sun-Canopus references as previously described.

The control modes that will be operational up to Earth acquisition in Mars orbit described briefly in these paragraphs indicate quite a large commonality of equipment with control modes in Mars orbit. This will be discussed in Section 5.2.

5.1.2 COARSE AND INTERMEDIATE POINTING ATTITUDE CONTROL MODES

Performance of laser communications to an Earth receiver from a Mars Orbiter in accordance with the selected system concept requires attitude control of the spacecraft and its primary optic (roll axis) to the apparent position of an Earth beacon, to a pointing accuracy of approximately 10^{-5} degrees of arc. Coupled with the requirement for spacecraft acquisition of this beacon and Canopus references from a previous orientation to the Sun and Canopus, where the accuracy of reorientation of the spacecraft roll axis can be done with an accuracy of about one degree, indicates an Earth sensor field of view requirement of better than one degree. The greater than 10^{5} sensor dynamic range to final resolution ratio designates the need for several control modes.

The Coarse Earth Pointing Control Mode assures reliable spacecraft roll axis acquisition of the Earth at the completion of commanded turns away from the Sun performed in the Inertial Mode. The precomputed commanded spacecraft turns, performed at approximately 0.1 degree per second in response to precise torquing of the pitch and yaw body mounted gyros permit roll control to Canopus to be maintained via the Canopus tracker. This is true in the case of the pitch axis as the Canopus tracker has a large field of view about its non-measuring axis (spacecraft pitch), permitting limited spacecraft pitch rotation without losing Canopus from the field of view of the tracker. Spacecraft roll control to the Coarse Canopus Tracker error signals during yaw rotation is performed in the normal manner.

Upon spacecraft roll axis acquisition of the Earth by the Coarse Earth Sensor, as detected by the control logic in the form of an Earth presence signal from the Coarse Earth Sensor, the spacecraft pitch and yaw axis control is switched to the attitude reference signals furnished by the Coarse Earth Sensor, while the Coarse Canopus Tracker is retained for roll error sensing. Rate signals about all axes are provided by the body-mounted gyro triad operating in the rate mode, and control torques are furnished by mass expulsion

actuators. Spacecraft rates of less than 0.005 degree per second, pitch and yaw pointing error within 3.5 minutes of arc, and roll error to within 7.0 minutes of arc are well within the state of the art in this mode. Attitude control within these specifications permits acquisition of the Earth and Canopus by the Intermediate Earth Sensor and Fine Canopus Sensor within their linear range.

Spacecraft attitude control is switched to the Intermediate Earth Pointing Control Mode upon receipt by the control logic of:

a. An Earth presence signal from the Intermediate Pointing Earth Sensor.

b. A Canopus presence signal from the Fine Canopus Sensor.

c. Spacecraft rate signals below the threshold corresponding to 0.005 degree per second.

The Intermediate Earth Pointing Control Mode provides proportional control about all three axes. Control torques are provided by Control Moment Gyro momentum storage devices in response to analog error signals developed by the Intermediate Earth Pointing Sensor and the Fine Canopus Sensor. Since operation in this control mode is initiated with sensed attitude errors within the linear range of the attitude sensors, acquisition is an initial condition. Control operation in this mode is similar to the Fine Pointing Mode which will be described in detail in the next section.

5.1.3 FINE POINTING ATTITUDE CONTROL MODE

The control system for the Fine Pointing Attitude Control Mode is shown in block diagram form in Figure 2-4. It features a Fine Earth Beacon Sensor which utilizes the light-gathering power of the primary optic and is aligned relative to its optical axis as described in Section 4.5 and Figure 2-1. It senses pitch and yaw attitude error with a resolution of 0.02 arc-second (3σ)*, relative to the apparent direction of the Earth beacon, in conjunction with diffraction-limited operation of the primary optic, and has response characteristics capable of sensing the 0.1-microsecond pulse-width laser beacon. Roll attitude

*Derived in Section 4.2.3 from S/N ratio of 60 derived in Section 3.6.2, Page 3-43.

errors are sensed by the Fine Canopus Sensor. Characteristics of the Fine Canopus Sensor and the Fine Earth Beacon Sensor, including its associated hold circuit to convert the pulsed output of its detectors to a continuous analog signal, are discussed in Section 5.2, with references to Appendix A.

Spacecraft control torques in this control mode are provided about the pitch and yaw axes by highly damped twin two-degree-of-freedom control moment gyro momentum exchange actuators. The uncompensated transfer function to achieve control about the spacecraft yaw axis for highly damped twin two-degree-of-freedom control moment gyro actuators as derived in Appendix E is:

$$\frac{\theta_y}{T_b} = \frac{2\,h\cos b}{I_y D_b \left(1 + \frac{I_c}{D_c} S\right) S^2} \tag{5-1}$$

and the pitch axis open-loop response as a function of inner and outer gimbal angles, since a single axis transfer function cannot be presented due to residual coupling from the y axis, as derived in Appendix E is:

$$\theta_z = \frac{2h\,(T_c \cos b \cos c - T_b \sin b \sin c)}{I_z D \left(1 + \frac{T_c}{D_c} S\right) S^2} \tag{5-2}$$

The high-response, low-open-loop gain characteristics inherent in the chosen configuration, as exhibited by the (vehicle angle)/(torque to CMG gimbal) transfer functions (Equations 5-1 and 5-2) are optimum when one considers:

a. The inherent very high gain required in the control loop, from attitude error sensing to the developed CMG gimbal torque, to make errors due to CMG gimbal axis friction and external disturbance torques negligible (see Appendix C).

b. The limitation imposed on control bandwidth by the sampling associated with the pulsed laser input.

Roll control torques are provided by twin single-degree-of-freedom gyros. This configuration suits the requirement for control about this single-vehicle axis, since the accuracy requirements are two orders of magnitude less severe and the control bandwidth limitation of a sampler is absent.

Analyses and mathematical models of the three-axis attitude control loops used in this control mode are presented in Section 5.4. Mathematical models of the control moment gyros are given in Section 5.3, with references to Appendices D and E. Control laws and compensation derived by these system analyses in conjunction with the sensor and torquer characteristics formulated were the bases for the system synthesized. Excerpts from these analyses in the form of control laws for the Fine Pointing Yaw and Pitch Attitude Control Loops, using highly damped twin two-degree-of-freedom control moment gyros, are given below and will be used in the discussion of the operation of this control mode.

Inner Gimbal Torques

$$T_{b3} = \frac{K\,(1+T_1S)}{(1+T_2S)}\,\theta_y^S - D_b\dot{B}_3 - M\,(B_3+B_4) + \begin{cases} K_{RL}\,\left[\omega_y - db\ \text{sign}\ (\omega_y)\right] & \text{if } |\omega_y| > db \\ 0 & \text{if } |\omega_y| \le db \end{cases} \tag{5-3}$$

$$T_{b4} = \frac{-K(1+T_1S)}{(1+T_2S)}\,\theta_y^S - D_b\dot{B}_4 - M\,(B_3+B_4) - \begin{cases} K_{RL}\,\left[\omega_y - db\ \text{sign}\ (\omega_y)\right] & \text{if } |\omega_y| > db \\ 0 & \text{if } |\omega_y| \le db \end{cases} \tag{5-4}$$

Outer Gimbal Torques

$$T_{c3} = \frac{-K(1+T_1S)}{(1+T_2S)}\,\theta_z^S - D_c\dot{C}_3 - M\,(C_3+C_4) + (T_{b3}+D_b\dot{B}_3)\tan B_3 \tan C_3 - \begin{cases} K_{RL}\,\left[\omega_z - db\ \text{sign}\ (\omega_z)\right] & \text{if } |\omega_z| > db \\ 0 & \text{if } |\omega_z| \le db \end{cases} \tag{5-5}$$

$$T_{c4} = \frac{K\,(1+T_1 S)}{(1+T_2 S)}\,\theta_z^S - D_c\dot{C}_4 - M\,(C_3+C_4) + (T_{b4}+D_b\dot{B}_4)\tan B_4 \tan C_4$$

$$+ \begin{cases} K_{RL}\left[\omega_z - db\ \text{sign}\ (\omega_z)\right] & \text{if } \omega_z > db \\ 0 & \text{if } \omega_z \le db \end{cases} \qquad (5\text{-}6)$$

The established value for the various parameters are:

$$K = 7.5 \text{ lb-ft/arc-sec}$$
$$T_1 = 0.5 \text{ sec}$$
$$T_2 = 0.05 \text{ sec}$$
$$D_b = D_c = 100 \text{ lb-ft/rad/sec}$$
$$M = 0.1 \text{ lb-ft/deg}$$
$$K_{RL} = 10 \text{ lb-ft/arc sec/sec}$$
$$db = 0.805 \text{ arc sec/sec}$$

An explanation of the various control law terms given in Equations 5-2 through 5-6 and shown in block diagram form in Figure 2-4 follows:

In the control law for each gimbal torque motor, a term involving the product of a large viscous damping constant and a gimbal rate term ($D\dot{B}$ or $D\dot{C}$) appear. These terms are present merely to give the gyros the desired highly damped characteristic. This is discussed in more detail in the "Feedback Loops for Parameter Control" section of Appendix E.

Terms of the form $K\,\frac{(1 + T_1 S)}{(1 + T_2 S)}\,\theta_i^S$ indicate that information from the attitude sensor θ_i^S is processed through a series compensation network. The value of K = 7.5 lb-ft/arc-sec was chosen because of the sensor characteristic and the initial conditions of acquisition.

The terms $M\,(B_3+B_4)$ and $M\,(C_3+C_4)$ are introduced in order to ensure that the corresponding gimbal angles are equal in magnitude and opposite in sign. If this condition is not

met, these terms are nonzero and provide corrective feedback torques until the constraint is satisfied.

The terms of the form $K_{RL}\left[\omega_i - \text{db sign}\,(\omega_i)\right]$ were added to shorten the acquisition and slewing times and to allow for a very large design safety factor with respect to the tolerable acquisition initial conditions. Without these terms (which would not be present if vehicle rate gyros failed), the previously described compensation network will successfully acquire with the worst expected initial conditions. However, due to the limited linear range of the sensor, derived rate information from the lead network exists only in the linear region near null, meaning that many overshoots are experienced during settling.

The remaining terms involving functions of gimbal angles are required to completely decouple the two axes.

Having completed the definition of the pitch and yaw axis fine-pointing control loops, operation during acquisition and attitude hold will be discussed briefly. It may be noted here that control during station switching is a mild form of acquisition, since the initial conditions of attitude error and rate are less severe.

Spacecraft attitude control is switched to the Fine Pointing Control Mode from the Intermediate Pointing Mode upon receipt by the spacecraft control logic of:

a. Signals from the pitch and yaw channels of the Intermediate Earth Pointing Sensor corresponding to pitch and yaw errors of less than 5 arc-seconds.

b. An Earth beacon presence signal from both pitch and yaw channels of the Fine Earth Beacon Sensor.

c. Signals from the spacecraft body-mounted gyros operating in the rate mode indicating spacecraft rates of less than 10 arc-seconds per second.

d. A signal from the Fine Canopus Sensor indicating a roll error of less than 14 arc-seconds.

e. Signals from the Control Moment gyros indicating gimbal angles of less than 10 degrees. (Reset of gimbal angles to zero through operation of mass expulsion actuators prior to mode switching is programmed if this condition is not within limits.)

Operation in the Fine Pointing Control Mode will begin with roll control maintained to the star Canopus through operation of roll single-degree-of-freedom control moment gyros in response to tracker error signals. Pitch and yaw channels of the Fine Pointing Beacon Sensor will most probably be in saturation as a result of the orientation of the roll axis to the Earth's center in the previous Intermediate Pointing Mode. Since the attitude sensor is roughly linear up to 0.2 arc-seconds where the signal saturates until the field of view is exceeded (see Figure 5-1), acquisition of the linear range should be accomplished well within the 90-arc-second field of view.

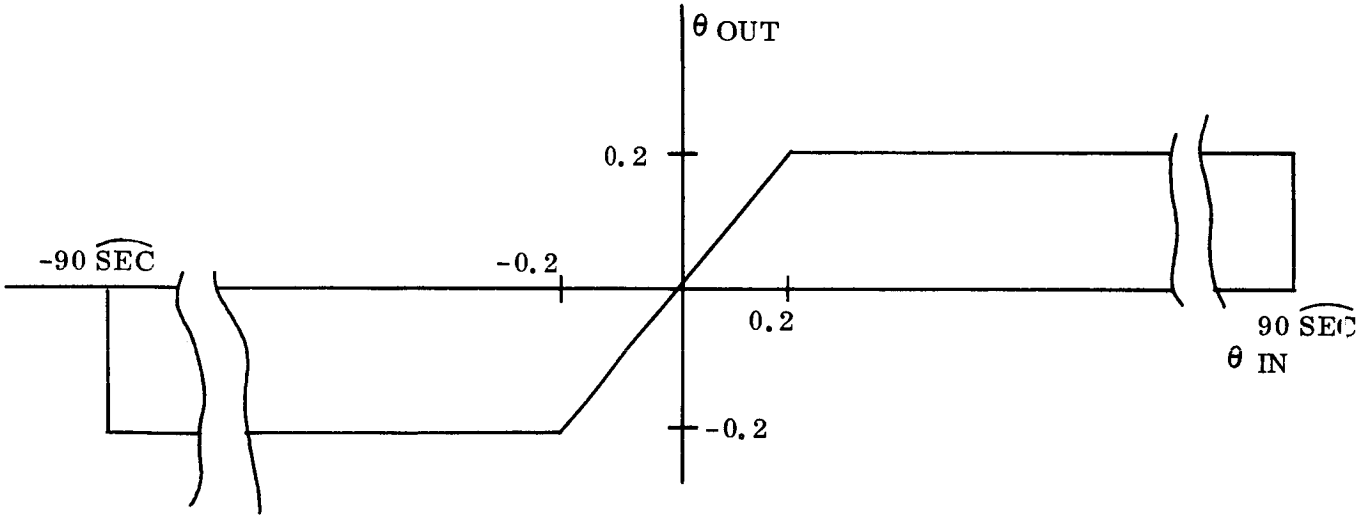

Figure 5-1. Sensor Input - Output Characteristic

Considering yaw axis control and referring to the simplified single-axis block diagram of Figure 5-2, the effect of the dominant loops may be noted. Acquisition is accomplished by combining the rate signal from the vehicle body-mounted yaw gyro, the yaw attitude error signal from the beacon sensor, and the rate signal from the CMG inner gimbal, in the CMG Inner Gimbal Torque Motor Control Amplifiers, where CMG torque motor commands

are derived. For the initial conditions considered, the amplifier would be saturated. It would command maximum control torques to be applied to both CMG inner gimbal torque motors of the twin two-degree-of-freedom CMG configuration, causing the inner gimbals to move and producing torques about the spacecraft yaw axis. (In this configuration the outer gimbals are aligned to the spacecraft yaw axis.)

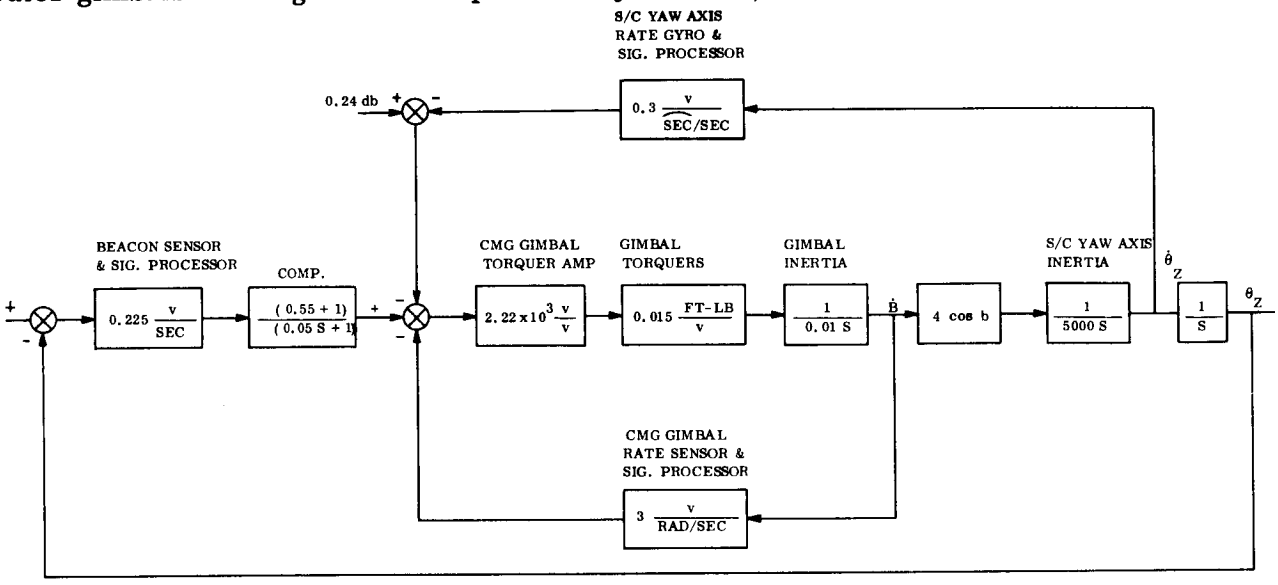

Figure 5-2. Simplified Block Diagram of Yaw Axis Fine Pointing Control Loop

The CMG gimbal dynamics are dominated by the viscous damping term. Thus a saturated sensor signal calling for 1.5 lb-ft of torque (0.2K) will very quickly generate a gimball rate of approximately $\frac{K\theta S}{D} = 0.015$ radian/second. The response time constant is I/D = 0.0001 second. The above gimbal rate exchanges momentum rapidly enough with the spacecraft so that the initial peak overshoot from the worst acquisition initial conditions (15 arc-sec error, 10 arc-sec/sec rate increasing the error) remains well within the field of view of the sensor. Note that to get the above-mentioned gimbal rate, it is not necessary to use a torque motor that can generate 1.5 lb-ft. of torque. This is because we have chosen to also have the torque motor generate the damping torque, thus the gimbal is accelerated by the difference. To illustrate this point, we purposely have chosen to have the amplifier that drives the torque motor saturate at a signal equivalent to 0.3 lb-ft. Therefore, a saturated sensor signal will accelerate the gimbal at $\frac{T_{sat}}{I} = \frac{0.3}{0.01} = 30$ radians/sec^2 until sufficient gimbal rate is developed to bring the amplifier out of saturation. Thus a smaller torque motor may be used with little sacrifice in response time. The vehicle rate

gyro helps to keep the amplifier in saturation until the vehicle rates are reduced below 0.8 arc-second per second as shown in Figure 5-3. When vehicle rates are reduced below this value, loop damping is provided by the series compensation network when the sensor is operating in its linear range.

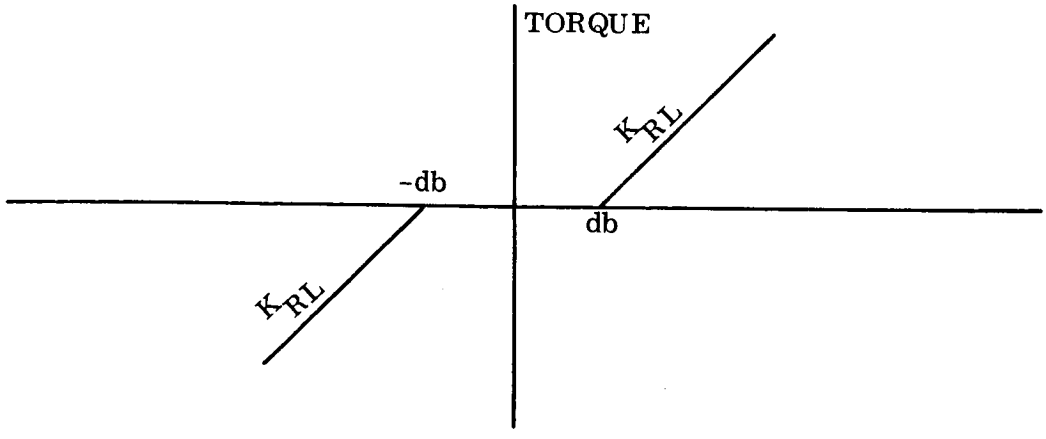

Figure 5-3. Torque Versus Vehicle Rate

Initial acquisition of the Fine Earth Beacon Sensor linear range in pitch is the same as in yaw with the exception that less attitude error exists as an initial condition.

Attitude hold in the Fine Pointing Control Mode is accomplished after the linear range of the sensor is acquired in both pitch and yaw, and pointing errors are reduced to 0.035 arc-second and 0.032 arc-second, respectively, through CMG operation in response to sensed attitude errors. The attitude control loop gain is high enough in each axis to make standoff errors due to friction on CMG gimbal axes and external disturbance torques negligible. The minor loops that keep corresponding gimbal angles equal in magnitude but opposite in direction and the uncoupling loops prevent cross coupling between axes and maintain the required pointing precision. Initiation of reset of the control moment gyros is required when gimbal angles exceed 45 degrees. An unloading jet torque of 0.01 ft-lb is provided in response to a logic command indicating reset is required.

Definition of the Fine Pointing Attitude Control Loop for the Roll axis is given in Figure 5-4.

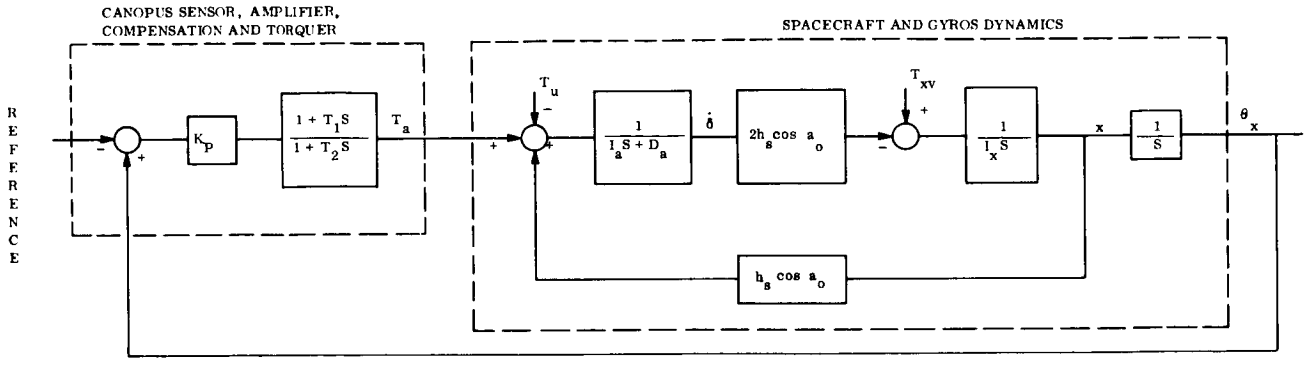

Figure 5-4. Block Diagram of Fine Pointing Attitude Control of Roll Axis

The control torque (torque applied by the gyro torque motor to the gimbal) is usually a function of the measurable state variables of the dynamic process. Because the purpose of the Fine Pointing Mode is that of attitude hold, the control torque is a function of the attitude error as measured by a Canopus Sensor. The static characteristics of the Canopus Sensor are shown in Figure 5-5.

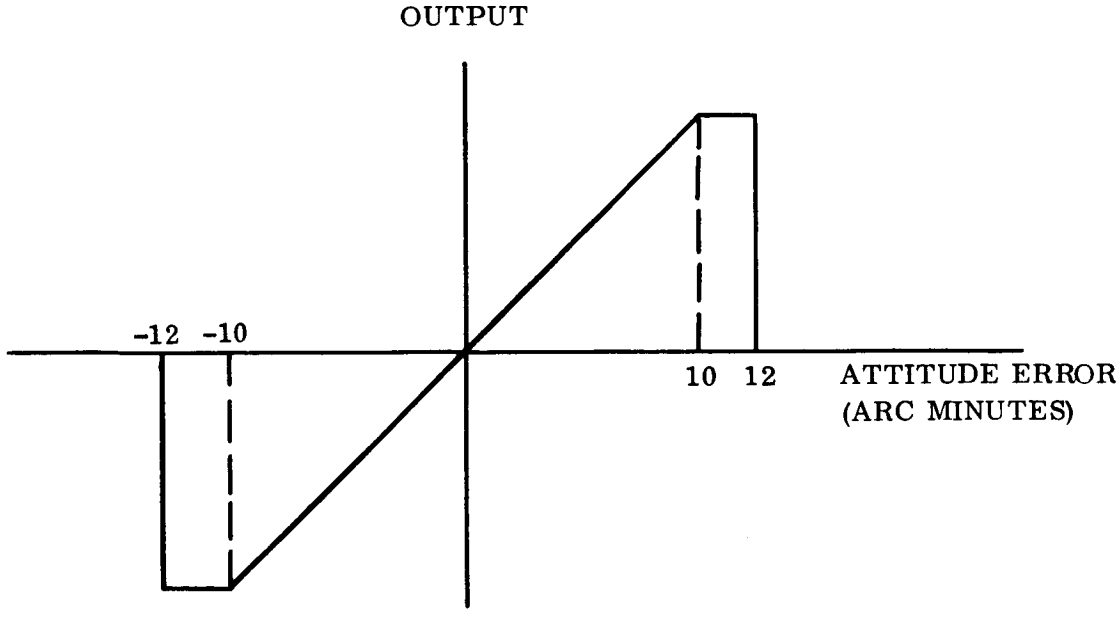

Figure 5-5. Static Characteristic of Canopus Sensor

The design of the roll axis control system was based upon selecting parameters to meet realizable hardware constraints coupled with obtaining both acceptable steady state and transient performance.

The system parameters used are as follows:

h_s = 2 ft-lb-sec (The control moment gyro angular momentum)

I_x = 5000 ft-lb-sec^2 (The spacecraft inertia about the roll axis)

$\frac{h_s}{I_a}$ = 2000 rad/sec $\longrightarrow I_a = 10^{-3}$ ft-lb-sec^2 (CMG gimbal inertia)

$\frac{D_a}{I_a}$ = 10 rad/sec $\longrightarrow D_a = 10^{-2}$ ft-lb/rad/sec (CMG gimbal damping)

$K_p = 5 \times 10^{-4} \frac{\text{ft-lb}}{\text{arc-sec}} = 100 \frac{\text{ft-lb}}{\text{radian}}$

$T_1 = \frac{1}{1.5}$ sec

$T_2 = \frac{1}{15}$ sec

The parameters used for the gyros and their torque motors are within present day state of the art while insuring a roll axis pointing accuracy of 1 arc-second.

The design analysis given in Section 5.4 established the feasibility of using two single-degree-of-freedom control moment gyros for fine roll control of the Mars orbiting spacecraft. The roll attitude control system is capable of acquiring from attitude errors within the Canopus Sensor's field of view.

It was seen from both the transient and steady-state performance that the gimbal damping is a critical design parameter and can be selected to satisfy both criteria. Also, the amount of damping needed can be accomplished with a standard eddy current damper. Unlike the pitch/yaw attitude control system, tachometer feedback of gimbal rate was not necessary.

5.1.4 CONTROL OF LASER BEAM POINTING

Having established spacecraft attitude control to the apparent direction of the Earth-based beacon and the star Canopus within the specifications for attitude hold (Table 2-5), it remains to intercept the Earth receiver with the spacecraft laser beam to begin the primary function of the mission. It is evident that the spacecraft laser beam must be angularly offset about the pitch and yaw axes established in the Fine Pointing Control Mode to accommodate the movement of the receiver with respect to the Mars Orbiter. The selected control concept for this mode defines the primary optic rigidly attached to the spacecraft structure to serve as both a receiver of Earth beacon radiation and a transmitter of the spacecraft laser beam in which the beam-pointing function can be separated from the attitude control system by use of a servoed optical element.

The approach proposed, shown in Figure 2-1, offsets the transmitted beam from the received beam (the Earth beacon pulsed laser) with a servoed tilting plate which varies the transmitted laser image position in the focal plane of the main telescope. Since offsets are required about both the pitch and yaw axes to provide the correct point-ahead, the tilting plate must be controlled about each of these axes. Since these angles are time varying and are a function of the position of the spacecraft and ground station relative to the celestial coordinate reference system and the relative velocity between them and the reference system, a complex mathematical model would be required for computation. It is likely that, due to uncertainties in ephemeris and spacecraft orbit tracking data, learning would be required through several spacecraft acquisitions of the ground station to improve the point-ahead computation model. Such modeling can best be performed on the ground. Thus, the selected approach proposed here is to compute the point-ahead angles on the ground and to transmit a point-ahead program to the spacecraft digital computer that is a function of the required position of the servoed optical elements and time.

Implementation of the servoed optics to perform the point-ahead function and to perform corrections to maintain diffraction limited operation of the optics is described in detail in Appendix F. The servo analysis of the proposed control loops is given in Section 5.4.

5.2 SPACECRAFT CONTROL SYSTEM COMPONENTS

5.2.1 SENSORS

The type and characteristics of various star trackers, Earth trackers, laser beacon trackers, gyros, etc., were considered in parallel with the formulation of control concepts in accordance with the tasks of the work statement. Upon selection of a mission as a basis for the precision triaxial control study, it was possible to formulate a control philosophy and identify components required for various control modes. This was summarized in Table 5-1.

Considering the electro-optical sensors required, no significant differences have been found between the requirements for star trackers and the requirements of a laser tracker. Over interplanetary ranges, a laser source has similar characteristics (as seen by the tracker) to that of a star. The main differences are laser parameters over which we have direct control: wavelength, power output, pulse rate, and polarization. The important aspect of these considerations is that star tracker technology is directly applicable to the problem of laser tracking.

Star/Earth/laser sensors for selected attitude control concept are of several varieties:

a. Coarse and Fine Canopus Trackers

b. Coarse and Intermediate Earth Sensors

c. Fine Laser Sensor for the 0.2 arc-second beamwidth configuration

d. Fine Earth Sensor. This was considered during the mission tradeoff studies and is applicable to the 2 arc-second beamwidth Earth pointing mission.

5.2.1.1 Coarse and Fine Canopus Trackers

Canopus trackers are employed in conjunction with integrating rate gyros for spacecraft third axis control. Accurate third axis control is necessary only to achieve point-ahead accuracy.

The tracker used for third axis control will nominally be directed at right angles to the main laser telescope axis. This requires a separate star tracking optical system; hence, it will require extreme mechanical stability between the two optical axes - on the order of a few arc seconds. This is the chief problem associated with the Canopus tracker - not tracker characteristics per se. Canopus is one of the brightest stars in the sky, and tracking accuracy in the arc-second range can readily be obtained with apertures in the 2- to 4-inch range. Mechanical gimbaling of the tracker to compensate for mechanical deformations with accuracies in the 1 arc-second range exceeds today's state of the art by an order of magnitude, and can not reasonably be used even in the 1975-1980 time period. Electronic gimbaling of some sort (in the non-measuring direction) is therefore required. This technique has been demonstrated in the OAO boresight tracker where the sensor null is electronically offset in increments of a few arc-seconds, and in the Mariner Canopus tracker where the sensor field of view is electronically stepped in the non-measuring direction. Improvements in these techniques can be expected by the 1975-80 time period of interest. Use of both a coarse and fine Canopus tracker is proposed in order to accommodate the wide required ratio of total offset range to offset accuracy. The Coarse Canopus Sensor has similar characteristics to the Mariner IV tracker, and is state of the art. The Fine Canopus Tracker has characteristics similar to the OAO boresight star tracker, and is also state of the art. Characteristics of these trackers are given in Appendix A.

It is emphasized again that the principal problem in third axis control is the required mechanical stability between the Fine Canopus Tracker and the main spacecraft telescope. This problem could perhaps be circumvented completely by eliminating the Canopus tracker and tracking some characteristic of the laser beam, e.g., its polarization. In this manner the main telescope is employed, and the mechanical stability problem disappears. Unfortunately, three-axis star trackers (or autocollimators) are only in their development infancy, and we know of no existing hardware except for laboratory models. These devices have achieved third axis sensing sensitivity of 10 to 20 arc-seconds. An order of magnitude improvement is necessary for the laser communication mission. A related problem involves the possible change of polarization of the laser beam as it passes through the Earth's atmosphere. Knowledge (preferably experimental data) is needed on the extent, if any, of atmospheric polarization change.

5.2.1.2 Coarse and Intermediate Earth Sensors

The Fine Earth Sensor or laser sensor utilizes the main spacecraft telescope for fine pointing. Coarse and/or Intermediate Earth Sensors are needed to orient the telescope axis with sufficient accuracy to permit the target (Earth or laser) to be within the fine sensor field of view.

The Earth varies in angular size from about 8 to 20 arc-seconds as viewed from Mars orbit. The Earth appears very bright from Mars - in the negative magnitude range. It also goes through phase as a function of time of the Earth-Mars orbital geometry. The finite size of the Earth and its phase has no significant effect on a short focal length star tracker, hence the Earth sensor is in reality a star tracker. Accuracy requirements for the Coarse Earth Sensor are well within the state of the art for acquisition of the Coarse Earth Pointing Control Mode. Its desired characteristics are given in Appendix A. A star tracker similar to the OAO boresight tracker would meet the requirements of the Intermediate Earth Sensor for this mission. The required tracker is 1965 state of the art. Appendix A summarizes the required tracker characteristics.

5.2.1.3 Fine Earth Sensor

For the wide beamwidth laser mission, the Earth must be tracked directly since a co-operating beacon is not employed. Even though this mission has been deleted from further consideration, the requirements of the Fine Earth Sensor have been examined and are reported here. The principal requirement of the sensor is that it must locate the geometrical center of the Earth (or some other known reference point) with an accuracy of about one-quarter the laser beamwidth or less, that is, to within about 0.5 arc-second. The main telescope objective (8-inch aperture) is used as the objective for this sensor. For typical missions the Earth appears only partially illuminated as seen from Mars. Since the spacecraft laser will be pointed at individual ground receiver stations whose positions change relative to Earth's image due to diurnal rotation, some stable point on or near the Earth's image must be used as a reference from which the transmitting axis can be offset. This point might be the geometric center of the Earth, the point of intersection of two orthogonal tangents (from which the location of the Earth's center can be determined through knowledge of the image size), or the center of illumination of the Earth's image.

The last of these has been rejected as a reference because, in the spectral region of the potentially useful detectors (essentially visible), the Earth's radiance is very nonuniform from point to point due to differences in the reflectivity of water and land masses and varies considerably with time as a function of weather conditions (cloud cover and snow fields) and seasonal changes. Furthermore, the photometric characteristics of the Earth's terminator as seen from space are not well known, thus introducing an uncertainty in the apparent "phase" of the Earth. Attempting to provide the spacecraft with continuous data on the location of the Earth's center of illumination with respect to its geometric (circular) center through a knowledge of the instantaneous radiance of every region on the Earth's surface would be a hopelessly complex task.

One may wish to consider the use of infrared rather than visual observation of the Earth. This method could use a detector sensitive in the far infrared to sense the emission rather than the reflection spectra. This approach overcomes the phasing problem, but by no means avoids the error introduced by a difference in the radiance center versus the geometrical center. A further compounding factor that makes this method less suitable is that the detectivity of infrared detectors is far inferior to photoelectric surfaces available in the visible region of the spectrum.

The second method available to the designer is to operate in the visible portion of the spectrum but completely avoid centroid measurements in favor of edge tracking. The most positive means of providing a reference point for pointing of the spacecraft laser is to sense the outer (nonterminator) edge of the Earth's image. Several potential means are available for the implementing of this approach, but at present no flight hardware has been developed that would operate on this principle. NASA (Ames), however, has under development an engineering model of a planet tracker operating on the edge-tracking technique. The tracker will employ an image tube and either an epicycle or gear tooth scan pattern as illustrated in Figure 5-6.

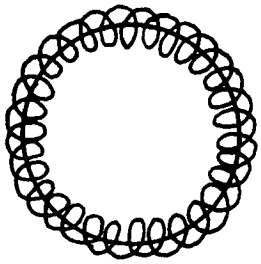

EPICYCLE

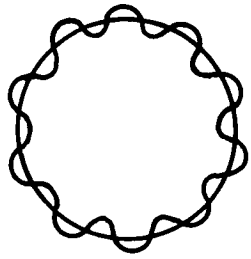

GEAR TOOTH

Figure 5-6. Epicycle and Gear Tooth Scan Patterns

For either scan pattern, the error signals are derived by phase detecting harmonics from the pulse width modulated detector output. The tracking scheme employed must permit pointing to within 1.6 arc-seconds of planet center for either axis. The goal for the development is 0.5 arc-second. The tracker is specified to be packaged in a cylinder 7 inches in diameter by 12 inches overall length and have a total weight under 10 pounds. Appendix A summarizes the pertinent design parameters of the tracker and the corresponding requirements for the present application. It is apparent that improvement in locating the geometric center of the Earth is necessary, and that electrical drift characteristics must be improved. We appraise the required Fine Earth Sensor as beyond existing hardware capability, but well within reach of a suitable development program that might be initiated in the next year or two.

5.2.1.4 Fine Earth Beacon Sensor

For all practical purposes, the laser beacon on Earth appears as a point source when viewed from Martian range; thus, the laser beacon tracker is essentially a star tracker. One essential difference, however, is that we have direct control over the laser, and can select its characteristics (within reasonable bound) to be consistent with sensor state of the art.

It is instructive to first consider whether a continuously transmitting beacon on earth is practical, or whether a high peak power pulsed laser (but not necessarily high average power) is more desirable. This involves a variety of considerations of potential star tracker types. Three basic type star tracking devices were considered.

5.2.1.4.1 Scanning, Nonstorage Devices

These devices are typified by the image dissector photomultiplier which scans the photocathode in the image plane in real time by electrostatically or electromagnetically deflecting the photoelectrons through a fixed aperture within the tube. The OAO boresight is based on this principle. The OAO gimbaled star tracker is a similar type device that employs mechanical chopping of the input light energy.

These type trackers detect the centroid of the image on the detector; hence, a continuously emitting laser beacon on Earth must have a fantastically high average power for this type sensor, i.e., the power delivered to the spacecraft detector must exceed the power from the total size of the Earth by a very large margin — perhaps 10^3 to 10^4 — in order to make the radiance centroid essentially coincide with the laser position. This is clearly a brute force approach that should be avoided.

The second approach is to pulse the laser at some small rate (perhaps 20/sec). This effectively provides chopping of the desired signal (laser) but not the Earth radiation which appears as a dc component. An electrical filter with a 20 Hz low-frequency cutoff effectively eliminates the Earth component of received energy.

The scanning, nonstorage type sensor does not operate well with a pulsed laser, however. The great difficulty with this type device is in achieving space and time coincidence of the laser image and the scanning aperture as projected on the photocathode. This problem is most acute during initial acquisition when relatively large fields of view are needed to establish initial contact. Let us assume that the beacon has been pointed to illuminate the spacecraft, and a coarse pointing device (probably tracking the Earth as a point source) has brought the laser beacon into the field of view of the fine pointing sensor. To assure that the sensor will detect the beacon's image on the photocathode, each detector element

must be viewed for at least one pulse repetition period (and more to provide for noise discrimination) to determine the presence or absence of the beacon. For a high resolution system with many detector elements, this may become a very time consuming process. This approach further assumes that the rate of image motion is low when compared to the scan rate. Furthermore, an extremely long focal length is required to provide the required resolution.

Use of scanning, nonstorage devices in conjunction with a pulsed laser is not adequate in the tracking mode either, as all detector elements being illuminated by the beacon image must be identified to locate the center. This process will require hundreds of laser firings, at least one for each element; thus, attitude data will be available at intervals of several seconds or tens of seconds. Since this is considered completely inadequate, this approach was not thought worthy of further consideration.

5.2.1.4.2 Scanning, Storage Devices

The image orthicon is the only member of this group having sufficient sensitivity for the intended application. The ability of the orthicon to store image data on the secondary target over extended periods eliminates the time and space coincidence problems of the image dissector (since the input data can be read out completely from all detector elements in a few hundredths of a second). However, in addition to the very long focal length (perhaps f/400) which the orthicon also requires for adequate resolution, there is a second peculiar problem which it introduces.

The orthicon, being a storage device, integrates input energy during the period between read-out sweeps. Thus, although a high peak power laser pulse may provide a very high instantaneous photocathode illumination, its duration is very short (about 100 nanoseconds), while the background optical noise (such as that from the sun-lit earth) continues to produce noise photoelectrons on the target. Thus the signal-to-noise ratio for incident background noise depends upon the total number of signal and noise photons received during the frame, or upon average rather than peak power. This is the same as saying that a 10 megawatt laser pulsed at 20 pulses/second of one microsecond duration each is no more effective than a 200-watt continuous wave laser. Some potential does exist for reducing

this noise integration effect by "pulsing" (activating) the photocathode in synchronism with the pulsed beacon, but it does not appear that this problem can be solved to the extent required.

We thus see that the conventional orthicon will respond only to average power, and little advantage can be gained by operation in conjunction with a pulsed laser. The very long required focal length of the telescope is a major factor in rejecting this approach since this introduces extremely complex optical problems for a diffraction limited system. Additionally, since each detector resolution element is far smaller than the telescope diffraction pattern, the actual distribution of energy within the diffraction pattern takes on critical importance - far more so than is warranted.

5.2.1.4.3 Nonscanning, Nonstorage, Image Dissecting Device

This type device is perhaps the simplest high precision star tracker available. The Stratoscope II fine pointing sensor is based on this principle. In this type tracker the laser image is focused at the apex of a pyramidal beam reflector whose mirrored sides split the laser image into four parts (for two-axis control).

This device is a centroid tracker just as the scanning, nonstorage type tracker is. We conclude, therefore, that the ground based laser should be pulsed to take advantage of the electrical filter discrimination that is possible against the nonpulsing earth reflection signal. Since we are not scanning, we do not have the problems associated with the scanning device. Additionally, focal length considerations are not critical for this type tracker, and a reasonable f/25 is selected.

The four-quadrant beam splitter utilizes the optical principle that a linear relationship exists between the angular motion in object space and the angular motion in image space. Actually, this relationship is linear only for paraxial conditions, but since fine pointing sensors usually operate over very limited angular ranges, this is a justifiable approximation. The beam splitter is used to physically divide the image and direct its radiation to several detectors so that motion of the image produces an electrical signal change. There

are many different ways to perform the beam splitting and to process the electrical signals, and one such method is described in Figure 5-7.

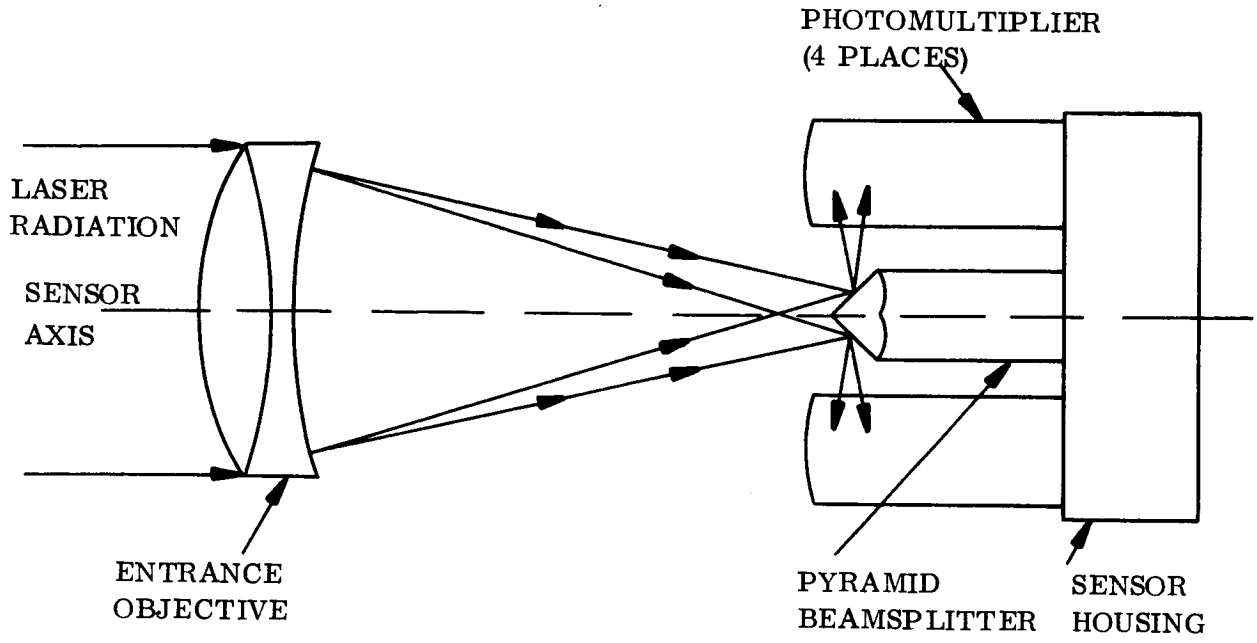

Figure 5-7. Beam Splitter

Radiation from the Earth beacon is converged to a focus at the tip of the beam splitter by the objective. The four photomultipliers are arranged so that the radiation which is specularly reflected from the beam splitter is collected by the photocathodes. Any angular moment of the reference produces a lateral movement of the image on the beam splitter; hence, a change in the radiant flux entering each photomultiplier results. Thus, by properly combining and summing the output current of the four photomultipliers, an angular movement of the stellar reference can be converted into an electrical signal change.

If one assumes that the sum of four photomultiplier outputs remains constant as long as the image is entirely within the bounds of the beam splitter, then the output signal on each axis is given by:

$$E_i = K \frac{2 d_i}{D}$$

where K is a constant, d_i is the lateral displacement (measured from the center of the beam splitter) of the image in the i^{th} direction, and D is the lateral diameter of the image. Once again, the assumption of paraxial rays has been utilized as well as the restriction that $d_i << D$. The exact expression for E_i is linear only for small excusions, d_i, with respect to the image diameter D. If one uses a diffraction limited objective, the lateral defocussed image size is given by:

$$D = 2f \left[\tan \alpha + \sin \theta\right]$$

where f is the objective focal length

α is the half angle of the stellar source

θ is the half-angle measured to the first minimum of the Fraunhofer diffraction pattern.

The lateral displacement, d_i, is given similarly by:

$$2 d_i = 2f \left[\tan \phi\right]$$

where ϕ is the angular displacement of the stellar source from the optical axis. Since all of these angles are quite small, the output, E_i, can be written:

$$E_i = \frac{K \phi_i}{(\alpha + \theta)}$$

When working with the beam splitter at the focal point of the objective, i.e., an in-image focus, $\alpha = \theta$, and

$$E_i = \frac{K}{2} \frac{\phi_i}{\theta}, \quad \theta = \frac{1.2 \lambda}{2d} \qquad -\theta < \phi_i < \theta$$

where

d = the objective aperture diameter

$\phi_i = \theta$

$E_i = E_{max} = \frac{k}{2}$

A plot of the transfer function is shown in Figure 5-8.

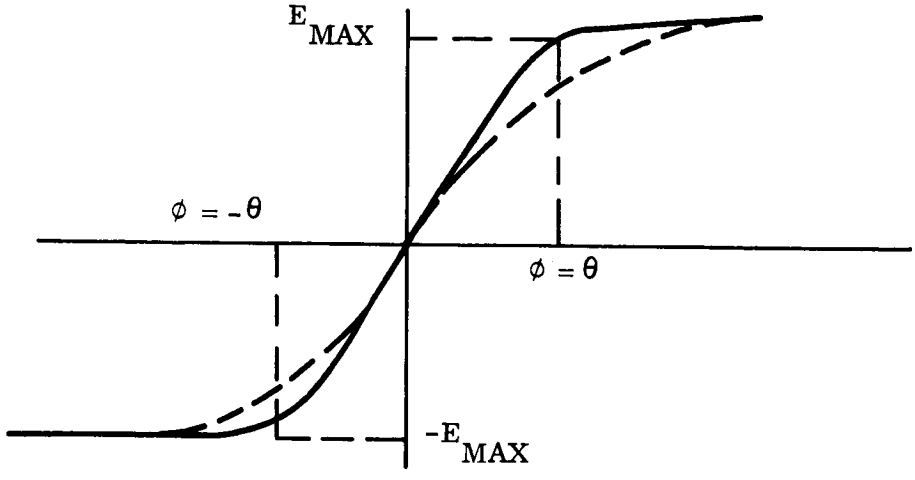

Figure 5-8. Transfer Function of Pyramid Beam Splitter Sensor

The dotted curve indicates the nature of the transfer function when the simplifying assumptions $d_i << D$ is not made.

The transfer function generated above has been assumed to be noiseless. In practice, of course, the one or more detectors are producing current at all times. This will lead to an rms noise voltage, N, corresponding to some equivalent angular error ϕ_n

$$N = \frac{E_{max}\,\phi_n}{\theta}$$

Since E_{max} is equivalent to the signal voltage, S, (all signal power contributing to the output of one detector),

$$\phi_n = \frac{N\theta}{S} = \frac{1.2\lambda}{d} \left(\frac{S}{N}\right)^{-1}$$

where

$\frac{1.2\lambda}{d}$ = the diffraction limited angular size of the image

$\frac{1.2\lambda f}{d}$ = the linear size for an equivalent focal length, f.

If the sensor is operated in a defocussed mode, the quantity $\frac{1.2\lambda}{d}$ is replaced by the angular size of the actual image used. For the defocussed condition, it is apparent that a larger S/N (and thus a larger Earth laser) is required to provide the same noise equivalent error, hence, penalizing the performance of the system. For this application $\frac{1.2\lambda}{D}$ = 0.2 arc-second at 6328Å, and the required ϕ_n is on the order of 0.0033 arc-second. This indicates that a minimum S/N of about 60 would be required.

We have previously shown (Section 3) that in a quantum noise-limited system the required S/N of 60 for the laser tracker is achievable for a laser peak power of 340 megawatts, a pulse width of 10^{-7} seconds, and a pulse repetition rate of 20 per second. These laser characteristics are not reasonably beyond the capability of existing single-crystal lasers. We can conclude that a tracker is needed that will operate near the theoretical quantum noise limit, and that advances in high peak power lasers are necessary to ensure the suitability of this mission. Appendix A summarizes the required tracker characteristics as compared to the Stratoscope II fine pointing sensor.

5.2.1.4.4 Hold Circuit for Fine Earth Beacon Sensor

The hold circuit required to convert the (pulsed) output of the Earth beacon sensor to an analog signal is somewhat different from a typical zero order hold circuit. Because the typical zero-order hold is employed to sample a continuous signal, no synchronization is involved except possibly between different samplers in the same circuit. Furthermore, the only constraint imposed upon the time allotted to sampling the input waveform is that imposed by the sampling rate itself.

In the case of the Earth beacon sensor output, synchronization must be provided to ensure that the pulses are sampled rather than the approximately zero-output of the sensor between Earth beacon pulses. Furthermore, the pulses to be sampled are very short (100 nanoseconds) with respect to the 50 milliseconds between pulses.

The synchronization necessitated by the pulsed nature of the Earth beacon sensor output can be provided by the Earth beacon sensor itself. A "sync" pulse can be provided by adding the outputs of the four photomultipliers within the Earth beacon sensor. The pulse will be relatively noise-free ($S/N \geq 60$), and the amplitude of the pulse will remain constant as long as the Earth beacon is within the sensor field of view.

The requirement to sample the Earth beacon sensor output within 100 nanoseconds necessitates a fast switching time of the components of the hold circuit. Since sampling occurs by charging up the capacitor in a circuit with a relatively low time constant, and the holding function is provided by an RC circuit with a high time constant, the resistance in the RC circuit must be changed by several orders of magnitude in the transition from sampling to holding. These requirements are met by the field effect transistor. A circuit to perform the sample and hold function is shown in Figure 5-9.

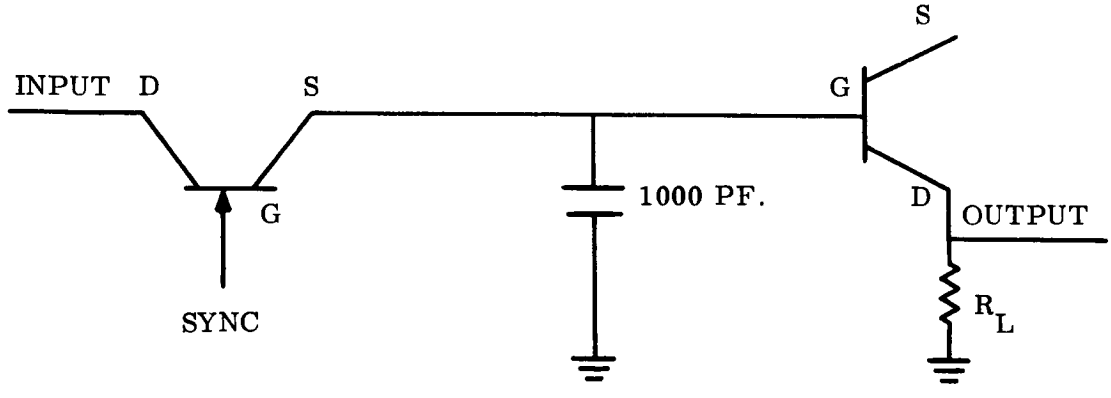

Figure 5-9. Sample and Hold Function Circuit

The RC time constant in the ON condition (during sampling) is 1000 pf times the resistance of the source-to-drain junction of the leftmost FET ($\cong$ 10 ohms) or 10 nanoseconds. The RC time constant in the OFF condition is 1000 pf times the parallel combination of the

resistance of the gate to drain circuit of the rightmost FET and the source-to-drain resistance of the leftmost FET (each ≅5000 M Ω) or 2.5 seconds. The rightmost FET circuit functions somewhat similarly to a cathode follower.

The above figures assumed state of the art hardware. Minor problems occur because of the source-to-gate capacitance of 25 pf draining charge from the 1000 pf capacitor and because of the 30 nanosecond switching time of the FET. Only slightly more sophisticated circuitry would be needed to solve these problems today. Improvements in these parameters can be expected by the 1975-80 period.

5.2.1.5 Inertial Sensors

Inertial sensors in the form of gyros are required in all control modes, except for the cruise mode during the interplanetary trip to Mars. In terms of components required on the spacecraft and exclusive of redundancy requirements, the need can be broken down into two packages.

a. A triad of floated rate integrating gyros aligned to the control axes of the vehicle with the necessary signal processing electronics and control logic to permit operation in the rate mode or in the rate-plus-position mode.

b. A single gyro aligned to the roll axis of the spacecraft to furnish a spacecraft roll position reference in all control modes in Mars orbit.

The selected gyro operating mode as a function of the control mode was summarized in Table 5-1.

5.2.1.5.1 The Three-Gyro Package

The performance requirements imposed on the gyro triad by the spacecraft attitude control modes are current state of the art. The rate mode operation required during initial attitude acquisition phases and attitude reacquisition phases after orbit and injection corrections have been performed, as well as rate-plus-position mode operation in the Inertial Control Mode, have been accomplished on Mariner, Ranger, and Surveyor spacecraft. The specifications for the three-gyro package to meet these requirements are presented in Appendix A.

5.2.1.5.2 The Roll Reference Gyro

The gyro requirements, compatible with the spacecraft attitude control system concept that the gyro furnish the roll reference during occultation of the star, Canopus, represent performance better than currently achieved by production components. The need to hold the inertial reference to about 6 arc-seconds over the 2-hour period of Canopus occultation represents a short term gyro drift requirement of better than 10^{-3} degrees per hour. Considering that the gyro reference will be updated by the Fine Canopus Sensor when the star is not occulted, the gyro biases may be removed during this period. Only the random drift is of concern during the time the gyro is called upon to serve as the roll attitude reference.

Since random drift performance as low as 10^{-2} degrees per hour can be achieved with present day components, and still better performance has been achieved by experimental components, it is reasonable to assume that gyros with the required performance will be available in the 1975 to 1980 time period.

The desired gyro characteristics to perform this inertial reference function are given in Appendix A.

5.2.2 CONTROL MOMENT GYROS

As a result of tradeoff studies reported in Appendix C, twin two-degree-of-freedom control moment gyros were selected to provide proportional control torques about the spacecraft pitch and yaw axes during the Fine Pointing Control Mode. The twin two-gimbal configuration is essentially current state of the art. However, the proposed method of gyro operation is deemed novel. It was derived to suit the system needs for high control loop static gain, low control bandwidth, and no significant time delays in application of control torques. The highly damped control moment gyros fill this bill. The gyro time constant, I_g/D, is of the order of 10^{-4} seconds, and the torque attenuation during the attitude hold phase of fine pointing (spacecraft rate-sensing gyro not in the loop) is given by $2h/D = 0.04$. It further suits the system needs by having the capability to provide high vehicle restoring control torque during acquisition of the Fine Pointing Mode from high vehicle rates by maintaining the gimbal torquers in saturation in response to sensed vehicle rates (spacecraft rate sensing gyro in the loop).

The design and use of the two-gimbal gyros is conventional to the extent that the individual momentum vectors are oriented in the opposite direction in the zero-momentum stored condition. When storing momentum, the corresponding gimbals of the pair move counter to each other to avoid cross coupling. A minor loop is included in the control package to maintain the corresponding gimbal angles equal and opposite.

High gyro damping is provided by an active loop from gimbal axis rate output to torquer input. Thus, to effect a change about the spacecraft yaw axis (aligned to the outer gimbal axis), motion is required about the inner gimbal axis, and the inner gimbals are torqued to achieve this result. The torque applied to the vehicle yaw axis is then the product of inner gimbal rate, twice the gyro spin momentum, and the cosine of the gimbal angle. A small motion occurs about the outer gimbal axis ($\frac{h}{D}$ inner gimbal axis motion). This small motion about the outer axis is made negligible through a minor loop that incorporates the control law stated in Section 5.1.

The twin single-degree-of-freedom gyros used for roll axis control operate in the more conventional manner which does not utilize tachometer feedback of gimbal rate. Gimbal torquers for all gyros are considered to be dc brushless motors. Gimbal bearing preloads are considered reduced after launch. Gimbal functions are derived for the conditions stated in Appendix C, as are gyro angular momentum and torquer size. All pertinent control moment gyro characteristics are summarized in Appendix A.

5.2.3 SPACECRAFT CONTROL COMPUTER

5.2.3.1 Introduction

The required spacecraft computer functions may be conveniently separated into (1) the guidance and control computations associated with interplanetary flight and injection into Mars orbit and (2) those computations required for vehicle stabilization to the selected attitude reference and control of its laser beam direction for communication to an Earth-based receiver. The former have been delineated, and for the most part implemented, for Mariner and Voyager type spacecraft and will not be repeated here.

The spacecraft attitude control computation for the laser communication mission starts after the injection maneuver which adjusts the spacecraft trajectory and velocity to attain the proper orbit about Mars.

The necessary computation for acquisition of the attitude reference may be essentially composed of analog logic and switching circuits of the type used on the Mariner spacecraft, with the exception that solid state switching is recommended in place of electromagnetic relays. During attitude hold to the laser beacon-Canopus reference, it is proposed that inputs to the control moment gyro torquers be computed by analog circuits from position and rate information about each axis. The actuator reset function may be implemented by analog circuits which respond to CMG gimbal pickoff signals as the torquer nears saturation and which command the transfer of momentum to space to reset the gyros.

The major portion of the spacecraft digital computer will be required to provide programmed command of the servoed optics to implement control of the laser beam motion during acquisition of the Earth-based receiver and to provide the proper point ahead for laser communication. The programmed sequential mode switching, commanded turn functions, and various back-up mode programs for attitude control of the spacecraft have storage and computational requirements that are small compared to those required for control of the servoed optics.

It is recommended that all point-ahead computations and corresponding tilting plate angles and corrective lens positions be computed on the ground. The program of the proper tilting plate angles and corrective lens position, as a function of time, should be transmitted to the spacecraft over the RF link and stored in the computer memory. At the correct time, as determined by the spacecraft computer clock, the proper tilting plate angles and corrective lens position will be read out of the memory as commands to the servoed optic control loops. The required update frequency of these commands was determined by mathematical analysis (Paragraph 5.2.3.3) to be 10 per minute to maintain the desired pointing accuracy. In order to avoid the possibility that failure of the RF link would temporarily stop spacecraft-Earth communications, a capability onboard the spacecraft to store the point-ahead data for 24 hours in advance is recommended. Using this

technique, the spacecraft digital computer is primarily a large memory with certain write-in and read-out capabilities; 14,400 37-bit words are required as determined by update frequency, range, and positional tolerances of the servoed optics loops, respectively.

5.2.3.2 Analog Computation

The analog computation functions to be performed during the acquisition of the beacon reference are as follows:

a. Switch command of the pitch and yaw axes from the gyro position-plus-rate reference to the Coarse Earth Sensor and gyro rate references upon receipt of an Earth presence signal from that sensor at the conclusion of the commanded turns. Actuate the proper mass expulsion thrusters to acquire the Earth. Pitch and yaw commanded turns may be accomplished without any spacecraft roll maneuver so as to maintain the Canopus reference, but a roll maneuver may be accomplished in case of an unscheduled loss of that reference. This is given in item b below.

b. Switch command of the roll axis to the roll search reference signal upon receipt of pitch and yaw signals indicating errors less than 0.2 degree, and pitch and yaw rates less than 0.05 degree per second. Upon receipt of Canopus presence signal, switch command of the roll axis to that sensor and to the roll rate gyro. Actuate the proper mass expulsion thruster during the acquisition maneuver.

c. Switch command of the pitch and yaw axes to the Intermediate Earth Sensor upon receipt of an Earth presence signal from that sensor and pitch and yaw signals from the Coarse Earth Sensor, indicating errors less than 4 arc minutes and rate signals less than 0.005 degree per second. Switch command of the roll axis to the Fine Canopus Sensor upon receipt of a Canopus presence signal from that sensor, and signals from the Coarse Canopus Sensor indicating an error less than 7 minutes of arc, and rate indication of less than 0.005 degree per second.

d. Activate the momentum storage subsystem when pitch, yaw, and roll rates less than 0.005 degree per second are indicated.

e. Switch command of the pitch and yaw axes to the Fine Earth Beacon Sensor when: a beacon presence signal is received from the Fine Error Sensor; pitch and yaw rate error signals indicate rates less than 10 arc seconds per second; signals from the Intermediate Earth Pointing Sensor and Fine Canopus Sensor indicate errors less than 5 arc seconds and 14 arc seconds, respectively.

During acquisition, rates are determined from gyros.

During the Fine Pointing Mode, analog signals from the beacon sensor signal processor, the vehicle rate gyro, and the control moment gyro gimbal rate sensor are processed in the appropriate gyro gimbal torquer summing amplifier, where the gyro gimbal torque motor signal is generated. In addition, trim signals from the gyro gimbal angle comparator amplifier and axis decouple signals from gimbal angle resolvers are processed in this component. Four such amplifiers are required. Analog logic is also required to sense CMG gimbal angles above 45 degrees and to gate mass expulsion actuators for reset of the CMG momentum vector.

5.2.3.3 The Digital Computer

Since the major portion of the spacecraft digital computer must be devoted to the point-ahead computation, it was analyzed in sufficient depth to determine the rate at which commands to the servoed optics must be updated, the resolution required, and the tradeoffs between "onboard" and ground based computation.

5.2.3.3.1 Servoed Optics Command Rate

The rate of change of the spacecraft-Earth laser station relative velocities is a figure of merit in determining how often the spacecraft point-ahead will have to be updated. The three components of spacecraft-Earth laser station cross range velocity were evaluated as follows:

a. The cross range velocity of the center of Earth with respect to the center of Mars; the component is slow varying, and its rate of change is negligible with respect to the others.

b. The velocity of the Earth based receiver with respect to the center of Earth. An upper bound to the rate of change of the Earth station cross range velocity is given by the product of the square of the Earth's angular velocity and the Earth's radius. This upper bound was computed to be 0.03 meter/second.

c. The spacecraft velocity about Mars. The rate of change of the spacecraft velocity about Mars can most conveniently be evaluated by considering its radial and angular components separately. The radial acceleration is given by:

$$A_r = \frac{G M_m a(1-e^2)}{r^3} - \frac{G M_m}{r^2}$$

where:

G is the universal gravitational constant

M_m is the mass of Mars

a is the semimajor axis of the orbit

e is the orbit eccentricity

r is the distance from the center of Mars to the spacecraft.

At the orbit perigee of 1000 K_m, A_r attains its maximum value of approximately 1 meter/sec^2.

The angular component of spacecraft acceleration is given by:

$$A_a = \frac{G M_m \, e \sin\theta \, (1 + e \cos\theta)^2}{A^2 (1-e^2)}$$

where:

θ is the true anomaly

A_a is a maximum near $\theta = 60^o$ where its value is approximately 0.7 meter/sec^2.

The rate of change of velocity about Mars is therefore bounded by:

$$\sqrt{1^2 + 0.7^2} \approx 1.2 \text{ meters/sec}^2.$$

The resultant rate of change of spacecraft relative velocity about Mars thus determines the rate at which the point ahead must be updated. The rate of change of the point ahead angle is given by:

$$\frac{\Delta \theta_{pa}}{\Delta t} = \frac{2 \Delta V}{c} \approx \frac{2 \times 1.2}{3 \times 10^6} \times 2 \times 10^5 \approx 0.0016 \ \frac{\text{arc sec}}{\text{sec}}$$

The error in commanded point-ahead angle should be held to 0.01 arc second, necessitating that the point-ahead be updated every six seconds about both axes about which point-ahead occurs.

5.2.3.3.2 Word Length

The number of bits in each word is determined by the desired tolerances in the tilting plate angle and corrective lens position of the servoed optics.

If the error introduced by the tilting plate control loop in pointing the laser about the axis where most of the point-ahead angle occurs is to be held to 0.01 arc second, the tilting plate must be controlled to an accuracy of $\pm$ 28 arc seconds.

Reasonable design goals under this constraint are to allocate $\pm$ 10 arc seconds to the tilting plate angle sensor, $\pm$ 2 to 4 arc seconds to the tilting plate torquer, and $\pm$5 arc seconds to the quantization of tilting plate command angles. The tilting plate would then be commanded with a range of operation of ±40 degrees and a resolution of ± 5 arc seconds for a range to resolution ratio of 29,000. It would thus require 15 bits for commanding the tilting plate with the range and resolution required.

The point-ahead angle about the second axis is implemented by a second degree-of-freedom of the tilting plate and can be accomplished with sufficient precision by allocating (as before) $\pm$ 10 arc seconds to the tilting plate angle sensor, 2 to 4 arc seconds to the tilting plate torquer, and $\pm$ 5 arc seconds to the quantization of tilting plate command angles. This necessitates that 15 bits be provided to command the tilting plate with the range and resolution required.

From Appendix F, corrective lens must be moved a distance of $\pm$ 0.124 inch with a resolution of $\pm$ 0.01 inch. Allocating $\pm$ 0.001 inch to the error introduced by quantization of lens position commands necessitates that 7 bits be allocated to the lens position command to provide the range and resolution required.

The number of words in the computer memory is determined by the 6-second update and 24-hour storage capability outlined above (24 x 60 x 10 = 14,400 words). The word length is determined by the desired tolerances in tilting plate angles and corrective lens position (15 + 15 + 7 = 37).

5.2.3.3.3 Ground-Based or Onboard Computation

Performance of all the point-ahead computations onboard the spacecraft involves periodic update of certain parameters in the stored point-ahead equations via the RF link, based upon improvement in the analytical model of the point-ahead computation as a result of determination of error in the received spacecraft laser beam. The point-ahead computation would be followed by computations of the tilting plate angular rotations about two axes and the corrective lens position. Solution of the point-ahead equations involves the multiplication and addition of a dozen or more 3 x 3 matrixes to derive the point-ahead angles about two axes in the spacecraft coordinate reference system. The expression for tilting plate angles must be determined from the complex expression:

$$D = t \sin i \left[1 - \left(\frac{1 - \sin^2 i}{n^2 - \sin^2 i} \right)^{1/2} \right]$$ developed in Appendix F.

Disadvantages of the onboard computation are almost overwhelming. Under this technique, control of spacecraft point-ahead is not completely Earth-based, and full use of computational facilities on Earth cannot be made. Use of conical scan and adaptive techniques for increasing pointing accuracy would be difficult to implement in this concept as perturbations upon normal point-ahead equations would be difficult to implement. The computer would be needlessly complex and, since the spacecraft is unmanned, maintenance could not be performed.

Use of an Earth-based computer to perform the point-ahead computations, and translate the results into the corresponding tilting plate angles and corrective lens positions, allows complete flexibility in determination of the correct analytical model of the point ahead situation and is the recommended technique. Under this technique, the results of the Earth-based computations are sent over the RF link and stored in the spacecraft computer, which is essentially a large memory. Every 6 seconds, new values of tilting plate angles and corrective lens position are read out of the spacecraft computer memory and sent as commands to the respective control loops.

Because the speed requirements of the spacecraft computer are very minimal, and because it is designed to read out the words in memory in a set order, the memory should be sequential. However, it is desirable to be able to update the memory more often than every 24 hours to take advantage of more up-to-date point-ahead information, and to be able to go into a programmed conical scan mode. For this reason, the write-in logic must be able to begin at any given place in memory and update any number of successive memory words. The read-out logic should also be able to change to any given place in memory and begin reading out successive words upon ground command.

Thus, a sequential memory with a limited random access capability is required. If such a device were built with state of the art hardware, it would be approximately 4000 cubic inches (16 x 16 x 16) in size, weigh 60 pounds, and require approximately 50 watts of power. Experience with existing hardware indicates that the random read-out capability could be most easily provided by reading out at a fast rate until the desired word has been reached. It is within the state of the art to read out the entire memory in 2 to 3 seconds. While operating in this fast read-out mode, 100 watts of power would be required.

5.3 MATHEMATICAL MODELS FOR THE SPACECRAFT CONTROL ACTUATORS

The function of the attitude control subsystem is to align the spacecraft with respect to some chosen reference frame. To correct any error in orientation requires that an appropriate angular velocity vector be imparted to the spacecraft to rotate it to the desired position. A unique 1 to 1 correspondence may be defined between the angular velocity and angular momentum vectors of the vehicle from a knowledge of its inertia profile. Control actuators classified as momentum exchange devices, such as control moment gyros and flywheels, control the angular velocity and thus the attitude of the spacecraft by transferring storage of angular momentum between themselves and the vehicle proper.

The tradeoff analysis reported in Appendix C indicates that the control actuators that best fit the selected mission's requirements are a combination of twin control moment gyros. The chosen mounting configuration is illustrated in Figure E-1, which appears at the end of Appendix E. By moving their respective spin vectors in a scissor-like fashion,

the two single-degree-of-freedom gyros exchange angular momentum with the spacecraft X-axis to which the primary optics is nominally aligned. Angular momentum is exchanged in the plane normal to the axis by appropriately scissoring the inner and outer gimbals of the two double-drgree-of-freedom gyros.

A complete set of coupled nonlinear differential equations is developed in Appendix D and summarized in Section E-11 of Appendix E. These equations define in the most general sense the functioning of the four control moment gyros. However, when the main interest is in precision pointing, characterized by small attitude errors and low vehicle angular rates, considerably simplified math models may be utilized. The techniques used in generating these simplified models are demonstrated in Appendix E.

5.3.1 SIMPLIFIED MATHEMATICAL MODEL FOR THE SPACECRAFT X-AXIS CONTROL ACTUATORS

From the discussion of the philosophy of operation with momentum exchange devices, it is apparent that the math model desired should indicate the stored angular momentum projected along the spacecraft X-axis by the single degree-of-freedom gyros as a function of the variables that effect a change.

The appropriate model is shown in Figure 5-10. It was obtained by rearranging Figure E-2, which was developed in Section E-4 of Appendix E. As discussed in Appendix E, the characteristics of the gyros are gimbal angle dependent, thus the simplified model was derived by considering perturbations about a nominal gimbal angle A. The signal flow graph indicates how the torque motor T_a, and vehicle motion w_x, create gimbal motion a, which in turn causes a perturbation $d\,h_x$ about the nominally stored momentum h_{xo}. The scale factor of 2 was introduced rather than indicating redundant information from the corresponding twin gyro which is operating similarly in the scissor-like fashion, thus providing half of the total projected momentum storage h_x. The letter s represents the LaPlace operator.

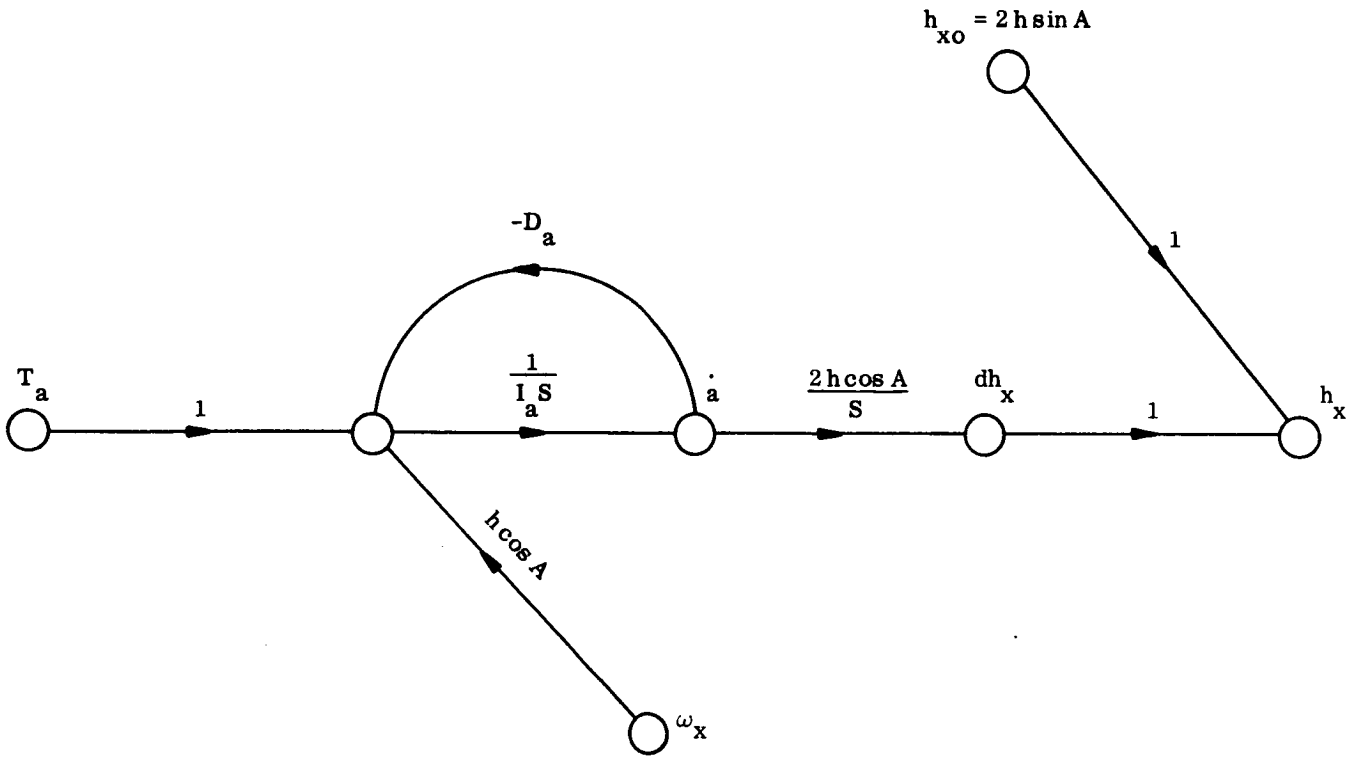

Figure 5-10. X-Axis Control Actuators — Math Model

5.3.2 SIMPLIFIED MATHEMATIC MODEL FOR THE SPACECRAFT Y-AXIS CONTROL ACTUATORS

Appendix E discusses how the double degree-of-freedom gyros may be utilized in the following three ways:

a. Pseudo single-degree-of-freedom mode

b. Lightly damped mode

c. Highly damped mode

The pseudo SDF mode was rejected because of the problem it presented in decoupling the Z-axis response from Y-axis excitation and the hardware complexity required to force it to operate in the single degree-of-freedom fashion.

The lightly damped mode was eliminated next because of its inherent highly underdamped gimbal dynamics that give rise to ringing and result in considerably less stability margin than is obtained when the gyros are used in the highly damped configuration.

The selected highly damped mode of operation may be modeled as shown in Figure 5-11. This model results from appropriately modifying Figure E-4,which is developed in Section E-4 of Appendix E. As indicated by the signal flow graph, the large gimbal damping is obtained by feeding gimbal rate information back into the torque motor. This completely dominates over the natural damping illustrated in Figure E-4. The high gimbal damping also makes interaction with the outer gimbal negligible. Thus, the gimbal motion,b,again results in a perturbation d h_y about the nominally stored Y-axis angular momentum h_{yo}. Again s represents the LaPlace operator and a factor of 2 was introduced rather than modeling redundant information for the twin gyro.

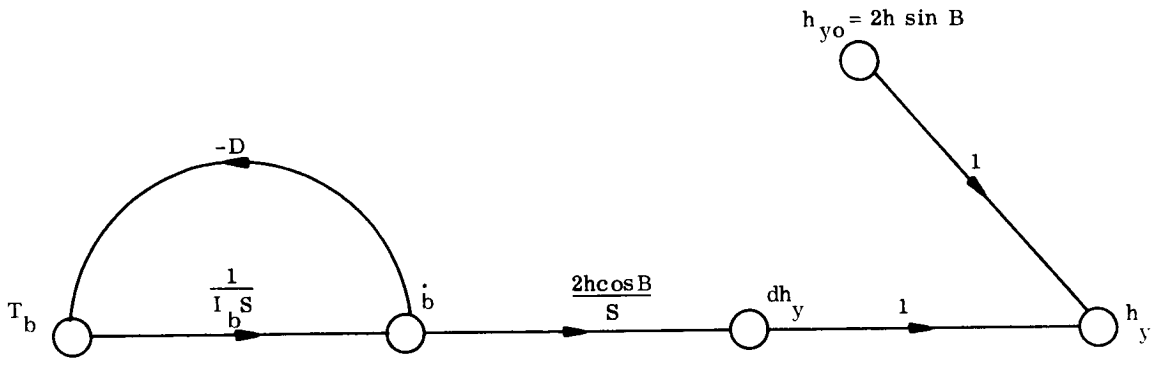

Figure 5-11. Y-Axis Control Actuators — Math Model

5.3.3 SIMPLIFIED MATHEMATICAL MODEL FOR THE SPACECRAFT Z-AXIS CONTROL ACTUATORS

As discussed in Section E-7 of Appendix E, it is impossible to uncouple the Z-axis from the Y-axis merely by choice of gyro parameters and that decoupling, if desired, must be achieved through the control law. The physical explanation of this phenomena is that stored momentum projected along the vehicle Y-axis is a function of only the inner gimbal positions of the double degree-of-freedom gyros. Thus, Y-axis control is readily obtained by properly modulating the position of the inner gimbals. Momentum stored along the vehicle Z-axis, however, is a function of both the outer and inner gimbal positions. Thus,

if Z-axis control is to be realized by modulating only the outer gimbals, inner gimal position change must be sensed and compensated for in the outer gimbal control law. Assuming this has been done as suggested in Section E-7, the simplified math model shown in Figure 5-12 results. Again the high gimbal damping is obtained through the feeding back of gimbal rate information into the torque motor, resulting in negligible interaction of both the perturbed and nominally stored momenta upon both gimbal angles.

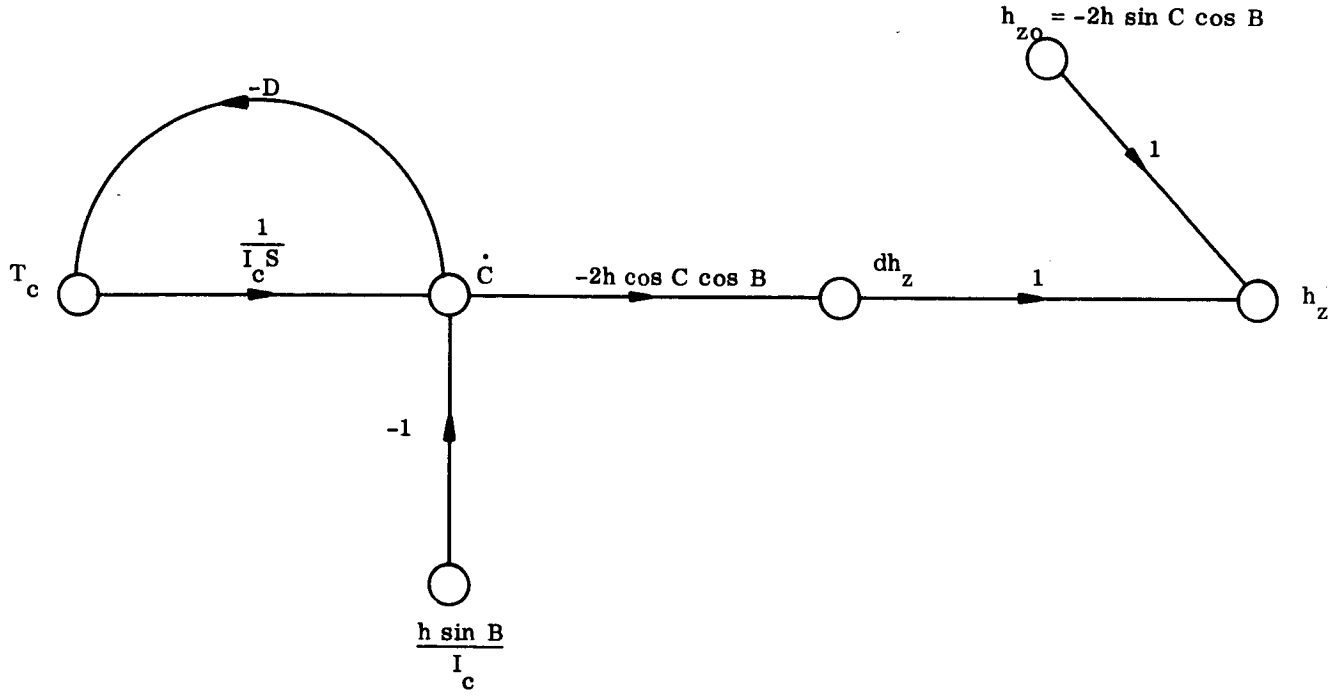

Figure 5-12. Z-Axis Control Actuators — Math Model

5.4 SPACECRAFT ATTITUDE CONTROL SYSTEM ANALYSIS

The control laws define the functional dependence of the torque motors upon the measurable system state variables. In choosing control laws to meet the system requirements, accuracy, stability, speed of response, and gimbal angle constraints must be considered. The control laws identified were chosen merely to show that the requirements could be met and no optimization with respect to any performance index has been performed.

5.4.1 SPACECRAFT X-AXIS ATTITUDE CONTROL LAWS

The control laws for the single degree-of-freedom gyros that control the vehicle X-axis are given to the LaPlace transform format as:

$$T_{a_1} = K_x \frac{(1 + T_{1x}\, s)}{(1 + T_{2x}\, s)} \theta_x - M_x (a_1 + a_2) \qquad (5\text{-}7)$$

$$T_{a_2} = -K_x \frac{(1 + T_{1x}\, s)}{(1 + T_{2x}\, s)} \theta_x - M_x (a_1 + a_2) \qquad (5\text{-}8)$$

The initial term in the first torque motor's control law indicates that the attitude information (θ_x) from the Canopus tracker is amplified (K_x) and that stability compensation is achieved with a lead network. The second torque motor, T_{a2}, has the identical term only with the polarity reversed in order to create the desired scissoring motion of the two gyro spin vectors. The second term in each case maintains this gimbal angle constraint by countering any tendency to drift away from the intended symmetrical movement.

The gain K_x was chosen from accuracy considerations, with gimbal stiction being the dominant source of error. The steady-state error resulting from superimposing the effects of a constant external disturbance torque, T_x, and gimbal running friction, f_r, on the linearized actuator math model shown in Figure 5-10 is:

$$\theta_x = \frac{1}{K_x} \left(\frac{T_x D_a}{2\, h \cos A} + f_r \right) \qquad (5\text{-}9)$$

With the peak disturbance torques (quoted in Section 4.1) and the running friction (Appendix C) both about 10^{-4} foot-pound, the gimbal freedom limited to plus and minus 60 degrees, and the D_a/h ratio much greater than unity, the error resulting from gimbal running friction clearly dominates. The condition for an even larger error exists when there are no disturbance torques acting, and the existing attitude error just fails to produce enough motor torque to exceed the starting friction (stiction) which always has a larger value than the running friction. Using a value of 3.6×10^{-4} pound-foot for the starting friction, K_x was chosen to be 5×10^{-4} pound-foot per arc second, which would limit the servo error to 0.7 arc second. (Refer to Appendix C, Sections C.5.1 and C.5.2.)

The gimbal damping D_a was chosen to be as large as possible (without using a rate sensor) by using standard eddy-current dampers to overdamp the gimbal dynamics, which lowers the loop crossover while eliminating the possibility of having a lightly damped resonant peak. The values for the time constants in the lead network were then chosen with the aid of the Bode plot shown in Figure 5-13.

A value of 0.1 pound-foot per degree was considered sufficient to maintain a tight constraint on the gimbal scissoring motion while still keeping this inner loop at a lower bandwidth than the attitude control loop.

All of the attitude control subsystem parameters are summarized in Table 5-2.

5.4.2 SPACECRAFT Y-AXIS ATTITUDE CONTROL LAWS

The control laws for the inner gimbals of the double degree-of-freedom gyros that control the vehicle Y-axis are:

$$T_{b_3} = K_y \frac{(1 + T_{1y}\, s)}{(1 + T_{2y}\, s)}\, \theta_y - D_b \dot{b}_3 - M_y (b_3 + b_4) + \begin{cases} E_{r1} \begin{bmatrix} (w_y - db \text{ sign } (w_y)) \end{bmatrix} & \text{if } |w_y| > db \\ \begin{bmatrix} 0 \end{bmatrix} & \text{if } |w_y| \le db \end{cases} \tag{5-10}$$

$$T_{b_4} = -K_y \frac{(1 + T_{1y}\, s)}{(1 + T_{2y}\, s)}\, \theta_y - D_b \dot{b}_4 - M_y (b_3 + b_4) - \begin{cases} E_{r1} \begin{bmatrix} (w_y - db \text{ sign } (w_y)) \end{bmatrix} & \text{if } |w_y| > db \\ \begin{bmatrix} 0 \end{bmatrix} & \text{if } |w_y| \le db \end{cases} \tag{5-11}$$

For reasons discussed in Section 5.3.2, the double degree-of-freedom gyros were chosen to operate in the highly damped mode. The terms $D_b \dot{b}_3$ and $D_b \dot{b}_4$ involving the product of a large viscous damping constant and a gimbal rate are present merely to give the gimbal dynamics the highly damped characteristic.

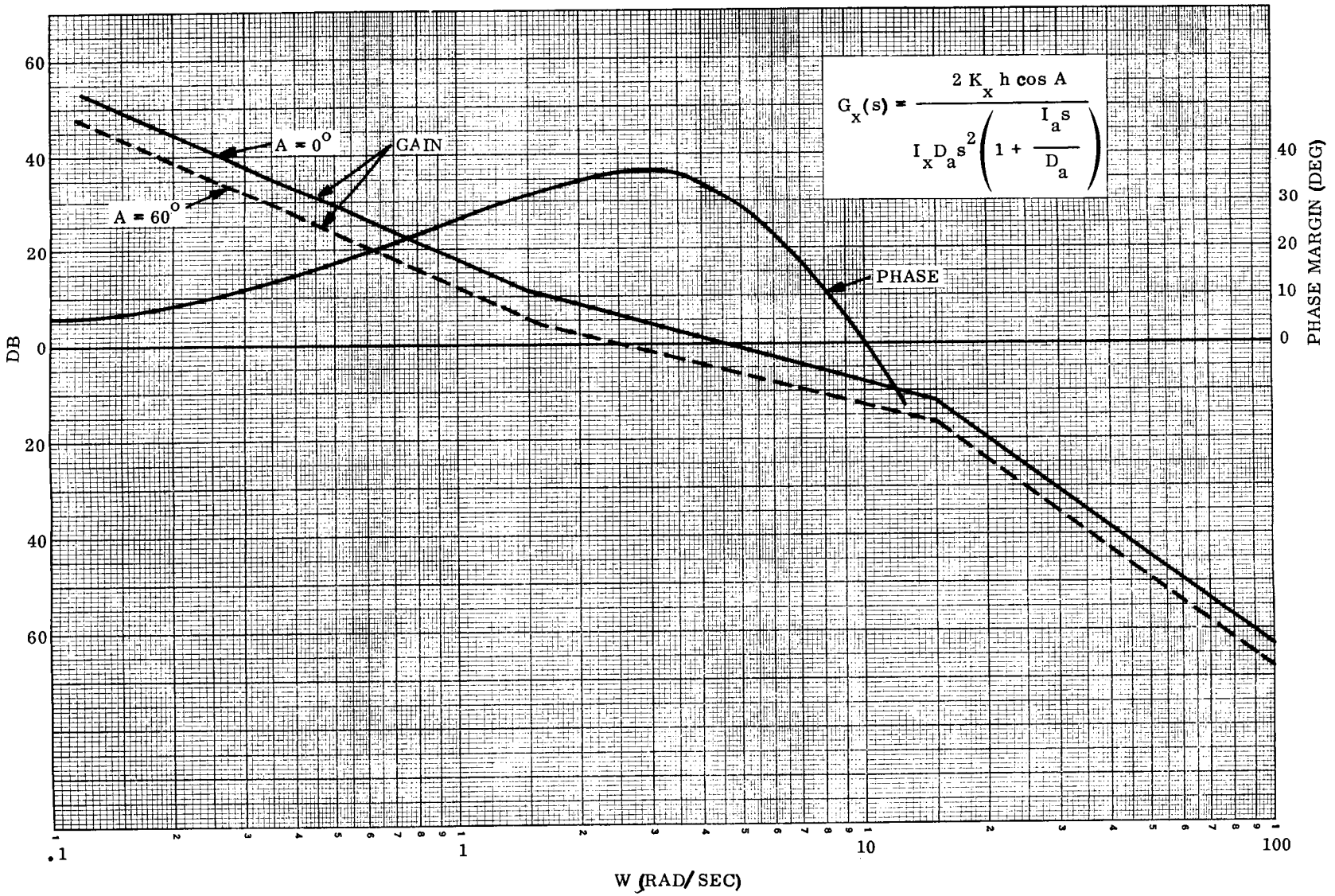

Figure 5-13. Bode Plot for X-Axis

Table 5-2. Summary of Attitude Control Subsystem Parameters

Symbol	Identification	Numerical Value
h	Spin momentum of each gyro	2 lb-ft-sec
I_x	Spacecraft X-axis inertia	5000 ft-lb-sec^2
I_y	Spacecraft Y-axis inertia	5000 ft-lb-sec^2
I_z	Spacecraft Z-axis inertia	5000 ft-lb-sec^2
I_a	Inertia of SDF gyro about gimbal axis	0.001 ft-lb-sec^2
I_b	Inertia of DDF gyro about inner gimbal axis	0.009 ft-lb-sec^2
I_c	Inertia of DDF gyro about outer gimbal axis	0.011 ft-lb-sec
D_a	SDF gyro viscous damping constant	0.01 ft-lb/rad/sec
D_b	DDF gyro inner gimbal viscous damping constant	90 ft-lb/rad/sec
D_c	DDF gyro outer gimbal viscous damping constant	110 ft-lb/rad/sec
K_x	X-axis gain, attitude to torque motor	5×10^{-4} ft-lb/arc sec
K_y	Y-axis gain, attitude to torque motor	7.5 ft-lb/arc sec
K_z	Z-axis gain, attitude to torque motor	7.5 ft-lb/arc sec
M_x	X-axis, gimbal angle constraint gain	0.1 ft-lb/deg
M_y	Y-axis, inner gimbal angle constraint gain	0.1 ft-lb/deg
M_z	Z-axis, outer gimbal angle constraint gain	0.1 ft-lb/deg
T_{1x}	X-axis lead time constant	0.667 sec
T_{2x}	X-axis lag time constant	0.0667 sec
T_{1y}	Y-axis lead time constant	0.5 sec
T_{2y}	Y-axis lag time constant	0.05 sec
T_{1z}	Z-axis lead time constant	0.5 sec
T_{2z}	Z-axis lag time constant	0.05 sec

Although equivalent expressions exist for the steady state error resulting from either gimbal friction or constant disturbance torques for the Y-axis as were presented for the X-axis, the choice of a gain of 7.5 pound-feet per arc second for K_y was dominated by considerations of the sensor characteristics and the initial conditions of acquisition. The attitude sensor is roughly linear up to 0.2 arc second where the signal saturates until the field of view is exceeded (at 90 arc seconds), at which point the signal vanishes. The sensor input-output characteristics are illustrated in Figure 5-14. The gimbal dynamics are dominated by the viscous damping terms when the control moment gyros are utilized in the highly damped mode. Thus, a saturated sensor signal calling for 1.5 pound-feet of torque ($0.2\ K_y$) will very quickly generate a gimbal rate of approximately $\frac{0.2\ K_y}{D_b} = 0.015$ radian per second.

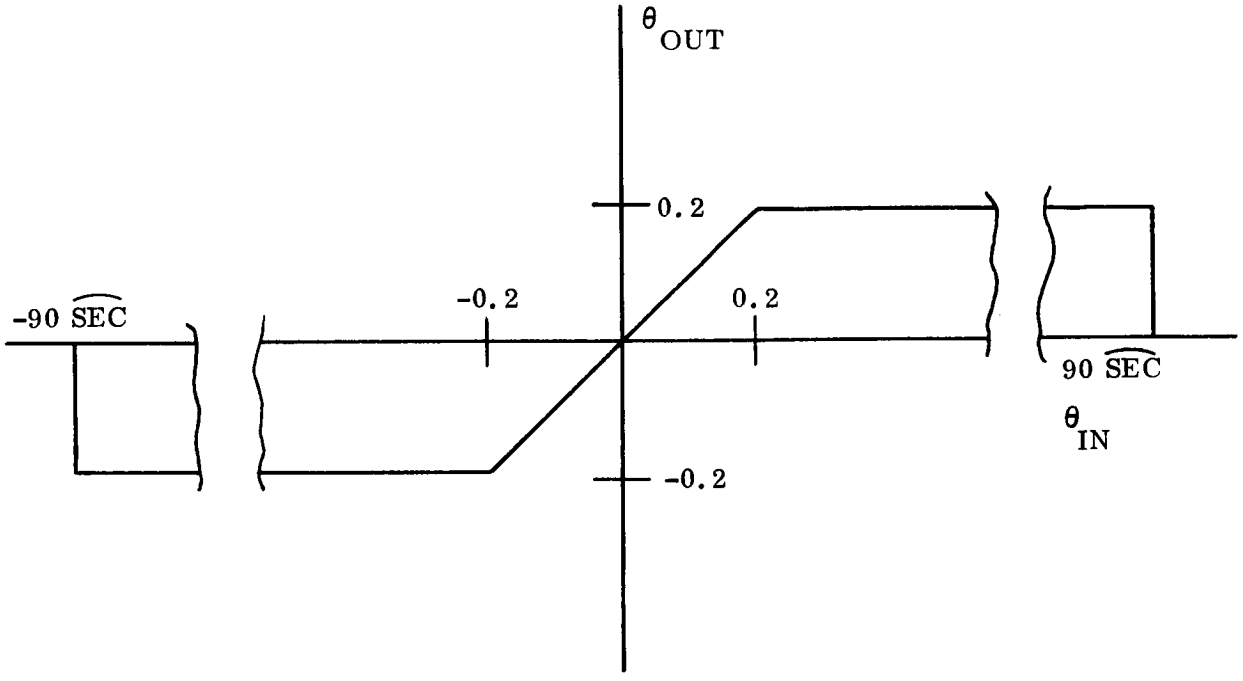

Figure 5-14. Sensor Input - Output Characteristics

The response time constant is $I/D_b = 0.0001$ second. The above gimbal rate exchanges momentum rapidly enough with the spacecraft so that the initial peak overshoot from the worst acquisition initial conditions (15 arc-seconds error, 10 arc-seconds per second rate increasing the error) remains within the field of view of the sensor. To get the mentioned gimbal rate, it is not necessary to use a torque motor that can generate 1.5 pound-feet of torque. This is because the torque motor also generates the damping torque, thus the gimbal is accelerated by the difference. To illustrate this point, the amplifier that drives the torque motor has purposely been chosen to saturate at a signal equivalent to 0.3 pound-foot. Therefore, a saturated sensor signal will accelerate the gimbal at $\frac{T\ sat}{I} = \frac{0.3}{0.01} = 30$ radians per second per second, until sufficient gimbal rate is developed to bring the amplifier out of saturation. Thus, a smaller torque motor may be used with little sacrifice in response time. Having thus chosen a value for K_y and knowing the uncompensated open loop transfer function reported in Appendix D, a lead compensation network was chosen with the aid of the Bode plot shown in Figure 5-15. The effect of the phase lag introduced by the sample and hold circuitry ($\frac{wT}{2}$, where T is the sampling period) is indicated.

The terms $M_y (b_3 + b_4)$ are again introduced in order to ensure that the corresponding gimbal angles are equal in magnitude and opposite in sign. If this condition is not met, these terms are nonzero and provide corrective feedback until the scissoring constraint is satisfied.

The terms of the form $K_{r1} (w_y - \text{db sign } (w_y))$ were added to shorten the acquisition and station switching times, and to allow for a large design safety factor with respect to the tolerable acquisition initial conditions. Without these terms (vehicle rate gyros failed), the previously described compensation network will successfully acquire from the worst expected initial conditions. However, due to the limited linear range of the sensor, derived rate information from the lead network exists only in the linear region near null, meaning that many overshoots are experienced during settling. Figure 5-16 illustrates this effect with a phase plane diagram. The sensor saturation causes the torque switching line to break vertically at ± 0.2 arc-second, resulting in very little damping until the trajectory remains within the linear range of the sensor. This situation can be improved by calling

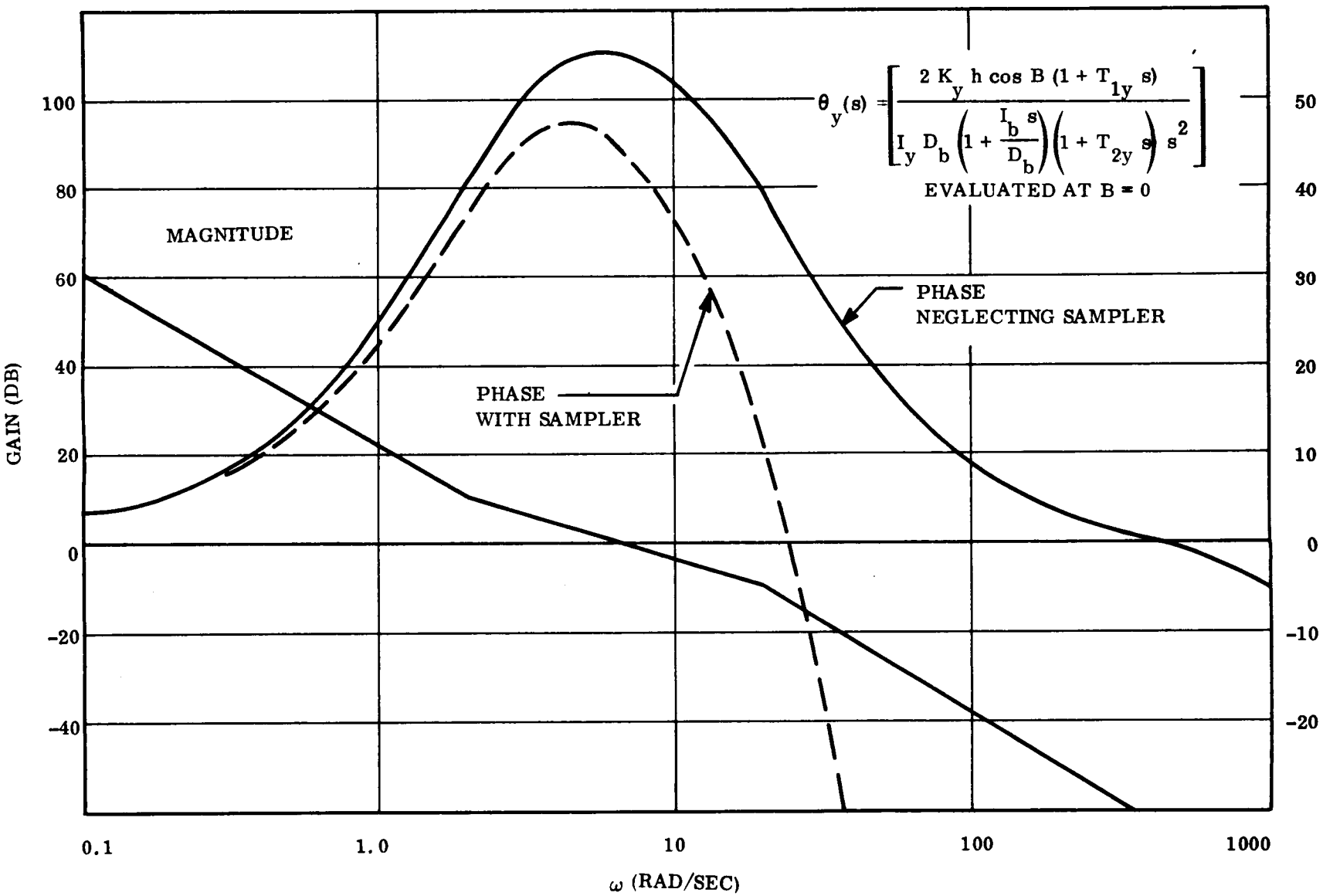

Figure 5-15. Bode Plot for Y-Axis

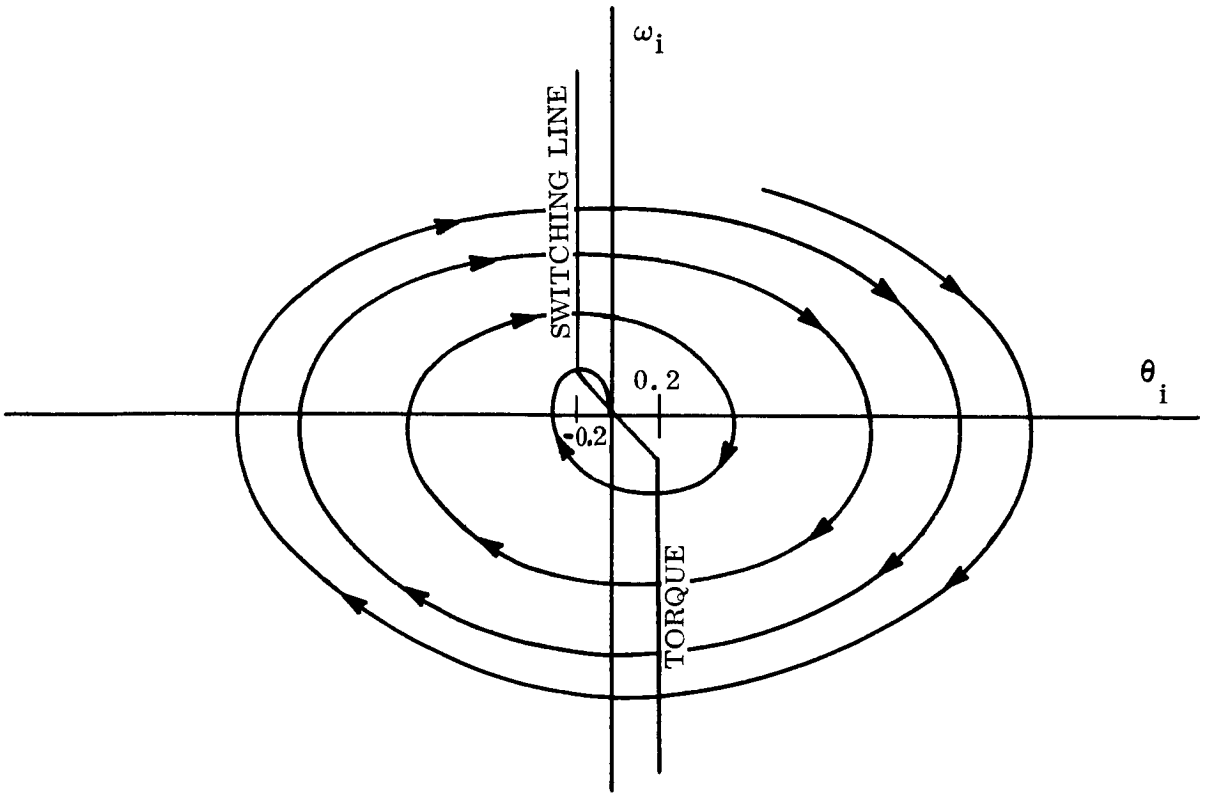

Figure 5-16. Phase Plane Without Rate Gyros

for more torque as indicated by passing signals from the spacecraft rate gyros through the characteristics shown in Figure 5-17. This approach has the advantage of only calling for more torque when the rates are high; the deadband removes the gyro from the loop at low rates, where the gyro is apt to have a poor signal to noise ratio. Utilizing the rate gyros in this manner converts the phase plane plot shown in Figure 5-16 to the one shown in Figure 5-18. This comparison is examined in greater detail in Section 6 (Control System Performance Verification).

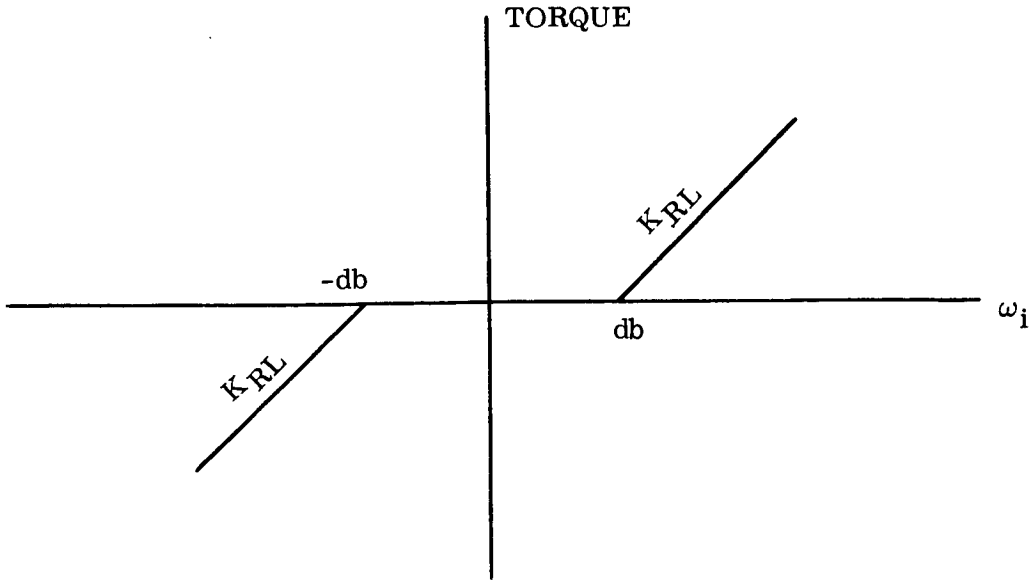

Figure 5-17. Torque vs. Vehicle Rate

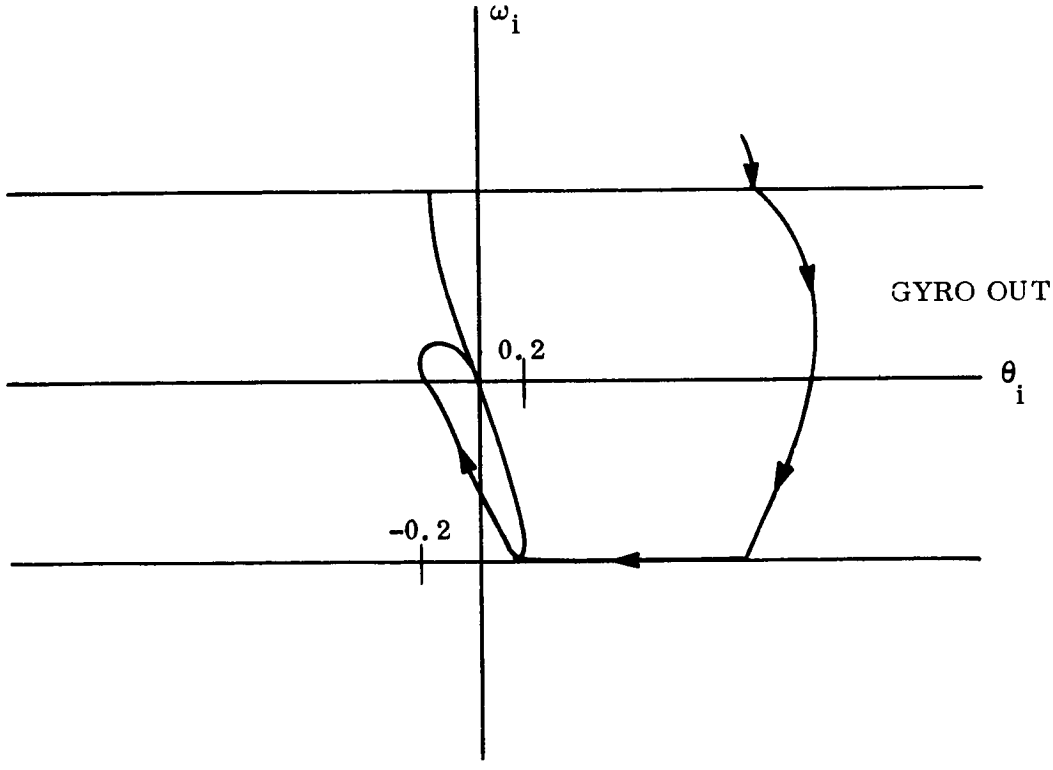

Figure 5-18. Phase Plane With Rate Gyros

5.4.3 SPACECRAFT Z-AXIS ATTITUDE CONTROL LAWS

Following the format used in the last two sections, the Z-axis attitude control laws are:

$$T_{c_3} = -K_z \frac{(1 + T_{1z}\, s)}{(1 + T_{2z}\, s)} \theta_z - D_c \dot{c}_3 - M_z (c_3 + c_4)$$

$$+ (T_{b_3} + D_b \dot{b}_3) \tan b_3 \tan c_3$$

$$- \begin{cases} K_{r_1} \left[(w_z - db \text{ sign } (w_z)) \right] & \text{if } |w_z| > db \\ \left[0 \right] & \text{if } |w_z| \leq db \end{cases} \qquad (5\text{-}12)$$

$$T_{c_4} = K_z \frac{(1 + T_{1z}\, s)}{(1 + T_{2z}\, s)} \theta_z - D_c \dot{c}_4 - M_z (c_3 + c_4)$$

$$+ (T_{b_4} + D_b \dot{b}_4) \tan b_4 \tan c_4$$

$$+ \begin{cases} K_{r_1} \left[(w_z - db \text{ sign } (w_z)) \right] & \text{if } |w_z| > db \\ \left[0 \right] & \text{if } |w_z| \leq db \end{cases} \qquad (5\text{-}13)$$

When both the inner and outer gimbal angles are large, the Z-axis responds to Y-axis excitation as is described in Appendix D and in Section 5.3.3. The control law decoupling suggested was incorporated into the outer gimbal torque motors in the form of the terms $(T_b + D_b \dot{b}) \tan b \tan c$. All other terms in the control laws are similar to those described for the Y-axis control laws. All of the control law parameters were summarized in Table 5-2.

5.4.4 ANGULAR MOMENTUM MANAGEMENT

The function of the control moment gyros is to exchange and store angular momentum. Precision pointing is maintained by absorbing the integrated disturbance torque momentum with the control moment gyros by repositioning the gimbals. In order that the capacity of the momentum exchange subsystem not be exceeded, a reset or unloading mechanism

must be implemented. This is accomplished by using the onboard reaction jet subsystem. Once any gimbal angle reaches 60 degrees, the appropriate axis is unloaded by firing a pneumatic jet. A 60-degree limit allows the gyro to store up to 87 percent of its available capacity, yet keeps the gyro operating in a regime where the gimbal dynamics are not seriously modified.

5.5 ANALYSIS OF SERVOED OPTICS CONTROL LOOPS FOR POINT AHEAD

The transmitted laser beam is deflected by a tilting plate with two degrees of freedom relative to the established spacecraft attitude reference. The point-ahead angles of the tilt plate are updated every 6 seconds by commands stored in the spacecraft's computer. These commands point the tilt plate relative to the spacecraft's pitch and yaw control axes.

5.5.1 BASIC CONFIGURATION

The basic configuration for the tilting plate control system is a two degree-of-freedom gimbal system. The tilting plate point-ahead angles are maintained in yaw and pitch by the inner and outer gimbals, respectively. In this configuration the pitch torquer must drive the entire inner gimbal (including the yaw control system), while the yaw torquer need only drive the tilting plate and the driven members of the yaw servo.

The servoed optics loop for either axis is shown in block diagram form in Figure 5-19. The components used in the control system are within present day state of the art, or can be obtained with modest improvements.

A digital pickoff was selected to meet the ± 10 arc-seconds previously allocated. This is consistent with the highest resolution available today. The pickoff was sized to accommodate ± 45 degrees rotation of the tilting plate with 15 bits required. This implies the least significant bit would correspond to ± 5 arc-seconds. Brushless dc motors and tachometers were selected because of their low noise characteristics.

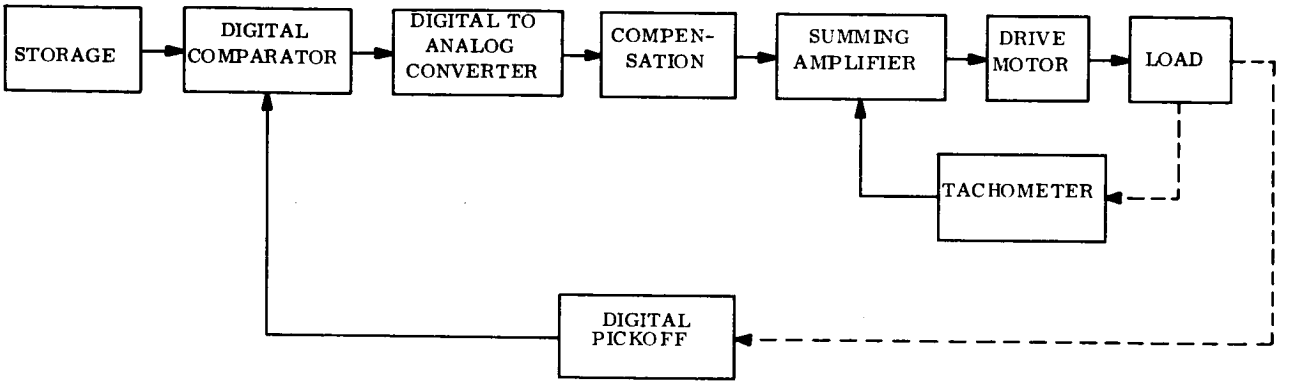

Figure 5-19. Single Axis Control System

The prime considerations in the analytical design of the servo subsystem were the high gain required to maintain the tilting plate pointing accuracy ($\pm$14 arc-seconds), and the desire for low control bandwidth to minimize noise in the loop and permit a minimum sampling frequency in the digital comparator. Rate feedback, series compensation and combinations of both were considered. Tradeoffs performed indicated that a reasonable computation rate (100 per second) can be achieved without resorting to a conditionally stable loop by using a combination of rate feedback and simple series compensation while providing a desirable overdamped response characteristic. Consideration was given in the loop design to minimizing the torque motor size (to minimize friction and power dissipation) while establishing a torque position error gain sufficient to make the position error, due to friction on the gimbal axes, negligible. Rate feedback was selected to provide desired damping within estimated projected noise limitations for the rate sensor. Control bandwidth was further reduced through the use of series lag compensation. The control bandwidth achieved was less than 10 Hz allowing digital computation of the order of 100 Hz, which is well within the state of the art. A zero order hold (ZOH) was considered for the digital to analog conversion.

5.5.2 YAW AXIS CONTROL SYSTEM DESIGN

Based upon the above configuration and existing components the yaw axis load was estimated to be:

$$\text{mass} < 0.01 \text{ slug}$$
$$I_L = 7 \times 10^{-5} \text{ lb-ft-sec}^2$$

With this load, the bearing static friction was estimated to be 10^{-5} ft-lb, and the running friction half that value.

For purposes of design, the yaw axis servoed optics loop can be represented by the linear sampled-data control system shown in Figure 5-20. The dynamics of the dc tachometer were neglected along with other high frequency rolloffs that greatly exceeded the system bandwidth. The various parameters shown in the block diagram are defined below:

- ψ : yaw point ahead angle
- I_L : moment of inertia of the inner gimbal (lb-ft-sec^2)
- K_t : torque sensitivity of motor (ft-lb/volt)
- K_n : motor back emf (volt/rad/sec)
- K_A : amplifier (volt/volt)
- K_R : tachometer feedback (volt/rad/sec)
- K_P : position sensor sensitivity (volt/sec)
- $G_c(s)$: compensation network
- T : comparator sampling period = 0.05 sec

Since the least significant bit corresponds to an error of 5 arc-seconds, the torque developed by this error must be greater than the friction torque of 10^{-5} ft-lb.

Therefore:

$$K_P K_A K_t (5 \text{ sec}) > 10^{-5} \text{ ft-lb/arc-sec}$$

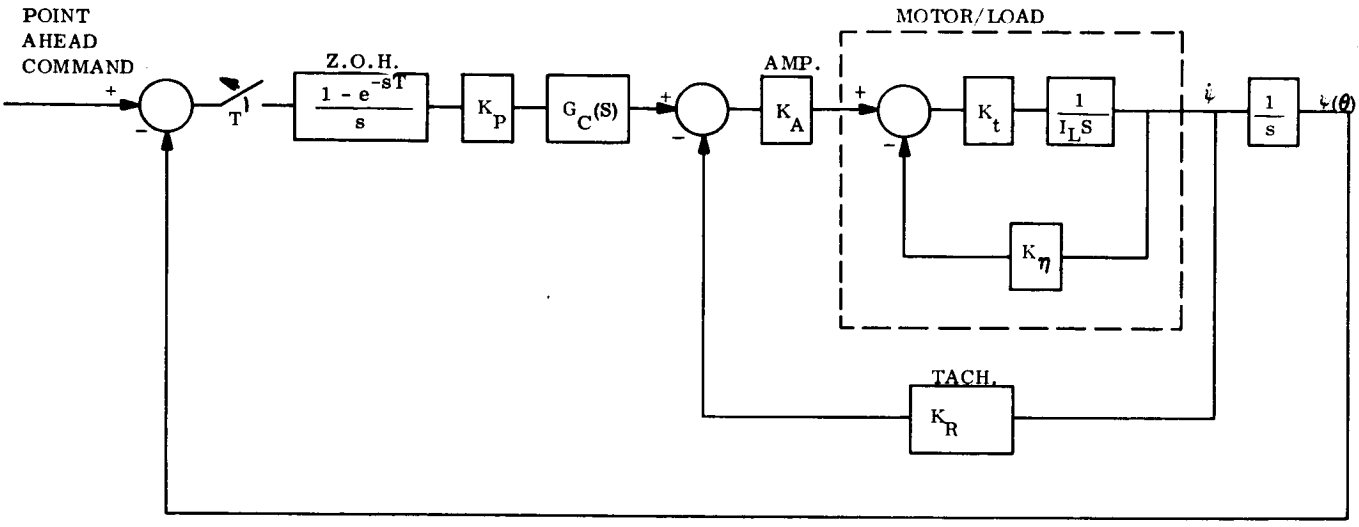

Figure 5-20. Block Diagram of Either Yaw (ψ) or Pitch (θ) Tilting Plate Servo

As a conservative design margin the control loop was sized to overcome 50 times the static friction torque for a 5 arc-second position error. With this margin of safety:

$$K_P K_A K_t = 10^{-4} \text{ ft-lb/arc sec}$$

Using this torque constraint and the limitation of present day components along with the bandwidth requirement, the selection of the parameters can be determined from standard control system design.

The block diagram of Figure 5-20 can be reduced to Figure 5-21 where:

$$\frac{K_n}{K_A K_R} << 1$$

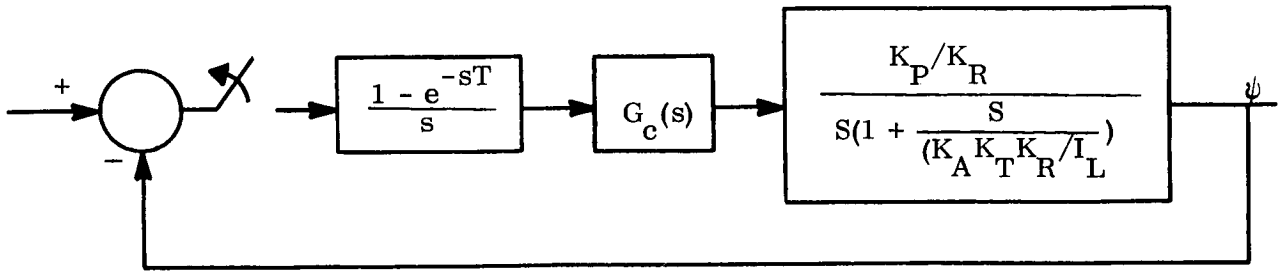

Figure 5-21. Block Diagram of Yaw Tilting Plate Servo, Negligible Back EMF

This approximation implies the back emf of the motor is negligible when compared to the damping produced by the tachometer feedback.

As a first approximation in design, the sampler and hold were neglected because the sampling frequency is much higher than the proposed bandwidth of the loop. With this approximation the open loop transfer function is

$$G(s) = \frac{K_P/K_R}{S\left(1 + \frac{S}{\frac{K_A K_t}{I_L} K_R}\right)}$$

Due to noise limitation,the position sensitivity was chosen as

$$K_P = 0.01 \text{ volt/arc second} = 2000 \text{ volt/radian}$$

The beat dc tachometers used with the summing amplifier limit the tach feedback gain to

$$K_R = 10 \text{ volt/radian/sec}$$

Using the static friction constraint with the parameters given above yields

$$K_A K_t = 10^{-2} \text{ ft-lb/volt}$$

and

$$G(s) = \frac{200}{S\left(1 + \frac{S}{1430}\right)}$$

To limit the bandwidth to 10 Hz, and still maintain an overdamped response with adequate phase margin, simple lag compensation was used.

The control system parameters chosen to satisfy the requirements are summarized below:

$$K_P = 0.01 \text{ volt/sec}$$

$$K_A = 50 \text{ volt/volt}$$

$$K_t = 2 \times 10^{-4} \text{ ft-lb/volt}$$

$$K_R = 10 \text{ volt/rad/sec}$$

$$G_c(s) = \frac{1 + \frac{S}{10}}{1 + \frac{S}{2}}$$

This torque sensitivity is consistent with a 1 in.-oz brushless dc motor.

Figure 5-22 is the resulting block diagram of the yaw axis tilting plate servo, with the sample and hold estimated by a frequency dependent lag. This approximation is valid when the bandwidth of the system is at least lower than the sampling frequency.

Figure 5-23 shows the bode and phase plot for the approximation shown in Figure 5-22. The system has 60 degrees of phase margin and 16 db of gain margin. The bandwidth is 10 Hz.

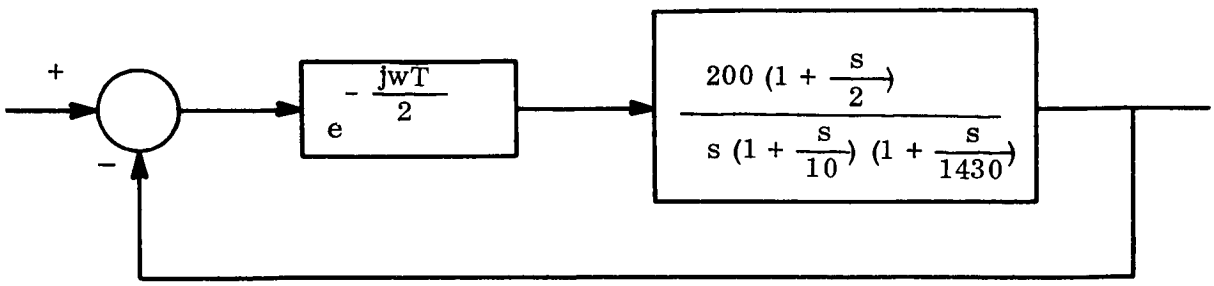

Figure 5-22. Block Diagram of Yaw Tilting Plate Servo, Sample and Hold Estimated by a Frequency Dependent Lag

In order to investigate the transient response of the yaw axis control system, Z-transform techniques were used. The lag with a break frequency of 143 rad/sec was neglected because it is much higher than the bandwidth of the system. With this approximation the system is shown in Figure 5-24.

$$G(z) = (1 - z^{-1}) \mathcal{Z} \left[200 \frac{(1 + \frac{S}{10})}{S^2 (1 + S/2)} \right]$$

$$G(z) \quad 40T \frac{[z - (1 - 10T)]}{(z - 1)[z - (1 - 2T)]} = 0.4 \frac{(z - 0.9)}{(z - 1)(z - 0.98)}$$

The unit step response is shown in Figure 5-25.

5.5.3 PITCH AXIS CONTROL SYSTEM DESIGN

As previously stated, the pitch axis of the tilting plate is controlled by the outer gimbal;

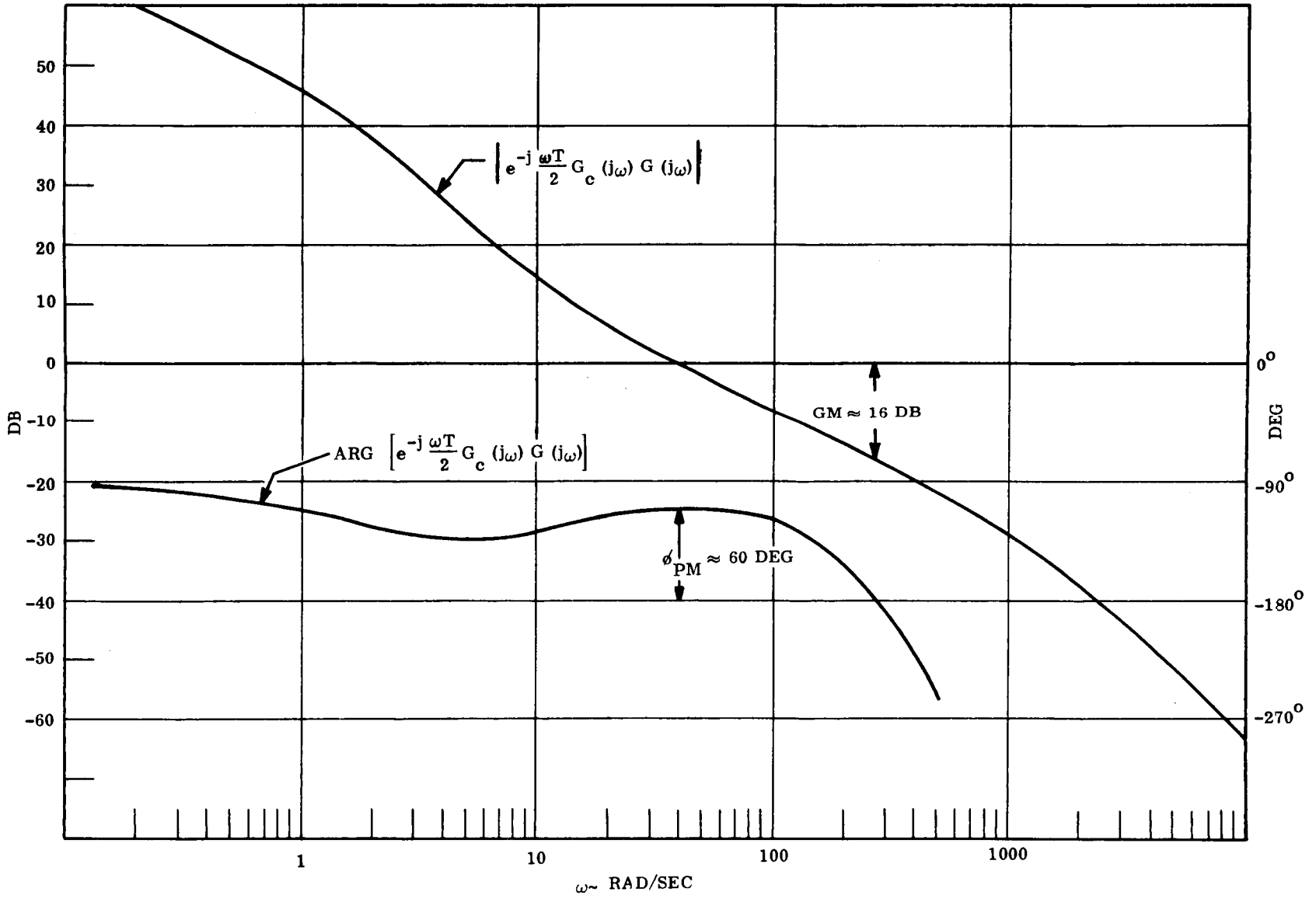

Figure 5-23. Bode and Phase Plot of Yaw Axis Tilting Plate Servo

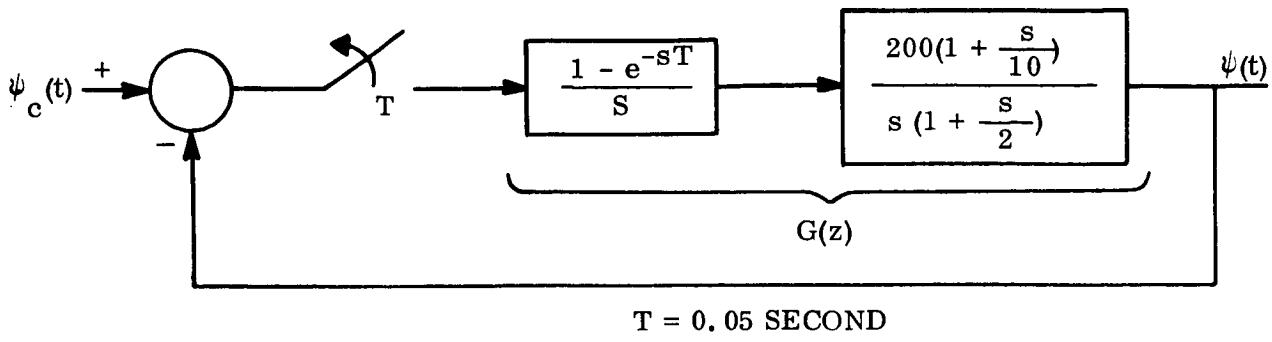

Figure 5-24. Investigation of the Transient Response of the Yaw Axis Control System

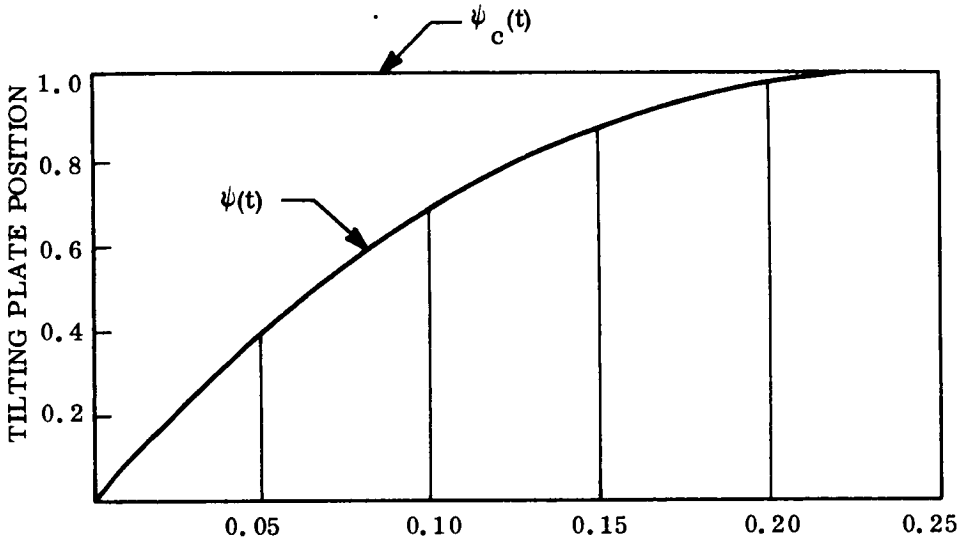

Figure 5-25. Response to Unit Step

therefore, its driven members include the entire yaw axis control system. With existing components, an estimate of the pitch load is:

weight ≈ 1 lb at launch

$I_L = 10^{-3}$ lb-ft-sec^2

With a load of 1 lb on the bearings, the static friction is about 10 times that of the yaw axis. Using this estimate, a 2 in.-oz brushless dc motor is adequate.

Using the position sensitivity and tachometer gain of the yaw axis servo, the closed loop performance of the pitch axis can be made the same as the yaw axis when:

$$K_t = 2 \times 10^{-3} \text{ ft-lb/volt}$$

$$K_A = 71.5 \text{ volt/volt}$$

A torque sensitivity of 2×10^{-3} ft-lb/volt is consistent with a 2 in.-oz brushless dc motor.

With the above parameters the transfer function of the plant (motor and load) is

$$G(s) = \frac{200}{S\left(1 + \frac{S}{1430}\right)}$$

This is the same transfer function as the yaw axis servo. Therefore, the compensation given in the yaw design can be used. The performance of the pitch servo is now the same as the yaw servo.

SECTION 6

CONTROL SYSTEM PERFORMANCE VERIFICATION WITH AN ANALOG COMPUTER SIMULATION

SECTION 6

CONTROL SYSTEM PERFORMANCE VERIFICATION WITH AN ANALOG COMPUTER SIMULATION

6.1 INTRODUCTION

To investigate the performance of the pitch (y-axis) and yaw (z-axis) attitude control system and check the concepts introduced into their control laws, an analog computer simulation was fabricated. The simulation was used to verify the acquisition and station switching capability of the control system using the twin two degree of freedom control moment gyros. The necessity of having a simulation to evaluate the control system performance during this mode of operation was dictated by the fact that fast nonlinearities (see Section 2.7 for discussion) of the sensors and torque motor summing amplifiers are encountered. The linear system techniques appropriately used to evaluate performance during fine attitude hold are in this case rendered inadequate.

6.2 THE ANALOG COMPUTER SIMULATION

The pitch and yaw axes of the attitude control system were simulated on a general purpose analog computer (EAI Model 231-R). The final form of the simulation utilized the twin two degree of freedom control moment gyros in the highly damped mode. Initially the simulation was used to examine the characteristics of the control actuators while being utilized in the lightly damped mode.

The equations which were used to represent the control moment gyros are presented in Appendix G. The resulting simulation diagram for the control actuators operating in the lightly damped mode is illustrated in Figure 6-1. Figure 6-2 shows the modified gimbal dynamics simulation for the actuators operating in the highly damped mode. Except for the additional damping, the descriptive equations remain the same. Thus, the simulation form remains identical, and only the scaling is changed. Due to this similarity the complete simulation is not repeated.

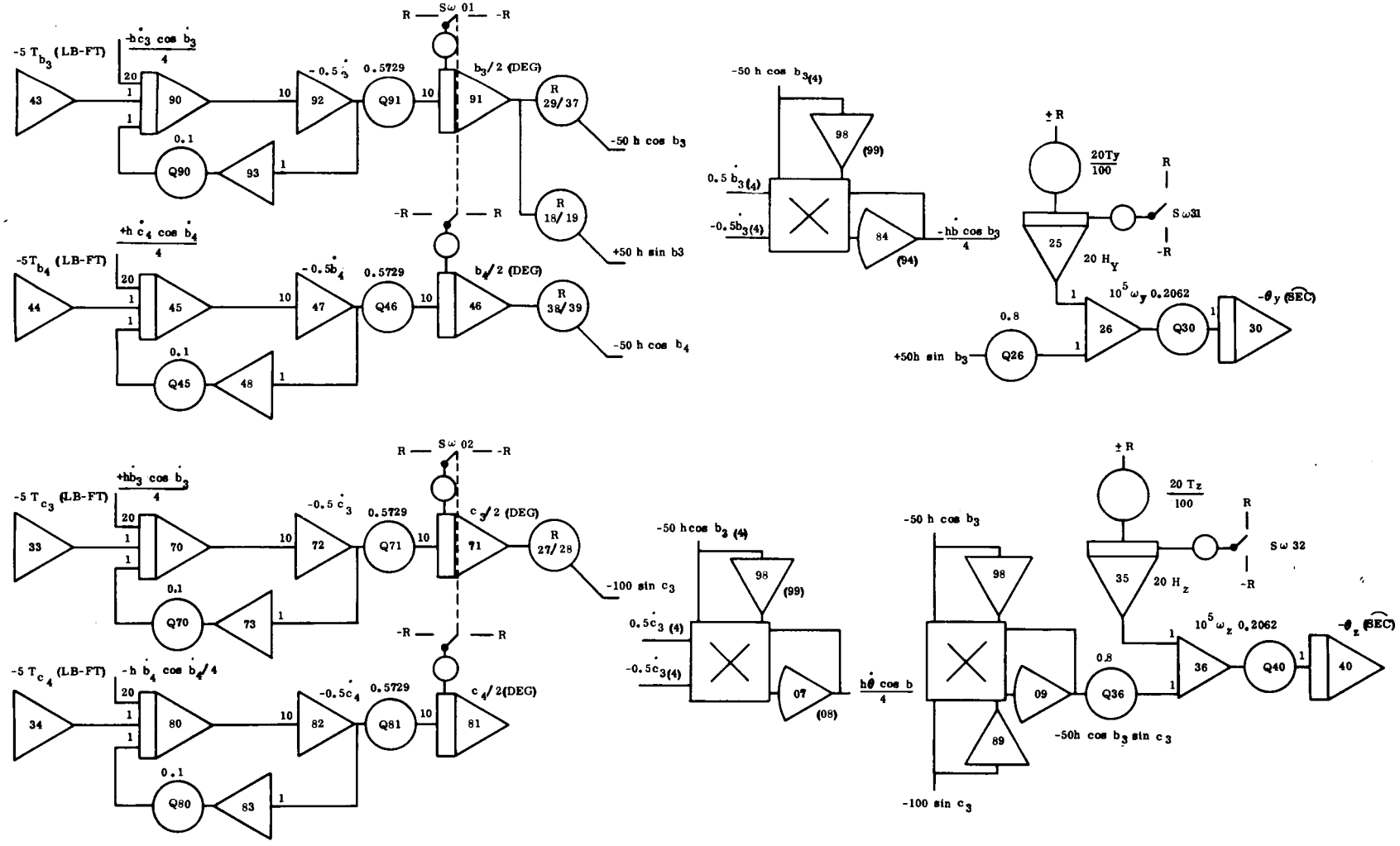

Figure 6-1. Simulation Block Diagram of Twin 2 DOF CMG's Used in the Lightly Damped Mode

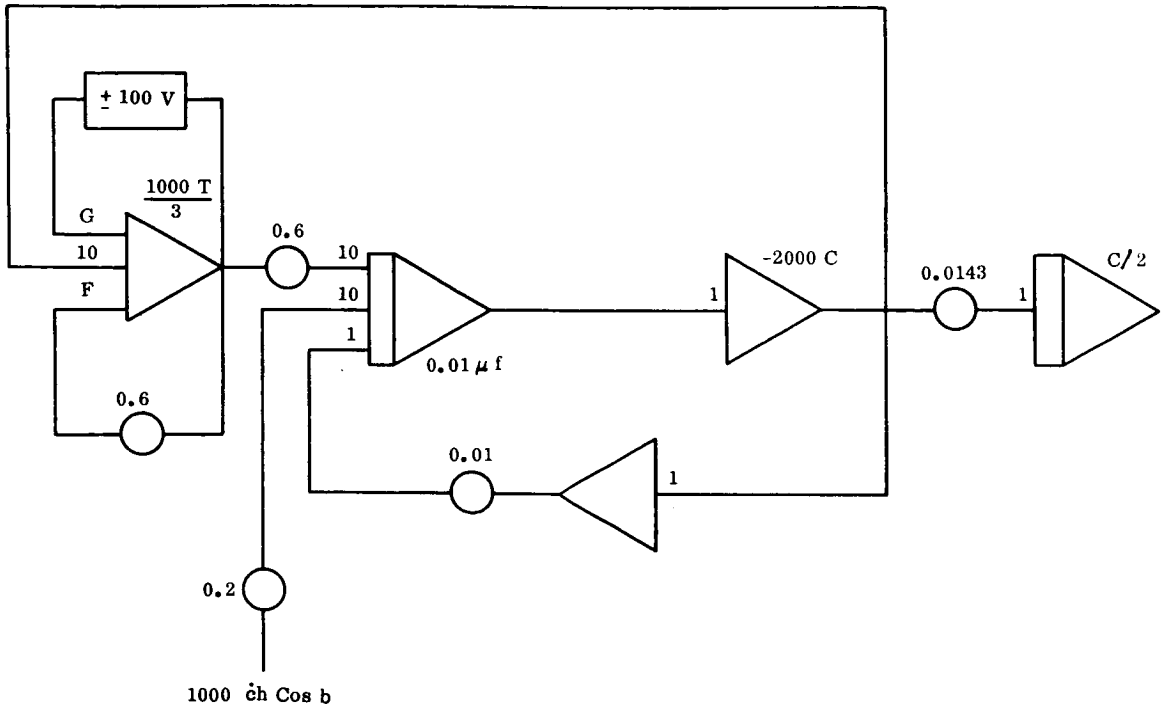

Figure 6-2. Modified Gimbal Dynamics for the Control Actuators Operating in the Highly Damped Mode

The form of the simulation for investigating the lightly damped mode of operation of the two degree of freedom control moment gyros included only the compensation network and the gimbal angle constraint loops as shown in Figures 6-3 and 6-4. The simulation operated at a 10 to 1 time scale reduction, i.e., ten seconds real time equals one second problem time. Due to the presence of the damped high frequency oscillation in the gimbal dynamics, solid state electronic resolvers were employed. Servo-mechanical resolvers were found to induce unrealistic perturbations from mechanic vibrations which arise in the servo nulling process.

The final form of the simulation utilizing the control moment gyros in the highly damped mode included sensor characteristics, compensation networks, gimbal angle constraint loops, the proposed decoupling function, rate loops, running friction, and unloading capability. They are presented in the simulation diagram form (Figures 6-1 through 6-3 and 6-5 through 6-8) along with a description where applicable. The time scale was real time. The gimbal dynamics simulation was revised to accommodate the increased damping and to

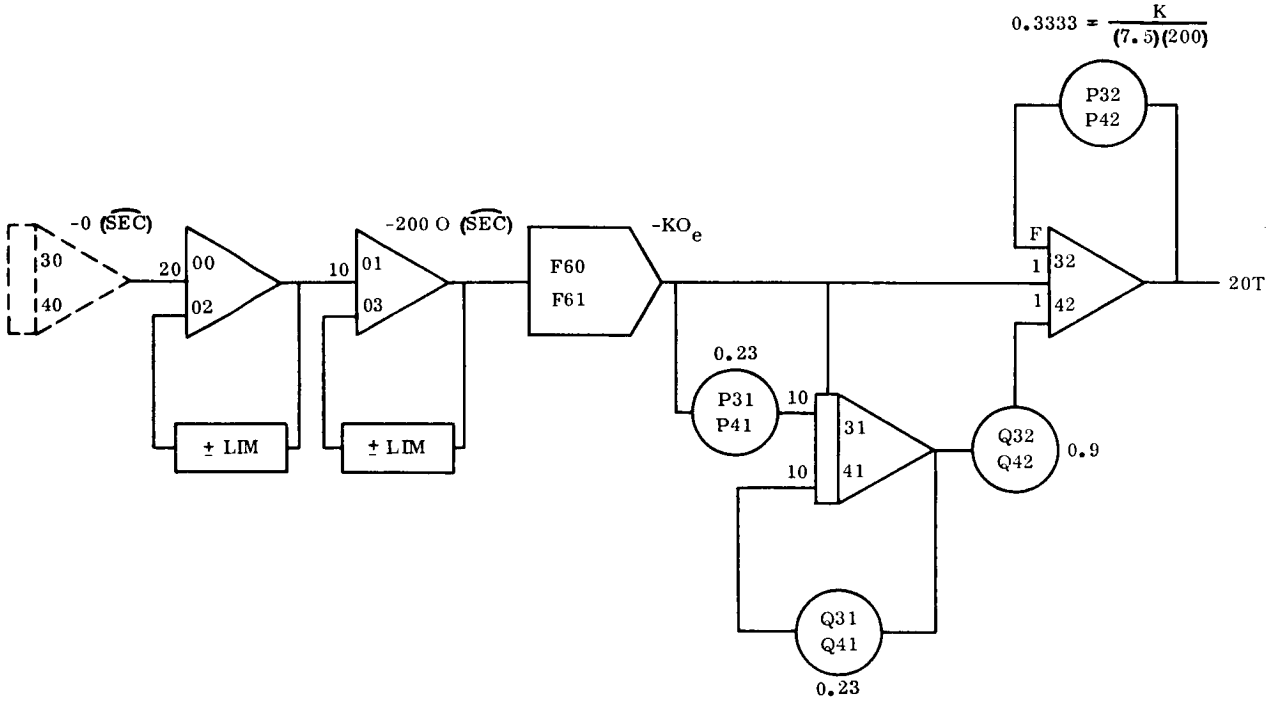

Figure 6-3. Control Loop for Twin 2 DOF CMG's

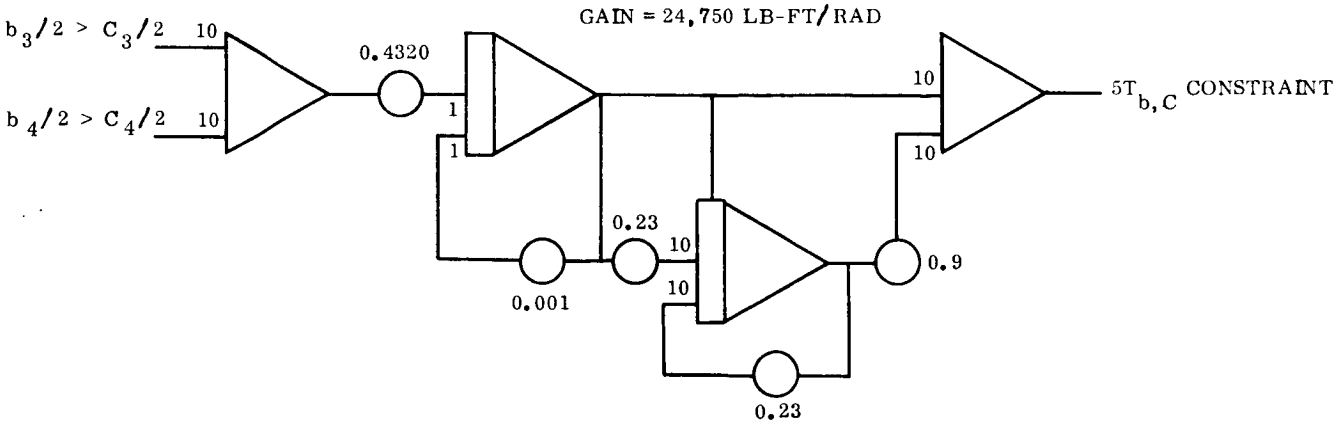

Figure 6-4. Constraint Loop for Twin 2 DOF CMG's Operating in the Lightly Damped Mode

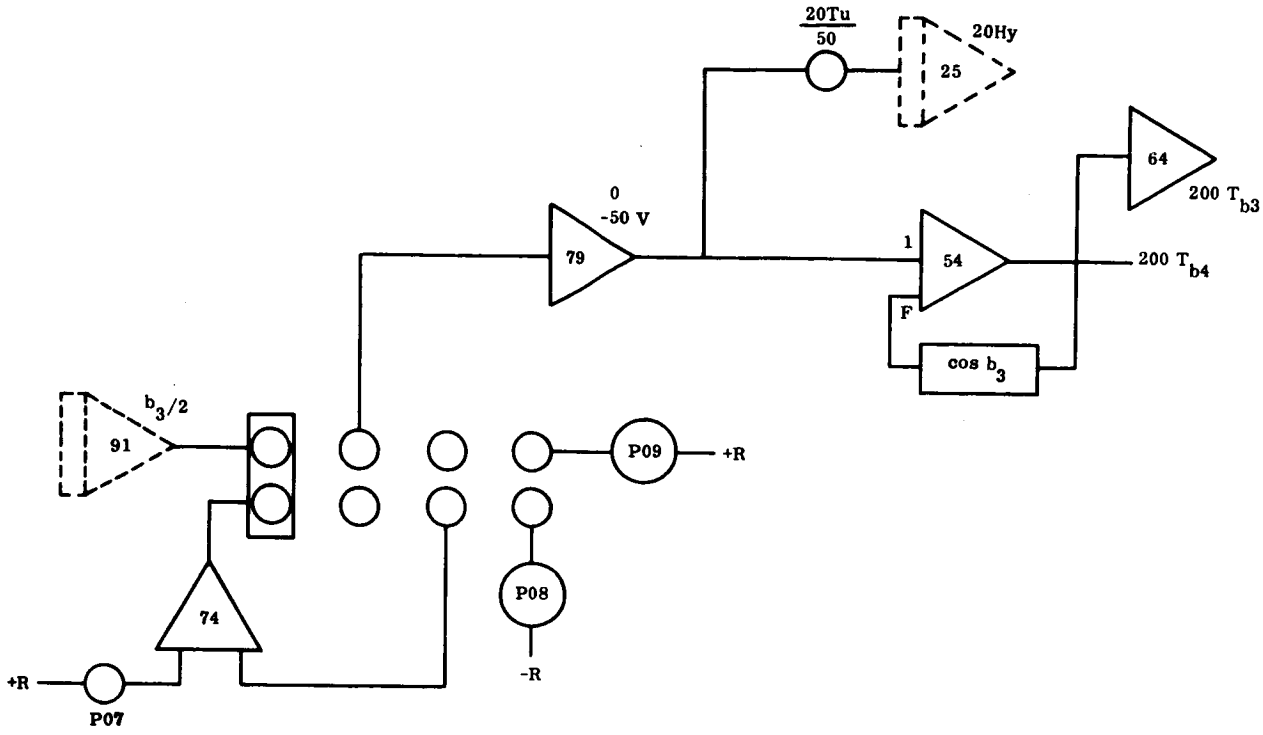

Figure 6-5. Unloading Circuit for the Inner Gimbals of the Twin 2 DOF CMG's

provide for the saturation of the torque motor summing amplifiers (Figure 6-1 as modified by Figure 6-2). The sensor characteristic used was the transfer function of the pyramid beam splitter fine beacon sensor described in paragraph 5.2.1.4, and it was simulated through use of a nonlinear function generator. Running friction was implemented with electronic switches in the CMG characteristic simulation shown by Figures 6-1 and 6-2.

The compensation network used is shown in Figure 6-3. The unloading circuit for the inner gimbals is shown in Figure 6-5. When a gimbal angle reaches sixty degrees, a pneumatic jet is actuated to impart a constant

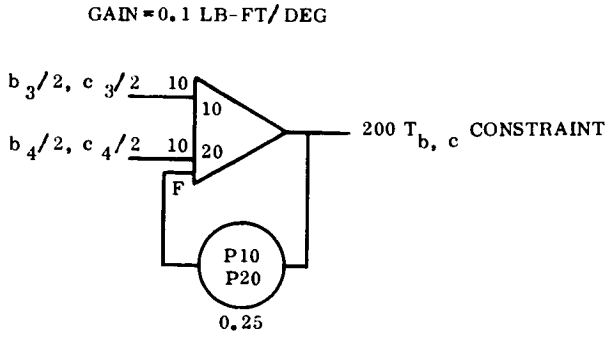

Figure 6-6. Constraint Loop for Twin 2 DOF CMG's Operating in the Highly Damped Mode

0.01 foot-pound of external torque to the vehicle and simutaneously an electrical signal calls for torques from the gimbal torque motors in order to maintain precision control even during unloading. The unloading is discontinued when the gimbal angles change sign. The gimbal angle constraint loops are shown in Figure 6-6. A decoupling function of the function of the form

$$T_c = (T_b + D_b \dot{b}) \tan b \tan c$$

was implemented as shown in Figure 6-7. The rate loop used is depicted in Figure 6-8.

6.3 IDENTIFICATION OF ANALOG RUNS AND THEIR PURPOSE

A total of twenty-eight acquisition and station switching runs have been documented (Figures 6-9 through 6-25). The purpose of the analog simulation was to verify the acquisition and station keeping capability of the spacecraft pitch and yaw axes and also to check the concepts discussed previously that were introduced into the control laws. In particular it is of interest to demonstrate the effect of the sensor saturation and the performance improvement realized by using the proposed rate loops. It is also significant to show how y-axis transients are strongly coupled over into the z-axis when both inner and outer gimbal angles are large unless decoupling is introduced through the control laws when the rate loops are inoperative.

The initial conditions for eighteen acquisition runs are listed in Table 6-1 along with indications of when the rate gyro loops and control law decoupling are being utilized. Similar information for the ten station switching runs appears in Table 6-2.

6.4 DISCUSSION OF ANALOG RUNS

Run 1 (Figure 6-9) represents a typical worst case acquisition demonstration for the pitch axis with the gyro rate loops inoperative. The numerous overshoots result from the loss of derived rate information from the lead network due to the limited linear range of the sensor. The heading "Torque Control" refers to the signal entering the torque motor summing amplifier from the lead network, and the effect of the sensor saturation is quite evident.

The heading, "Torque Constraint", refers to the control law term that keeps the corresponding twin gimbal angles equal in magnitude and opposite in sign. This channel of information also functions as a total twin gimbal angle mismatch indicator since the scale factor is known to be 0.1 foot-pound per degree. "Torque Total" refers to the output of the torque motor summing amplifier which has as inputs the two previously mentioned terms plus the viscous damping torque signal obtained with tachometer feedback. This worst case set of conditions required a settling time of 70 seconds.

Run 1 (Figure 6-9) should be compared to Run 3 (Figure 6-10), which has the same initial conditions. The drastic improvement in the acquisition characteristics results from using the gyro rate loops. The settling time is reduced to about 21 seconds.

Run 9 (Figure 6-15) exchanges the initial conditions of Run 1 (Figure 6-9) between the pitch and yaw axes to indicate a yaw axis worst case acquisition demonstration. Run 11 (Figure 6-16) is the yaw axis acquisition counterpart of Run 3 (Figure 6-10) since the gyro rate loops are operative. When the gimbal angles are small, the pitch and yaw acquisition characteristics are almost identical.

Run 2 (Figure 6-9) was obtained by increasing the initial pitch rate of Run 1 until the first attitude overshoot just missed exceeding the sensor field of view at 90 seconds of arc. Run 4 (Figure 6-10) repeats the initial conditions of Run 2 (Figure 6-9), but with the gyro rate loops operative to again shown how the acquisition capability is enhanced. Again, Run 10 (Figure 6-15) is the yaw axis counterpart of Run 2 (Figure 6-9), and Run 12 (Figure 6-16) is the yaw version of Run 4 (Figure 6-10).

Run 5 goes back to the spacecraft rate and position conditions of Run 1 (Figure 6-9), only now with angular momentum initially stored on the control moment gyros by virtue of their forty-five degree gimbal angles. With no gyro rate loops or control law decoupling, this run clearly demonstrates the severe coupling of the y-axis transient over into the z-axis (Figure 6-12) since both gimbal angles are appreciable. This run should really be considered finished after the first 23 seconds, since the field of view limitation of the sensor was not modeled. Run 6 (Figure 6-13) then dramatically demonstrates the

benefit of decoupling through the control law. Run 7 (Figure 6-14) indicates the value of the gyro rate loops operating even without the control law decoupling. The rate loops help by virtue of their ability to keep all transients small. Run 8 (Figure 6-12) shows the response with both the rate loops and decoupling operative. The conclusion formed from considering Runs 5 through 8 (Figures 6-11 through 6-14) is that when both inner and outer gimbal angles have significant magnitude, either the control law decoupling or rate loops or both must be operative in order to prevent severe coupling of y-axis transients over into the z-axis.

Run 13 through 18 (Figures 6-17 through 6-20) demonstrate the acquisition characteristics with and without the rate loops, with transient conditions initially on both pitch and yaw.

Station switching is just a special case of acquisition where the vehicle angular rates are nominally small. With the decoupler circuitry utilized, the ten station switching exercises shown in Runs 19 through 28 (Figures 6-21 through 6-25) indicate adequate control system performance with the gyro rate loops either operative or failed.

Table 6-1. Acquisition Runs

Run	o_y sec	$\dot{o}_y$ sec/sec	o_z sec	$\dot{o}_z$ sec/sec	$b_3 = -b_4$ deg	$c_3 = -c_4$ deg	Gyro	Decoupler
1	15	10	0	0	0	0	Out	Out
2	15	19	0	0	0	0	Out	Out
3	15	10	0	0	0	0	In	Out
4	15	19	0	0	0	0	In	Out
5	15	10	0	0	45	45	Out	Out
6	15	10	0	0	45	45	Out	In
7	15	10	0	0	45	45	In	Out
8	15	10	0	0	45	45	In	In
9	0	0	15	10	0	0	Out	Out
10	0	0	0	15	19	0	Out	Out
11	0	0	15	10	0	0	In	Out
12	0	0	15	19	0	0	In	Out
13	15	10	5	5	0	0	Out	In
14	15	19	5	5	0	0	Out	In
15	15	10	5	5	0	0	In	In
16	15	19	5	5	0	0	In	In
17	15	10	5	5	45	45	Out	In
18	15	10	5	5	45	45	In	In

Table 6-2. Station Switching Runs

Run	σ_y sec	w_y sec/sec	σ_z sec	w_z sec/sec	$b_3 = -b_4$ deg	$c_3 = -c_4$ deg	Gyro
19	15	0	0	0	0	0	Out
20	15	0	0	0	0	0	In
21	15	0	0	0	45	45	In
22	15	0	0	0	45	45	Out
23	0	0	15	0	0	0	Out
24	0	0	15	0	0	0	In
25	0	0	15	0	45	45	In
26	0	0	15	0	45	45	Out
27	-15	0	0	0	45	45	In
28	0	0	-15	0	45	45	In

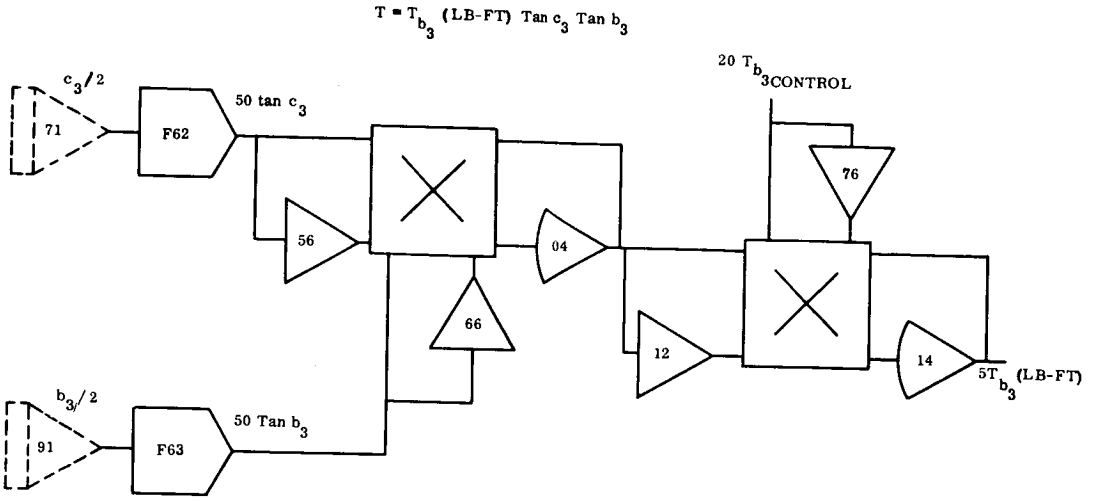

Figure 6-7. Decoupling Loop for the Twin 2 DOF CMG's Operating in the Highly Damped Mode

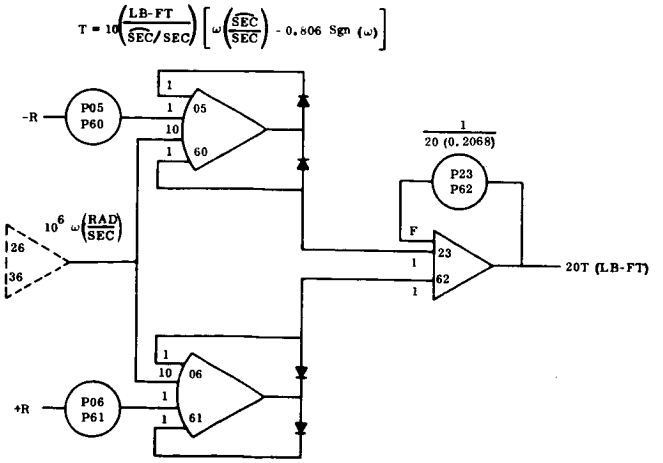

Figure 6-8. Rate Loop for the Twin 2 DOF CMG's Operating in the Highly Damped Mode

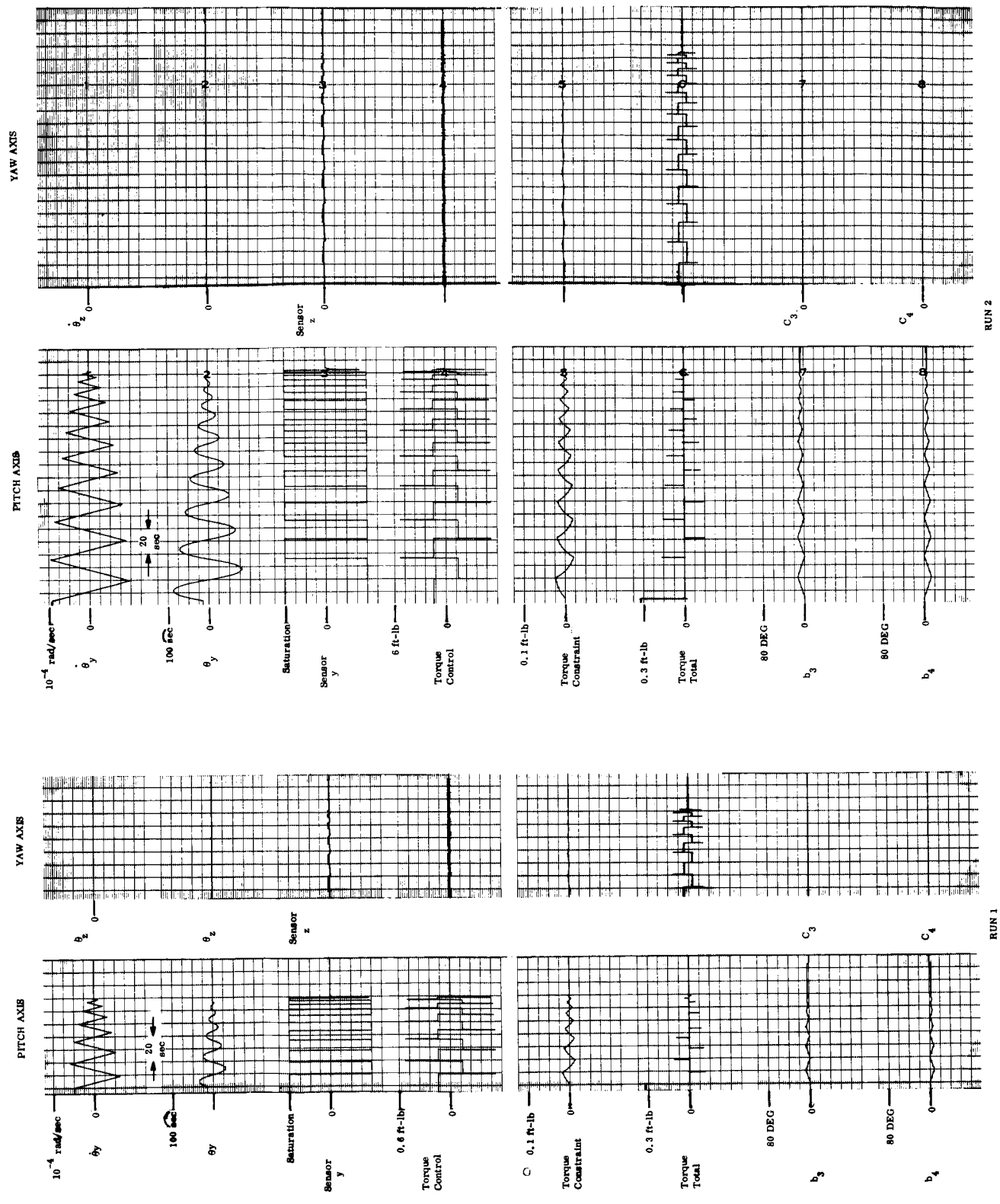

Figure 6-9. Analog Simulated Acquisition, Runs 1 and 2

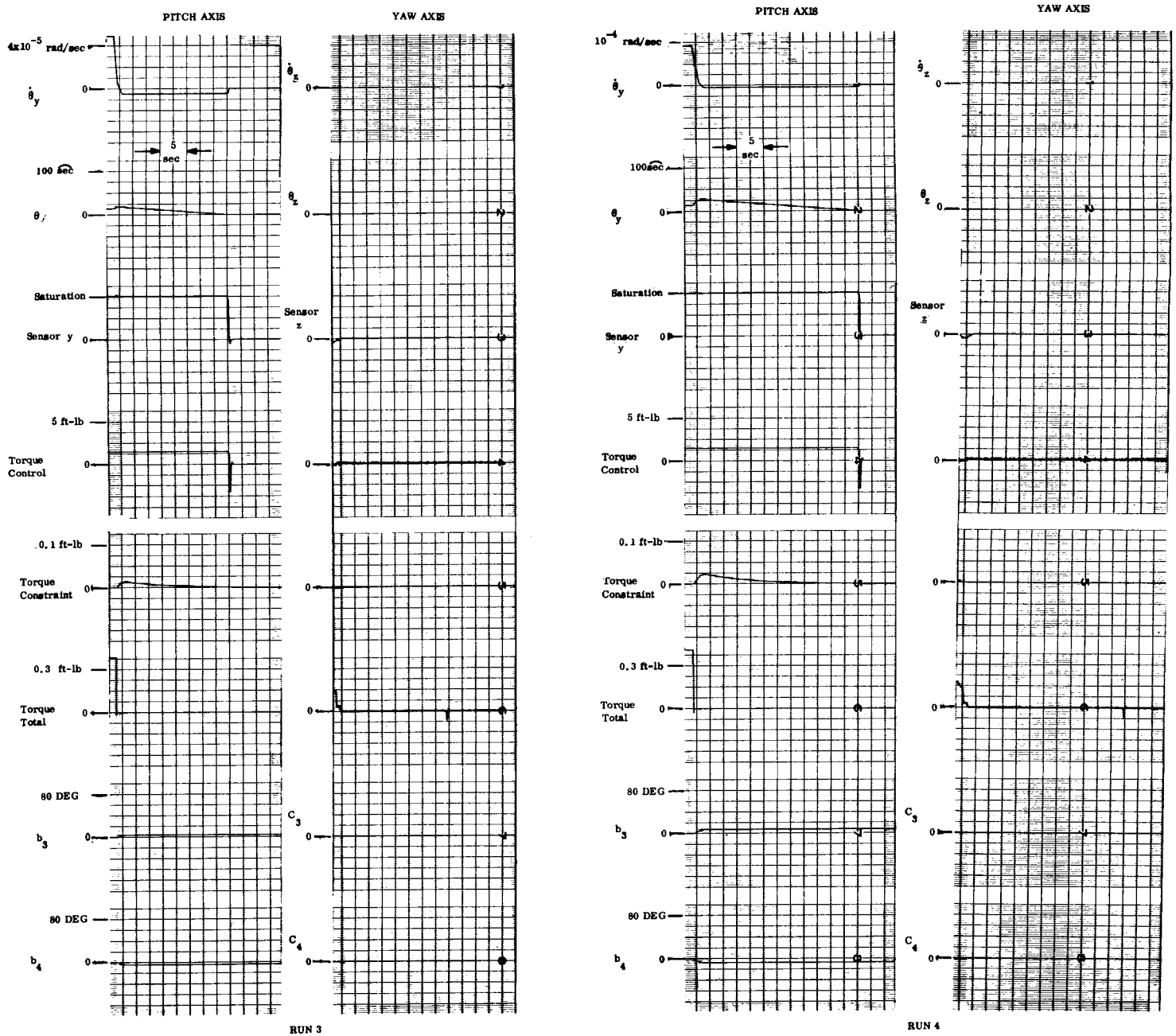

Figure 6-10. Analog Simulated Acquisition, Runs 3 and 4

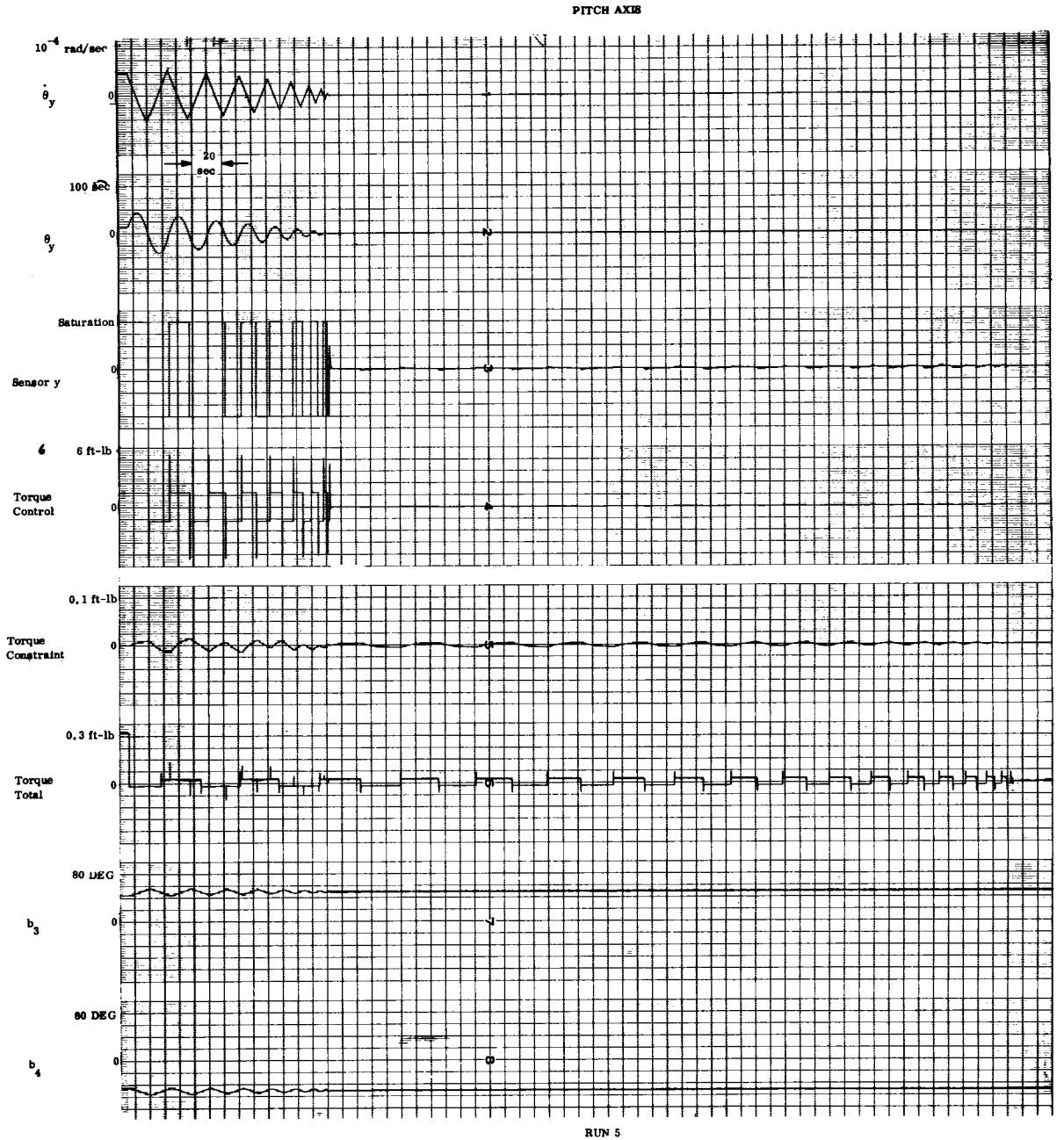

Figure 6-11. Analog Simulated Acquisition, Run 5, Y-Axis Parameters

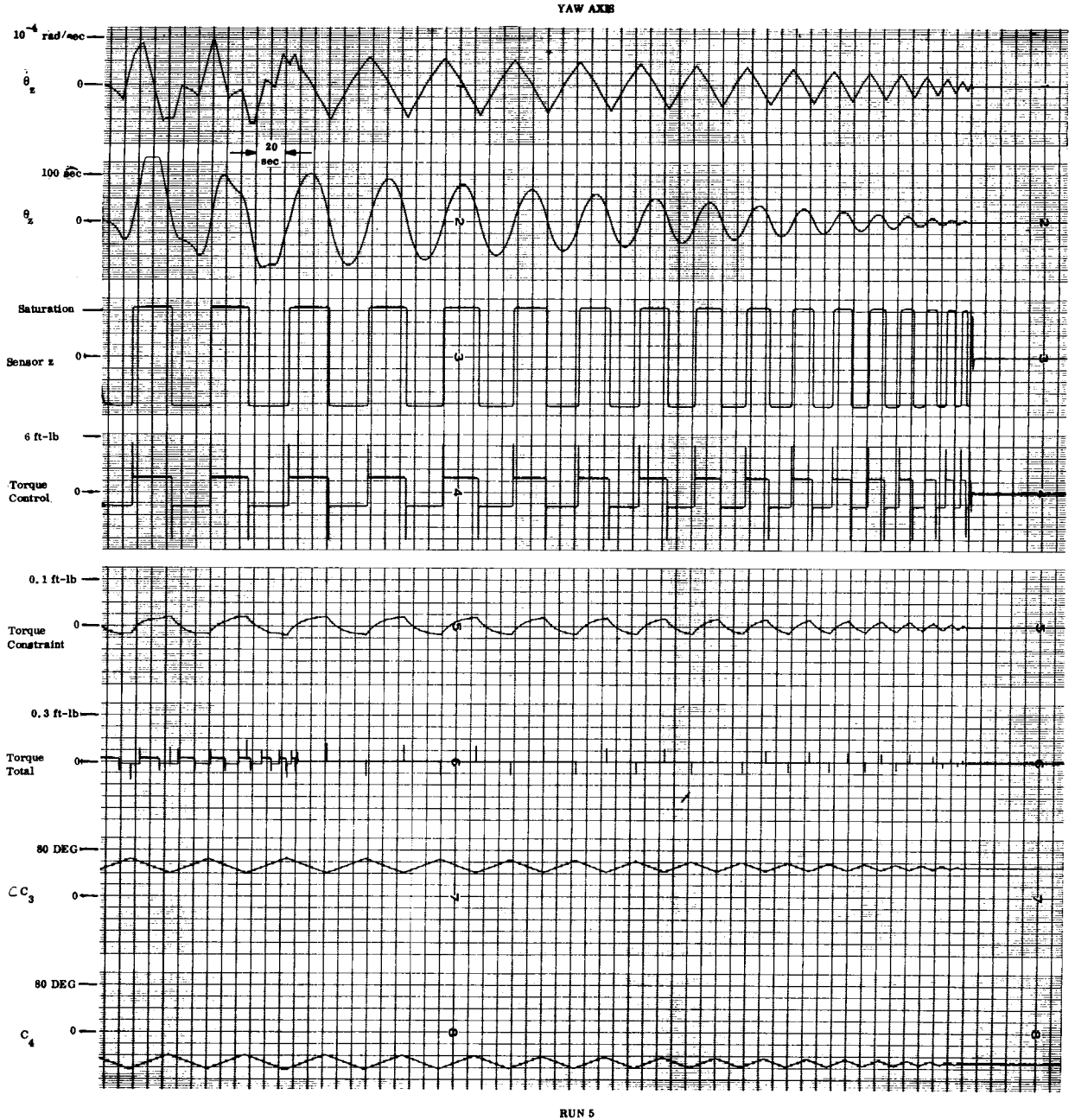

Figure 6-12. Analog Simulated Acquisition, Run 5, Z-Axis Parameters

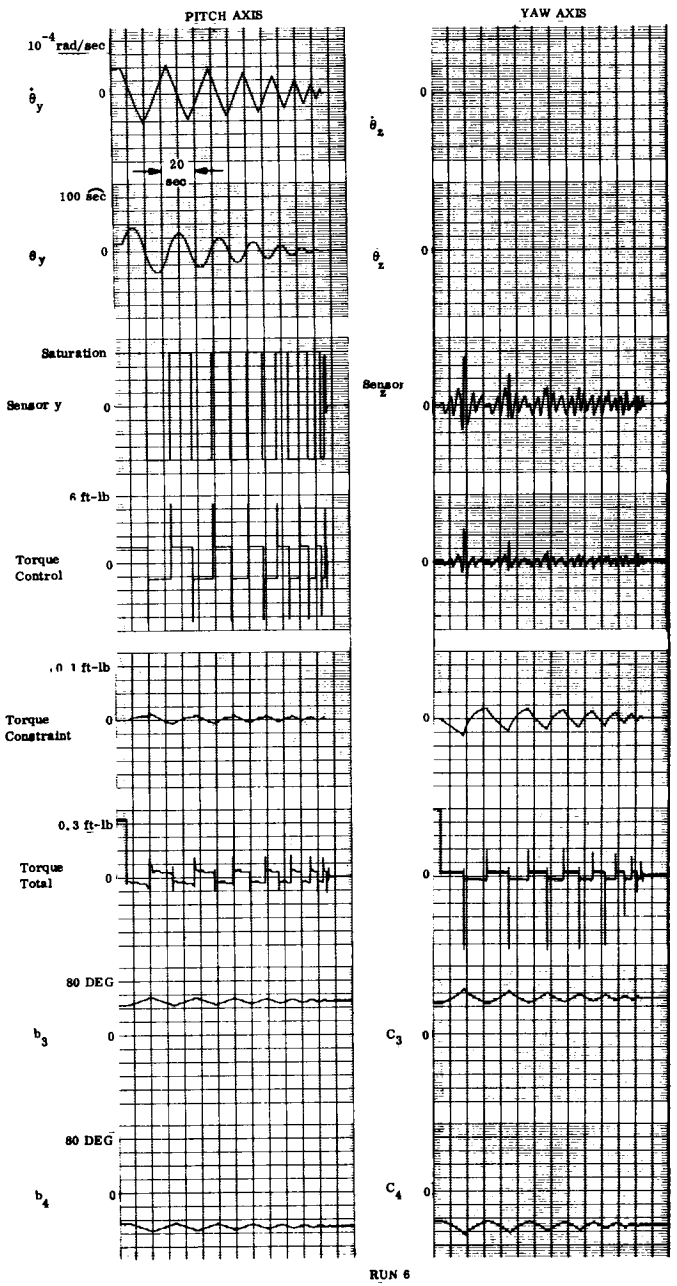

Figure 6-13. Analog Simulated Acquisition, Run 6

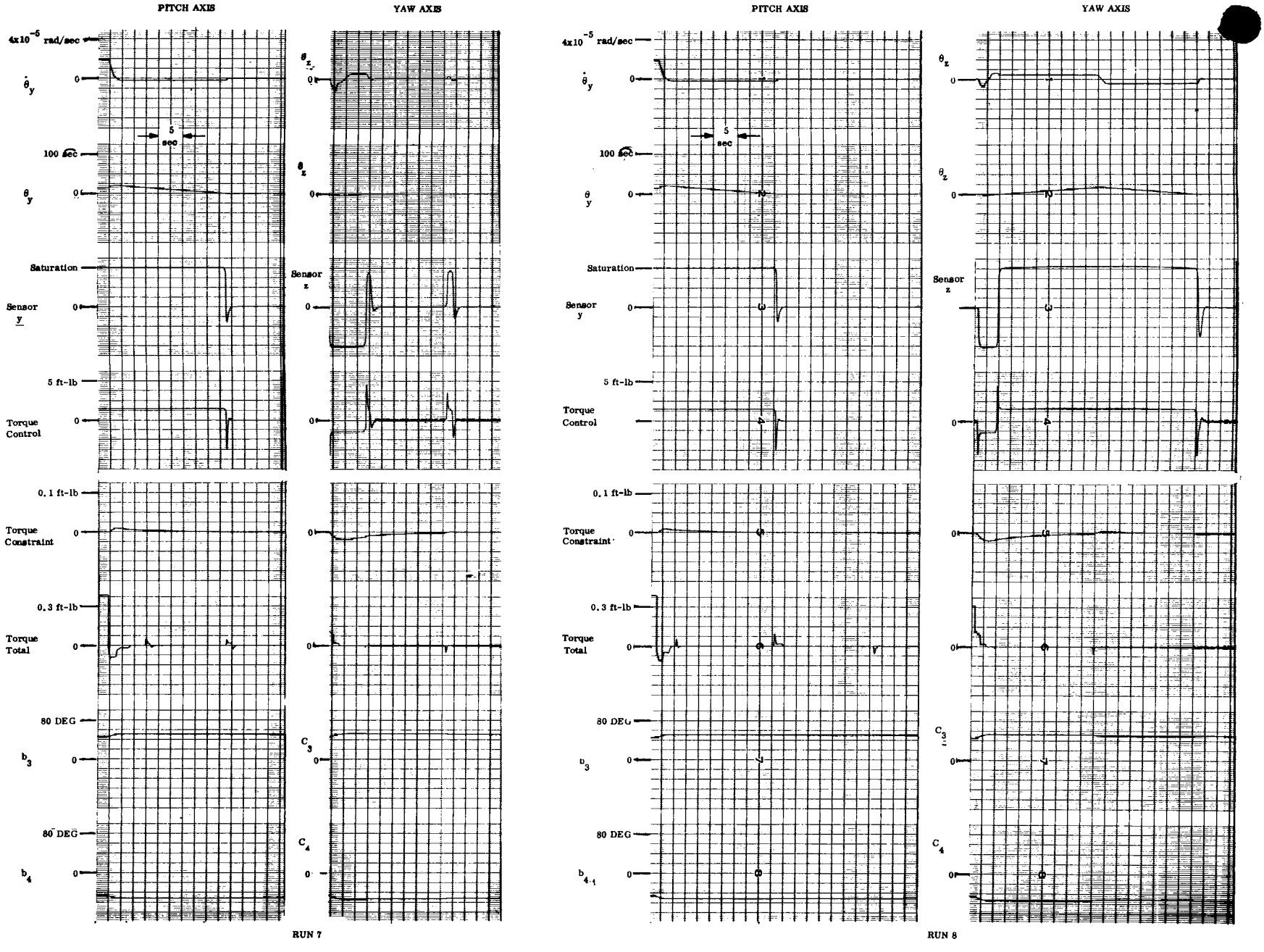

Figure 6-14. Analog Simulated Acquisition, Runs 7 and 8

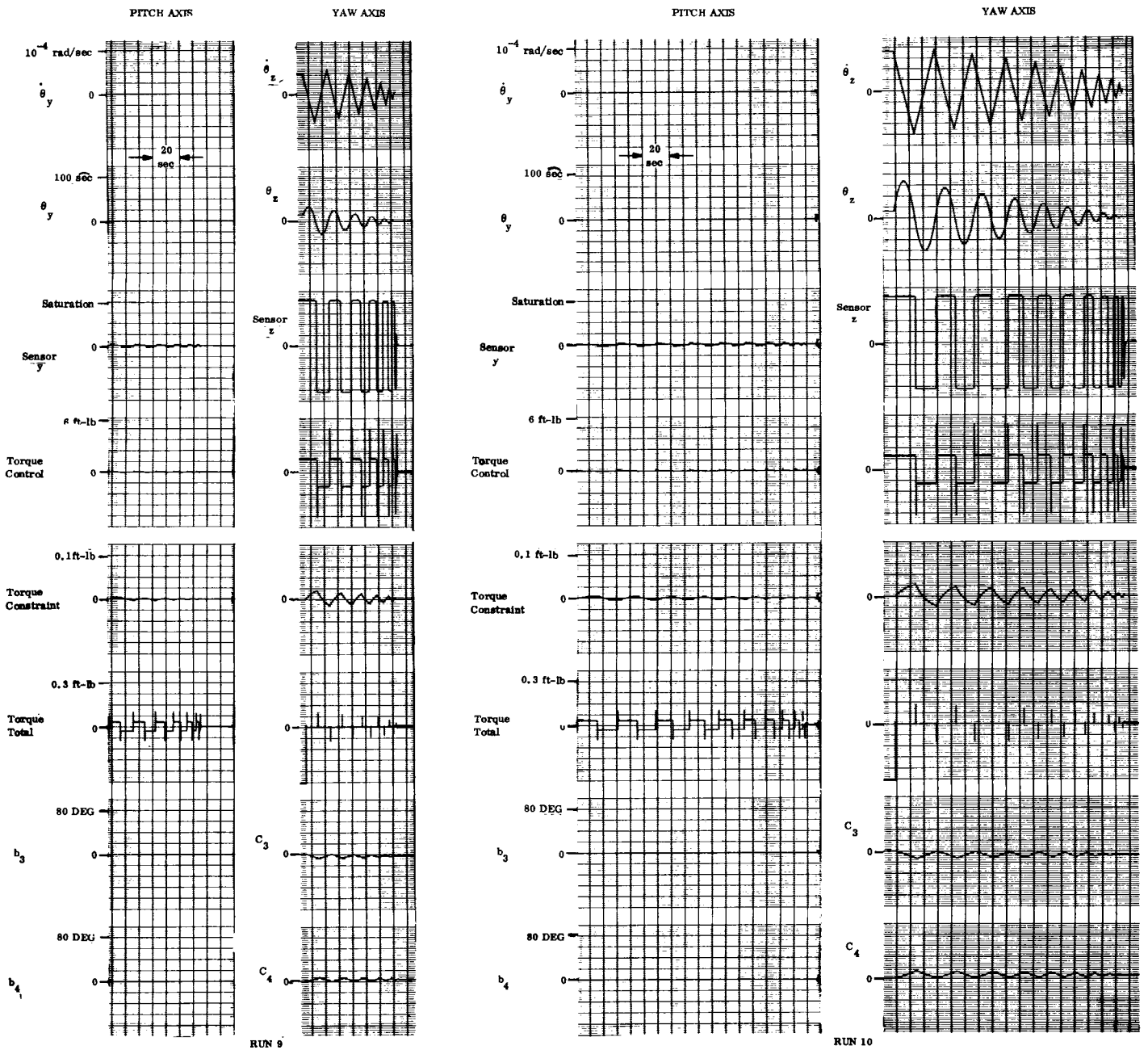

Figure 6-15. Analog Simulated Acquisition, Runs 9 and 10

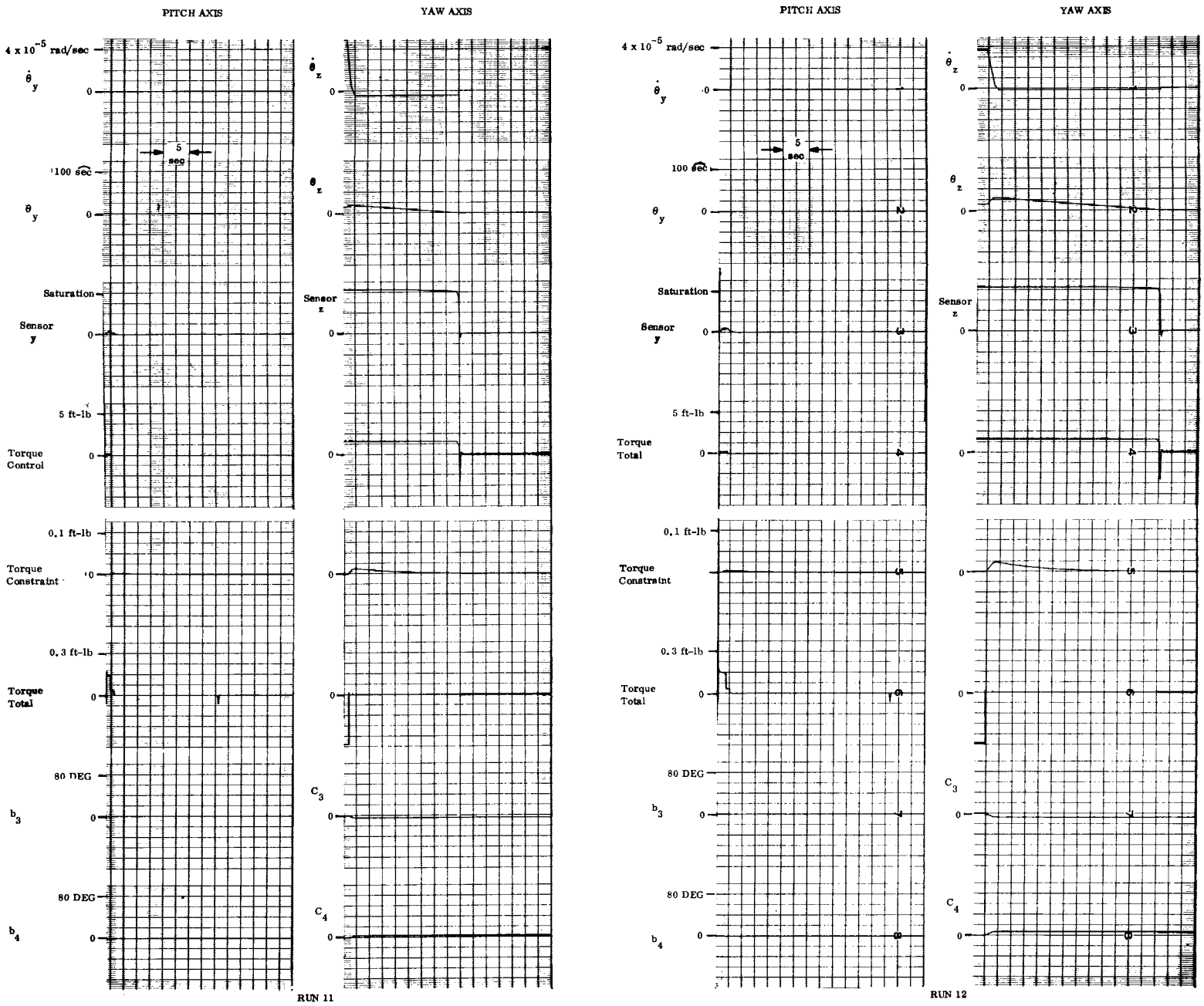

Figure 6-16. Analog Simulated Acquisition, Runs 11 and 12

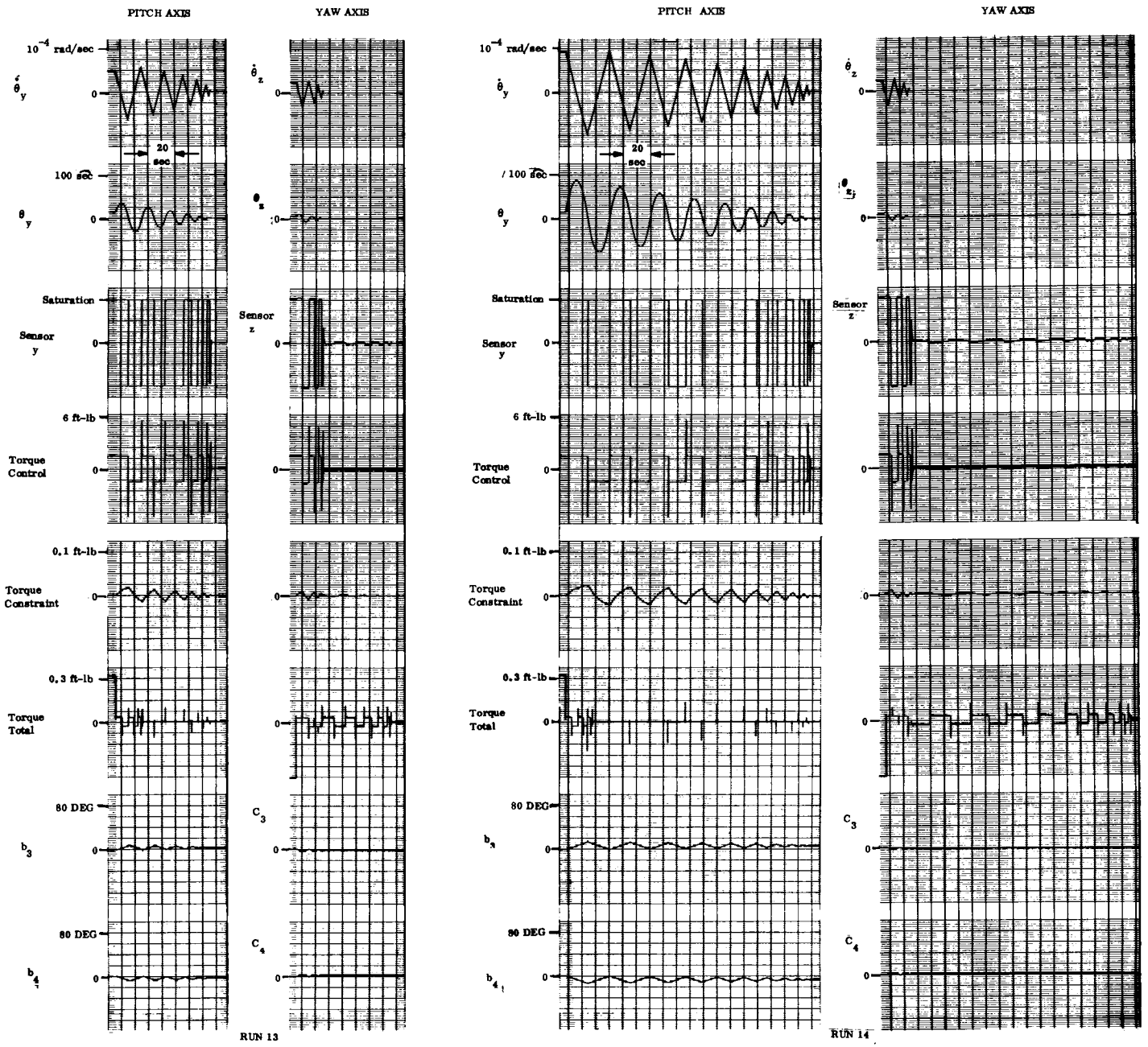

Figure 6-17. Analog Simulated Acquisition, Runs 13 and 14

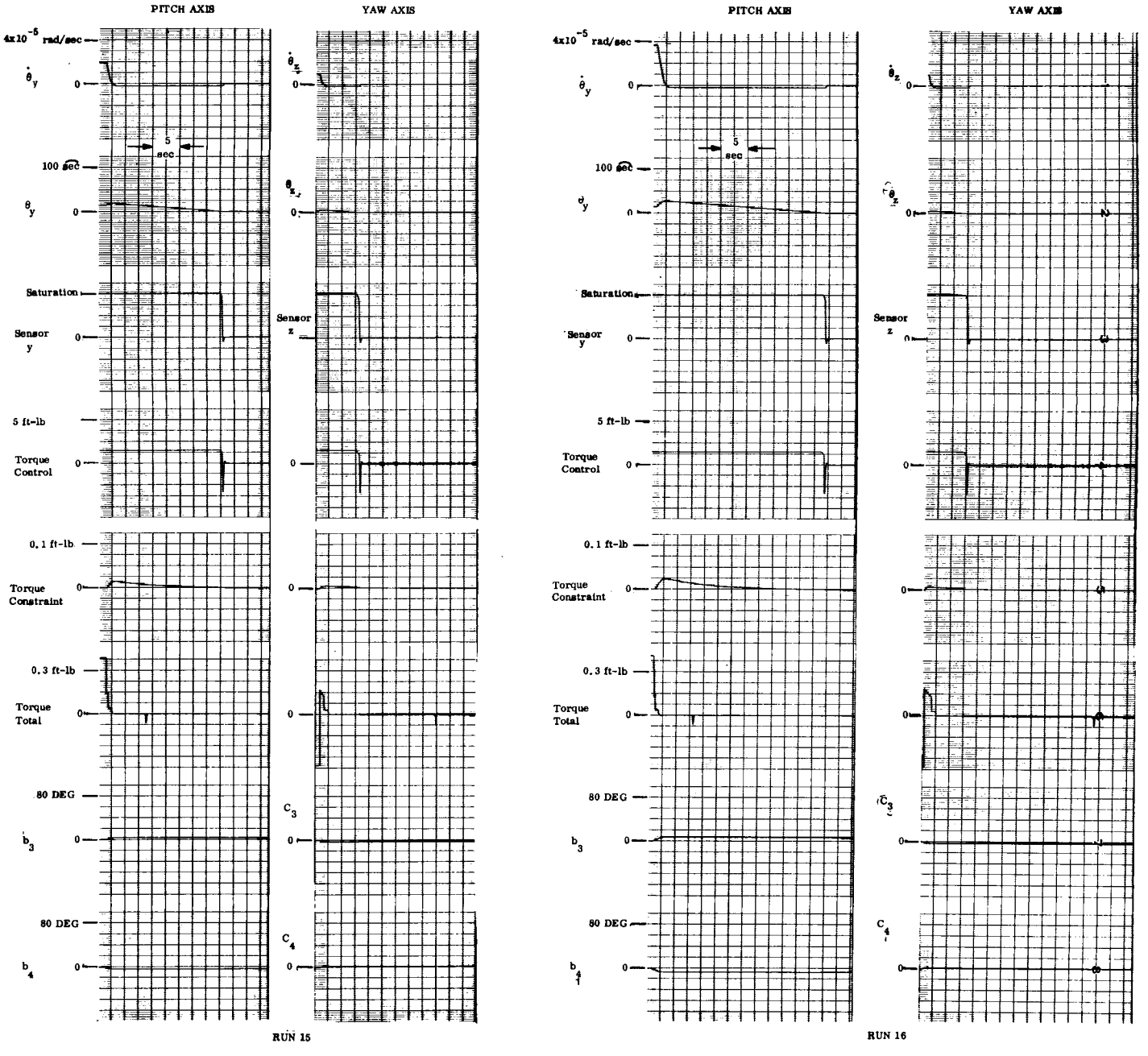

Figure 6-18. Analog Simulated Acquisition, Runs 15 and 16

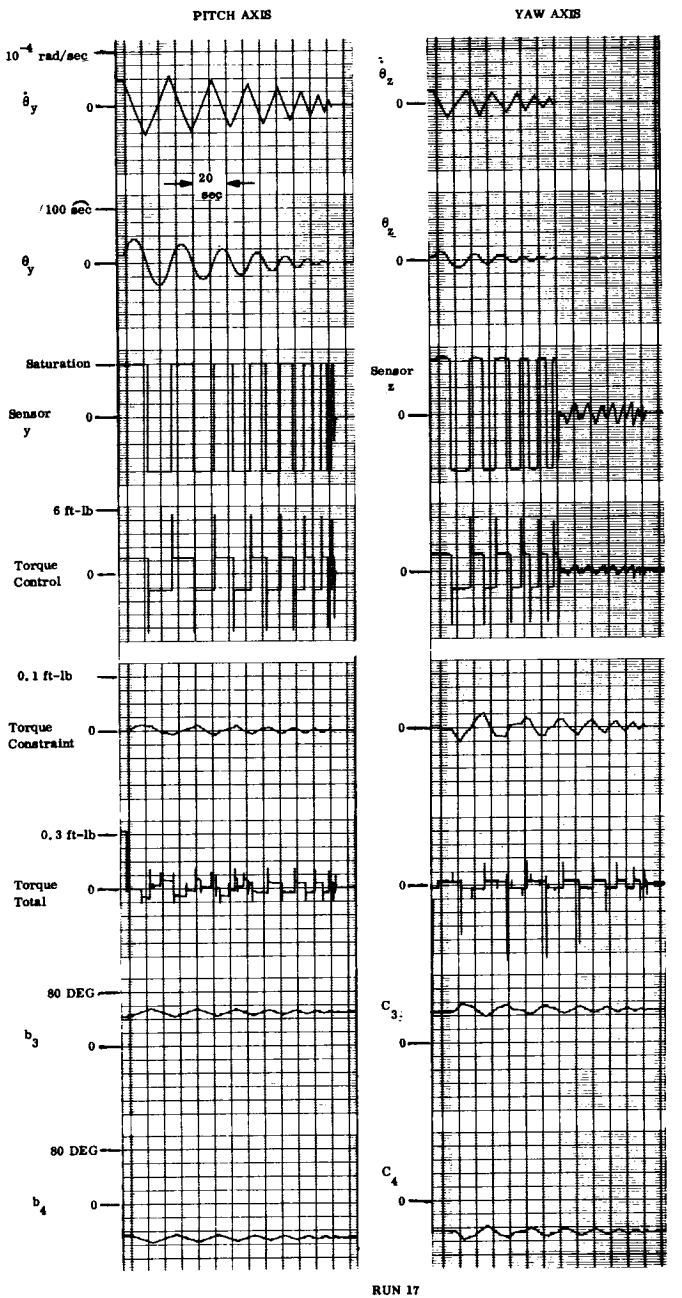

Figure 6-19. Analog Simulated Acquisition, Run 17

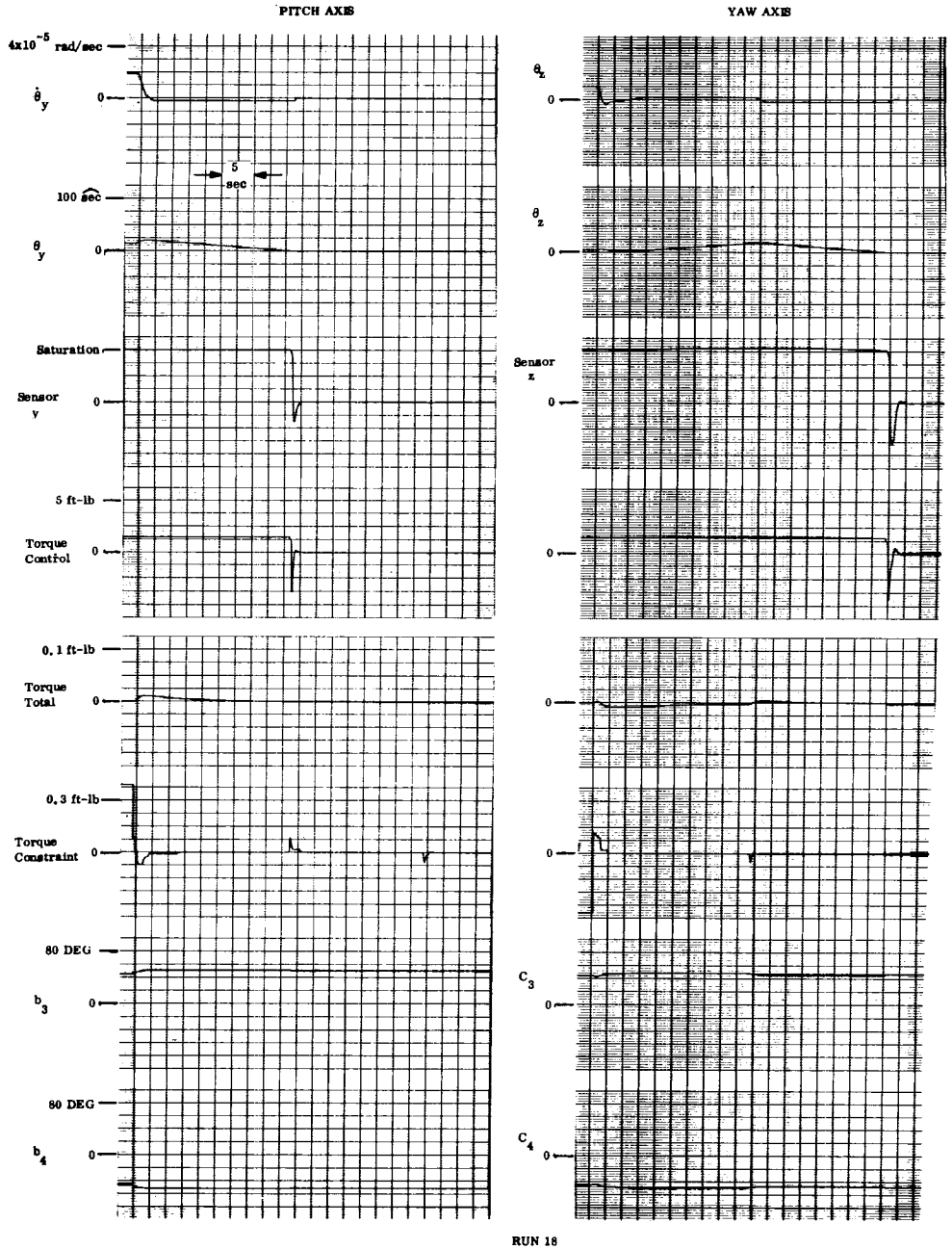

Figure 6-20. Analog Simulated Acquisition, Run 18

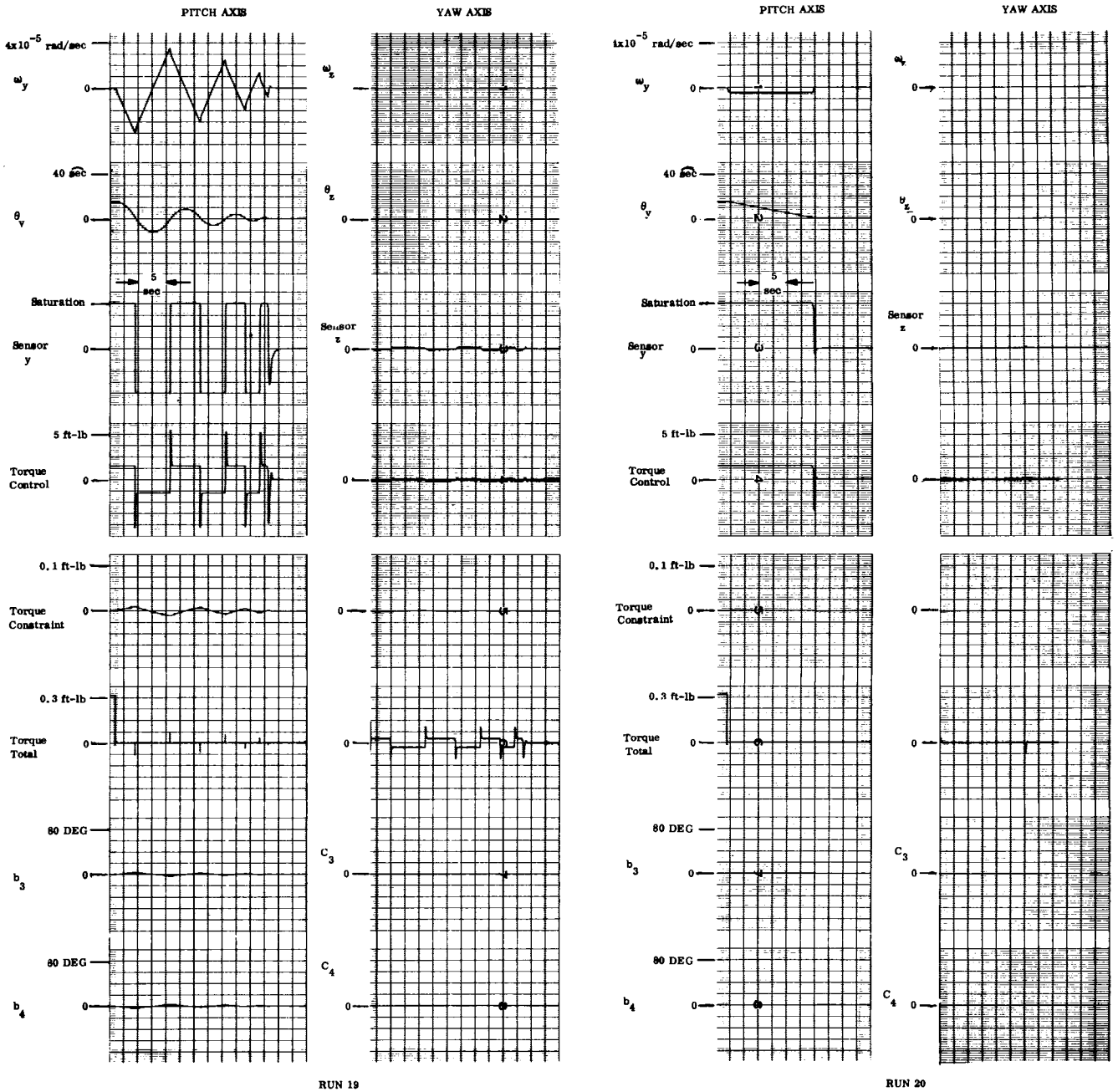

Figure 6-21. Analog Simulated Station Switching, Runs 19 and 20

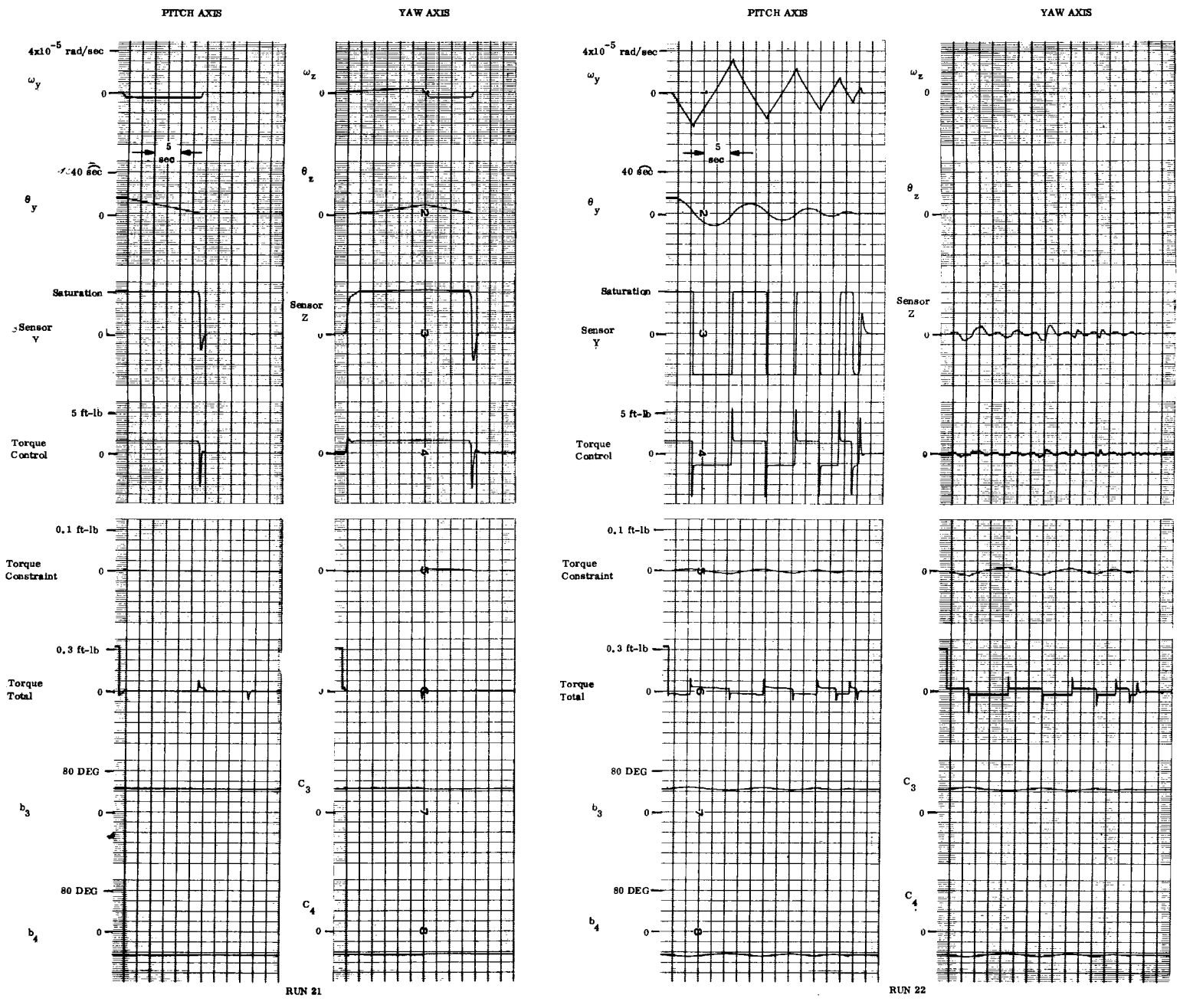

Figure 6-22. Analog Simulated Station Switching, Runs 21 and 22

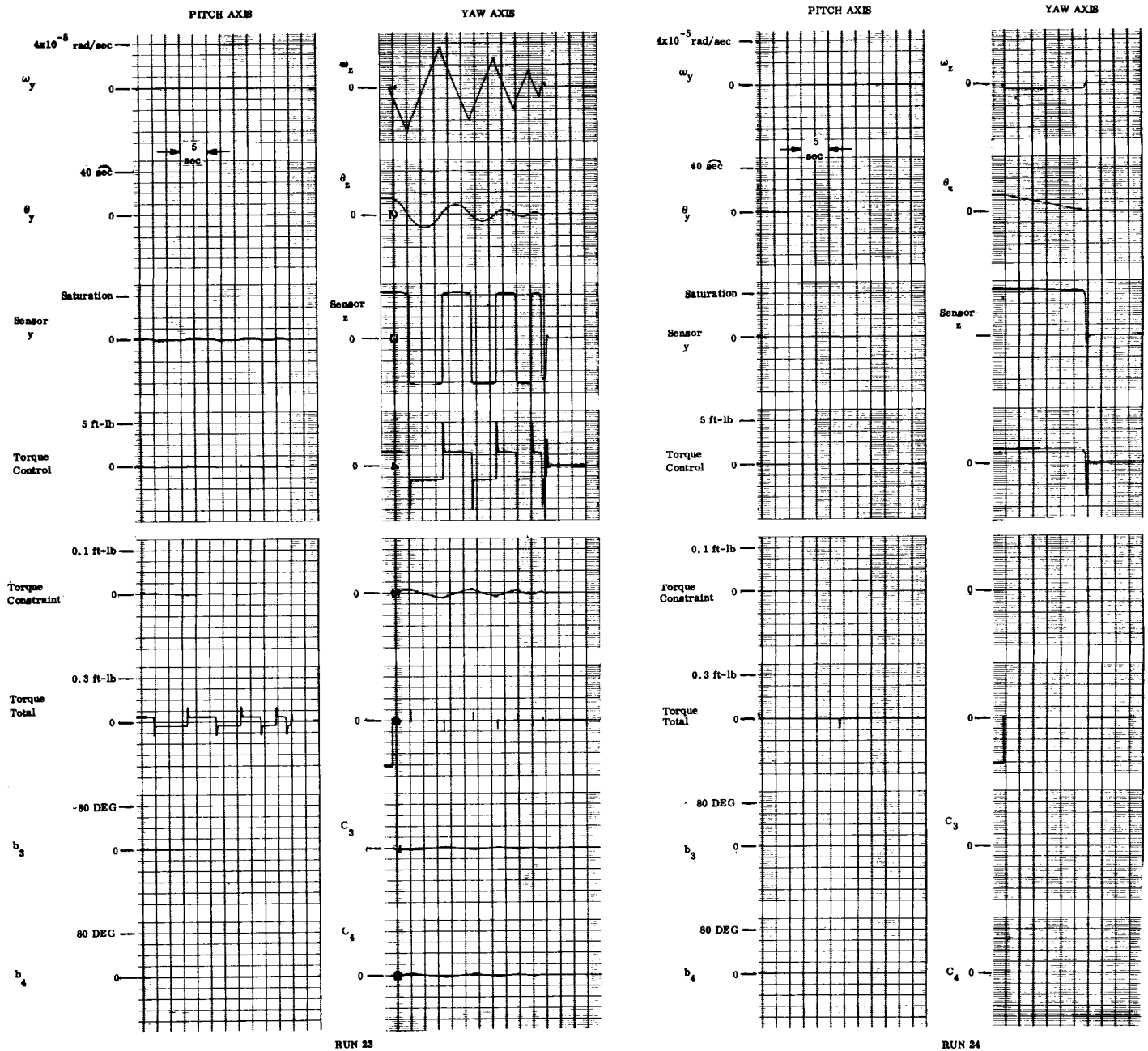

Figure 6-23. Analog Simulated Station Switching, Runs 23 and 24

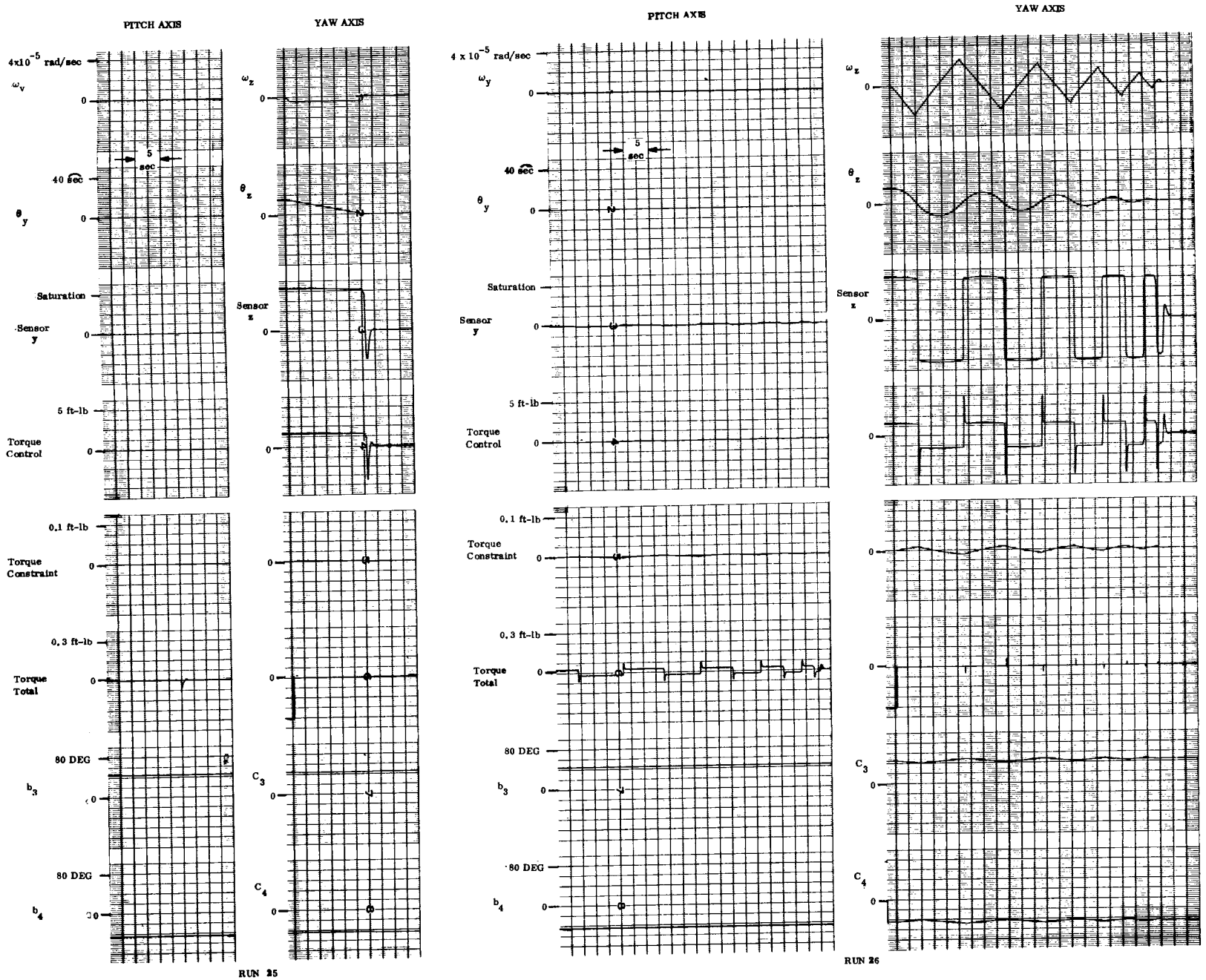

Figure 6-24. Analog Simulated Station Switching, Runs 25 and 26

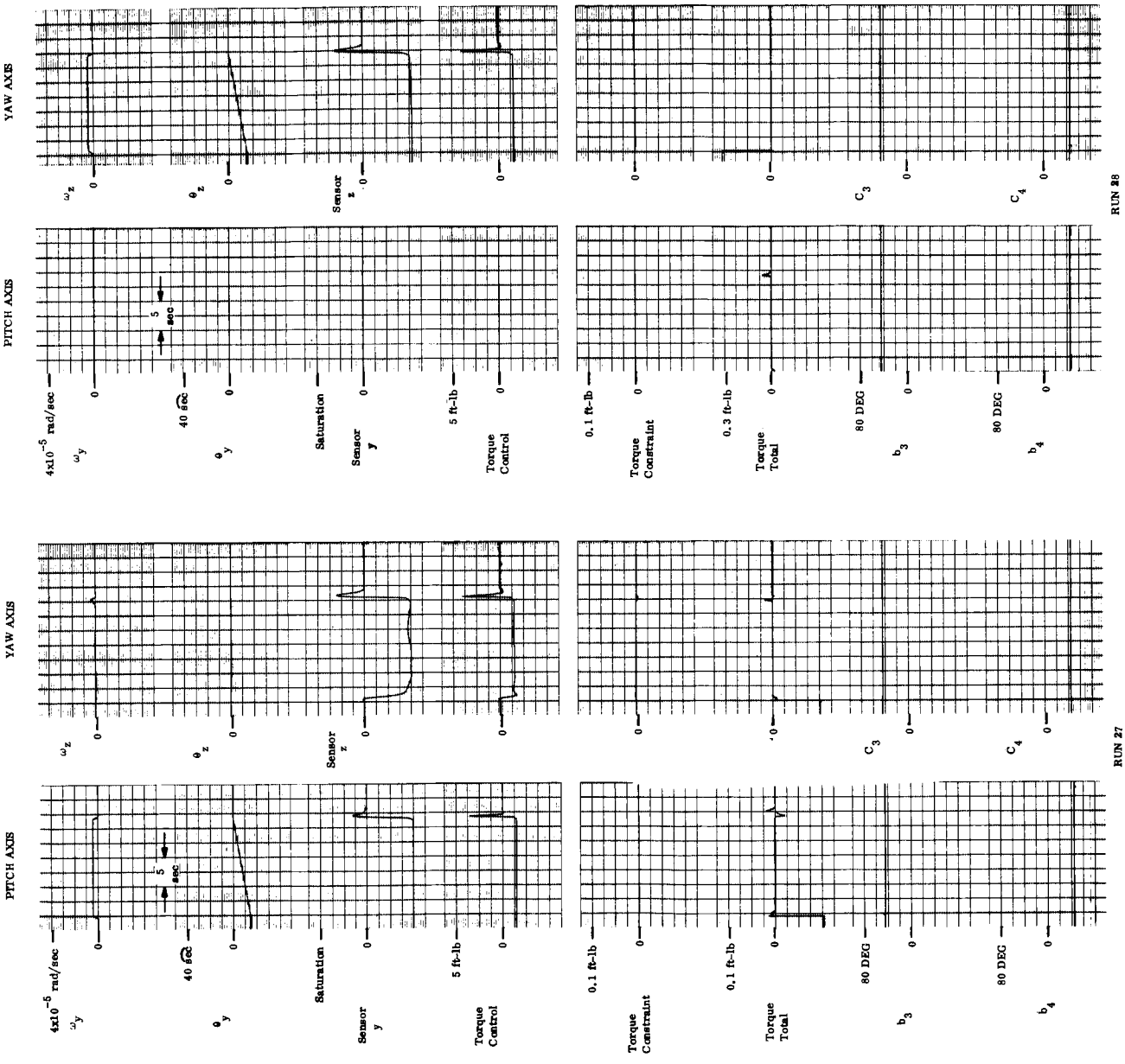

Figure 6-25. Analog Simulated Station Switching, Runs 27 and 28

APPENDIX A

COMPONENT SPECIFICATIONS

APPENDIX A

COMPONENT SPECIFICATIONS

A.1 INTRODUCTION

Summarized in this section are the significant characteristics of the spacecraft control components identified with the successful performance of a laser communications mission to Earth from a Mars orbiter tracking an Earth laser beacon. In some instances, existing equipment is referenced where it can provide the desired performance or where modifications or expected improvement in performance in the time period of interest may reasonably be expected.

A.2 ELECTRO-OPTICAL SENSORS

Three optical sensors are required for spacecraft pitch and yaw attitude control to provide the required field of view to acquire the Earth after spacecraft injection into Mars orbit, and the high resolution required for fine pointing to the Earth laser beacon during laser communications. The Fine Earth Beacon Sensor makes use of the primary optic to collect sufficient beacon emitted energy and is aligned relative to its optical axis. The Intermediate and Coarse Earth Sensors are boresighted to the primary so that their pitch and yaw attitude alignment nominally coincides with the Fine Earth Beacon Sensor.

Two optical sensors are required for spacecraft roll control to provide the required field of view for acquisition of the star Canopus and the moderately high resolution for roll axis control during the fine attitude control of the spacecraft during laser communications. Each of the Canopus sensors makes use of its own optics and is aligned to the other and nominally normal to the optical axis (spacecraft roll axis), because the latter is determined by the Fine Earth Beacon Sensor. Desired characteristics of these components are given in Tables A-1 through A-5.

Since the ratio of field of view to resolution required of the Coarse Earth Sensor is on the order of 60 to 1, and the resolution required is only 5 minutes of arc, such a sensor is obviously within present day state of the art. The desired performance specifications are listed in Table A-1.

Table A-1. Coarse Earth Sensor Characteristics

Size	less than 24 x 24 x 24 in.
Weight	less than 20 pounds
Power Dissipation	less than 10 watts
Detector	probably an electronically scanned image dissector tube
Field of View	$\pm$ 2.5 degrees
Total Pointing Error	$\pm$ 2.5 arc minutes

The Canopus sensor used on Mariner IV meets all requirements for the Coarse Canopus Sensor of both Earth-Mars laser communications missions except that the resolution needs to be improved. This does not present a significant problem, as considerably superior star sensors could be built today if needed. The characteristics of the Mariner IV Canopus sensor and those required of the Coarse Canopus Sensor for the two Earth-Mars laser communications missions are shown in Table A-2.

The OAO boresight type star tracker is adequate for use as the Intermediate Earth Sensor. It also meets all requirements for the Fine Canopus Sensor, except that it is not capable of being gimballed through large (15 degrees) angles in its present version and the field of view would have to be increased. The characteristics of the OAO boresight star tracker are listed in Table A-3.

A sensor like the Stratoscope II may be used for the laser beacon sensor. The parameters will be changed from those of the Stratoscope II, so as to be compatible to the main probe telescope. The laser beacon on Earth has been sized to provide the required signal to noise ratio chosen. The characteristics of the Stratoscope II and those required for the beacon tracking mission are shown in Table A-4.

Table A-2. Coarse Canopus Sensor Characteristics

	MARINER IV CANOPUS SENSOR	DESIRED CHARACTERISTICS
Size	4-1/2 x 5 x 11 in.	NS
Weight	4.95 lb.	NS
Power Dissipation	5 watts for acquisition 3 watts for tracking	NS
Input Voltage	50 volts, 2400 Hz square wave	NS
Detector	Electrostatic image dissector	NS
Star Magnitude Sensitivity	Variable	NS
Optical System Type	Catadioptric with aperture compensation	NS
Focal Length	0.8 in.	NS
Focal Ratio	f/0.6 geometric f/1.0 effective	Same
Field of View	0.89^{o} x 11^{o} instantaneous 4^{o} x 11^{o} scanned 4^{o} x 32^{o} total	NS
Scale Factor	8 volts/degree $\pm$ 20%	Same or Better
Typical Roll Error Noise	0.015 degree peak-to-peak	$\pm$ 0.04 degree
Null Stability (Mech. and Elec.)	$\pm$ 0.125 degree	$\pm$ 0.1 degree
Total Pointing Error	$\pm$ 0.265 degree	Same or Better
Signal/Peak Noise	16/1	

NS - Not significant as long as parameters do not differ greatly from Mariner IV Canopus Sensor parameters

Table A-3. Intermediate Earth Sensor and Fine Canopus Sensor Characteristics

Weight	25 lb total
Power Dissipation	8 watts
Input Voltages	28 vdc and 10 vdc
Detector	Image dissector multiplier phototube, magnetic deflection
Star Magnitude Sensitivity	+ 6 magnitude faintest
Objective Aperture (clear)	2.7 in. diameter
Focal Ratio	f/1.8
Instantaneous Field of View	± 5 arc-minutes
Desired Instantaneous Field of View	± 12 arc-minutes
Total Angular Electrical Offset Capability	± 1.5 degrees
Offset Increment	15 arc second steps to 15 arc minutes and one arc-minute steps to 90 minutes of arc
RMS Noise Equivalent Error	Approx. 1/3 arc second, 3rd magnitude Approx. 2 arc seconds, 6th magnitude
Error Gradient	1.2 volts/ minute @ 3rd magnitude 0.7 volts/ minute @ 6th magnitude
Null Stability	1-3 arc seconds @ 6th magnitude
Signal/ Noise Ratio	6 @ 6th magnitude 30 @ 3rd magnitude
Total field of view about one axis normal to nominal optical axis for Canopus sensor only (Electrical or mechanical gimbaling)	± 16 degrees

Table A-4. Fine Earth Sensor Characteristics for the Beacon Tracking Mission

	STRATOSCOPE II	DESIRED
Type	Pyramid beamsplitter with four photomultipliers	Same
Detector	No. 7265 photomultipliers (S-20 photocathode)	Same
Linear Range	± 0.1 arc-seconds	± 0.2 arc-seconds
Total (saturated) Range	± 1 arc-minute	± 1.5 arc-minutes
Electrical Bandwidth	700 Hz	10 MHz
Objective Aperture	36-in. diameter	30-in. diameter
Effective Focal Length	1800 in.	750 in.
Effective Focal Ratio	f/50	f/25
Noise Equivalent Error	0.016 arc-second	0.01 arc-second
Signal to Noise Ratio		60 (when detecting 340 megawatt pulses of 100 nanosecond duration at 108 miles range. Laser wavelength is 6943 Angstroms)

A sensor based upon the NASA-Ames high precision planet tracker currently under development could be used for the Fine Earth Sensor if the Earth tracking mission were performed. Since the Fine Earth Sensor need not meet the small size and weight restrictions imposed upon the NASA-Ames version, but need only conform to the main spacecraft telescope, the required improvement in resolution is feasible. The minimum acceptable and design goal specifications for the NASA-Ames trackers are listed in Table A-5 along with the desired characteristics of the Fine Earth Sensor for the Earth tracking mission.

Table A-5. Fine Earth Sensor for the Earth Tracking Mission

	MINIMUM ACCEPTABLE	DESIGN GOAL	DESIRED FOR FINE EARTH SENSOR
Size		7 in. diameter x 12 in. length	Must conform to main probe telescope
Weight		< 10 lb	< 30 lb
Power Dissipation	< 10 watts	< 5 watts	< 25 watts
Detector	Image tube (either vidicon or reconotron)	Same	Same
Field of View	± 2.25 arc-min.		± 1.5 arc-min
Error Signal Slope for Specified Planets	180 ± 36 mv/sec		
Noise Equivalent Angle	0.2 arc-seconds	0.1 arc-second	0.04 arc-second
Linear Slope Limits	± 1.67 arc-seconds	± 2 arc-seconds	± 1 arc-second
Frequency Response 0 to 5 Hz 5 to 10 Hz	 ± 1 db ± 3 db		 ± 1 db ± 3 db
Phase Shift at 1 Hz	< 10 degrees		
Offset Error (Mech. and Elec.)	± 1.6 arc-seconds	± 0.5 arc-second	± 0.2 arc-second
Drift		< ± 1 arc-second	± 0.2 arc-second

A.3 INERTIAL SENSORS

Inertial sensors are required for the performance of the following functions:

a. Sense spacecraft rates during all acquisition modes.

b. Provide an inertial position reference during commanded turns or rocket engine firing for trajectory corrections during the interplanetary flight or corrections after attainment of Mars orbit.

c. Provide a roll axis attitude reference during occulation of Canopus by Mars during laser communication from Mars orbit.

These functions are provided in two basic gyro packages. The first is a triad of body-mounted rate integrating gyros with associated loop closing electronics making the gyro capable of operation in the rate or rate-plus-position mode. The second package contains a single gyro, exclusive of redundancy, representing a modest advance in the state of the art with respect to drift over gyros available today. Only the random component of gyro drift is of concern because the Fine Canopus Sensor can be used to update the gyro attitude information during most of any given orbit.

The random component of gyro drift must be held to 6 arc seconds over a two-hour period, based upon the control system performance required and the occulation characteristics of the orbit selected. The desired characteristics of the two gyro packages are given in Tables A-6 and A-7.

The Gyro Control Assembly contains a triad of three orthogonally mounted state-of-the-art rate integrating gyros. The package contains the three gyros, their loop closing electronics, the temperature control amplifier,and power supply for all gyro functions. The significant characteristics of the package and the individual gyros are listed in Table A-6.

The Roll Reference Gyro Package contains a single strapdown gas bearing or electrostatic gyro, gyro electronics, temperature control amplifier, and power supply for all gyro package functions. The significant performance characteristics are given without reference to physical characteristics since the gyro represents an advance in the state of the art. See Table A-7.

A.4 CONTROL MOMENT GYROS

The control moment gyro configuration consists of a twin two-degree-of-freedom gyro package to absorb angular momentum about the spacecraft pitch and yaw axes, and a twin single-degree-of-freedom package to absorb angular momentum about the spacecraft roll axis.

Table A-6. Gyro Control Assembly

Power Dissipation	
3ø 800 Hz at 26 v	10 watts avg 16 watts peak
50 at 20 kHz	10 watts avg 15 watts peak
Size	7 x 6 x 6 in.
Weight	10 lbs
Gyro Data	
Non-g sensitive drift	
Short term	0.1 deg/hr
30-day stability	0.2 deg/hr
Random	0.01 deg/hr
g sensitive drift	
Short term	0.1 deg/hr/g
Long Term	0.3 deg/hr/g
Random	0.01 deg/hr/g
g^2 sensitive drift	
Anisoelastic	0.05 deg/hr/g^2
Attitude angle	0.01 deg/hr/g^2
Max. torquing rate	15 deg/sec
Torquer linearity	0.01 percent
Signal Generator SF	30 v/rad
Signal Generator linearity	1 percent
Temp. Environment (nonoperating)	0° to 212° F
Operating Temperature	180° F
Operating Life	20,000 hours

The gimbal axes of the single gimbal CMG's are aligned in parallel in the same gimbal structure with their rotor angular momentum vectors aligned normal to the gimbal axes, and in opposite directions in the nominal zero momentum stored condition. The rotors operate at synchronous speed to obviate cross coupling torques. Brushless dc torquers

Table A-7. Roll Reference Gyro

Gyro Data	
Non-g sensitive drift	
Short term (not trimmed)	0.01 deg/hr
30-day stability	0.05 deg/hr
Random drift	0.0008 deg/hr
g sensitive drift	
Short term	0.02 deg/hr/g
30-day stability	0.07 deg/hr/g
Random drift	0.002 deg/hr/g
g^2 sensitive drift	
Anisoelastic	0.02 deg/hr/g^2
Attitude Angle	0.02 deg/hr/g^2
Temp. Environment (nonoperating)	0°F to 212°F
Operating Life	8,000 hr

are used to drive the gyro gimbals with eddy-current damping used to stabilize the gyro loop. Minimum gimbal axis friction is derived from the reduction in bearing preload in orbit and by use of the brushless torquers. The significant design and performance characteristics for the twin single-degree-of-freedom CMG's are given in Table A-8.

The double gimbal control moment gyro package is similar to the single gimbal unit except for the addition of a gimbal ring between the mounting frame ring and the rotor gimbal structure; the outer gimbals are aligned parallel in the mounting frame. The inner gimbal axes and gyro rotor axes complete the orthogonal alignment at the zero momentum condition with rotor spin vectors in opposite directions. The gimbal axis design again features brushless dc gimbal torquers and minimum preload bearings, but an active damping loop is closed around each gimbal axis to achieve the desired highly damped mode of operation. The significant design and performance characteristics are given in Table A-9.

Table A-8. Twin Single Degree of Freedom Control Moment Gyros

		PER GYRO	TOTAL
Rotor Momentum	ft-lb-sec	2	4
Gimbal Inertia	ft-lb-sec^2	0.001	
Gimbal Damping	ft-lb/rad/sec	0.02	
Gimbal Running Friction	in.-oz	0.035	
Gimbal Static Friction	in.-oz	0.07	
Gimbal Reset		$\pm$ 60^o	
Maximum Gimbal Angle (STOPS)		$\pm$ 65^o	
Weight	1 lb		16
Power	watts avg watts peak		8 12

Table A-9. Twin Two Degree of Freedom Control Moment Gyros

		PER GYRO	TOTAL
Rotor Momentum	ft-lb-sec	2	4
Gimbal Inertia	ft-lb-sec^2	0.01	
Gimbal Damping	ft-lb/rad/sec	100	
Gimbal Running Friction	in.-oz	0.035	
Gimbal Static Friction	in.-oz	0.07	
Gimbal Reset		45^o	
Maximum Gimbal Angle (STOPS)		60^o	
Weight	lb		25
Power	watts avg watts peak		12 20

A.5 SPACECRAFT ATTITUDE CONTROL ELECTRONICS

The computation required for the proposed spacecraft control system can be divided into those computations required for attitude control of the spacecraft to the attitude reference and those required for positioning the servoed optics for "steering" the transmitted laser beam. It is proposed that the spacecraft attitude control computations be performed by analog circuits, with the exception of programmed sequential mode switching which will be accomplished by command programs received from the ground and stored in the spacecraft computer to institute a timed change in spacecraft attitude to a prescribed orientation in space for path corrections or other purposes.

These programming functions for spacecraft attitude control and all commands to the servoed optics for control of laser beam pointing can be accomplished in the spacecraft digital computer, which is discussed under the Point Ahead Control System (A.6.1), because the servoed optics considerations dominate its sizing and performance characteristics.

A.5.1 ANALOG ELECTRONICS

The analog electronics for attitude control of Mariner spacecraft during the interplanetary trip to Mars have been completely specified for that spacecraft and are applicable to this mission and so will be considered present aboard the spacecraft. The Mariner specifications will not be repeated herein, but the functions performed and components employed will be listed to show how some of this equipment can be used to advantage in Mars orbit for the mission that is the subject of this study. The pertinent control functions and equipment are as follows:

a. Attitude control switching amplifiers on all three axes which control mass expulsion actuators in response to sensor attitude error signals and spacecraft rate information from body mounted gyros.

b. Analog roll search and acquisition control logic, which determines the completion of initial Sun acquisition from pitch and yaw attitude errors and rates, commands a slow roll search and determines acquisition of Canopus from star brightness and star presence signals, and switches roll control to the command of the Coarse Canopus Tracker.

c. Derived rate electronics which determine spacecraft rates after completion of the acquisition of the Sun and Canopus and permit the gyros to be turned off.

d. Autopilot electronics which control the position of the rocket engine thrust vector control actuators during rocket engine firings for spacecraft path corrections.

This same equipment may be used in the Coarse Earth Pointing mode after the spacecraft has been placed in Mars orbit. Upon completion of commanded turns about the spacecraft pitch and yaw axes to orient the spacecraft roll axis from the Sun to the Earth, and receipt of an Earth presence signal from the Coarse Earth Sensor, inputs to the pitch and yaw switching amplifiers (part (a) above) will be switched from spacecraft Sun Sensors to the Coarse Earth Sensor. Thus, acquisitions of the Earth and Canopus in Mars orbit can be accomplished with Mariner-type control equipment, which is the initial condition for specification of control electronics for the laser communications mission. The spacecraft attitude control electronics, required for the interplanetary trip and acquisition of the Earth and Canopus in Mars orbit, will have a volume of about 450 cubic inches, a weight of about 13 pounds, and will dissipate an average and peak power of about 10 and 25 watts, respectively.

Additional attitude control electronics, which will be described here, are required for the fine pointing to the Earth laser beacon. This equipment will be common for the Intermediate Pointing Control Mode and Fine Pointing Control Mode. The initial conditions for operation of these electronic units occur when the spacecraft pitch and yaw attitude errors relative to the Earth reference are less than 3.5 minutes of arc, the roll attitude error relative to Canopus is less than 7 minutes of arc, and spacecraft rates about all axes are less than 0.005 degree per second. Upon receipt by the control logic of Earth presence, Canopus presence, and rate signals indicating spacecraft stabilization within these limits, control is switched to the Intermediate Pointing Control Mode which employs the Intermediate Earth Sensor, fine pointing attitude control electronics, and control moment gyro torquers. This equipment serves to reduce pointing errors and rates to those that are permitted for acquisition of the Earth beacon by the Fine Earth Beacon Sensor, and stabilization of the spacecraft to the beacon and Canopus to the

accuracy required for laser communications. This equipment may best be described in terms of its components (Tables A-10 and A-11) and by referring to Figure 2.3.

Table A-10. CMG Torque Motor Summing Amplifier Characteristics

Gain	$2.22 \times 10^3 \pm 5\%$
Frequence Response	Flat to 300 rad/sec
Offset and Drift (Ref. to Output)	100 mv max
Noise (Ref. to Output)	100 mv RMS max
Saturation	$\pm$ 22 v $\pm$ 10%

Table A-11. Fine Pointing Mode Position Amplifier Characteristics

Gain	$1 \pm 5\%$
Offset and Drift (Ref. to Output)	100 microvolts max
Noise	100 microvolts RMS max
Saturation	> 100 millivolts
Frequency Response Characteristic	$\frac{(0.5S+1)}{(0.05S+1)}$ *

*Additional lags above 100 rad/sec are permitted provided they contribute no more than 3 degrees phase lag at 6 rad/sec

A.6 POINT AHEAD CONTROL SUBSYSTEM

A two-gimbaled device is used in conjunction with a tilting plate to accomplish the spacecraft point ahead angle. The tilting plate deflects the spacecraft laser beam by an amount dependent upon the angle between the laser beam and the normal to the tilting plate surface. The tilting plate must be gimballed about two axes because of the two axes about which the point ahead angle occurs.

A digital computer is used to store tilting plate commands sent from the Earth and to send a command to the tilting plate control loops every six seconds to update the pitch and yaw point ahead angles. Position-plus-rate feedback is used in the point ahead control loops to provide the desired response characteristics. Also, electronics consisting of adders, digital-to-analog converters, amplifiers, and compensation are required in the control loops. Therefore, in addition to the digital computer and torque motors, the control loops also utilize control electronics, tachometers, and digital encoders.

A.6.1 SPACECRAFT DIGITAL COMPUTER

The requirements that the spacecraft digital computer must meet are not stringent; an acceptable computer could easily be built today. The computer is essentially a large memory which is read out in a sequential mode, at the very slow rate of one word every six seconds,to issue the command to the tilting plate mechanism to update the point ahead angle. It is desirable to be able to jump to a new place in memory and begin reading out in a sequential manner from that place so as to take advantage of improved point ahead information. The best way to accomplish this is to simply read out at a fast rate until the desired place in memory has been reached. Therefore, provision is made for reading out the memory at a rate such that the entire memory can be read out in two or three seconds,essentially resulting in the capability to jump from one place in memory to any other place during the 6-second interval between point ahead commands. A convervative estimate of the characteristics of the spacecraft digital computer required are given below:

Weight	60 lb
Power Dissipation	50 watts, continuous 100 watts for 2-3 seconds when in the fast read-out mode
Voltage	4 vdc $\pm$ 5%
Size	4000 in.^{3} (possibly 16 x 16 x 16)
Memory Word Length	37 bits

Storage Capability		14,400 words (for 24 hours of point ahead information)
Read Out Speed:	Slow Mode	1 word/6 seconds
	Fast Mode	approx. 5000 words/second

A.6.2 DC TORQUE MOTORS

The torque levels required are very minimal due to the low inertias of the point ahead loop. The torque motor used for pitch control needs to be slightly larger than that used for yaw because the pitch loop corresponds to the outer gimbal of a two-gimbal device. Thus, the motor must torque all hardware on the inner gimbal as part of its load.

Brushless dc motors were selected for this application because their friction characteristics are very minimal. The only disadvantage of these motors for general applications is the fact that the torque available from the motor begins to fall off as the angle between the shaft and the null position exceeds 45 to 60 degrees. However, this is no disadvantage for this application because the maximum angular range of tilting plate rotation is limited by other consideration to $\pm$40 degrees. Typical characteristics of dc torquers which could be used to meet the point ahead control loop requirements are listed below. These specifications are clearly within present day state of the art.

	Yaw	Pitch
Continuous Torque Rating	1 in.-oz	2 in.-oz
Weight	2 oz	3 oz
Size	1.0 in. diameter x 0.7 in.	1.7 in. diameter x 0.5 in.
Power	3 watts	6 watts
Torque Sensitivity	2×10^{-4} ft-lb/volt	2×10^{-3} ft-lb/volt
Back EMF	0.01 volts/rad/sec	0.02 volts/rad/sec
Angular Motion	$\pm$60 degrees	$\pm$60 degrees
Electrical Time Constant	2×10^{-4} sec	5×10^{-4} sec
Rotor Inertia	2.5×10^{-6} lb-in-sec^2	1.0×10^{-5} lb-in-sec^2
Resistance	200 ohms	75 ohms

A.6.3 TACHOMETERS

The tachometers used in the pitch and yaw point ahead loops were selected to be of the brushless dc variety (as are the motors) because of their low friction. The tachometers were selected to be identical although a different choice of the control system parameters (which can be varied) would have resulted in the characteristics of the two tachometers differing slightly. The tachometers are within the state of the art; their specifications are given below:

Weight	3 oz
Size	1.5 in. diameter x 0.75 in.
Power	-
Sensitivity	10 volts/rad/sec
Resistance	3000 ohms
Electrical Time Constant	5×10^{-4} seconds

A.6.4 DIGITAL ENCODER

A digital encoder was selected over an analog transducer as the position sensor because of noise problems associated with high resolution analog devices, and because the commanded tilting plate angle is already in digital form. Under this scheme, the output of the encoder is either compared by a bit check or subtracted from the commanded angle, and the result converted to an analog signal for use by the control loop.

The digital encoder characteristics were selected to be compatible with the bit allocation of the tilting plate commands. Thus, while the encoder utilizes only 15 bits, it must be considered as a 17-bit encoder because 17 bits would be required to accomplish a full 360-degree rotation. The characteristics listed below are attainable today (based upon a survey of the literature) except that some improvement needs to be made to meet the size and weight allocations. The small weight is desirable because the encoder disk is part of the load of the inner and outer gimbal control loops, and the entire inner gimbal encoder is part of the outer gimbal torquer load. If difficulties are experienced in reducing the encoder weight, two options are available:

a. Increasing the torquer size and control loop amplifier gain

b. Locating the parts of the encoder which do not need to be gimballed elsewhere in the structure and using flexible electrical leads between the two parts of the encoders.

The desired encoder characteristics are listed below:

Weight	4 oz
Size	3.25 in. diameter x 1.25 in.
Power	5×10^{-4} seconds
Encoder Disk Size	2.5 in. diameter x 0.2 in.
Encoder Disk Inertia	1.5×10^{-5} ft-lb-sec^2
Response Time	5×10^{-4} seconds
Least Significant Bit	10 arc seconds (results in $\pm$5 arc seconds due to quantization)
Error in Line (Least Significant Bit) Location on the Disk	$\pm$10 arc seconds
Total Number of Bits Used	15
Range of Operation	$\pm$45 degrees

A.6.5 CONTROL ELECTRONICS

Nothing associated with the digital to analog conversion, or the addition, amplification, and compensation required for the pitch and yaw point ahead control loops suggests a need for improvement upon present day state of the art. Typical specifications for the control electronics required to accomplish these functions are given below:

Weight	5 lb
Size	5 x 5 x 5 in.
Power	8 watts
Input Voltage	4 vdc

APPENDIX B

THERMAL AND STRUCTURAL CONSIDERATIONS

APPENDIX B

THERMAL AND STRUCTURAL CONSIDERATIONS

B.1 INTRODUCTION

The specific problem areas investigated include:

a. Maintaining alignment between the telescope, servoed optics, and laser.

b. Rejecting the heat dissipated in the RTG power supplies in such a manner as to not deteriorate the pointing accuracy via excessive heat impingement upon optical elements and misalignments due to thermal gradients.

c. Rejecting heat dissipated by the laser and optimum location of the laser within the spacecraft.

d. Maintaining alignment of the third axis (Canopus) sensor to the optical axis.

e. Location of the orbit injection rocket.

f. Location of the remaining equipment on board the spacecraft.

g. Estimation of the spacecraft moments of inertia.

B.2 SUMMARY OF RESULTS

The design of a Mars orbiting spacecraft employing a 0.2 arc-second beam in the 1975-80 period will present some serious thermal control and structural problems. However, use of advanced techniques and materials indicates that the design is feasible.

The spacecraft will probably be somewhat cylindrical in shape (on the order of 17 feet long and 4 feet in diameter) with RTG power supplies, mounted exterior to the spacecraft, extending the outer diameter to approximately 10 feet. Figures B-1 and B-2 are sketches of the overall spacecraft design.

The spacecraft structural design will probably consist of two structures: (1) an inner structure of invar, which has a low coefficient of thermal expansion, supporting the main telescope, optical elements, spacecraft laser and third axis star sensor; and (2) an outer

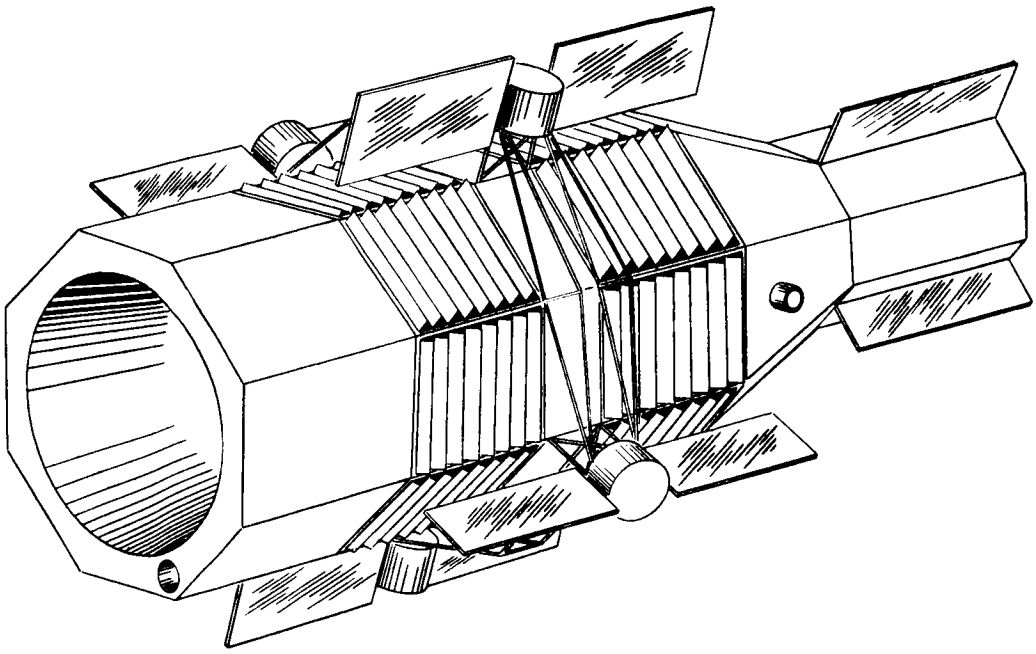

Figure B-1. Sketch of Spacecraft

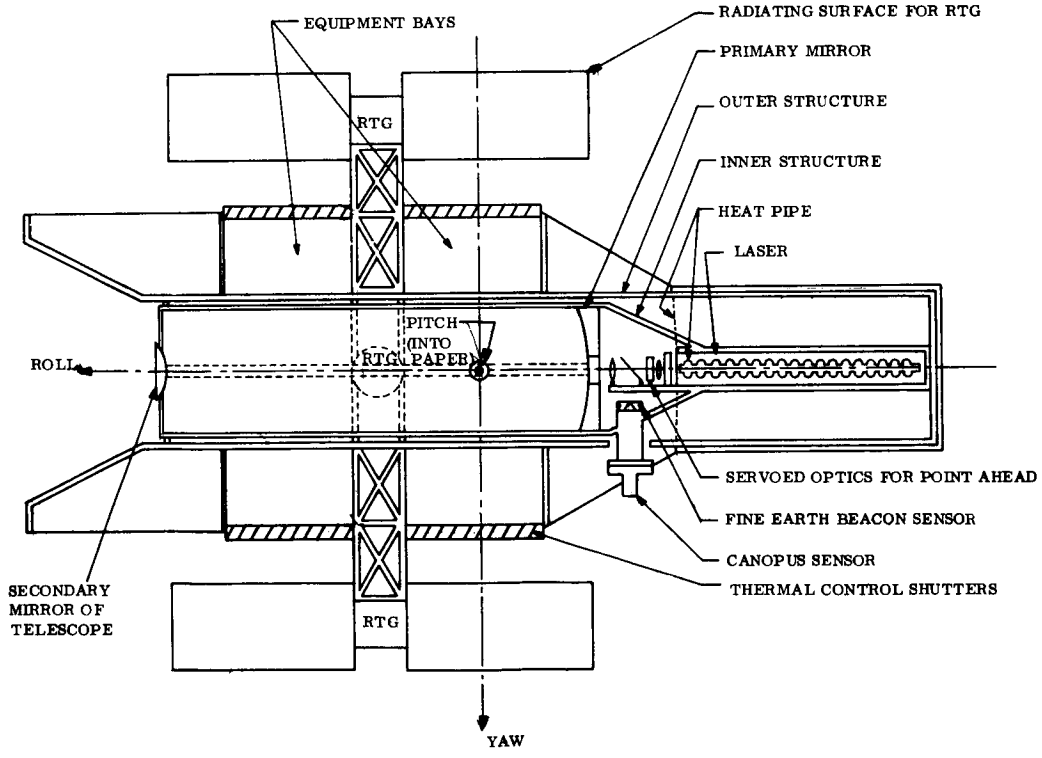

Figure B-2. Cutaway Sketch of Spacecraft

structure of aluminum. Embossed aluminized mylar insulation will be used between the two structures and between the outer structure and the spacecraft skin.

The RTG power supplies should be located external to the spacecraft because of the high amount of heat (a total of 20 kw) dissipated within the RTGs and should be supported by a framework of a metal such as stainless steel, which has a low thermal conductivity. The radiating vanes of the RTG power supplies should be oriented so that little of the radiated heat is directed at the spacecraft.

The spacecraft laser should be located approximately in line with the optical axis of the telescope. The use of a heat pipe, which dissipates 2 kw of heat, is recommended for thermal control of the spacecraft laser. A heat pipe is a passive device which conducts the heat given off by the spacecraft laser to the exterior of the spacecraft, where it is radiated to space.

The telescope structure should be thermally isolated from the rest of the spacecraft by embossed aluminized mylar insulation. The telescope structure should be jointed to the laser structure through a rigid thermal barrier of 1/4-inch laminated fiberglas. The optical elements, such as the servoed optical elements for point-ahead, should be located within a housing coated with a material with a high solar absorptivity, such as optical velvet, to reduce the noise at the fine pointing sensor caused by reflections at the surfaces of the optical elements.

Thermal control of the telescope structure is required to ensure that the temperature variation over time along the telescope structure is held to 2.7°F. This is well within present day state of the art. The temperature variation across the structure aligning the spacecraft laser, servoed optics, and fine pointing sensor must be held to 0.1°F. While advanced thermal control studies (such as the analysis performed for the MOT study) indicate such a temperature control can be maintained, The maintenance of this degree of thermal control is one of the most serious problems a laser communications mission detailed design would have to concentrate upon.

The rocket engine used for midcourse correction and orbitial injection does not present any serious structural and thermal problems during the mission because it can be jettisoned prior to the start of laser communications. The rocket should be located at the same end of the spacecraft as the main telescope, for structural reasons with its thrust vector aligned approximately along the optical axis and through the spacecraft center of mass.

B.3 THE TELESCOPE STRUCTURE

The major problem in maintaining alignment of the telescope section of the spacecraft structure is to maintain the correct distance between the primary and secondary mirrors (the required tolerance is on the order of 10^{-3} to 10^{-4} inches). The temperature tolerance required to accomplish control of the distance between these mirrors is given by:

$$\Delta T = \frac{\Delta L}{\alpha L} \qquad \text{(B-1)}$$

where

L = the distance between the primary and secondary mirrors ($\cong 8$ ft)

α = the coefficient of thermal expansion of the structural material used

Because of the high precision to which alignment must be held, invar or some similar material is recommended for the telescope structure because of its low (0.7×10^{-6}) coefficient of thermal expansion.

then

$$\Delta T = \frac{10^{-4}}{0.7\,(10^{-6})\,96} = 1.5^{\circ}C = 2.7^{\circ}F \qquad \text{(B-2)}$$

In the region of $-20^{\circ}C$, the coefficient of thermal expansion of invar is an order of magnitude lower, and the tolerance of thermal control can be somewhat relaxed. The extent to

which such a low temperature and variation in temperature can be maintained is dependent upon how well the telescope structure can be thermally isolated from the RTG power supplies and the spacecraft laser. Both direct sunlight and sunlight reflected from Mars are prevented from entering the telescope by the attitude control maintained during the mission and through use of a small sunshield. Confidence in maintaining structural rigidity and thermal control of a large spacecraft telescope is evidenced in such analyses as that performed for the MOT study (Reference B-1) which not only involved a much larger telescope but concluded that aluminum, a material with a much larger coefficient of thermal expansion ($\alpha \simeq 20 \times 10^{-6}$), would be adequate for the telescope structure (although the optics were servoed in the MOT design to maintain the distance between mirrors and their alignment).

A second problem associated with the telescope structure is the bending of the structure due to a thermal gradient across the structure (normal to the optical axis). Because the angle between the sun to spacecraft line and one side of the spacecraft varies throughout the mission (while the other side of the spacecraft never sees the sun) and because the orbit selected is such that sun occulation does occur, adequate thermal insulation must be provided to minimize the variation in telescope structural temperature normal to the optical axis. The tolerance in temperature variation is given by

$$\Delta T = \frac{2\, d\theta}{\alpha L} \qquad \text{(B-3)}$$

where

θ = the angular deflection of the telescope structure

d = the distance across the telescope structure, which can be assumed to be ≥ 2.5 ft

L = the length of the telescope structure ($\cong 10$ ft)

There is little advantage in holding θ to less than one arc-second (since the maximum point-ahead angle is 75 arc-seconds with respect to the earth beacon signal), and the telescope must be configured to maintain diffraction limited operation throughout such a range. There is no need to maintain θ below the 0.2 arc-second of the spacecraft laser beamwidth because a distortion θ affects both incoming and outgoing beams, respectively. It is the relationship between the spacecraft laser and the beacon sensor that must be maintained to such an alignment tolerance. The temperature variation across the telescope structure must therefore be held to a tolerance of $\Delta T \cong 4^{o}C$ (or $7.2^{o}F$).

Neither the $2.7^{o}F$ tolerance in temperature variation along the optical axis nor the $7.2^{o}F$ tolerance in temperature variation across the spacecraft presents serious thermal control problems as long as the effects of the RTG power supplies and the spacecraft laser are suitably controlled. Approximately 150 pounds of structure is capable of providing sufficient rigidity to the spacecraft telescope to keep the natural bending frequencies of the telescope well above the attitude control frequencies.

B.4 THE RTG POWER SUPPLIES

Suitable thermal isolation of the RTG power supplies from the spacecraft telescope can be provided by locating the RTGs external to the spacecraft. Assuming the power supplies provide 2 kw of electrical power at 10 percent efficiency, approximately 20 kw of heat must be radiated to space.

The configuration selected utilizes four power supplies with 5 kw of heat dissipation each. The power supplies are mounted on a ring of tubes of a metal with a relatively low thermal conductivity such as stainless steel. The ring is attached by supports to the spacecraft outer structure in several places. Associated with each power supply is approximately 15 square feet of surface area to maintain the desired temperature, which can be accomplished by two vanes approximately 18 inches by 40 inches. These vanes should be oriented such that the optical axis of the telescope lies approximately in the plane of the surface of the vane so that the heat radiation toward the spacecraft is minimized.

To provide adequate insulation of the telescope structure, the RTG power supplies should be mounted at least one foot from the exterior of the spacecraft. The use of approximately 30 layers of embossed aluminized mylar (a total thickness of 0.3 inch) insulation exterior to the telescope structure is recommended.

B.5 THE SPACECRAFT LASER

Rejecting the heat dissipated by the spacecraft laser in a manner compatible with the attainment of high pointing accuracy is one of the more formidable tasks of the laser communications mission. Lasers operating on the earth are cooled by a water jacket surrounding the laser (sufficient water is pumped through the jacket to maintain the desired operating temperature of 100°C or less). Pumping water to cool a spacecraft laser, however, is undesirable because of the relatively large high frequency disturbance torques induced by the pump motor and turbulence of the water. The recommended solution is to use a heat pipe, which is a passive device and utilizes the temperature difference between the spacecraft laser and the cold of space to radiate the heat to space in an efficient manner. (The laser-heat pipe combination is shown in Figure B-3.)

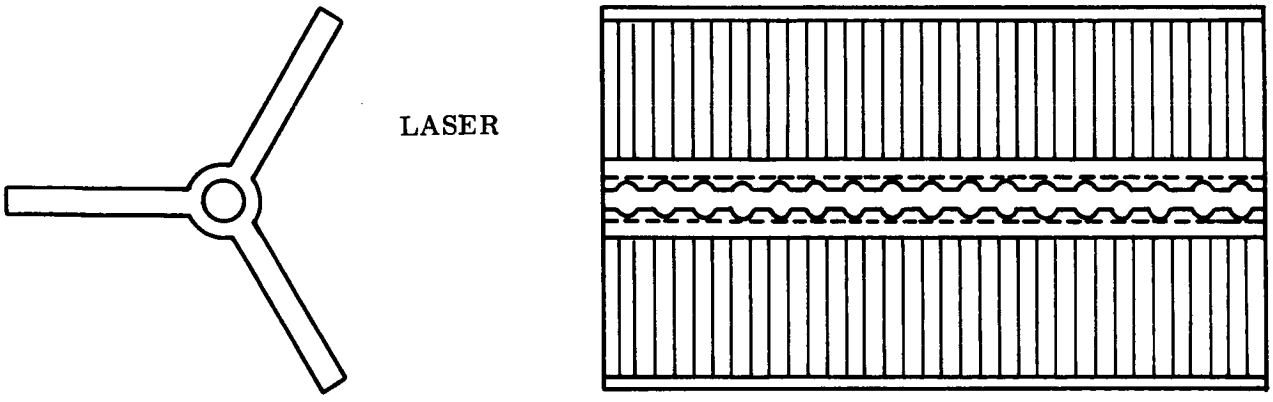

Figure B-3. Laser-Heat Pipe Combination

A water jacket surrounds the laser, and the water heated by the laser flows outward in the pipes in each vane due to the vapor pressure of the boiling water. The vanes extend outside the spacecraft and radiate the heat of the water to space. The heat pipe may be

sized roughly by assuming a laser operating temperature of 100°C and the portion of the vanes external to the spacecraft to be at a temperature of 80°C. For an emissivity of 1, the vanes will radiate 82 watts/ft^2 of surface area. Assuming an emissivity of 0.9 (which is reasonable because of the relative cold of outer space), $\frac{2 \times 10^3 \text{ watts}}{(82)\ (0.9) \text{ watts/ft}^2} = 27 \text{ ft}^2$ of vane surface area will be required external to the spacecraft. Since all three vanes need be approximately 4 feet long, the vanes must protrude beyond the spacecraft skin a total of $\frac{27 \text{ ft}^2}{(3)\ (2)\ (4)\ \text{ft}} = 1.1$ ft, which is minimal.

The heat pipe is a very attractive concept for this application because it involves no moving parts. While the heat pipe definitely shows promise of meeting the laser temperature control requirements, it must be pointed out that 100°C laser temperature goal is pushing the heat pipe to nearly its maximum performance because of two considerations:

a. The relatively high concentration of heat it must dissipate. A laser sized to meet the 10 watt output at 0.5 percent efficiency (2 kw input power) would be on the order of 4 feet long with a bore of approximately 1/2-inch diameter. Fortunately, the heat is dissipated at the walls of the laser due to arcing and is nearly uniform in intensity throughout its length. The concentration of heat is therefore approximately

$$\frac{(2 \text{ kw})\ (12 \text{ in./ft})}{(4 \text{ ft})\ )1/2\ \pi \text{ in.})} \cong 4 \text{ kw/ft}^2 \qquad \text{(B-4)}$$

This is relatively high.

b. If the desired temperature of operation were decreased significantly, the effect of sunlight incident upon the vanes would not be negligible, and the vane size would have to be greatly increased. The power available from sunlight in the vicinity of Mars is approximately 55 watts/ft^2, and there is a limit to how effectively this can be prevented from heating the vanes through positioning of the vanes in the spacecraft shadow, which becomes more acute as the vanes grow in size.

Since solar heating is not a serious problem, it appears most advantageous to locate the vanes symmetrically (120 degrees apart) to provide uniform cooling of the spacecraft laser. Because of the attitude control maintained during the mission, only one of the sides of the spacecraft sees the sun, and the vane located on that side can be positioned so that the sun

is nearly in the plane of the vane at all times, minimizing the interference of incident solar energy upon the radiation of the laser's heat. Because of the relatively small size of the vanes, the remaining vanes can be located to remain in the spacecraft's shadow throughout the mission.

The location of the vanes symmetrically about the heat pipe is most practical if the spacecraft laser is approximately in line with the optical axis of the telescope. If the spacecraft laser is not in line with the telescope optical axis, the vanes in the heat pipe will have unequal surface areas within the spacecraft (assuming the spacecraft is nearly symmetrical about the telescope optical axis) which will result in an unequal cooling of the spacecraft laser and a nonsymmetrical distribution of temperatures within the spacecraft leading to thermal bending problems. If the laser and servoed optics for the point ahead are folded via mirrors so that the spacecraft laser lies parallel to the telescope and next to it as shown in the sketch below, large and difficult to control temperature gradients across the telescope structure will result. This will lead to thermal bending of the telescope structure. Thus, the preferred design is to place the laser and servoed optics for point-ahead approximately in line with the telescope optical axis.

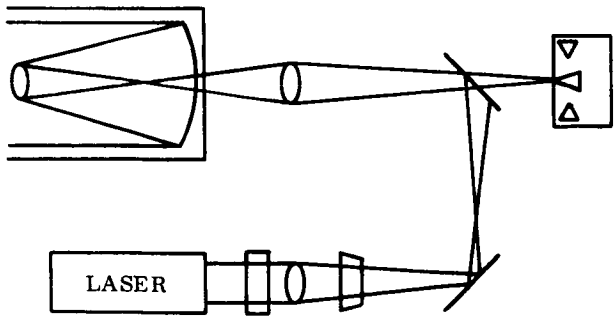

B.6 STRUCTURE FOR THE SPACECRAFT LASER, SERVOED OPTICS, AND FINE POINTING SENSOR

Maintaining alignment between the spacecraft laser, servoed optics for point ahead, and the fine Earth (beacon) sensor is the most critical thermal and structural problem because:

a. The alignment between these components represents the alignment between the incoming Earth beacon beam and outgoing spacecraft laser beam, which is critical because of the open loop nature of the point-ahead angle.

b. The alignment required is precise due to the narrow (0.2 arc-second beamwidth) spacecraft laser beam.

The problem is compound because the spacecraft laser will be operating at 100°C, and the telescope will be operating near 0°C (with the structure aligning the spacecraft laser, servoed optics for point-ahead, and fine Earth sensor connecting the laser to the telescope).

Consideration of the sizes of the laser, servoed optics, and fine Earth sensor and of the structural problems of interconnecting them dictate that the structure should be on the order of 1 ft across. The spacecraft laser will be approximately 4 ft long, and optical considerations dictate that approximately 2.5 ft of structure length be allocated to the servoed optics for fine pointing, fine earth sensor, and remaining optical elements (excluding the main telescope). Assuming an invar beam, the temperature gradient across the beam should be held to

$$\Delta T = \frac{2\, d\theta}{\alpha L}$$

$$= \frac{(2)\,(1)\,(0.025)(5 \times 10^{-6})}{(0.7 \times 10^{-6})\,(6.5)} = 0.055^{\circ}C = 0.1^{\circ}F \qquad \text{(B-5)}$$

Such a temperature control constitutes the most serious thermal problem of the mission. However, advanced thermal analyses such as that performed for the MOT study (Reference B-1) indicate thermal control to such a tolerance is feasible. Thermal control to such a tolerance is enhanced by the following factors:

a. The heat dissipation within the laser will not vary significantly with time since it is dependent upon the electrical power input (which can be controlled with precision) to the laser.

b. The heat pipe is capable of maintaining the laser temperature at a reasonably constant value through uniform radiation of laser heat to space over time.

c. The laser can be somewhat thermally isolated from the structure while maintaining rigid alignment to the structure by the use of mounting blocks of a material such as laminated Fiberglas. A 1/4-inch thickness of this material would provide at least 30°C of temperature isolation with sufficient structural rigidity. In addition, a barrier of 30 layers of embossed aluminized mylar should be placed between the spacecraft laser and optical elements, except for a clearance along the optical path.

To maintain thermal isolation between the telescope structure and the structure of the laser and optical elements, a gasket-type thermal barrier should be made using a 1/4-inch thick layer of laminated Fiberglas. To minimize the effect of longitudinal temperature variations along the spacecraft laser, the laser should be attached rigidly to the structure (through the laminated Fiberglas mounting blocks) at the end of the laser from which the beam emerges and should be attached in such a manner that the other end is free to move along the structure. If this design is not used, a longitudinal variation in temperature could lead to differing expansion of the laser and structure. This would cause a bending of both the laser and the structure. An additional thermal barrier of 30 layers of embossed aluminized mylar should be placed between the telescope and the other optical elements, with a sufficient opening in the barrier for the spacecraft laser beam and collected Earth beacon energy to pass through.

To minimize the noise to the fine Earth sensor due to reflection by the optical elements of spacecraft laser energy, the optical elements should all be contained in a housing which is coated with a material with a high solar absorptivity such as optical velvet (solar absorptivity 0.95 to 0.96). In addition, housings with optical velvet should be placed about each individual optical element to the degree permitted by the range of possible positions of the spacecraft laser and collected Earth beacon beams for the particular optical element involved. The levels of reflected energy are too low to lead to thermal problems, so that absorption of the energy to minimize noise to the fine Earth sensor can be carried out via the optical velvet coating to provide an adequate signal-to-noise ratio at the sensor.

The noise problem is further alleviated by tuning the sensor optical filter to the Earth beacon frequency, which can be different than the spacecraft laser frequency.

B.7 THE THIRD AXIS SENSOR STRUCTURE

The problem of maintaining alignment of the star sensor used for the third axis reference can best be solved by shielding the sensor and its associated structure so that it does not see the sun, the RTG power supplies, or the vanes of the laser heat pipe.

To thermally isolate the telescope and spacecraft laser structures from heat sources they need not be exposed to, the use of an outer structure made of a metal with a reasonably low coefficient of thermal expansion, such as aluminum, is recommended. This structure should be separated from the inner structure by a good insulator such as mylar. A thermal shield can then be built up from this structure to completely shield the Canopus sensor and its invar structure from the sun, RTG power supplies, and laser heat pipe radiating surfaces so that the sensor and structure are exposed only to the constant temperature of outer space, except for periods when Mars occults Canopus. Because of the low solar reflective properties of Mars, for the short (less than one hour) periods of time when Mars will be illuminating the star sensor and associated structure (and thermal control design for a long thermal time constant), Mars reflected sunlight is not anticipated to cause serious thermal bending problems to the third axis sensor structure.

The third axis sensor will be mounted on a beam which is normal to the beam of the spacecraft laser and optical elements and which is attached to that beam in the vicinity of the optical elements. Thermal control of this beam must be sufficient to maintain an alignment of 3 arc-seconds (allowing 3 arc-seconds to thermal and 4 arc-seconds to other miscellaneous structural distortions such as those caused by launch). The variation in temperature across the beam must therefore be held to

$$\Delta T = \frac{2\, d\theta}{\alpha L}$$

$$= \frac{(2)\,(.05)\,(3)\,(5 \times 10^{-6})}{(0.7 \times 10^{-6})\,(2)} = 10.7^{\circ}C = 19^{\circ}F \qquad \text{(B-6)}$$

which does not present a serious thermal problem. An invar beam of 25 pounds weight is sufficient to maintain structural rigidity.

Since the beam supporting the third axis sensor must be rigidly attached to the beam supporting the laser and optical elements to maintain the precise alignment required, the two beams may be regarded as forming a single structure. The only reason they were listed separately was to determine the thermal control required for each section of the structure to maintain the overall alignment dictated by mission considerations.

B.8 THE ROCKET ENGINE

The rocket engine for midcourse correction and orbit insertion should be located so that its thrust vector goes through the spacecraft center of mass and is in a direction in which the structural effects of the thrust can best be tolerated. For the mission under consideration, this direction corresponds to the spacecraft optical axis, since the major parts of the spacecraft structure are located to maintain alignment to this axis.

Therefore, the rocket should be located at the telescope end of the structure (as it is structurally desirable to have it near the heavy RTG's) and aligned to the optical axis of the spacecraft. Considerations related to the interplanetary flight do not pose any difficulties for such a placement of the rocket engine. Location of the rocket engine in such a manner is also desirable because the same spacecraft control axes can be used for the interplanetary flight as are used during the laser communications phase of the mission.

The outer structure of the spacecraft should be built up somewhat in the area of the rocket to handle the thrust of the rocket and adequately support the 4300 pounds of the rocket and fuel.

Because there is no need for the rocket engine once a suitable orbit of Mars has been attained, the rocket and fuel tanks will be jettisoned prior to commencement of laser communications. In addition, immediate jettison after burn greatly alleviates thermal problems caused by the rocket.

The remaining equipment on board the spacecraft, such as the RF communications package, the spacecraft computer, attitude control electronics, etc., can be located either in the area between the vanes of the heat pipe or mounted in bays within the spacecraft in the region of the RTG supports. While there is no strong reason for either choice, locating the remaining equipment in the region of the RTG supports is recommended because it better isolates these variable sources of heat from the portion of the spacecraft structure supporting the laser and optical elements.

B.9 REFERENCES

B-1. "A System Study of a Manned Orbital Telescope", prepared for NASA Langely Research Center by Aerospace Group, The Boeing Company, under contract NAS 1-3968, D2-84042-1, October, 1965.

APPENDIX C

TORQUER SUBSYSTEM TRADEOFFS

APPENDIX C

TORQUER SUBSYSTEM TRADEOFFS

C.1 INTRODUCTION

A comprehensive tradeoff study was conducted to determine the best of the several varieties of torquing subsystems, considered to be available in the 1975-1980 time period, to meet the attitude control and stabilization requirements derived from the selected mission involving high data rate laser transmission to Earth from a Mars orbiting vehicle. These subsystems included:

a. Mass Expulsion
    1. Bipropellant
    2. Monopropellant
    3. Cold Gas
    4. Varieties of Micropound Thrusters
b. Control Moment Gyros
    1. Twin Two-Degree-of-Freedom plus Twin Single Degree-of-Freedom Gyros
    2. Three Pairs of Single Degree-of-Freedom Gyros
    3. Four Off-Axis Single Degree-of-Freedom Gyros
c. Reaction Wheels
    1. Conventional
    2. Fluid Flywheel

The Torque Adaptive Control Technique currently under development at the General Electric Company was considered an example of computation logic which could make efficient use of the capabilities of the broad range of mass expulsion media considered.

The tradeoff studies were based on mathematical analyses of the ability of each of the candidate systems to acquire the Fine Pointing Control Mode and to maintain the required precision attitude hold, the weight and power consumption of the candidates, and their availability in the time period of interest. Reliability, the most nebulous area in the tradeoff structure, was factored in on a comparative basis which considered the development necessary to get the reliability as a governing factor.

In the subsequent paragraphs, the tradeoff conclusions will be summarized followed by the criteria, torquer descriptions, and details of the tradeoffs upon which the recommendations were based.

C.2 SUMMARY OF RESULTS

The tradeoff studies in the precision vehicle control area indicate that the three control moment gyro systems present the most attractive methods of obtaining the desired control. The single degree-of-freedom gyros may be slightly more applicable within the bounds of a strictly paper study, but for the precision control required about two axes to stabilize the narrow laser beam to Earth, the less complex loop stabilization favors the two degree-of-freedom gyros.

The single degree-of-freedom control moment gyros have a small advantage over inertia wheels for third-axis control in the areas of a lower peak power requirement and a more linear gain characteristic.

The torquing subsystem recommended for analytical design purposes, derivation of mathematical model, and simulations to be performed during the latter half of the study is as follows:

a. Twin two degree-of-freedom control moment gyros to be used for two-axis spacecraft attitude control to the Earth-based laser beacon reference.

b. Twin single degree-of-freedom gyros to be used for third-axis attitude control of the spacecraft to the Canopus reference.

c. Reset of the control moment gyros using a low level mass expulsion system.

C.3 TORQUING SUBSYSTEM FUNCTIONAL REQUIREMENTS

As previously stated, the spacecraft control system must aim its laser beam ahead of the apparent location of the proper Earth-based receiver to compensate for transmission lags and the spacecraft motions in orbit, the relative motion of Earth and Mars in their orbits, and the motion of the receiver as the Earth rotates on its axis during these lags. The method derived to accomplish this is to orient the spacecraft with its fixed telescope to an Earth beacon-Canopus reference and to acquire the Earth receiving station through a laser beam steering servoed optic system in response to computed point-ahead and acquisition commands relative to that reference. The functions reserved for the spacecraft attitude control torquing subsystem are:

a. To align and stabilize the spacecraft roll axis, (X_c) designated by the optical axis of its fixed telescope, to the sensed incoming radiation from the Earth-based beacon in response to attitude and rate signals.

b. To align and stabilize the spacecraft in roll in response to position-error signals from the Fine Canopus Sensor or gyro reference, and rate signals.

c. To periodically slew the spacecraft from one Earth Station to another as necessitated by Earth rotation. The maximum slew angles are of the order of 10 arc-seconds in yaw and 3 arc-seconds in pitch, as tracking an alternate station is initiated by signals derived from errors in the saturated region of the fine error sensor.

d. To control the spacecraft attitude and rates in response to signals from gyros and coarse and intermediate attitude sensors during the acquisition sequences leading to the capture of the Earth-based target-Canopus attitude reference system.

Considering the requirement for fine stabilization of the spacecraft in pitch and yaw to within 0.03 arc-second of the Earth-based target radiation and to within 7 arc-seconds of the Earth-based target-spacecraft-Canopus plane in roll, an error apportionment of 0.01 arc-second and 3 arc-seconds, respectively, is allowed for the control "standoff" error.

Stabilization of the spacecraft in the intermediate pointing mode to within 5 arc-seconds of the Earth radiation target and within 15 arc-seconds of the Earth-spacecraft-Canopus plane with vehicle rates less than 0.005 degree per second are considered reasonable. The optimum point in the acquisition sequence for the momentum storage devices to take over control is after stabilization to the intermediate pointing references to these performance requirements.

The major disturbance torques are considered to be due to solar pressure and gravity gradient, where the maximum values as given in Figure C-1 are:

Solar Pressure Torque (T_s) = 1.6×10^{-5} ft-lb

Gravity Gradient (T_{gg}) = 2.2×10^{-4} ft-lb

The combined torques will vary in time, but an estimation of the torque impulse transferred to the spacecraft from these sources may be determined, considering the solar pressure to be a constant destabilizing torque having a cumulative momentum effect, while the gravity gradient torque has changes in polarity during an orbital period which results in a partially cyclic torque impulse effect.

The extreme cases of gravity gradient momentum transfer are shown in Figure C-1.

Considering the case of totally cumulative gravity gradient momentum transfer to the spacecraft, the area under the T_{gg}-time curve for one half orbital period may be approximated by:

$$H = \int_0^{T_{o/2}} \frac{T_{gg\ max}}{2} (1-\cos 2t)\, dt = \frac{T_{gg\ max}}{2} \frac{T_o}{2} = 0.25\, T_{gg\ max} T_o$$

where T_o = the orbital period $\approx$ 26,000 seconds.

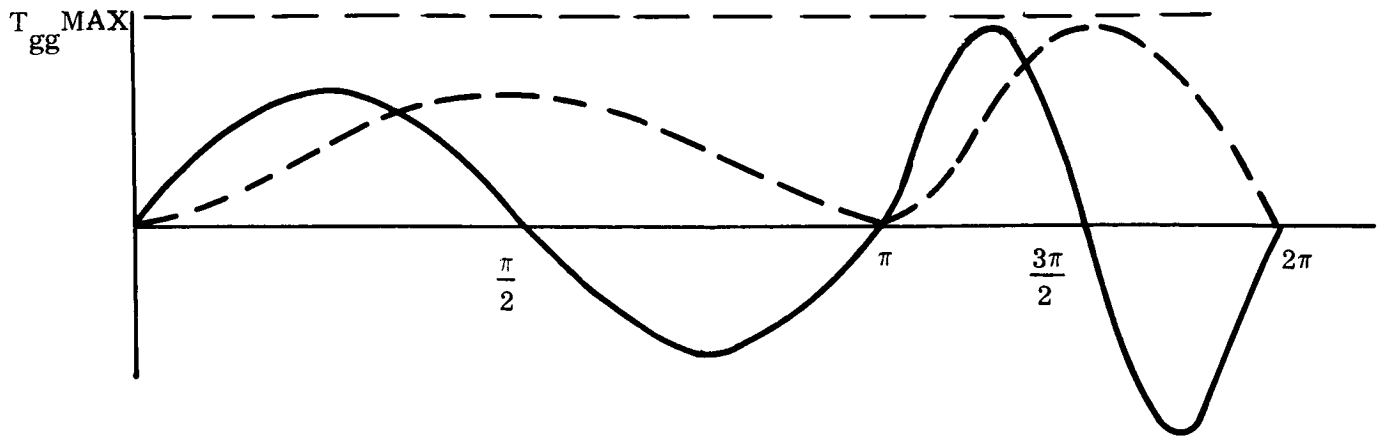

where $T_{gg\ max}$ (for each axis) was obtained by maximizing the following expression for gravity gradient torques.

$$\begin{bmatrix} T_{ggx} \\ T_{ggy} \\ T_{ggz} \end{bmatrix} = \frac{3GM_m}{Ro^3} \begin{bmatrix} A_{32}A_{33}\left[I_{yy} - I_{zz}\right] \\ A_{33}A_{31}\left[I_{zz} - I_{xx}\right] \\ A_{31}A_{32}\left[I_{xx} - I_{yy}\right] \end{bmatrix}$$

where: R_o = circular orbit radius. $Ro_{min} = 4.43 \times 10^6$ m for a 1000 km x 10000 km orbit
G^o = universal gravitational constant = 6.67×10^{-11} nt - m^2/kg^2
M_m = mass of Mars = 6.38×10^{23} kg
A_{31}, A_{32}, A_{33} = direction cosines between local vertical and spacecraft axes
$(A_{3p}\, A_{3g\,max} = 0.5)$
I_{xx}, I_{yy}, I_{zz} = vehicle inertias (max difference of inertia assumed = 300 slug-ft^2)
results in $T_{ggmax} = 2.18 \times 10^{-4}$ ft-lb

For solar pressure torques (which are much less):

$$\left|T_s\right| = \left|F\right| a \sin\theta$$

where $\left|F\right| = PA \cos\theta$ for totally absorbed radiation (worst case).

θ = angle between force vector (at center of pressure) and the center of pressure to center of mass line. $(\sin\theta\ \cos\theta)_{max} = 0.5$

a = distance between center of pressure and center of mass, assumed to be no greater than 0.5 ft.

A = surface area upon which solar radiation is incident (assumed a max of 30 m^2).

P = volume energy density in the solar radiation field, assumed less than the near earth density of 0.47 dynes/m^2.

Therefore, $\left|T_s\right| \leq 1.55 \times 10^{-5}$ ft-lb

Figure C-1. Gravity Gradient Momentum Transfer

For the completely cyclic case, the largest torque impulse to be transferred to the spacecraft per half orbit may be approximated by:

$$H = \frac{2}{\pi} T_{gg\ max} \frac{T_o}{4} = 0.16\, T_{gg\ max} T_o$$

A spacecraft control torquing subsystem may take advantage of the cyclic nature of the gravity gradient torque by providing a counter torque while storing the disturbance torque impulse in a suitable momentum storage device during one-half of the cycle and reversing the process when the disturbance torque polarity reverses. The momentum storage subsystem should be designed to minimize the number of resets (unloading) required by providing sufficient capacity to store the maximum disturbance torque impulse anticipated during one-half of the cycle plus a suitable margin. The combined momentum transferred to the spacecraft per axis per half orbit considering a worse case is given by:

$$H = \int T_{sp}\, dt + T_{gg}\, dt$$

$$= (1.6 \times 10^{-5} + 0.5 \times 2.2 \times 10^{-4}) \frac{26000}{2} = 1.64 \text{ ft-lb sec}$$

C.4 DESCRIPTION OF CANDIDATE SYSTEMS FOR TRADEOFF

C.4.1 TWIN TWO-DEGREE-OF-FREEDOM CONTROL MOMENT GYROS (2 DOF CMG)

A single 2 DOF CMG can be used to provide control about two axes. However, cross coupling into the third axis from the torquer controlling the inner gimbal is present. This coupling can be reduced by restricting outer gimbal angular motion, but a correspondingly larger wheel is required to transfer the desired momentum.

The use of twin CMG's eliminates this problem by providing equal and opposite torques on the third axis due to matched gimbal angles. A third axis control system capable of absorbing spurious cross coupling is necessary when this is used.

C.4.2 TWIN SINGLE-DEGREE-OF-FREEDOM CONTROL MOMENT GYROS (1 DOF CMG)

Twin 1 DOF CMG's have been looked at in various studies, such as the Manned Orbital Telescope, and have been concluded to be satisfactory for our type system. Twin 1 DOF CMG's provide control about one axis, and cancel one another's cross coupling effects into the other two axes.

C.4.3 INERTIA WHEEL

The inertia wheel provides single-axis control with little cross coupling effects when vehicle rates are low. The rate of change of wheel speed is the means used for momentum exchange. The General Electric Company has successfully flown inertia wheel control systems in space for more than 1 year on the Nimbus satellite.

C.4.4 FLUID FLYWHEEL

The fluid flywheel is a single-axis device providing momentum exchange as long as a rate of change in fluid rate exists. Little, if any, cross coupling between axes exists when vehicle rates are low. The fluid flywheel can be considered as a special case of the inertia wheel.

C.4.5 GLOPAC

GLOPAC (Gyroscopic Low Power Attitude Control) is the name applied to a system under development at General Electric Company's Light Military Electronics Department since 1960. The system uses four symmetrically mounted single-axis control moment gyros to stabilize and control space vehicles. The system is most applicable to vehicles with symmetrical momentum transfer requirements such as the one discussed here.

The system has (1) undergone extensive mathematical and analog analysis, (2) tested on three different air bearing simulations, and (3) demonstrated attitude hold capabilities of less than 20 arc-seconds under high disturbance torque conditions (simulator unbalance and air motion).

Because of gyroscopic cross coupling in the system, it does not lend itself readily to the type analysis discussed here, especially when nonlinear effects are important. Thus, the ultimate precision attitude hold capabilities of the system cannot be shown without an extensive analog (or digital) simulation. Intuitively, it is felt that the system has the same accuracy potential as the other more easily analyzed systems, but that dynamically it may be somewhat slower.

Because of the response requirements during acquisition and the difficulties of analysis, a study of the magnitude reported here cannot fully assess the comparative merits of the GLOPAC system.

C.4.6 MASS EXPULSION SYSTEM

The mass expulsion system is a one, two, or three axis system using controlled thrusters for control. Its use, thus far, has been mainly for relatively coarse control. New concepts in thrusters giving very small thrust levels make this system worthy of consideration for our purposes. A key to the use of these techniques is the control logic computations which enables efficient use of the low thrust. Torque adaptive control logic is now under development.

C.5 ACTUATOR TRADEOFFS

The tradeoffs were performed in two parts — the two-axis tradeoff and the third-axis tradeoff. This was because of the attitude tolerance difference of $\pm$ 0.03 arc-second for the pitch and yaw axis and $\pm$ 7 arc-seconds for the roll axis.

The two-axis tradeoff considers candidate systems previously described. The third-axis tradeoff considers all the candidate two axis systems, except the twin 2 DOF CMG's which are excluded for obvious reasons.

Tables C-1 and C-2 summarize the two-axis and-third axis tradeoffs developed in Sections C.5.1 through C.5.5 of this report.

Table C-1. Two-Axis Tradeoff

	PERFORMANCE, 5	RELIABILITY, 4	POWER, 3	WEIGHT, 2	AVAILABILITY, 1
10	2G	W	M	GP	1G, W
9	GP, 1G, W	2G, GP		2G, 1G	
8		1G	1G		2G
7			2G, GP		GP
6	M		W		
5				W	
4		M		M	M
3					
2					
1					
DROPPED	F				

SYMBOLS:
M - Mass Expulsion
F - Fluid Flywheel
GP - GLOPAC
1G - 1 DOF CMG
2G - 2 DOF CMG
W - Inertia Wheel

Table C-2. Third Axis Tradeoff

	PERFORMANCE, 5	RELIABILITY, 4	POWER, 3	WEIGHT, 2	AVAILABILITY, 1
10	1G	W	M	GP	1G, W
9	W, GP	1G, GP			
8			1G	W, 1G	
7			GP		GP
6	M		W		
5				M	
4		M			M
3					
2					
1					

SYMBOLS:
M - Mass Expulsion
GP - GLOPAC
1G - 1 DOF CMG
W - Inertia Wheel

The candidate systems can be ranked by multiplying rating and parameter weighting values from Tables C-1 and C-2. For the two-axis tradeoff, the results are:

2 DOF CMG	133 pts
GLOPAC	129 pts
1 DOF CMG	129 pts
Inertia Wheel	123 pts
Mass Expulsion	90 pts

From this ranking, the three gyro systems appear to be the most suitable for the mission.

For the third axis, GLOPAC and mass expulsion values are extrapolated from the two-axis tradeoff and rank as before:

1 DOF CMG	136 Pts
GLOPAC	129 Pts
Inertia Wheel	129 Pts
Mass Expulsion	80 Pts

The gyro systems appear to be slightly more suitable than the Inertia Wheel with virtually no difference between the control moment gyro systems.

C.5.1 TWIN TWO-DEGREE-OF-FREEDOM CONTROL MOMENT GYRO (2 DOF CMG)

Figure C-2 shows a simplified single axis vehicle control loop using a twin 2 DOF CMG system, in the highly damped mode.

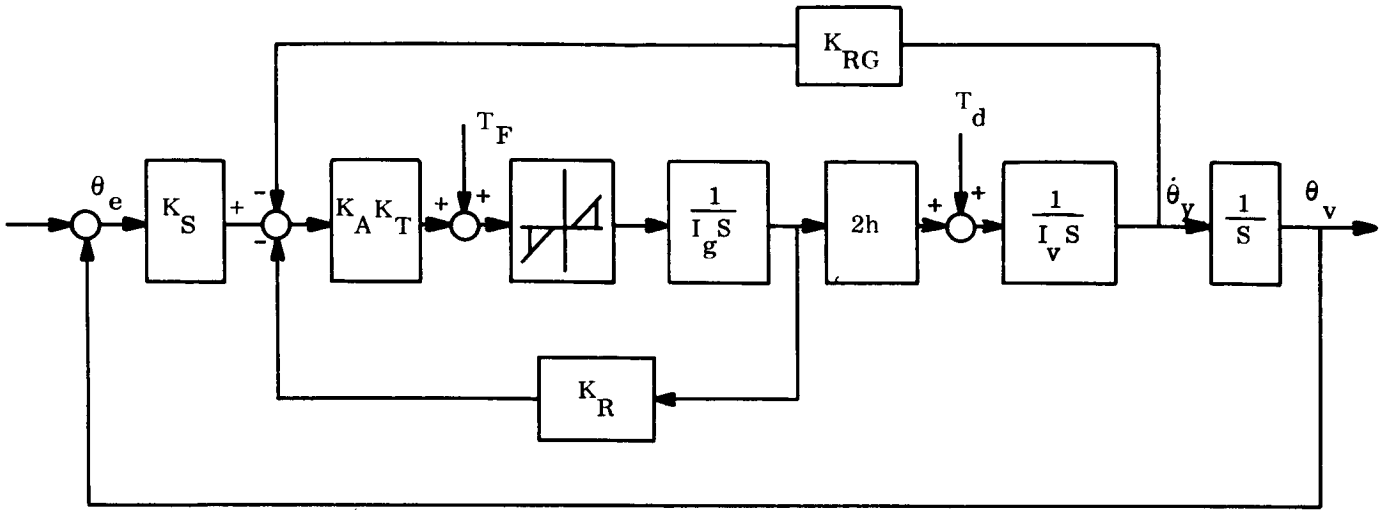

Figure C-2. Single Axis Vehicle Control Loop

The twin 2 DOF CMG's were selected for the two-axis system because of lesser power and weight requirements and the 1 DOF CMG's for the third axis. As mentioned previously, the GLOPAC system was dropped because of its difficulty of analysis (beyond the scope of this study) and because of the intuitive feeling that this system might be too sluggish to meet response requirements during acquisition.

For this control moment gyro configuration (using two gyro wheels per axis), the combined momentum capacity should be:

$$\vec{H}_t = H_y \vec{Y} + H_z \vec{Z}$$

where Y and Z are two axes of control. Considering a disturbance torque impulse of 1.64 ft-lb/sec about the two axes simultaneously.

$$H_t = \sqrt{H_y^2 + H_z^2} = 2.32 \text{ ft-lb/sec}$$

To include a margin reduction in spacecraft rates during initial acquisition, etc., the value of momentum storage capacity H_t used is 4 ft-lb/sec. The momentum capacity of each individual gyro at reset is 2.0 ft-lb/sec, and the required spin vector momentum for each gyro is 2.0 ft-lb/sec.

The gain of the control loop should be sufficient to maintain vehicle control about a single axis with a gimbal angle at 60 degrees, the assumed reset position. In the ideal situation, the torque applied to the vehicle T_a is equal to the torque disturbances T_d. Considering the nonlinearities caused by friction on the gyro gimbal axes T_f from bearings, gimbal torque motor hysteresis, etc., in addition to T_d; the control gain for fine pointing attitude hold must provide the required torque to overcome T_f and T_d with an attitude error within allowable limits.

Referring to C-4, T_a for attitude hold in the fine pointing mode can be determined from

$$T_a = \left(K_s \theta_e - \dot{\theta}_v K_{rg}\right) K_A K_T - \left(T_F + \frac{T_d}{2h} K_A K_T K_R\right)$$

where K_s = Sensor gain
K_a = Amplifier gain
K_T = Torquer gain
K_R = Gyro gimbal rate sensor gain
$D = K_S K_T K_R$ the gyro gimbal damping = 100

θ_v may be considered essentially zero except during station switching and acquisition, so during fine pointing attitude hold the overall loop gain K required to limit the standoff error to 0.01 arc-second may be found

$$K = K_s K_a K_T = \frac{\left(T_F + \frac{T_d}{2h} K_s K_T K_R\right)}{\theta_e \cos B}$$

Assuming the combined friction torque to be 5.2×10^{-4} ft-lb and T_a to be a maximum of 2.34×10^{-4} ft-lb., and for a maximum gyro gimbal angle of 60 degrees a torque five times above threshold is provided for a 0.1 arc-second position error, we have

$$K = \frac{5\left(5.2 \times 10^{-4} + 2.36 \times 10^{-4} \frac{x100}{4}\right)}{0.01 \cos 60^{o}}$$

$$= 6.4 \text{ ft-lb/arc sec}$$

This is a fairly high gain, but it probably should be even higher for acquisition or station switching. For attitude hold a CMG gimbal torquer size of 0.064 ft-lb would be sufficient.

The maximum vehicle rate which can be adsorbed in two axes simultaneously without saturation of the CMG's is

$$\dot{\theta}_v = \frac{H \sin 45^o}{I_v} = \frac{4\ (0.707)}{5000} = 5.6 \times 10^{-4}\ \frac{\text{rad}}{\text{sec}} = 0.032\ \frac{\text{deg}}{\text{sec}}$$

The CMG torque capability for acquisition may be sized by starting from the initial conditions that (1) the spacecraft is stabilized to within 5 arc seconds of the center of the Earth, (2) the Intermediate Earth Pointing Sensor is being used, and (3) the ground station is at the edge of the Earth disc (10 arc-seconds maximum from the Earth's center); and assuming it is possible to reduce the vehicle rate to zero during the time the beacon is within the 1.5 arc-minute range of the sensor. Considering the maximum initial rate to be 0.032 degree per second, the average rate during deceleration is 0.016 degree per second and the Fine Earth Beacon Sensor range would be exceeded in

$$t_{acq} = \frac{\Delta\theta}{\dot{\theta}_{avg}} = \frac{75 \text{ arc-seconds}}{0.016\ \frac{\text{deg}}{\text{sec}} \times 3600} = 1.3\ \widehat{\text{sec}}$$

Assuming negligible torquer reaction time the spacecraft must be decelerated at

$$\ddot{\theta}_{max} = \frac{\dot{\theta}_{max}}{t_{acq}} = \frac{0.032}{1.3} = 0.024\ \frac{\text{deg}}{\text{sec}^2}$$

The average torque on the vehicle during this period would be

$$T_{avg} = \ddot{\theta} I_v = \frac{0.024}{57.3} \times 5000 = 2.1 \text{ ft-lb}$$

The torques indicated here for acquisition of the fine pointing mode are considerably higher than those required for attitude hold, but the initial rates derived from momentum storage capability are also higher than will exist at the start of acquisition. Considering stabilization of the spacecraft in the Intermediate Pointing Mode to be to 10 arc-seconds per second, the acquisition time, deceleration and torque required on vehicle should be

$$t_a = \frac{\Delta\theta}{\dot{\theta}_{avg}} = \frac{75 \text{ arc-sec}}{5 \frac{\text{arc-sec}}{\text{sec}}} = 15.0 \text{ seconds}$$

$$\ddot{\theta}_v = \frac{\dot{\theta}_{v\ max}}{t_a} = \frac{10 \text{ arc-sec/sec}}{15 \text{ sec}} = 0.67 \text{ arc-sec/sec}^2$$

$$T_{veh} = \ddot{\theta}_v I_v = 0.67 \frac{\text{arc-sec}}{\text{sec}^2} \times 5 \times 10^{-6} \frac{\text{rad}}{\text{arc-sec}} \times 5000 = 0.017 \text{ ft-lb}$$

Considering that during acquisition the vehicle attitude sensor and/or rate gyro keeps the CMG gimbal torquers in saturation, the required 0.017 ft-lb can be supplied by a very small gyro gimbal torquer. As long as the gyro gimbal torquer is kept in saturation by a large spacecraft attitude or rate error, the gyro gimbals will be accelerated, increasing gimbal rate and increasing the torque applied to the vehicle. Because the minimum gyro gimbal torque required for the attitude hold mode is only 0.064 ft-lb, the gimbal torque motor can be chosen with margin to spare as 0.3 ft-lb or 0.15 ft-lb for each gyro gimbal torquer. This enables the acquisition of the fine pointing mode to take place well within the saturation limits of the fine pointing sensor and control moment gyros.

The estimated running friction of the gimbal bearings required by the gyro discussed here is about 2×10^{-5} ft-lb per bearing and the static frictions is about 4×10^{-5} ft-lb per bearing. The friction torque characteristic of a 0.15 ft-lb brushless torque motor is estimated at approximately 10^{-4} ft-lb. Since two bearing sets and two torque motors per axis are required by the mechanization, the total stiction type torque per axis is about 3.6×10^{-4} ft-lb, well below the 5.2×10^{-4} assumed for computations.

Considering the 6.4 ft-lb/arc-sec gain requirement for K for attitude hold, a value of 7.5 ft-lb/arc-second was selected for this parameter to allow some margin. Considering this parameter value the controller open loop gain for pitch and yaw spacecraft axes is

$$\text{Open Loop Gain} = \frac{K\ 2h}{D\ I_v}$$

$$= \frac{7.5 \text{ ft-lb/}\widehat{\text{sec}} \times 2 \times 10^5 \frac{\widehat{\text{sec}}}{\text{rad}} \times 4}{100 \times 5000 \text{ ft-lb-sec}^2} = 12 \text{ sec}^{-2}$$

The estimated weight of two 2 DOF CMG's and associated electronics is about 25 lb.

Power (for induction motors) required to run the gyros will be approximately 8 watts. Additional losses due to AC inversion will add another approximately 4 watts for about 12 watts total. Peak power requirements will occur very infrequently during acquisition of the fine pointing mode.

Two DOF CMG's have been built and successfully run, although none has been used in space thus far. A summary of the torquing subsystem parameters are as follows:

Controller Open Loop Gain	Approximately	12 sec^{-2}
Controller Torquer Gain $K_s K_a K_t$		7.5 ft-lb/arc-sec
Weight (2 Axes)		25 lb
Power Required (2 Axes)		12 watts average 20 watts peak

C.5.2 TWIN SINGLE-DEGREE-OF-FREEDOM CONTROL MOMENT GYRO SYSTEMS (1DOF CMG)

Figure C-3 shows a simplified block diagram of a twin 1 DOF CMG system.

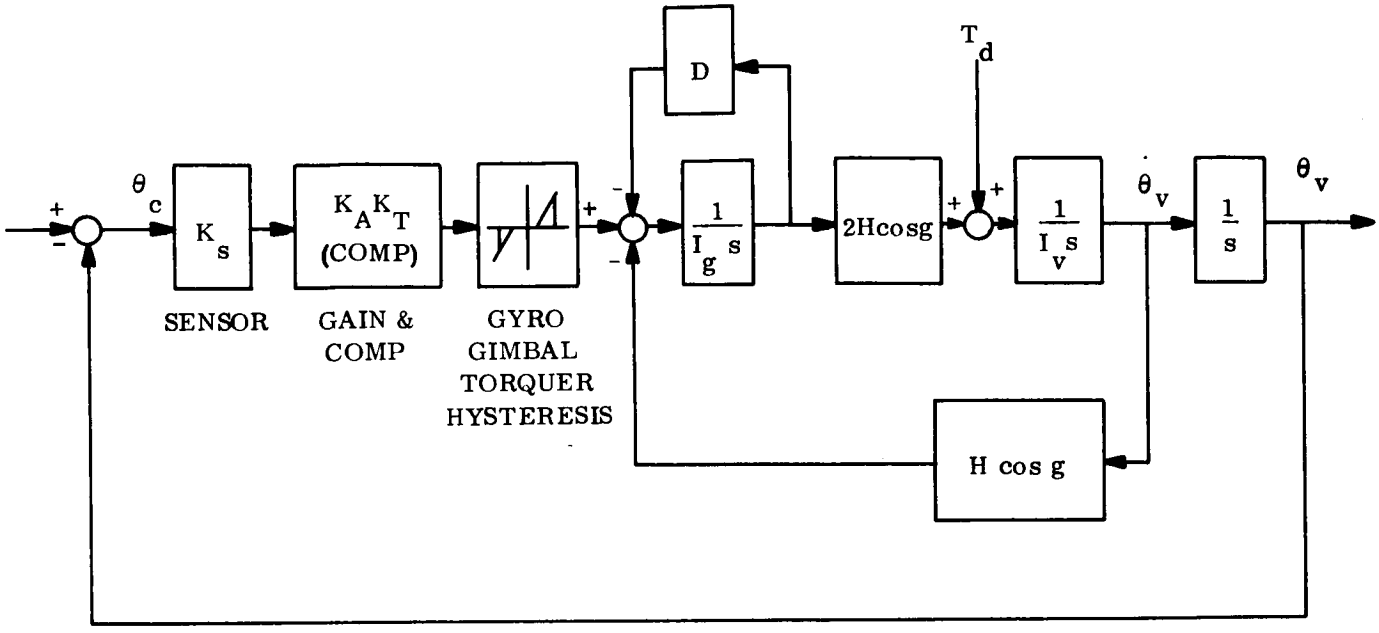

Figure C-3. Block Diagram of a Twin 1 DOF CMG System

In this configuration, the momentum capacity of the twin gyro combination on each axis need only be 3 ft-lb-sec at reset to store the disturbance torque impulse per half orbit with some margin. The Manned Orbital Telescope study included a single-axis analog simulation of its fine pointing mode in which this type of torquing subsystem was shown to be capable of stabilizing the spacecraft to the reference within 0.01 arc second. This was using a much larger vehicle (1.3×10^5 ft-lb-sec^2) and much larger CMG capacity (300 ft-lb-sec each). Based on this, twin 1 DOF CMG's should have no trouble meeting the tolerance here.

For two axis control of the Mars orbiter, the two twin 1 DOF CMG's weigh more and require higher average power than the twin 2 DOF CMG's by virtue of the 4-gyro versus 2-gyro implementation. An advantage of the 1 DOF configuration is its inherent torque amplification. However, the loop gain from attitude error to the gimbal bearing torquer output to a counter gimbal bearing friction, torquer friction characteristic, and disturbance torques for fine

pointing attitude errors of less than 0.01 arc-second is only approximately a factor of thirty less than that required for fine pointing hold utilizing 2 DOF gyros.

$$K = K_s K_a K_t = \frac{5\ T_F}{\theta_e} = \frac{5 \times 5.2 \times 10^4}{0.01} = 0.26\ \frac{\text{ft-lb}}{\text{arc-sec}}$$

In this case, the gain is determined solely by the torque threshold of the two gyro gimbals per control axis.

Utilizing twin 1 DOF CMG torquers the spacecraft exhibits a single-axis attitude control loop in which the transfer function definition without compensation essentially is:

$$\text{Open loop} = \frac{K_s K_a K_t}{H^* S\left(\frac{I_v I_g}{2H^2} S^2 + \frac{I_v D}{2H^2} S + 1\right)}$$

In which considering $H = 2000\ I_g$ (a very good approximation) and $H^* = H \cos \gamma$

$$\frac{1}{\omega^2} = \frac{I_v I_g}{2H^2} = \frac{I_v}{4000\ H^*}$$

$$\frac{2\mathcal{L}}{\omega} = \frac{I_v D}{2H^2} = \frac{D}{I_g} \frac{I_v}{4000\ H^*} = \frac{D}{I_g \omega^2}$$

and considering $I_v = 5000$ ft-lb/sec^2 and $H = 2$ ft-lb/sec

$$\omega = \sqrt{\frac{4000 \times 2}{5000}} = 1\pi 26 \text{ rad/sec}$$

and for $\mathcal{L} = 0.7$

$$\frac{D}{I_g} = 2 = 1.77 \text{ sec}^{-1}$$

which for the particular subsystem values being considered exhibits an open loop gain of

$$\frac{K_s K_a K_t}{H^*} = \frac{0.26 \times 2 \times 10^5}{2} = 2.6 \times 10^4 \text{ sec}^{-1}$$

Application of this type controller to the Mars orbiting spacecraft and laser communication mission being considered would yield a very high response and require a nonlinear sensor amplifier combination or complex compensation or both. It would be more applicable if larger values of momentum storage were desired.

The system weight is estimated at 15 pounds for each axis or about 30 pounds total for two axes. The power should be about 3 watts for each gimbal torquer for 12 watts total. Control electronics should be about 4 watts for a total of about 16 watts. Peak power should be less than 20 watts. Previous comments about the brushless DC torquer also apply here.

A summary of parameters for two axis control is as follows:

Controller Open LoopGain	Approximately	26,000 sec^{-1}
Control Torquer Gain $K_s K_a K_t$		0.25 ft-lb/arc-sec
Weight (2 Axes)		30 lb
Power Required (2 Axes)		16 watts average 22 watts peak

The momentum capacity for a twin 1 DOF CMG for third-axis control should be a minimum of 3 ft-lb-sec at reset as before. The gain required to overcome torquer friction need be

$$K = K_s K_a K_t = \frac{5 \times 5.2 \times 10^4}{3} = 7.25 \times 10^{-4} \quad \frac{\text{ft-lb}}{\text{arc-sec}}$$

and the open loop gain requirements are:

$$\frac{K_s K_a K_t}{H^*} = \frac{7.25 \times 10^{-4} \times 2 \times 10^5}{2} = 72.5 \text{ sec}^{-1}$$

Standard compensation techniques will ensure stable control. A summary of parameters for third axis control is as follows:

Controller Open Loop Gain	72 sec^{-1}
Weight (1 Axis)	16 lb
Power Required (1 Axis)	8 watts average 12 watts peak

C.5.3 THE INERTIA WHEEL

Figure C-4 shows a simplified version of a typical inertia wheel controller.

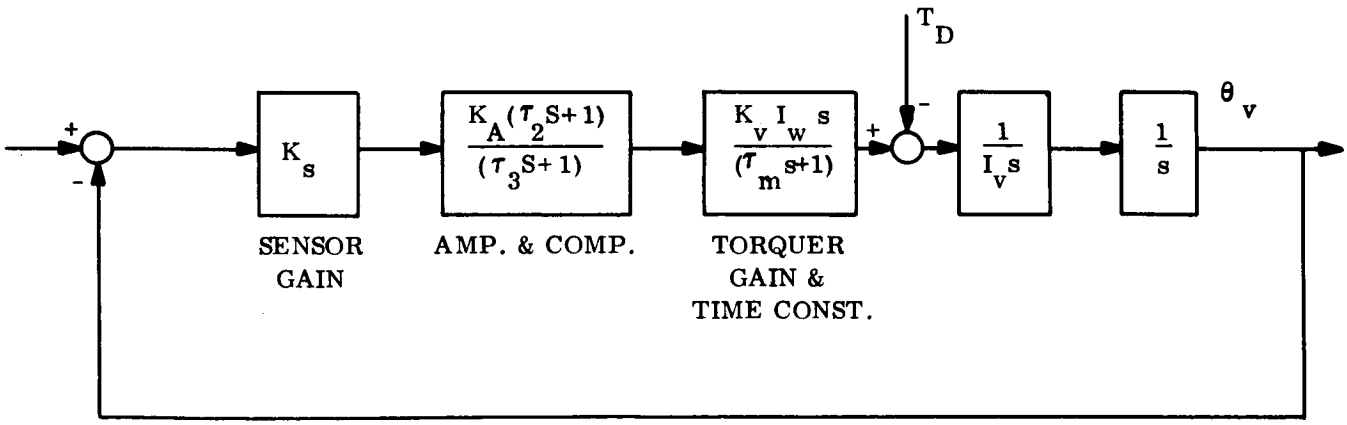

Figure C-4. Inertia Wheel Controller, Simplified Version

The continuous relatively high speed rotation of the inertia wheel avoids the gimbal static friction nonlinearity of control moment gyros, but the control loop has an inherent nonlinear torque characteristic demonstrated by reduction in torque availability and associated reduction in response as the wheel stores momentum.

Considering the transfer function of the vehicle rate for a torque disturbance input

$$\frac{\dot{\theta}_v(S)}{T_d(S)} = \frac{(\tau_m S + 1)(\tau_3 S + 1)}{I_v S (\tau_m S + 1)(\tau_3 S + 1) + K_v I_w K_s K_a (\tau_2 S + 1)}$$

and the steady state response to counter an external torque of magnitude T_d for a half orbit of 13,000 seconds

$$\frac{\theta_v}{T_d}(t) = \frac{13,000 \text{ seconds}}{K_v I_w K_s K_a} \quad \frac{\text{rad}}{\text{ft-lb}} = \frac{26 \times 10^8}{K_v I_w K_s K_a} \quad \frac{\text{arc-sec}}{\text{ft-lb}}$$

Considering a maximum amount of standoff error of 0.01 arc second due to the maximum disturbance torque of 2.36×10^{-4} ft-lb implies a closed loop gain of

$$\frac{\theta_v}{T_d} = \frac{0.01}{2.36 \times 10^{-4}} = 42.5 \quad \frac{\text{arc-sec}}{\text{ft-lb}} = 21.2 \times 10^{-5} \quad \frac{\text{rad}}{\text{ft-lb}}$$

which makes the gain

$$K_v K_w K_s K_a = \frac{13,000 \text{ sec}}{21.2 \times 10^{-5} \frac{\text{rad}}{\text{ft-lb}}} = 6.13 \times 10^7 \quad \frac{\text{ft-lb/sec}}{\text{rad}}$$

and the open loop gain is

$$\frac{K_v I_w K_s K_a}{I_v} = \frac{6.13 \times 10^7}{5 \times 10^3} = 12,200 \text{ sec}^{-1}$$

The torque requirement for acquisition is the same as for the twin 2 DOF CMG configuration namely 0.2 ft-lb average. A conceptual design is given in Figure C-5 that maintains high stall torque during acquisition and provides excess momentum storage capability during fine pointing attitude hold.

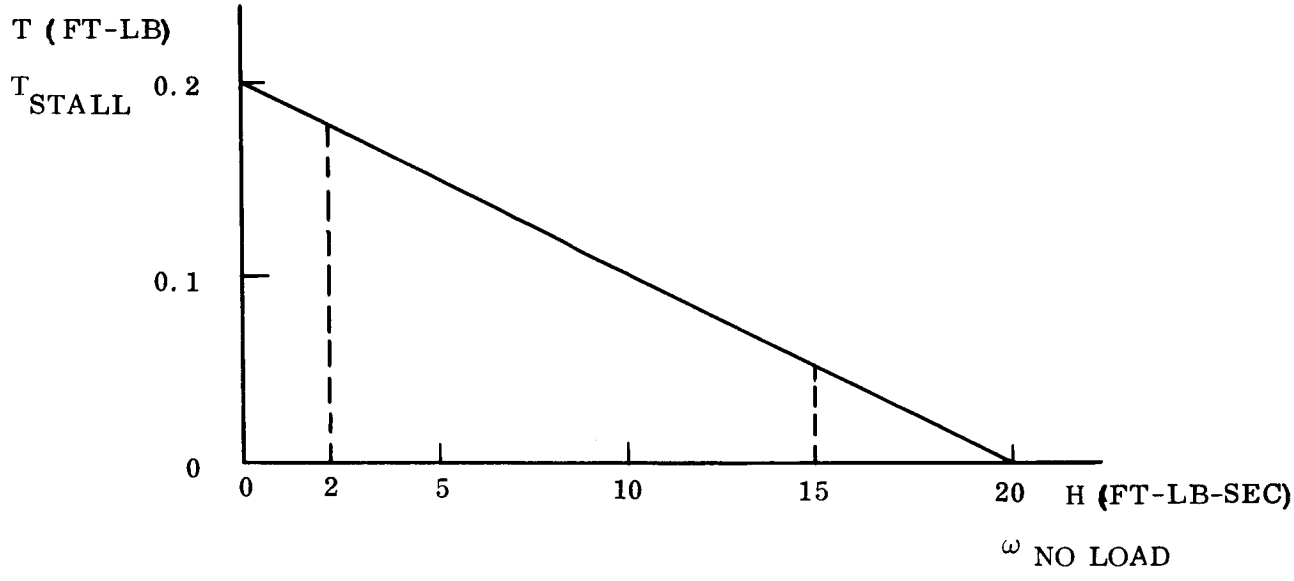

Figure C-5. Conceptual Design for Acquisition Torque Requirements

For H_{max} = 20 ft-lb/sec and T_{stall} = 0.2 ft-lb at zero speed

$$\tau_m = \frac{H_{max}}{T_{stall}} = \frac{20}{0.2} = 100 \text{ sec}$$

$$K_s K_a K_t = \frac{6 \times 10^7}{100} = 6 \times 10^5 \frac{\text{ft-lb}}{\text{rad}} = 3 \frac{\text{ft-lb}}{\text{arc-sec}}$$

and torquer saturation is reached at 0.067 arc second.

For

$$K_t = \frac{0.2}{20} \frac{\text{ft-lb}}{\text{v}} = 0.01 \frac{\text{ft-lb}}{\text{v}}$$

$$K_s K_a = \frac{3}{0.01} = 300 \frac{v}{\text{arc-sec}} = 6 \times 10^7 \frac{v}{\text{rad}}$$

and the required wheel inertia considering a maximum speed of 1000 $\frac{\text{rad}}{\text{sec}}$ is

$$I_w = \frac{20}{1000} = 0.02 \text{ ft-lb/sec}$$

These parameters yield an order of magnitude greater momentum storage capability with a wheel that has approximately the same inertia as the OAO fine wheel, but a motor stall torque 20 times greater.

Inertia wheels are used to stabilize OAO in its fine pointing mode (0.1 arc-sec), and have been demonstrated in space as controllers for several orbiting vehicles. Nimbus inertia wheel controllers have a life in space in excess of one year.

A summary of characteristics for the pitch and yaw axes is as follows:

Open Loop Attitude Control Gain	Approximately	12,000 sec^{-1}
Weight (2 Axes)		40 lb
Power Required (2 Axes)		20 watts average 120 watts peak

The momentum capacity for third axis control should be a minimum of 3 ft-lb/sec at reset. The gain required to limit standoff error to 3 arc-sec is

$$K_s K_a K_t \tau_m = \frac{13000 \text{ sec } 2.36 \times 10^{-4}}{3 \text{ arc-sec}/2 \times 10^5} \text{ ft-lb} = 2 \times 10^5 \frac{\text{ft-lb/sec}}{\text{rad}}$$

and the minimum open loop gain is

$$\frac{K_s K_a K_t \tau_m}{I_v} = \frac{2 \times 10^5}{5 \times 10^3} = 40 \text{ sec}^{-1}$$

Providing a stall torque of 0.1 ft-lb for acquisition of the reference

$$\tau_m = \frac{H_{max}}{T_{stall}} = \frac{4}{0.1} = 40 \text{ sec}$$

Standard compensation techniques will ensure stable control. A summary of parameters for third axis control is as follows:

Controller Open Loop Gain	4000 sec^{-1}
Weight (1 Axis)	8 lb
Power Required (1 Axis)	10 watts average 36 watts peak

C.5.4 FLUID FLYWHEEL SYSTEM

Figure C-6 shows a signal flow graph of a linearized single-axis fluid flywheel control loop.

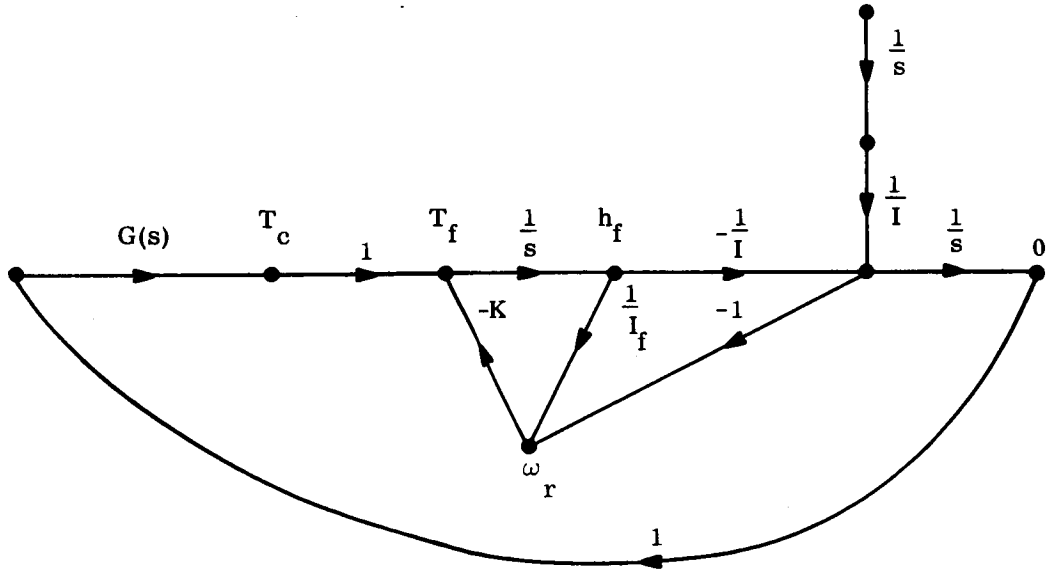

Figure C-6. Single-Axis Fluid Flywheel Control Loop

The open-loop transfer function from the control torque signal to the angular position output is

$$\frac{O}{T_c}\left(\begin{matrix}\text{open}\\ \text{loop}\end{matrix}\right) = \frac{-I_f}{K\,(I + I_f)\left(1 + \frac{I_f\, I\, S}{K\,(I + I_f)}\right) S} \approx -\frac{1}{I\,(1 + S)\,S}$$

since the inertia of the vehicle is much greater than the inertia of the fluid in the flywheel ($I >> I_f$) and a time constant $\frac{I_f}{K}$ of one second is typical.

The short time constant of a fluid flywheel makes it very attractive for applications where rapid momentum exchanges (fast manuevers) are required. However, the mechanism responsible for the short time constant, namely, the large energy loss due to fluid friction, drains excessive power while the fluid is storing angular momentum as is required for precision pointing. In addition, the large open loop gain necessary for precision pointing would require cascaded compensation networks (or a rate gyro that cleanly senses very small rates) to lower the bandwidth of the control loop to where it would be compatible with the constraints dictated by the sampled data sensor signal processing.

Because the fluid flywheel did not readily fit the control actuator requirements of this particular mission, it was dropped from further consideration.

C.5.5 MASS EXPULSION SUBSYSTEM

A mass expulsion subsystem provides an efficient source of control torque for (1) removal of spacecraft separation rates after launch, (2) rapid acquisition of, and (3) control to the prescribed interplanetary attitude reference, and (4) for performance of commanded turns for midcourse corrections and Earth acquisition.

Mass expulsion is also the prime means of transferring absorbed momentum to the external environment during accomplishment of the mission objective, which dictates precise pointing of the spacecraft to Earth for laser communication from Mars orbit. When used in

conjunction with any momentum storage device for this purpose, the momentum storage device can be sized for (1) acquisition of the fine pointing mode, (2) slewing during station switching, and (3) to absorb the cyclic torque disturbance impulse. The combination, as implemented, will minimize the controller subsystem weight.

For the assumed 1975 to 1980 time period, mass expulsion is also a control torque candidate for fine pointing when one considers new concepts in very low level thrusters and adaptive control logic techniques.

From the above discussion it is evident that for any spacecraft torquing subsystem a multi-level mass expulsion system will be required. The high level system for (1) acquisition of the attitude reference after launch during the interplanetary trajectory and (2) acquisition of the Earth reference is state of the art, and as such they are assumed to be present on the spacecraft and will not be discussed further.

Fine pointing using only mass expulsion torquing will be presented here, followed by a discussion of mass expulsion for reset in conjunction with previously mentioned alternate fine pointing control concepts using momentum storage devices. The minimum thruster size to maintain the required fine pointing is given by the relation

$$F = \frac{I_v \omega_v}{r_v t_i N}$$

where $I_v = 5000$ ft-lb/sec^2, the vehicle moment of inertia

$r_v = 10$ ft, the thruster moment arm

$t_i = 0.01$ sec, the thruster pulse time

$N = 50$ the number of thruster pulses derived from the adaptive control scheme to maintain pointing accuracy

$\omega_v = 1.37 \times 10^{-7}$ rad/sec $= 0.0274 \frac{\text{arc-sec}}{\text{sec}}$ the vehicle rate induced by 2.34×10^{-4} ft-lb disturbance torque, T_D, acting from the maximum -0.03 arc-sec error until the thruster is turned on by +0.01 arc-sec error detected by the fine error sensor

$$F = \frac{5000 \times 1.37 \times 10^{-7}}{10 \times 10^{-2} \times 50} = 1.37 \times 10^{-4} \text{ lb thrust}$$

The total thrust of a two thruster couple

$$2F = 2.74 \times 10^{-4}$$

Thrusters smaller than this will allow the spacecraft to go out of pointing tolerance. Larger thrusters can be used at the expense of higher gas consumption. The thruster size should be set at $1.37 \times 10^{-4} < F < 10^{-3}$.

Control system performance and required fuel weight are heavily dependent upon the control logic. Torque tolerant adaptive control logic has recently been developed under Air Force Contract AF 33(657)-9180. In this concept, the optimum control criteria to allow for a large parameter variation would make the thrust on time

$$t_{on} = \frac{1.51 I_v \theta}{F r_v T_d}$$

where I_v, F, and r_v are as before

T_d = time in deadband

θ = the angular deadband measured from null

This computation can be easily mechanized by a series of straight-line approximations as illustrated in Figure C-7. The computed control impulse will equal the straight-line approximation shown dotted in the plot. The straight-line approximations are made by a relatively simple digital system whose block diagram is shown in Figure C-8.

As the vehicle enters the deadband, a nine-stage binary counter is started at the higher of the low frequency clock rates (F_1). Counting continues at this rate until the vehicle leaves

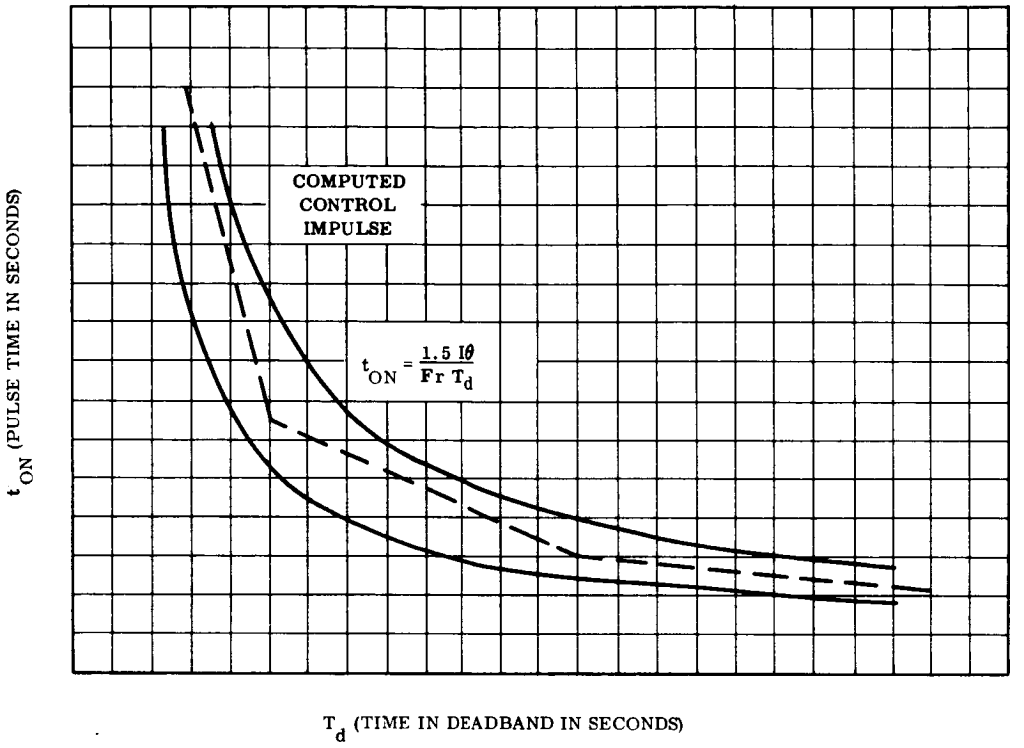

Figure C-7. Time-in-Deadband Control Logic Straight-Line Measurement

the deadband. As the vehicle leaves the deadband, a corrective pulse is initiated at the high frequency (F_f). The ON time of this pulse will depend upon the count remaining in the binary counter. If the deadband time is long (low vehicle energy) the control pulse is short because the remaining count is small. A short deadband time (high vehicle energy) computes a long control pulse because the count remaining is large.

When the deadband time, T_d, is greater than the intersection of the first two straight lines, the lowest frequency oscillator F_2 is switched on. This will compute a pulse time (t_{on}) which lies along the second straight line. Each additional straight line will require an additional oscillator which is relatively simple, requiring only one counter and a total number of oscillators equal to one more than the number of straight lines used in the approximation.

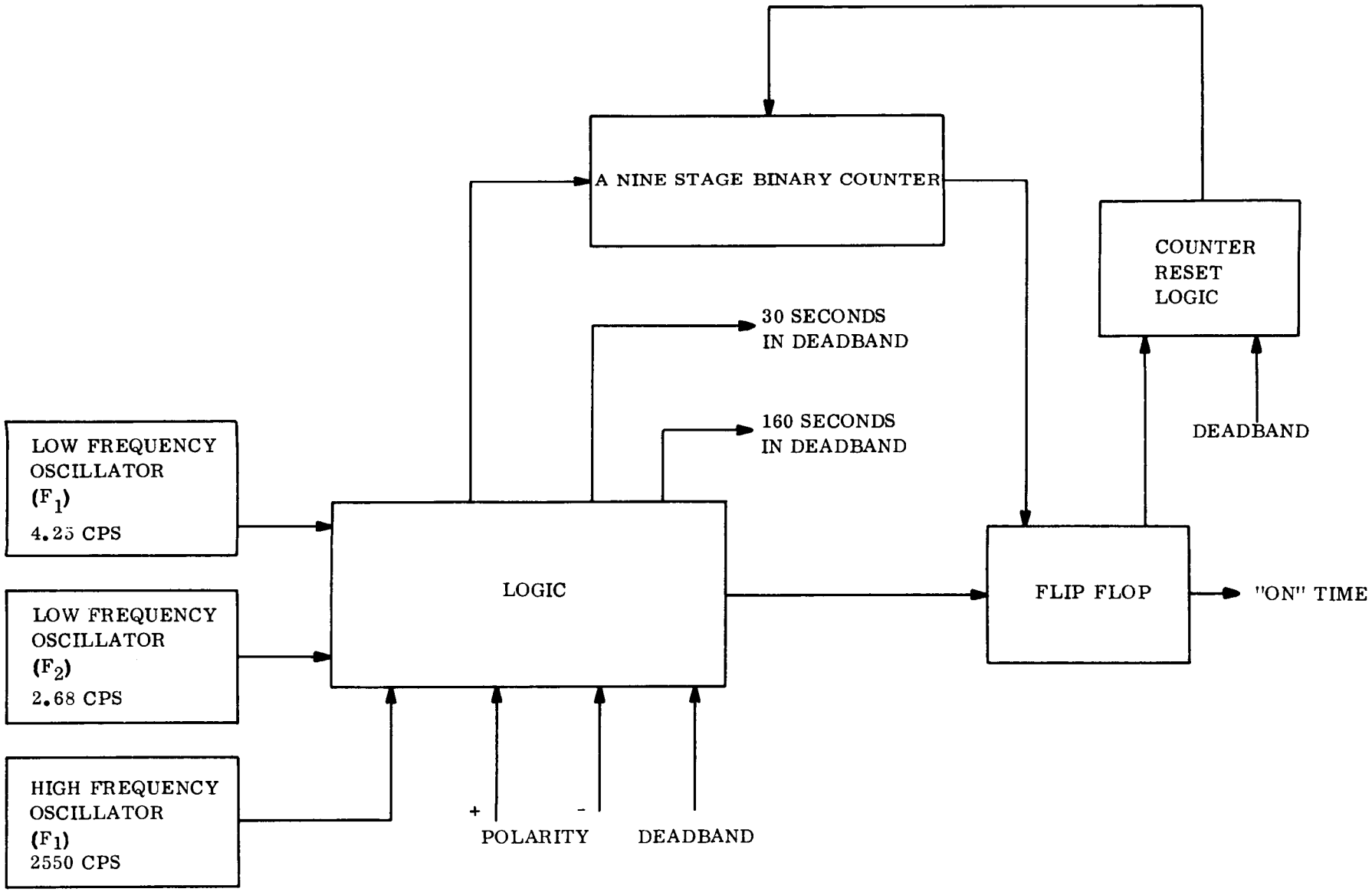

Figure C-8. Block Diagram of the ON-Time Computation as a Function of Vehicle in Deadband

The general equations are:

$$F_f t_{on} = k - F_1 T_d \qquad T_d < A$$

$$F_f t_{on} = k - k_1 (F_1 - F_2) - F_2 T_d \qquad A < T_d < B$$

$$F_f t_{on} = k - k_1 (F_1 - F_2) - k_2 (F_2 - F_3) - F_3 T_d \qquad B < T_d < C$$

The minimum computed pulse t_{on} will be determined by the electrical and mechanical limitations of the solenoid valve and the thruster design.

The previous discussion has been confined to the undisturbed limit cycle. The external torques acting upon the vehicle will consist of steady-state, cyclic, impulse and any combination of the three. The period of the cyclic torques will, in general, be equal to the orbit period so that for most limit cycle frequencies these torques appear as slowly varying and may be considered as constant during several limit cycles. The impulse torques such as those imparted by meteorite impact are random in nature and have widely varying energy levels. The lower energy levels can be handled by conventional control logic techniques while the high levels will require a reacquisition of the vehicle through the more conventional means (lead network, rate gyro, etc.). Fortunately, the probability of a high energy impulse is quite low. Therefore, the reacquisition periods which require relatively large fuel expenditures will be infrequent.

The presence of a disturbing torque is indicated by determining the polarity of the vehicle as it leaves its position deadband. If the signs alternate, the disturbing torques have had minor effects upon the control. If the signs are the same, a significant bias torque exists. Referring again to Figure C-2 the minimum pulse is first limited to its value at A. Three vehicle crossings are sampled as to sign when the vehicle leaves its deadband. If these signs alternate the minimum pulse is reduced to B; if the signs are the same, the minimum pulse is held at A. This process is continued until the smallest impulse is obtained for the particular disturbing torque condition. If the disturbing torque is zero, a minimum impulse is achieved.

System weight for two axis operation including propellant is approximately 100 pounds for hot gas systems. It is doubtful that this type propellant could be used because of fouling of optical surfaces in the spacecraft. Cold gas systems would be almost twice the weight. The average power required for control logic network values and associated electronics is about 10 watts.

A summary of parameters of the mass expulsion subsystem for relatively fine pointing is as follows:

Thruster Size Needed	1.4×10^{-4} to 10^{-3} lb
Subsystem Weight	100 to 200 lb
Average Power	10 watts

The capability of mass expulsion actuators as vehicle control torquers for fine pointing in the range of 0.01 arc-second has not been simulated or demonstrated analytically. The low performance rating in this torquer tradeoff study is based on the doubtful performance to the tolerances required in the fine pointing mode.

Torquing subsystems employing momentum storage devices require a means of "reset" or "unloading" as they approach their storage capacity. Mass expulsion is an accepted method. The thrusting must be sized to accomplish reset without introducing a transient that would result in an out of tolerance pointing error. A value of unloading torque a factor of twenty less than the control torque of the momentum storage device is a reasonable value, based upon past experience and the simulation of the control actuators chosen. Considering a thruster couple, the thrust should be about

$$F = \frac{T_{m/20}}{r_r \times 2} = \frac{0.2/20}{10 \times 2} = 0.0005 \text{ lb}$$

A continuous torque of 0.01 ft-lb from thruster couples of this size would completely unload the maximum disturbance torque impulse in about 160 seconds. (The amount of momentum unloaded is a function of the characteristics of the disturbance torque profile; and typically, less than the full stored momentum is removed at one firing.)

The system weight to accomplish unloading is dependent upon the orbital cumulative disturbance torque impulse.

The total momentum transfer per orbit is

$$H_o \int^{T_o} T_d \, dt$$

Assuming that the gravity gradient torque is at least in part cyclic and the solar pressure torque is always of one polarity, the torque impulse for six months per axis is estimated to be:

$$\begin{aligned} H &= (T_s + 0.4\, T_{gg\ max})\, T_d \\ &= (0.16 \times 10^{-4} + 0.4 \times 2.2 \times 10^{-4})\, 15.7 \times 10^{6} \\ &= 1640 \text{ ft-lb sec per axis} \end{aligned}$$

To counter this a total of

$$I_{mp} = \frac{1640}{10} \text{ ft-lb sec} = 164 \text{ lb-sec per axis}$$

is required (assuming a lever arm of 10 feet). Considering the use of cold gas, because of the continuous use of optics throughout the mission, a specific impulse of 60 seconds (lb-sec/lb of gas) is assumed to compute gas weight.

$$W_g = \frac{I_{mp}}{I_{sp}} = \frac{164}{60} = 2.73 \text{ lb per axis}$$

Twice this value is assumed to provide gas for acquisition and a margin of safety. Allowing for one stuck valve type failure per axis, the gas lost and the gas consumed in correcting the resulting disturbance must be added. To still have enough gas to complete the mission, we must now triple the weight. The required gas weight per axis for the six-month Mars orbiting mission is estimated to be 16 pounds per axis or a total of about 50 pounds for all

three axes. Considering weight of tankage, valves, regulators, piping, etc., the weight of the pneumatic system including gas is about 80 pounds. An estimated additional 20 percent in weight is required for the interplanetary trip making a total pneumatic subsystem weight of 96 pounds for a torquing subsystem design utilizing momentum storage devices.

C.5.6 RELIABILITY

At this stage, an actual reliability prediction complete with probabilities of success in a six-month mission would be pure guess work. Too many factors such as individual hardware components for each system are undefined and developments in the next 15 years may increase (or decrease) reliability to unexpected levels. With this in mind, this section will attempt to compare the reliability of each system relative to one another, based on current levels and expected areas of improvement. In this comparison, the fluid flywheel is neglected, because this actuator has been previously shown to be unsuitable for this mission. The current reliability is estimated to be as follows:

	Reliability Prediction (6 Months)*
Inertia Wheel	0.99
4 Gyros (GLOPAC)	0.98 (estimated)
6 Gyros (3 Axis Twin 1 DOF CMG)	0.98
Twin 2 DOF CMG - 1 DOF CMG 3 Axis Control	0.97
Mass Expulsion	0.94

The mass expulsion rating will probably drop drastically because we are using much smaller thruster sizes, and these smaller sizes are much more susceptible to clogging. The four gyro system (GLOPAC) will probably improve to an even higher rating than the 1 CMG system, since fewer gyros are used (4 versus 6) and corresponding less bearings and torques are involved.

*Based on probability of equipment lasting. Degradation of system is not included. A system such as GLOPAC would suffer the least degradation if one gyro failed.

The 2 DOF CMG - 1 DOF CMG three axis system should improve as development work in 2 DOF CMG's progresses. This is a relatively new area, and improvement can be expected.

An expected comparison of reliability without reliability figures is given below. The rating is just to give a rough comparison of expected levels.

System	Expected Rating
4 Gyro (GLOPAC) or Inertia Wheel	10
Twin 2 DOF CMG or 1 DOF CMG (3 Axis Control)	9
6 Gyro (3 Axis 1 DOF CMG)	8
Mass Expulsion	4

C.5.7 DEVELOPMENT AREAS

In the area of control moment gyros, work in improving spin bearing reliability is needed. Work in the area of hydrodynamic bearings may solve this problem, but a way must be found for them to survive launch and start-up.

In conventional bearings, the launch period may be survived by using a heated element to preload the bearings. This may be a plate that presses against the bearing when hot and clears when cool.

The brushless DC spin and torque motors hold great promise in providing efficient spin motor and gimbal torquing devices. Both of these devices are currently under development at General Electric. If the current rate of development is continued, flight-proven versions should be available within the next five years.

Torquer losses due to hysteresis and stiction could be eliminated by the use of "pulse stretching" circuits. These circuits add a small current to the normal current, so that current output is similar to the illustration in Figure C-9.

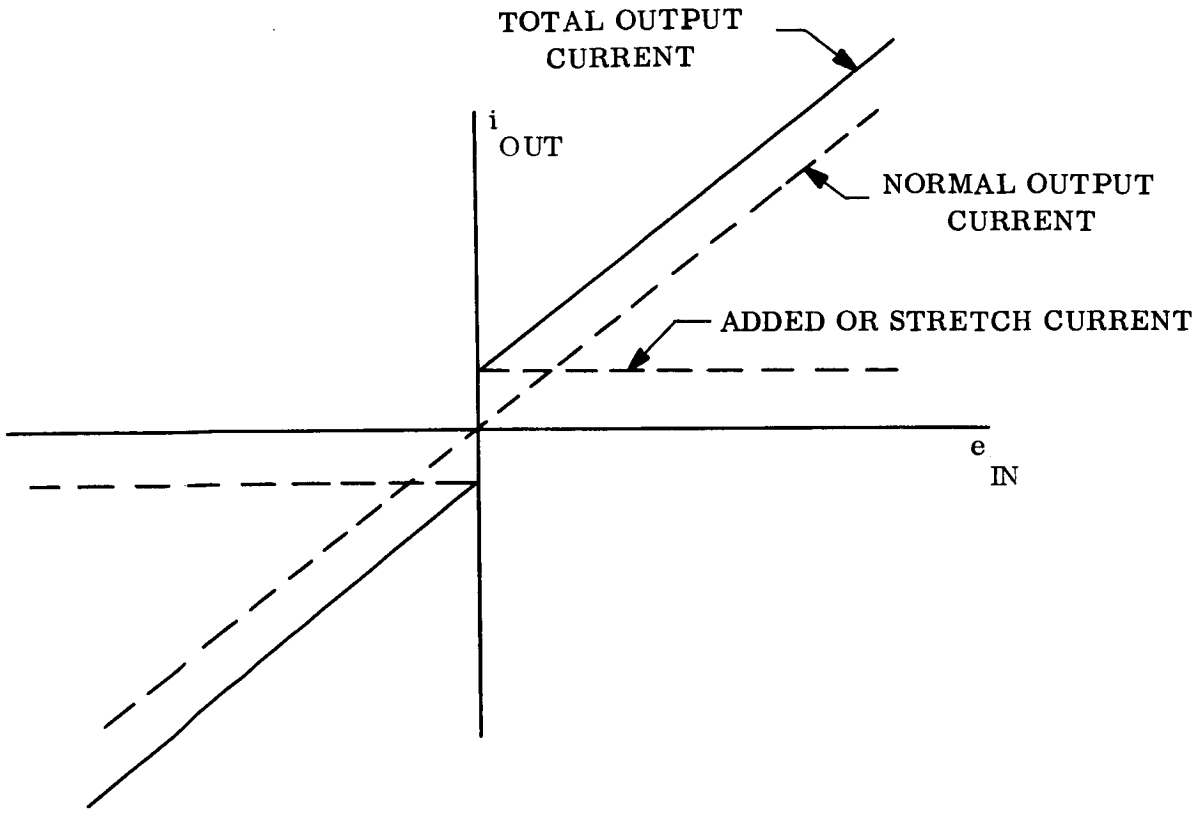

Figure C-9. "Pulse Stretching" Circuit Current Output

This type of power circuit is also in an advanced stage of development at General Electric.

In the area of mass expulsion, the main need is low level thrusters (10^{-4} - 10^{-3} lb) with high reliability over long periods. General Electric has evolved SPET (Solid Propellant Electrical Thruster) which is a promising microthruster, and perhaps this could be developed for larger thrust levels.

The fluid flywheel's main need is more efficient power conversion equipment and higher magnetic fluxes in EM motors. This system is very promising and potentially one of the most reliable we have, but the gains required are very excessive.

APPENDIX D

DEVELOPMENT OF THE CONTROL MOMENT GYRO MATHEMATICAL MODELS

APPENDIX D

DEVELOPMENT OF THE CONTROL MOMENT GYRO MATHEMATICAL MODELS

D.1 INTRODUCTION

The tradeoff analysis documented in Appendix C indicates that the control actuators that best fit the requirements of the selected mission are a combination of twin control moment gyros. One axis is controlled using twin single degree-of-freedom gyros and the other two axes are controlled using twin double degree-of-freedom gyros. This appendix derives the mathematical models for these control actuators.

D.2 THE EQUATIONS OF THE VEHICLE DYNAMICS

There is only one basic physical law that is used in this appendix and all that follows from it is just algebraic manipulation. The law is that, referred to an inertial space, torque is the time rate of change of angular momentum.

$$\overline{T}_I = \dot{\overline{H}}_I \qquad \text{(D-1)}$$

The above equation, with the subscript indicating that the vectors are referenced to an inertial frame, is the simplest algebraic statement of the dynamics law.

Sometimes it is convenient to use other reference systems because parameters of interest may then appear in a simpler form. In this appendix the various reference bases will be identified by a trio of mutually orthogonal unit vectors. The transformations between bases are then unitary which means that the inverses of the matrixes representing the transformations are just their transposes (for a real vector space). Transformations are necessary to bring vector quantities that are to be combined into a common frame of reference.

When analyzing a rotating rigid spacecraft, the use of a vehicle fixed reference frame has certain advantages. First, the inertias of the vehicle are time-invariant since the mass of the spacecraft has a constant distribution with respect to the vehicle fixed reference

frame. Second, since sensors are fixed to the spacecraft, their outputs are also most simply described in a vehicle frame. The dynamics equation (D-1) is transformed from the inertial to a vehicle fixed frame as follows:

$$\bar{T}_V = A_{VI}\,\bar{T}_I = A_{VI}\,\dot{\bar{H}}_I = A_{VI}\left[A_{IV}\,\dot{\bar{H}}_V + \dot{A}_{IV}\,\bar{H}_V\right]$$

$$= \dot{\bar{H}}_V + A_{VI}\,\dot{A}_{VI}\,\bar{H}_V \qquad \text{(D-2)}$$

The notation used here is that the matrix A_{ij} represents the transformation of vector quantities from the j frame into the i frame. From the earlier discussion it is noted that the inverse transformation is simply the transpose of the matrix. It is well known that the time derivative of the direction cosine matrix A_{VI} is

$$\dot{A}_{VI} = \begin{bmatrix} 0 & w_z & -w_y \\ -w_z & 0 & w_x \\ w_y & -w_x & 0 \end{bmatrix} A_{VI} \qquad \text{(D-3)}$$

Taking the transpose of (D-3) and substituting back into (D-2) yields the dynamics equation referred to a vehicle fixed frame.

$$\bar{T}_V = \dot{\bar{H}}_V + \begin{bmatrix} 0 & -w_z & w_y \\ w_z & 0 & -w_x \\ -w_y & w_x & 0 \end{bmatrix} \bar{H}_v \qquad \text{(D-4)}$$

In Equation D-4, the three terms necessary to specify the skew-symmetric matrix are the components of the relative velocity vector between the vehicle-fixed and inertially fixed frame .

$$\begin{bmatrix} w_x \\ w_y \\ w_z \end{bmatrix} = w_v \qquad \text{(D-5)}$$

The skew-symmetric matrix is often denoted by the shorthand notation

$$\begin{bmatrix} 0 & -w_z & w_y \\ w_z & 0 & -w_x \\ w_y & w_x & 0 \end{bmatrix} = \bar{w}_v \times \qquad \text{(D-6)}$$

The strictly mechanical connotation is valid only in three-space, and it is felt that the matrix representation follows naturally from the derivation. Although sensor outputs and inertia values may take on a simpler form in the vehicle fixed frame, Equation D-4, is algebraically more complex than Equation D-1. The form of computation (analog or digital computer) called upon to solve the equations (considering the submodels that support the dynamics law) should indicate which approach is superior. Note that there is nothing mysterious about the last group of terms in Equation D-4 which naturally result from viewing the dynamics law from a noninertial basis.

Assuming that the vehicle fixed form of the dynamics law has been chosen, it is apparent that two vectors must be known before the dynamics law can be integrated. These are the system momentum vector $\bar{H}_V$ and the relative velocity $\bar{w}_v$. The total system angular momentum consists of the part $I\bar{w}_v$ which is associated with the rotating spacecraft and and the rest ($\bar{h}_v$) which is stored on the moving control parts.

$$\bar{H}_V = I\bar{w}_v + \bar{h}_v \qquad \text{(D-7)}$$

The inertia matrix (I) describes the integrated mass distribution of the spacecraft with respect to the chosen vehicle fixed basis. Many analysts at this point substitute

Equation D-7 back into Equation D-4, perform the indicated time differentiation, and eventually solve the resulting system of equations for the angular acceleration vector ($\dot{\bar{W}}_v$). This is actually a formal change of state variable from the angular momentum indicated by the natural physical law into angular velocity. This change of state variable results in a considerably more complicated statement of the dynamics law, particularly when the chosen vehicle basis results in products of inertia being present and when such practical engineering considerations as misalignment of the mass expulsion thrusters and momentum storage devices are included. This problem reformulation also gives rise to the concept of "internal" system torques such as reaction torques from changing the state of the momentum storage devices, numerous inertia and so called gyroscopic crosscoupling torques which derive their origin from the final group of terms in Equation D-4, where Equations D-1 and D-4 only concern themselves with "external" system torques such as environmental disturbances and those from mass expulsion control actuators. Finally, the change of state variables is not necessary to determine the angular velocity vector ($\bar{w}_v$). By monitoring the angular momentum stored by the control parts, the angular velocity vector can be computed by rewriting Equation D-7 in the following form:

$$w_v = I^{-1} (\bar{H}_V - \bar{h}_v) \qquad \text{(D-8)}$$

D.3 THE EQUATIONS FOR THE SINGLE DEGREE-OF-FREEDOM TWIN GYROS

Reaction wheels, control moment gyros, fluid flywheels, etc., are nothing more than angular momentum storage devices. A fluid flywheel or a reaction wheel stores angular momentum by dictating the angular velocity of the controlled mass; i.e., the liquid metal in the fluid flywheel or the speed of the motor rotor. Control moment gyros store momentum by changing the "direction" of the constant speed rotors.

Figure D-1 illustrates the operation of the twin single degree-of-freedom gyros. The vehicle fixed reference basis is defined in D-1a. The nominal zero position for the twin gyros is shown in D-1b where the spin vectors are opposed resulting in no momentum storage. After the gyros have been torqued through equal and opposite angles, the addition of the spin vectors results in a net momentum storage along the vehicle x-axis (D-1c). Neglecting misalignment, the momentum cannot be stored along the y-axis and as long as

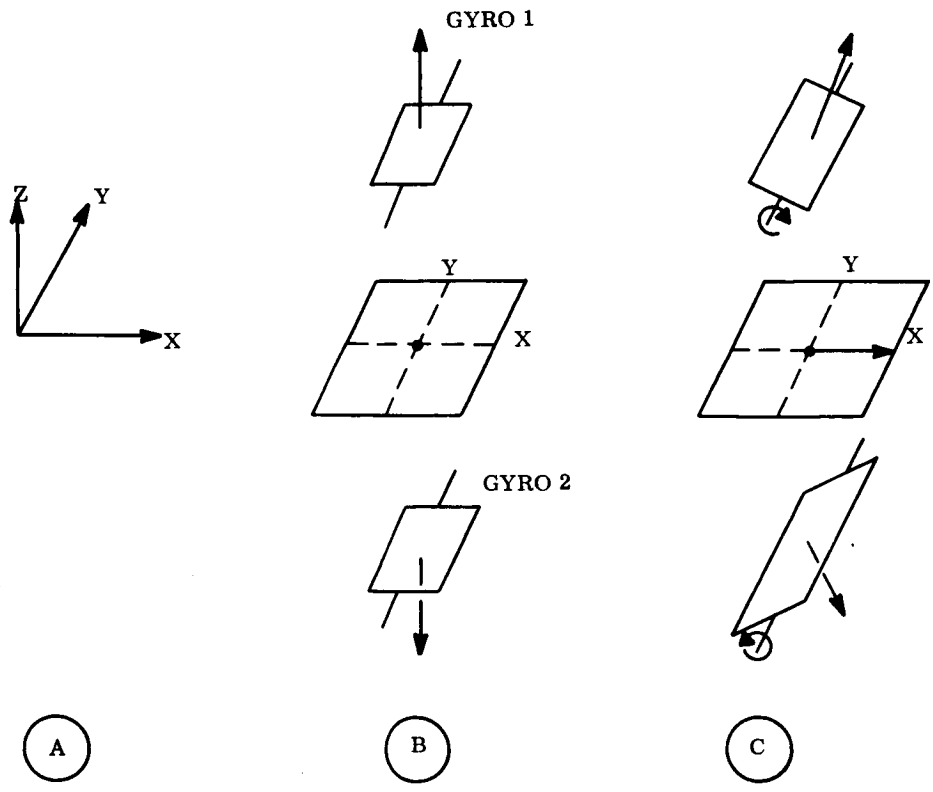

Figure D-1. Single Degree-of-Freedom Twin Gyro Operation

the spin momentums have the same magnitude and are torqued through equal and opposite angles, the z-axis components also cancel. This explains why the gyros are used in pairs.

Each individual gyro may be analyzed as a separate subsystem. Gyro 1 will be denoted as the single degree-of-freedom gyro indicated in Figure D-1 as having its gimbal axis always aligned to the vehicle y-axis and having its rotor spin momentum aligned with the positive vehicle z-axis when the gimbal angle is zero. A positive rotation of the gimbal through an angle of 90 degrees would align the spin axis momentum with the vehicle positive x-axis. A rotating basis that coincides with the vehicle fixed frame is useful here since the external torque seen by the gimbal of the first gyro always appears along the y-axis. This would also be true of a basis fixed in the gimbal which in addition expresses the spin momentum in a constant form. However, since the momentum of the moving control parts will eventually be resolved along the vehicle axes, the former choice appears preferable. Therefore the dynamics equation for the first gyro (indicated by the superscript) is:

$$\begin{bmatrix} \dot{H}_x^{(1)} \\ \dot{H}_y^{(1)} \\ \dot{H}_z^{(1)} \end{bmatrix} = \begin{bmatrix} T_x^{(1)} \\ T_y^{(1)} \\ T_z^{(1)} \end{bmatrix} + \begin{bmatrix} 0 & w_z & -w_y \\ -w_z & 0 & w_x \\ w_y & -w_x & 0 \end{bmatrix} \begin{bmatrix} H_x^{(1)} \\ H_y^{(1)} \\ H_z^{(1)} \end{bmatrix} \qquad \text{(D-9)}$$

As previously discussed, the elements of the skew-symmetric matrix are the components of the vehicle angular velocity vector.

The total angular momentum of the first gyro system is the superposition of moments associated with rotation of the gyro package, the relative motion of the gimbal, and the amount stored by the spin vector.

$$\begin{bmatrix} H_x^{(1)} \\ H_y^{(1)} \\ H_z^{(1)} \end{bmatrix} = \begin{bmatrix} I_1 & 0 & 0 & w_x \\ 0 & I_a & 0 & w_y \\ 0 & 0 & I_1 & w_z \end{bmatrix} + \begin{bmatrix} 0 \\ I_a \dot{a}_1 \\ 0 \end{bmatrix} + \begin{bmatrix} h_s \sin a_1 \\ 0 \\ h_s \cos a_1 \end{bmatrix} \qquad \text{(D-10)}$$

Here $\dot{a}_1$ indicates the time rate of change of the gimbal angle a_1 and h_s is the spin momentum. It is assumed that the gyro is designed to be inertially cylindrical so that the inertias referred to the vehicle fixed basis are independent of the gimbal angle. From Equation D-10 it is observed that the portion of momentum stored by the first gyro that is already included on the momentum of the spacecraft (whose inertias include those of the gyro at rest) is:

$$\bar{h}_v^{(1)} = \begin{bmatrix} h_s \sin a_1 \\ I_a \dot{a}_1 \\ h_s \cos a_1 \end{bmatrix} \qquad \text{(D-11)}$$

This means that the only variables needed to identify $\bar{h}_v^{(1)}$ are $\dot{a}_1$, and a_1. The second component of Equation D-10 may be solved for $\dot{a}_1$.

$$\dot{a}_1 = \frac{H_y^{(1)}}{I_a} - w_y \tag{D-12}$$

The gimbal angle a_1 may be obtained by integrating Equation D-12 and $H_y^{(1)}$ from integrating the second component of Equation D-9.

$$\begin{aligned} \dot{H}_y^{(1)} &= T_y^{(1)} + w_x H_z^{(1)} - w_x H_x^{(1)} \\ &= T_{a_1} - D_a \dot{a}_1 + h_s (w_x \cos a_1 - w_z \sin a_1) \end{aligned} \tag{D-13}$$

In Equation D-13, T_{a1} is the torque from the torque motor and $D_a \dot{a}_1$ is the damping torque resisting the relative motion between the spacecraft and the gimbal and D_a is the damping coefficient.

The equations for the second gyro may be obtained by changing the superscript from one to two (a_1 to a_2), and by replacing h_s by minus h_s.

$$\bar{h}_v^{(2)} = \begin{bmatrix} -h_s \sin a_2 \\ Ia\, \dot{a}_2 \\ -h_s \cos a_2 \end{bmatrix} \tag{D-14}$$

$$\dot{a}_2 = \frac{H_y^{2}}{I_a} - w_y \tag{D-15}$$

$$\dot{H}_y^{(2)} = T_{a_2} - D_a \dot{a}_2 - h_s (w_x \cos a_2 - w_z \sin a_2) \tag{D-16}$$

Equations D-11 through D-16 completely define the twin single degree-of-freedom gyros. A few points are worth noting before proceeding to the twin double degree-of-freedom gyros which are algebraically more complex although their physical operation is similar. First, if $a_1 = -a_2 = a$, the stored momentum from the twin package is:

$$\bar{h}_v^{(1)} + \bar{h}_v^{(2)} = \begin{bmatrix} 2\, h_s \sin a \\ 0 \\ 0 \end{bmatrix} \qquad \text{(D-17)}$$

which is the desired result indicated in Figure D-1c. Thus, the signals to the torque motors from the control law should be equal in magnitude and opposite in sign. Note also from Equations D-13 and D-16 that (with $|a| < 90^o$) a rate about the vehicle x-axis will cause both gyros to turn their spin momenta in opposite directions towards the vehicle rate vector and thus absorb it when no signal is sent to the torque motors. Thus, the gyros act not only as actuators but also as rate sensors. Note also that, if there is a rate about the vehicle z-axis (with $0 < |a| < 90^o$), the gyros tend to turn their spin momenta in the same direction towards the vehicle rate vector to absorb it. This is undesirable since the function of this set of gyros is to control x-axis vehicle motion. For this reason, along with the fact that the torque motors and gyros are not exactly identical, a constraint loop is employed that compares a_1 and $-a_2$ (or $\sin a_1$ and $-\sin a_2$) and corrects any difference through the torque motors.

D.4 THE EQUATIONS FOR THE DOUBLE DEGREE-OF-FREEDOM TWIN GYROS

The nominal zero position of the double degree-of-freedom twin gyros with respect to the spacecraft is shown in Figure D-2. By turning the outer gimbal angles in equal amounts and in opposite directions ($c_3 = -c_4 = c$), momentum may be stored along the vehicle z-axis while turning the inner gimbals in a similar manner ($b_3 = -b_4 = b$) allows momentum to be stored along the vehicle y-axis. Combining these two options enables momentum to be stored anywhere in the y-z vehicle plane.

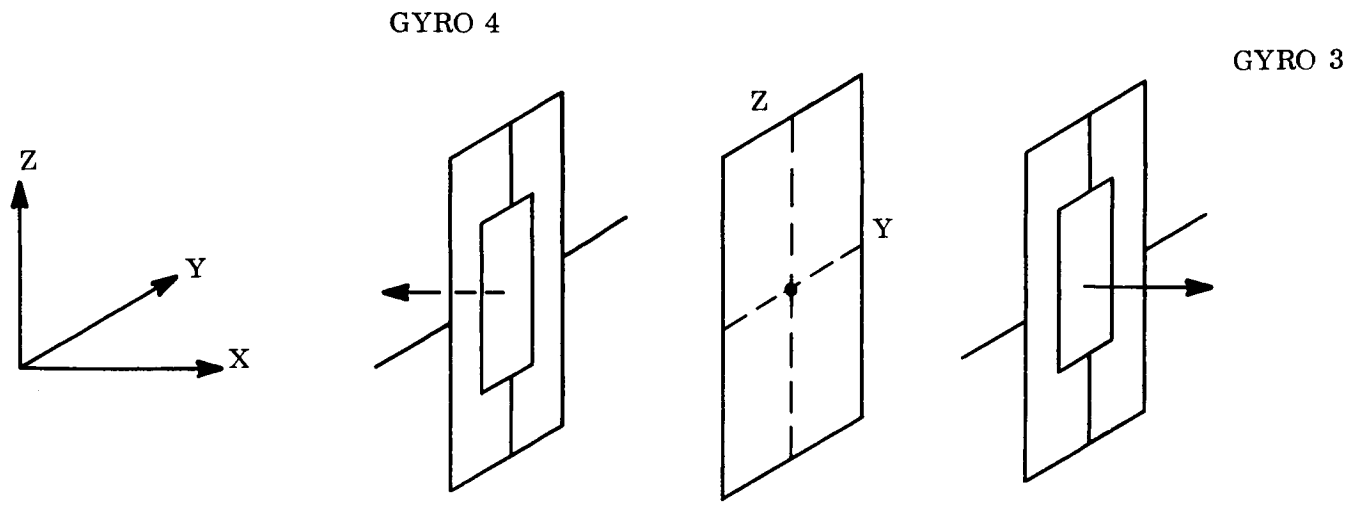

Figure D-2. Double Degree-of-Freedom Twin Gyro Operation

Each gyro may again be analyzed as a separate subsystem. Gyro 3 will be denoted as the double degree-of-freedom gyro indicated in Figure D-2. Its outer gimbal axis is always aligned to the vehicle y-axis. When its gimbal angles are zero, the inner gimbal axis is aligned with the vehicle z-axis and its spin vector momentum is aligned to the vehicle x-axis. A positive 90-degree rotation of the outer gimbal ($c_3 = 90^o$, $b_3 = 0$) would align the spin vector with the vehicle negative z-axis while a positive 90-degree rotation of the inner gimbal ($c_3 = 0$, $b_3 = 90^o$) would align the spin vector with the vehicle positive y-axis.

A rotating basis that is fixed to the outer gimbal and coincident to the vehicle basis when the gimbal angles are zero is a convenient choice since the torque motors will always act along two of the basis vectors. The relative angular velocity of this basis with respect to an inertial frame is the superposition of the vehicle angular velocity and the angular velocity of the outer gimbal expressed in the gimbal fixed basis.

$$\begin{bmatrix} W_x \\ W_y \\ W_z \end{bmatrix}_G = \begin{bmatrix} \cos c_3 & 0 & -\sin c_3 \\ 0 & 1 & 0 \\ \sin c_3 & 0 & \cos c_3 \end{bmatrix} \begin{bmatrix} w_x \\ w_y \\ w_z \end{bmatrix}_V + \begin{bmatrix} 0 \\ \dot{c}_3 \\ 0 \end{bmatrix}$$

$$= \begin{bmatrix} w_x \cos c_3 - w_z \sin c_3 \\ w_y + \dot{c}_3 \\ w_x \sin c_3 + w_z \cos c_3 \end{bmatrix} \qquad \text{(D-18)}$$

Here again, the total angular momentum of the third gyro system is the superposition of momenta associated with the rotation of the gyro package, the relative motion of the gimbals, and the amount stored by the spin vector.

$$\begin{bmatrix} H_x^{(3)} \\ H_c^{(3)} \\ H_b^{(3)} \end{bmatrix} = \begin{bmatrix} I_c & 0 & 0 \\ 0 & I_c & 0 \\ 0 & 0 & I_c \end{bmatrix} \begin{bmatrix} w_x \cos c_3 - w_z \sin c_3 \\ w_y \\ w_x \sin c_3 + w_z \cos c_3 \end{bmatrix} + \begin{bmatrix} 0 \\ I_c \dot{c}_3 \\ I_b \dot{b}_3 \end{bmatrix}$$

$$+ \begin{bmatrix} h \cos b_3 \\ h \sin b_3 \\ 0 \end{bmatrix} \qquad \text{(D-19)}$$

The double degree-of-freedom gyro is assumed to be designed so that it is inertially spherical so that the inertias are independent of the gimbal angles. Note, however, that the inner gimbal I_b (inferior to the outer gimbal) has a different inertia (smaller than I_c). The momentum stored by the third gyro not already included in the momentum of the spacecraft is:

$$\bar{h}_G^{(3)} = \begin{bmatrix} h \cos b_3 \\ I_c \dot{c}_3 + h \sin b_3 \\ I_b \dot{b}_3 \end{bmatrix} \tag{D-20}$$

Expressing this stored momentum in components along the vehicle-fixed basis results in

$$\bar{h}_v^{(3)} = \begin{bmatrix} \cos c_3 & 0 & \sin c_3 \\ 0 & 1 & 0 \\ -\sin c_3 & 0 & \cos c_3 \end{bmatrix} \bar{h}_G^{(3)}$$

$$= \begin{bmatrix} h \cos b_3 \cos c_3 + I_b \dot{b}_3 \sin c_3 \\ I_c \dot{c}_3 + h \sin b_3 \\ I_b \dot{b}_3 \cos c_3 - h \cos b_3 \sin c_3 \end{bmatrix} \tag{D-21}$$

Thus, to determine the momentum stored by the double degree-of-freedom gyro the inner and outer gimbal angles and their time derivatives must be determined. The outer and inner gimbal angle time can be obtained from the last two components of Equation D-19.

$$\dot{c}_3 = \frac{H_c^{(3)} - h \sin b_3}{I_c} - w_y \tag{D-22}$$

$$\dot{b}_3 = \frac{H_b^{(3)} - I_c (w_x \sin c_3 + w_z \cos c_3)}{I_b} \tag{D-23}$$

The gimbal angles can be obtained by integrating Equations D-22 and D-23 while integrating the following two equations will yield $H_c^{(3)}$ and $H_b^{(3)}$.

$$\dot{H}_c^{(3)} = T_c^{(3)} + W_x H_b^{(3)} - W_z H_x^{(3)}$$

$$= T_{c_3} - D_c \dot{c}_3 + (w_x \cos c_3 - w_z \sin c_3) I_b \dot{b}_3$$

$$- (w_x \sin c_3 + \cos c_3) h \cos b_3 \qquad \text{(D-24)}$$

$$\dot{H}_b^{(3)} = T_b^{(3)} + W_y H_x^{(3)} - W_x H_c^{(3)}$$

$$= T_{b_3} - D_b \dot{b}_3 + (w_y + \dot{c}_3) h \cos b_3$$

$$- (w_x \cos c_3 - w_z \sin c_3) h \sin b_3 \qquad \text{(D-25)}$$

Again, T_{c_3} and T_{b_3} are the torques from the outer and inner gimbal torque motors and D_c and D_b are the damping coefficients.

The equations for the fourth gyro are obtained by simply changing the appropriate subscripts and superscripts and replacing h by minus h. Then

$$\bar{h}_v^{(4)} = \begin{bmatrix} I_b \dot{b}_4 \sin c_4 - h \cos b_4 \cos c_4 \\ I_c \dot{c}_4 - h \sin b_4 \\ I_b \dot{b}_4 \cos c_4 + h \cos b_4 \sin c_4 \end{bmatrix} \qquad \text{(D-26)}$$

$$\dot{c}_4 = \frac{H_c^{(4)} + h \sin b_4}{I_c} - w_y \qquad \text{(D-27)}$$

$$\dot{b}_4 = \frac{H_b^{(4)} - I_c (w_x \sin c_4 + w_z \cos c_4)}{I_b} \qquad \text{(D-28)}$$

$$\dot{H}_c^{(4)} = T_{c_4} - D_c \dot{c}_4 + (w_x \cos c_4 - w_z \sin c_4) I_b \dot{b}_4 + (w_x \sin c_4 + w_z \cos c_4) h \cos b_4 \quad \text{(D-29)}$$

$$\dot{H}_b^{(4)} = T_{b_4} - D_b \dot{b}_4 - (w_y + \dot{c}_4) h \cos b_4 + (w_x \cos c_4 - w_z \sin c_4) h \sin b_4 \quad \text{(D-30)}$$

Equations D-21 through D-30 define the twin double degree-of-freedom gyros. Note that if the appropriate gimbal angles are equal and opposite ($b_3 = -b_4 = b$, $c_3 = -c_4 = c$) then the momentum stored by this set of gyros is:

$$\bar{h}_v^{(3)} + \bar{h}_v^{(4)} = \begin{bmatrix} 2 I_b \dot{b} \sin c \\ 2 h \sin b \\ -2 h \cos b \sin c \end{bmatrix} \quad \text{(D-31)}$$

Constraint loops are implemented that compare b_3 to minus b_4 and c_3 to minus c_4 (or compares their sines) and corrects any differences through the torque motors. This is done for the same reasons mentioned in the discussion of the single degree-of-freedom gyros. It is even more important with the double degree-of-freedom gyros since the gimbals must be made insensitive not only to certain components of the vehicle angular velocity vector but also to the motion of its own co-gimbal (inner to outer and vice-versa).

D.5 SUMMARY

The appendix has presented a set of mathematical models for single and double degree-of-freedom control moment gyros. The assumptions made are that the gyros are designed so that their inertias are independent of their gimbal orientations, and that the twin gyros are similar. The task of investigating differences in the twins, mass unbalance and other anomalies falls under the heading of an error analysis which was not the purpose of this development.

Equation D-4 describes the dynamics of a rigid spacecraft in terms of the total system angular momentum expressed in a vehicle fixed basis. Equation D-4 is solved (integrated) for the total angular momentum, and Equation D-8 is used to obtain the vehicle angular velocity vector. Equation D-8 requires a knowledge of the portion of the total angular momentum that is stored on the moving control parts. For the control moment gyros described, this is obtained by superimposing the results of Equations D-11, D-14, D-21, and D-26.

$$\overline{\overline{h}}_v = \sum_{i=1} \overline{h}_v^{(i)} = \overline{h}_v^{(1)} + \overline{h}_v^{(2)} + \overline{h}_v^{(3)} + \overline{h}_v^{(4)} \qquad \text{(D-32)}$$

A system synthesis to meet the mission requirements would identify the constant gyro parameters and specify the control laws. The control laws define the functional dependence of the torque motor upon the system state vector.

APPENDIX E

DEVELOPMENT OF CONTROL MOMENT GYRO TRANSFER FUNCTIONS FOR ATTITUDE HOLD

APPENDIX E

DEVELOPMENT OF CONTROL MOMENT GYRO TRANSFER FUNCTIONS FOR ATTITUDE HOLD

E.1 INTRODUCTION

Appendix D developed the complete set of coupled nonlinear differential equations that define the operation of both the single degree of freedom (SDF) and double degree of freedom (DDF) control moment gyros (CMG's). Although these equations, which are summarized in Section E.11, specify the operation of the CMG's and define a baseline for the simulation engineer, they do not clearly indicate guidelines for the control engineer to follow in formulating control laws. This appendix takes the next logical step and develops numerous single axis attitude hold transfer functions which should aid the control engineer in defining attitude hold control laws and in choosing the necessary compensation networks.

E.2 SUMMARY OF RESULTS

CMG's are inherently more complex to analyze than flywheels. The reason for this is the following. The attitude hold mode of spacecraft control is characterized by small attitude errors and low vehicle angular rates. In other words, the vehicle has little response to external disturbance torques because the momentum storage devices respond to absorb the integrated torque history. Flywheels absorb this angular momentum by changing the angular velocity of their controlled mass while CMG's accomplish this by reorienting the direction of their spin vector momentums. Thus, in the case of an inertially pointed spacecraft in the attitude hold mode, the direction of the individual flywheel's momentum vector remains relatively fixed in inertial space; and only the magnitude changes. This means that the single-axis equations for attitude hold become linear and uncoupled (assuming that the hardware components are operating in a linear regime).

In the case of the SDF CMG, control is obtained by rotating the gyro spin vector momentum about a fixed orthogonal to the one being controlled. This results in single-axis attitude hold equations that are still nonlinear. In the case of the DDF CMG, control is realized by rotating the spin vector momentum about an axis which, in general, is neither fixed nor orthogonal to the axis being controlled. Therefore, their single axis attitude hold equations

remain nonlinear and coupled. Thus, in the case of the CMG's used for attitude hold, we must face up to the analytical problems that a flywheel system experiences while tumbling. The CMG system compensates for this additional analytical complexity with extreme flexibility. With appropriate electrical feedback loops, almost any desired characteristics can be obtained, the only real limitation being the ingenuity of the control engineer. Thus, CMG's may very well be the control actuators of the future with the potential of replacing flywheels for all applications.

Gyro parameters, particularly the h/D ratio (spin momentum to viscous damping ratio) play a dominant role in determining the CMG's operation. Using the mounting configuration illustrated in Figure E-1, several possible utilizations are presented. This set should not be construed to be all inclusive, but some reasonable cut-off point had to be chosen. The resulting transfer functions are too numerous to be repeated here, however, the appropriate equations will be identified.

The transfer function from the x-axis attitude hold which is provided by the twin SDF CMG's is identified by Equation E-27. The twin DDF CMG's are used to control the vehicle y and z axes, with the outer gimbal axes always aligned to the vehicle y-axis as is indicated in Figure E-1. Three ways of utilizing the DDF CMG's are considered. They are

a. The lightly damped ($\frac{h}{D}$ large) or "free" gyro mode

b. The heavily damped ($\frac{h}{D}$ small) mode

c. The pseudo-SDF mode

It turns out that the z-axis cannot be uncoupled from the y-axis (even though the y-axis is uncoupled from the z-axis) by choice of gyro parameters alone; and that complete decoupling, if desired, must be achieved through the control law. Therefore, the y-axis transfer functions are Equation E-52 for the lightly damped gyro, Equation E-56 for the heavily damped gyro, and Equation E-70 when used in the pseudo SDF mode. Due to the residual coupling mentioned above, a z-axis transfer function cannot be presented (except when one of the

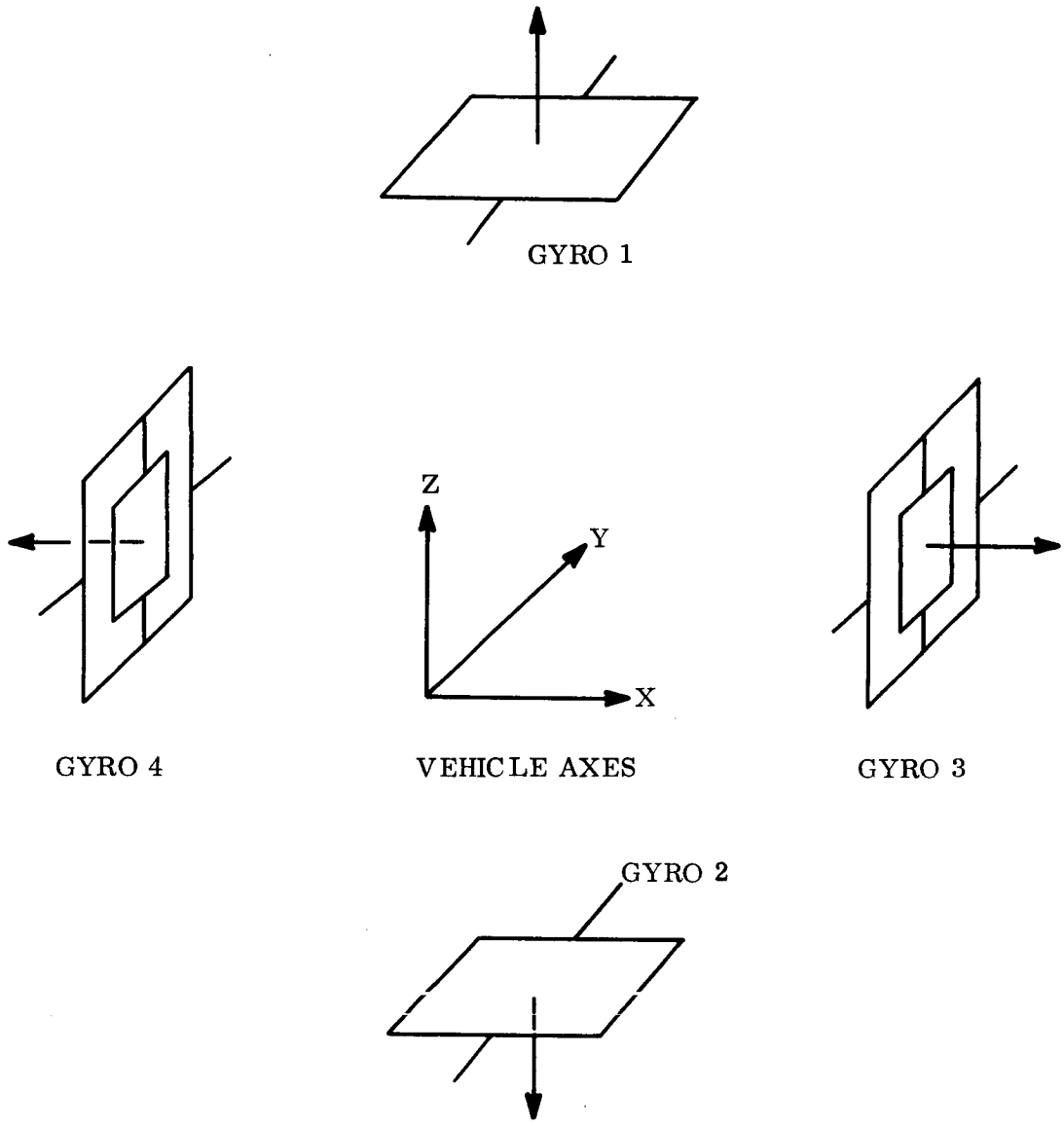

Figure E-1. Mounting Configuration for CMG's

gimbal angles is small); and therefore, the z-axis open-loop response as a function of both inner and outer gimbal torque motors is presented. This is done in Equation E-64 for the lightly damped gyro, Equation E-65 for the highly damped gyro, and Equation E-75 when used in the pseudo SDF mode.

A precautionary reminder and demonstrative example are given in Section E.10 emphasizing that these transfer functions only pertain to the system during attitude hold.

E.3 A REDUCED SET OF COUPLED NONLINEAR DIFFERENTIAL EQUATIONS THAT ARE VALID FOR INVESTIGATING ATTITUDE HOLD

The complete set of equations listed in Section E.11 may be considerably reduced for purposes of investigating system behavior during attitude hold. For precision operation of the CMG's in pairs, the twin gimbal angles must be closely equal in magnitude and opposite in sign. The control laws must be chosen to create this effect, and constraint loops implemented to prevent any long term errors. Knowing this ($a_1 = -a_2$, $b_3 = -b_4$, $c_3 = -c_4$) only two of the four gyros need be considered. Also realizing that the gimbal coupling and damping torques predominate in the lightly and highly damped gyro modes allows the complete set of equations to be reduced to the following.

$$\dot{H}_i = T_i, (i = x,\ y,\ z) \qquad \text{(E-1, E-2, E-3)}$$

$$w_i = \frac{H_i - h_i}{I_i}, (i = x,\ y,\ z) \qquad \text{(E-4, E-5, E-6)}$$

$$\dot{\theta}_i = w_i, (i = x,\ y,\ z) \qquad \text{(E-7, E-8, E-9)}$$

$$h_x = 2\,h \sin a_1 \qquad \text{(E-10)}$$

$$h_y = 2\,h \sin b_3 \qquad \text{(E-11)}$$

$$h_z = 2\,h \cos b_3 \sin c_3 \qquad \text{(E-12)}$$

$$\dot{a}_1 = \frac{H_y^{(1)}}{I_a} - w_y \qquad \text{(E-13)}$$

$$\dot{b}_3 = \frac{H_z^{(3)}}{I_b} \qquad \text{(E-14)}$$

$$\dot{c}_3 = \frac{H_y^{(3)} - h \sin b_3}{I_c} \tag{E-15}$$

$$\dot{H}_y^{(1)} = T_a - D_a \dot{a}_1 + w_x h \cos a_1 - w_z h \sin a_1 \tag{E-16}$$

$$\dot{H}_c^{(3)} = T_c - D_c \dot{c}_3 \tag{E-17}$$

$$\dot{H}_b^{(3)} = T_b - D_b \dot{b}_3 + \dot{c}_3 h \cos b_3 \tag{E-18}$$

Attitude parameters have been introduced in Equations E-7, E-8, and E-9. Some of the terms above will be deleted and some terms ignored above will be reintroduced when investigating and pseudo SDF mode with appropriate discussion at that time.

E.4 SINGLE AXIS ATTITUDE HOLD TRANSFER FUNCTION FOR THE SDF CMG'S

These gyros control the vehicle x-axis (see Figure E-1). Therefore, the appropriate equations to use (with $w_y = w_z = 0$) are E-1, E-4, E-7, E-10, E-13, and E-16. As mentioned in the summary, these equations are still nonlinear; however, this difficulty can be circumvented by linearizing them about an operating point as follows. Let

$$a_1 = A + a \tag{E-19}$$

where A is the constant operating point and a is a small perturbation about this operating point. Then

$$\sin a_1 \approx \sin A + a \cos A \tag{E-20}$$

$$\cos a_1 \approx \cos A - a \sin A \tag{E-21}$$

The linearized equations for the x-axis then become the following.

$\dot{H}_x = T_x$ (From Equation E-1)

$$w_x = \frac{H_x - 2h \sin A - 2h(\cos A)a}{I_x} \tag{E-22}$$

$$\dot{\theta}_x = w_x \tag{E-23}$$

$$\dot{a} = \frac{H_y^{(1)}}{I_a} \tag{E-24}$$

$$\dot{H}_y^{(1)} = T_a - D_a \dot{a} + w_x h (\cos A - a \sin A)$$

$$\approx T_a - D_a \dot{a} + w_x h \cos A$$

$$\text{for } |\cos A| >> |a \sin A| \tag{E-25}$$

These linearized equations (E-1, E-22, E-23, E-24, E-25) result in the signal flow graph shown in Figure E-2. The graph determinant G_x (defined in footnote Reference +) is

$$G_x = \frac{2h^2 \cos^2 A}{I_a I_x s^2} \left[1 + \frac{D_a I_x s}{2h^2 \cos^2 A} + \frac{I_a I_x s^2}{2h^2 \cos^2 A} \right] \tag{E-26}$$

The open loop uncompensated transfer function for the x-axis utilizing the twin SDF CMG's is then

$$L_x(s) = \frac{\theta_x}{T_a} = \frac{-2h \cos A}{I_x I_a s^3 G_x} = \frac{-1}{h \cos A \left[1 + \frac{D_a I_x s}{2h^2 \cos^2 A} + \frac{I_a I_x s^2}{2h^2 \cos^2 A} \right] s} \tag{E-27}$$

+ "The Art of Formulating Signal Flow Graphs" Report PIBMRI-869-60 by L. Brown, Jr. and W.A. Lynch of the Polytechnic Institute of Brooklyn Microwave Research Institute, 18 October 1960.

Note that dependent upon vehicle and gyro parameters that the quadratic may have complex roots or factor into two real roots. In any event the roots are gimbal angle dependent. The control engineer should be wary in the lightly damped case since the underdamped resonance peak moves back towards lower frequencies and the open loop gain simultaneously increases as the gimbal angle moves away from zero. He may want to highly overdamp the quadratic in order to factor it into a root near the one "way out" in order to help in lowering the system bandwidth. It should be obvious that the gimbal angle magnitude should not be allowed to get too close to ninety degrees.

E.5 FEEDBACK LOOPS FOR PARAMETER CONTROL

The vehicle inertia is something the control engineer must tolerate. The spin vector momentum will be determined from the mission requirements such as pointing in the presence of disturbance torques or perhaps a minimum slewing rate if the CMG's are used to reorient the spacecraft. Once this is chosen the gimbal inertia is roughly determined by the gyro maker's rule of thumb that

$$\frac{h}{I} = 2000 \text{ radians/second} \qquad \text{(E-28)}$$

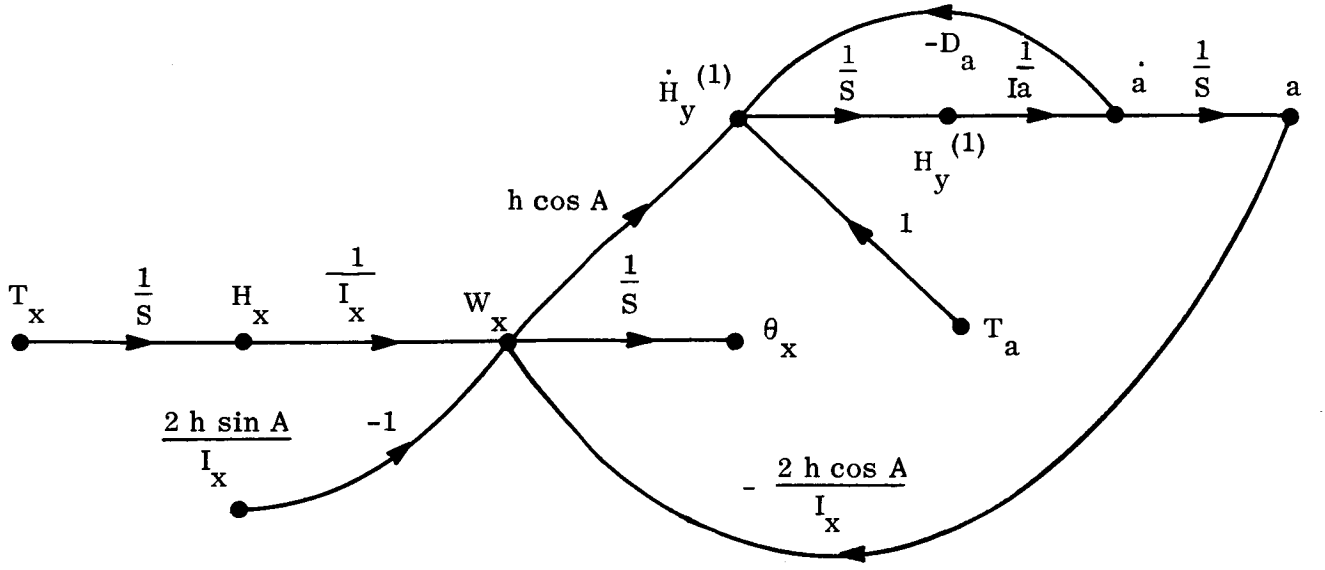

Figure E-2. Signal Flow Graph, X-Axis

There are physical limitations to the viscous damping coefficient D that can be obtained with either eddy current dampers, fluids, or the back emf of the torque motor. However, the discussion at the end of Section E.4 points out the desirability of having complete control over the parameters that determine the transfer function. The transfer function can be easily modified by using feedback loops from the vehicle rate (rate gyros) and gimbal rate (tachometer, perhaps) through the torque as shown in Figure E-3.

The resultant transfer function becomes

$$\frac{\theta_x}{T_a} = \frac{-1}{(h \cos A + K_g)\left[1 + \frac{(D_a + K_t) I_x s}{2 h \cos A (h \cos A + K_g)} + \frac{I_a I_x s^2}{2 h \cos A (h \cos A + K_g)}\right] s} \quad \text{(E-29)}$$

Thus, for example, if the CMG's were being utilized in a highly damped mode (K_t large, K_g small) for precision attitude hold, and the attitude sensor failed, the rate gyro could be switched in (K_g large) to enhance the rate sensing, rate absorption characteristics of the CMG's to have them hold the attitude by rapidly absorbing any disturbances.

These feedback techniques also pertain to the DDF CMG's which will be examined next.

E.6 SINGLE AXIS ATTITUDE HOLD TRANSFER FUNCTIONS FOR THE VEHICLE AXIS ALIGNED WITH THE OUTER GIMBALS OF THE TWIN DDF CMG'S (LIGHTLY AND HIGHLY DAMPED MODES)

From Figure E-1, we see that we are now considering y-axis control. The appropriate equations to use (with $w_x = w_z = 0$) are E-2, E-5, E-8, E-11, E-14, E-15, E-17, and E-18. As mentioned in the summary these equations are nonlinear and coupled. They are linearized using the same technique employed on the x-axis equations.

$$b_3 = B + b \quad \text{(E-30)}$$

$$\sin b_3 \approx \sin B + b \cos B \quad \text{(E-31)}$$

$$\cos b_3 \approx \cos B - b \sin B \quad \text{(E-32)}$$

The y-axis linearized equations are therefore

$$\dot{H}_y = T_y \text{ (From Equation E-2)}$$

$$w_y = \frac{H_y - 2\,h \sin B - 2\,h\,(\cos B)\,b}{I_y} \tag{E-33}$$

$$\dot{\theta}_y = w_y \tag{E-34}$$

$$\dot{b} = \frac{H_b^{(3)}}{I_b} \tag{E-35}$$

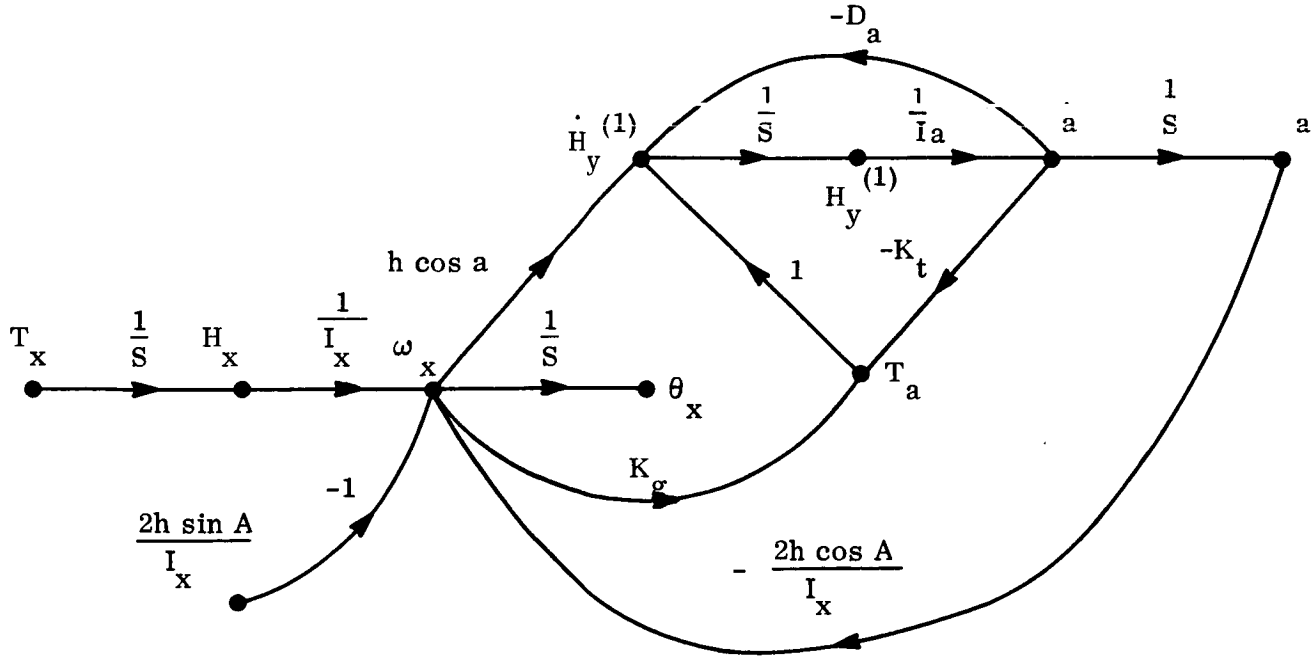

Figure E-3. Feedback Loops for Transfer Function Control

$$\dot{c} = \frac{H_c^{(3)} - h \sin B - h (\cos B)\, b}{I_c} \tag{E-36}$$

$$\dot{H}_c^{(3)} = T_c - D_c \dot{c} \tag{E-37}$$

$$\dot{H}_b^{(3)} = T_b - D_b \dot{b} + \dot{c}\, h (\cos B - b \sin B)$$

$$\approx T_b - D_b \dot{b} + \dot{c}\, h \cos B$$

$$\text{for } \left| \cos B \right| >> \left| b \sin B \right| \tag{E-38}$$

These linearized equations result in the signal flow graph indicated by Figure E-4. The graph determinant G_y is

$$G_y = \left(\frac{h^2 \cos^2 B + D^2}{I^2 s^2} \right) \left[1 + \frac{2 D I s}{h^2 \cos^2 B + D^2} + \frac{I^2 s^2}{h^2 \cos^2 B + D^2} \right] \tag{E-39}$$

with

$$\frac{D_b}{I_b} = \frac{D_c}{I_c} \tag{E-40}$$

$$D^2 = D_b D_c \tag{E-41}$$

$$I^2 = I_b I_c \tag{E-42}$$

for convenience since I_b and I_c are nearly but not quite equal. Also let

$$M = \frac{2 D I}{h^2 \cos^2 B + D^2} \tag{E-43}$$

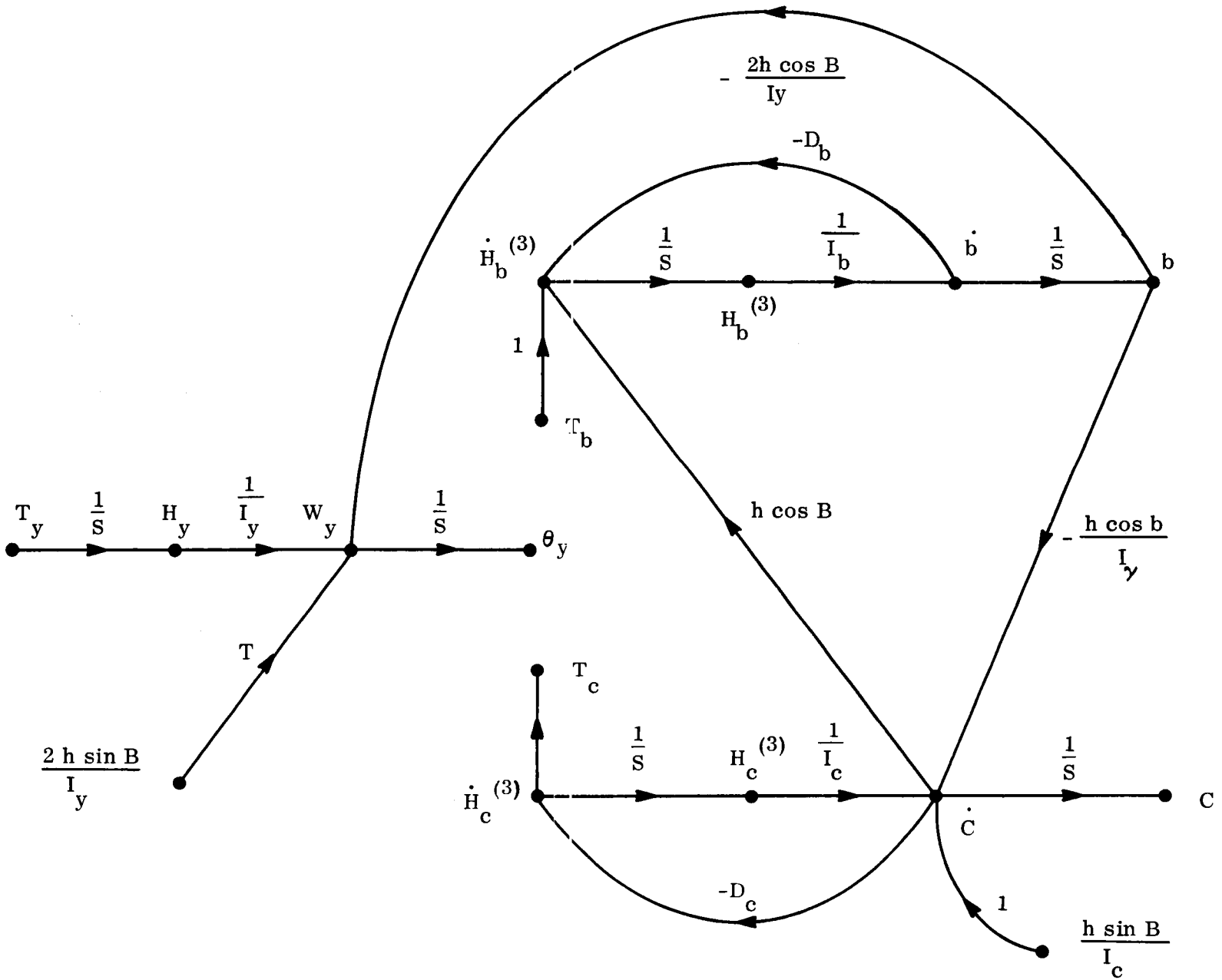

Figure E-4. Y-Axis Signal Flow Graph for Both Lightly and Highly Damped Gyros

$$N = \frac{I^2}{h^2 \cos B + D^2} \tag{E-44}$$

Before presenting the open-loop transfer functions some intermediate transfer functions must first be presented as will soon be evident.

$$\frac{b}{T_b} = \frac{\left(1 + \frac{D_c}{I_c s}\right)}{I_b s^2 G_y} = \frac{D_c\left(1 + \frac{I_c s}{D_c}\right)}{(h^2 \cos^2 B + D^2)(1 + M s + N s^2) s} \tag{E-45}$$

$$\frac{c}{T_c} = \frac{\left(1 + \frac{D_c}{I_b s}\right)}{I_c s^2 G_y} = \frac{D_b\left(1 + \frac{I_b s}{D_b}\right)}{(h^2 \cos^2 B + D^2)(1 + M s + N s^2) s} \tag{E-46}$$

$$\frac{b}{T_c} = \frac{h \cos B}{I_c I_b s^3 G_y} = \frac{h \cos B}{(h^2 \cos^2 B + D^2)(1 + M s + N s^2) s} \tag{E-47}$$

$$\frac{c}{T_b} = \frac{-h \cos B}{I_c I_b s^3 G_y} = \frac{-h \cos B}{(h^2 \cos^2 B + D^2)(1 + M s + N s^2) s} \tag{E-48}$$

Thus, in general, if you torque with one torque motor (inner or outer) both gimbals move. The relative motion is

$$\left.\frac{b}{c}\right|_{T_b} = \frac{-D_c\left(1 + \frac{I_c s}{D_c}\right)}{h \cos B} \tag{E-49}$$

and

$$\left.\frac{c}{b}\right|_{T_c} = \frac{-D_b\left(1 + \frac{I_c s}{D_c}\right)}{h \cos B} \tag{E-50}$$

These last two equations clearly point out the importance of the h/D ratio and immediately suggest how the y-axis transfer function can be made dependent upon only one of the torque motors, either in the inner or the outer. Consider

$$h^2 \cos^2 B >> D^2 \tag{E-51}$$

The DDF CMG's are then in the lightly damped or "free" gyro mode as it is sometimes called. Then, to move the inner gimbals in the desired manner, you must torque the outer gimbals in the same direction. (See Figure E-5.) The appropriate transfer function is

$$L_y^{(1)}\left(h^2 \cos^2 B >> D^2\right) = \frac{\theta_y}{T_c} = \frac{-2}{I_y\left(1 + \frac{2 d s}{w_n} + \frac{s^2}{w_n^2}\right) s^2} \tag{E-52}$$

where

$$w_n^2 = \frac{h^2 \cos^2 B}{I^2} \tag{E-53}$$

$$d = \frac{D}{h \cos B} \tag{E-54}$$

Note that the "free" gyro has a maximum natural frequency of 2000 radians/seconds (at $B = 0$) for almost any gyro because of the gyro maker's rule of thumb (Equation E-28) and that this lightly damped resonant peak moves towards lower frequencies as the inner gimbal angle moves away from zero. This fact should be carefully noted by the control engineer.

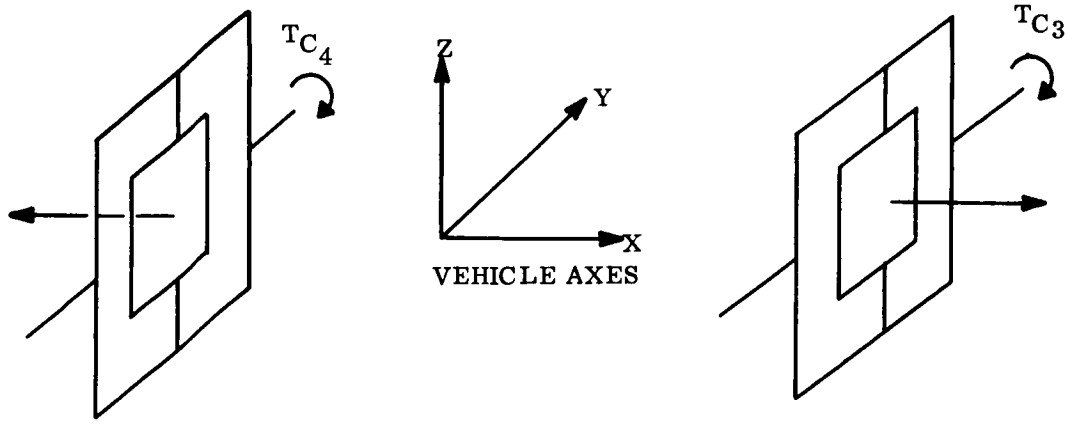

$$T_{C_3} = T_{C_4}$$

A.) LIGHTLY DAMPED OR "FREE" GYRO CONTROL SCHEME

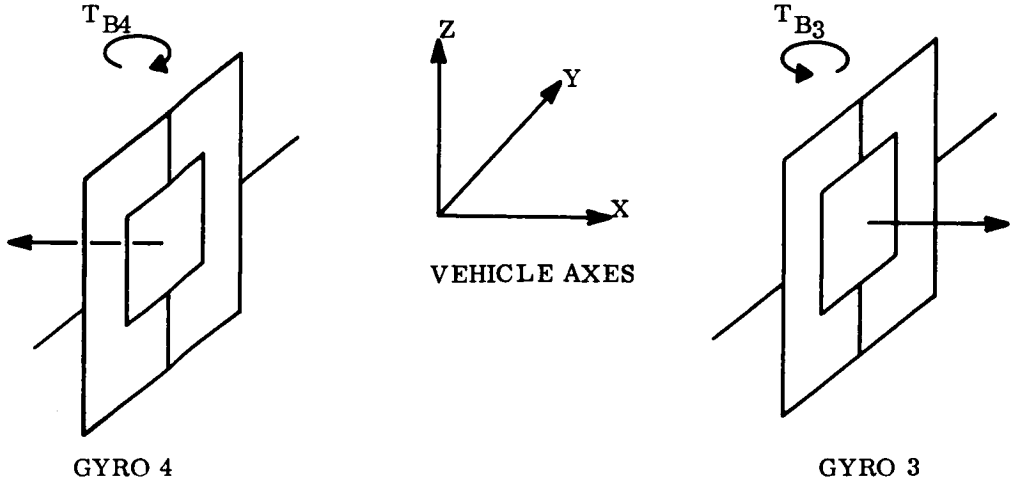

$$T_{B_3} = T_{B_4}$$

B.) HIGHLY DAMPED AND PSEUDO SDF CONTROL SCHEMES

Figure E-5. Y-Axis Control Schemes

Next consider

$$D^2 >> h^2 \cos^2 B \tag{E-55}$$

The gyro is now in the highly damped mode, and to move the inner gimbals in the desired manner you must torque the inner gimbals in opposite directions. (Refer to Figure E-5.) The appropriate transfer function in this case is

$$L_y^{(2)} \; (D^2 >> h^2 \cos^2 B) = \frac{\theta_x}{T_b} = \frac{-2 h \cos B}{I_y D_b \left(1 + \frac{I_b s}{D_b} \right) s^2} \tag{E-56}$$

This transfer function is certainly a more desirable form than that of the "free" gyro since it has a lower crossover. Since $\frac{D}{h}$ is large, the lag in the denominator occurs at a very large frequency; and you do not have to worry about the resonant peak. However, to realize the large D/h ratio will probably require the tach feedback loop mentioned in Section E.5. This is not all bad because it enables you to get by with as small a torque motor as is required by the "free" gyro.

E.7 SINGLE AXIS ATTITUDE HOLD EQUATIONS FOR THE VEHICLE AXIS NOMINALLY ALIGNED WITH THE INNER GIMBALS OF THE TWIN DDF CMG'S (LIGHTLY AND HIGHLY DAMPED MODES)

From Figure E-1 we see that we are now considering z-axis control. The appropriate equations to use (with $w_x = w_y = 0$) are E-3, E-6, E-9, E-12, E-14, E-15, E-17, and E-18. These nonlinear coupled equations are again linearized.

$$\sin b_3 \approx \sin B + b \cos B \tag{E-31}$$

$$\cos b_3 \approx \cos B - b \sin B \tag{E-32}$$

$$c_3 = C + c \tag{E-57}$$

$$\sin c_3 \cos b_3 \approx \sin C \cos B + c \cos C \cos B - b \sin C \sin B \tag{E-58}$$

Thus the linearized equations are

$$\dot{H}_z = T_z \tag{E-3}$$

$$w_z = \frac{H_z + 2h\,(\sin C \cos B + c \cos C \cos B - b \sin C \sin B)}{I_z} \tag{E-59}$$

$$\dot{\theta}_z = w_z \tag{E-60}$$

$$\dot{b} = \frac{H_b^{(3)}}{I_b} \tag{E-35}$$

$$\dot{c} = \frac{H_c^{(3)} - h \sin B - h(\cos B)b}{I_c} \tag{E-36}$$

$$\dot{H}_c^{(3)} = T_c - D_c \dot{c} \tag{E-37}$$

$$\dot{H}_b^{(3)} \approx T_b - D_b \dot{b} + \dot{c}\, h \cos B \tag{E-38}$$

These linearized equations result in the signal flow graph indicated in Figure E-6.

The graph determinant is again

$$G_z = \frac{h^2 \cos^2 b + D^2}{I^2 s^2} \left[1 + M s + N s^2\right] \tag{E-61}$$

The response of the z-axis position to torque motor excitation is

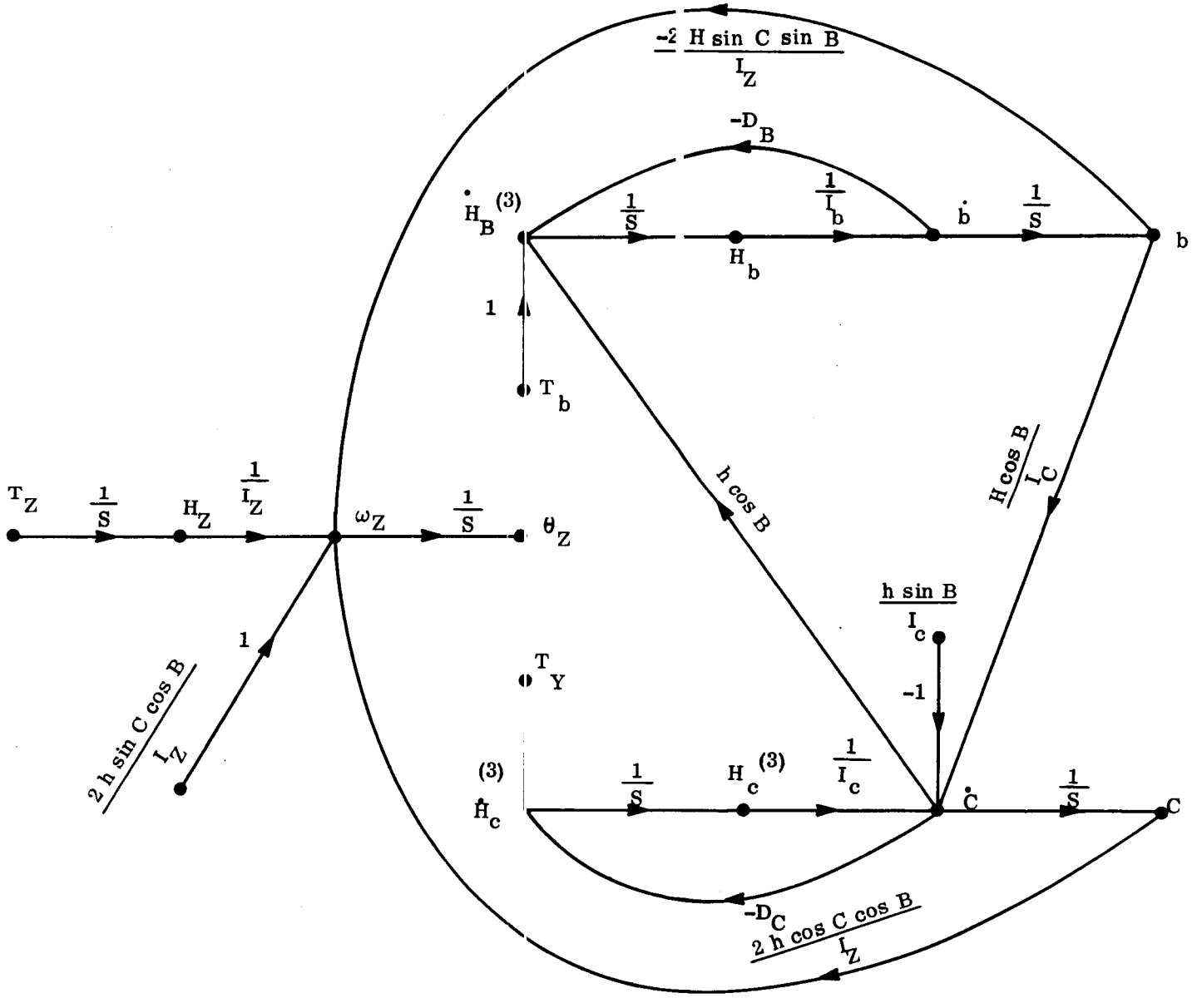

Figure E-6. Z-Axis Signal Flow Graph for Lightly and Highly Damped Gyros

$$\theta_z = \frac{\theta_z}{b}\frac{b}{T_c} + \frac{\theta_z}{c}\frac{c}{T_c}T_c + \frac{\theta_z}{b}\frac{b}{T_b} + \frac{\theta_z}{c}\frac{c}{T_b}T_b \qquad \text{(E-62)}$$

Putting the appropriate transfer functions into the last equation yields

$$\theta_z = \frac{2h\cos B\left[D_b \cos C\left(1 + \frac{I_b s}{D_b}\right) - h \sin C \sin B\right] T_c}{I_z (h^2 \cos^2 B + D^2)(1 + M s + N s^2) s^2}$$

$$- \frac{2h\left[h \cos C \cos^2 B + D_c \sin C \sin B\left(1 + \frac{I_c s}{D_c}\right)\right] T_b}{I_z (h^2 \cos^2 B + D^2)(1 + M s + N s^2) s^2} \qquad \text{(E-63)}$$

In the case of the lightly damped or "free" gyro the last equation reduces to

$$\theta_z\,(h^2 \cos^2 B >> D^2) = \frac{2\left[\sin B \sin C\, T_c - \cos B \cos C\, T_b\right.}{I_z \cos B\left(1 + \frac{2 d s}{w_n} + \frac{s^2}{w_n^2}\right) s^2} \qquad \text{(E-64)}$$

In the case of the highly damped gyro, Equation E-63 reduces to

$$\theta_z\,(D^2 >> h^2 \cos^2 B) = \frac{2h\left[\cos B \cos C\, T_c - \sin B \sin C\, T_b\right]}{I_z D_c\left(1 + \frac{I_c s}{D_c}\right) s^2} \qquad \text{(E-65)}$$

Thus, by choice of gyro parameters alone, complete uncoupling can not be obtained even for the attitude hold mode. Equations E-64 and E-65 indicate that unless the control law is used to decouple the z-axis from the y-axis when both gimbal angles are away from zero, the z-axis will respond to any y-axis excitation, and the z-axis can not settle out until

after the y-axis has. An example of control law decoupling for the highly damped case would be

$$T_{c_1} = f(\theta_z) + T_{b_3} \tan b_3 \tan c_3 = - T_{c_4} \qquad \text{(E-66)}$$

indicating that the signal to the inner gimbal torque motors would have to be processed through the appropriate tangent resolvers.

E.8 THE Y-AXIS UNCOMPENSATED OPEN-LOOP TRANSFER FUNCTION UTILIZING THE TWIN DDF CMG'S IN THE PSEUDO SDF MODE

The DDF CMG's are here defined to act in the pseudo SDF mode when all gimbal coupling is purposely restrained. This may be realized through mechanical gearing or electronic feedback through the torque motors. For example, if the outer gimbals are torqued in opposite directions, the natural tendency of the inner gimbals to move in the same direction is opposed, thus giving the DDF gyro and SDF appearance. Two equations from the previous y-axis analysis must be modified. Equation E-15 becomes

$$\dot{c}_3 = \frac{H_c^{(3)} - h \sin b_3}{I_c} + \left(\frac{h \sin b_3}{I_c} \right) = \frac{H_c^{(3)}}{I_c} \qquad \text{(E-67)}$$

The terms in parentheses represents the effect of the gimbal coupling constraint. Equation E-18 also changes to

$$\dot{H}_b^{(3)} = T_{b_3} - D_b \dot{b}_3 + \dot{c}_3 h \cos b_3 - (\dot{c}_3 h \cos b_3) + w_y h \cos b_c \qquad \text{(E-68)}$$

In the last equation the effect of the constraint in opposing gimbal coupling is quite evident and a new term ($w_y h \cos b_3$) has been added. This term, which was negligible for the previous y-axis investigation, now becomes significant. For example, if it had been included in the earlier analysis, the lightly damped mode transfer function would have come out as

$(h^2 \cos^2 B >> D^2$, including the $w_y h \cos B$ term)

$$L_y^{(1)} = \frac{-1}{DI\left(1 + \frac{I_y s}{2DI}\right)\left(1 + \frac{2 d s}{w_n} + \frac{s^2}{w_n^2}\right)s} \approx \frac{-2}{I_y\left(1 + \frac{2 d s}{w_n} + \frac{s^2}{w_n^2}\right)s^2} \qquad \text{(E-69)}$$

since the time constant $\frac{I_y}{2 D I}$ comes out to be extremely large. The signal flow graph for the y-axis pseudo SDF mode is given in Figure E-7. The open loop uncompensated transfer function is just

$$L_y^{(P)} = \frac{\theta_y}{T_b} = \frac{-1}{h \cos B\left(1 + \frac{D_b I_y s}{2 h^2 \cos^2 B} + \frac{I_b I_y s^2}{2 h^2 \cos^2 B}\right)s} \qquad \text{(E-70)}$$

which we note is identical to the x-axis function defined in Equation E-27.

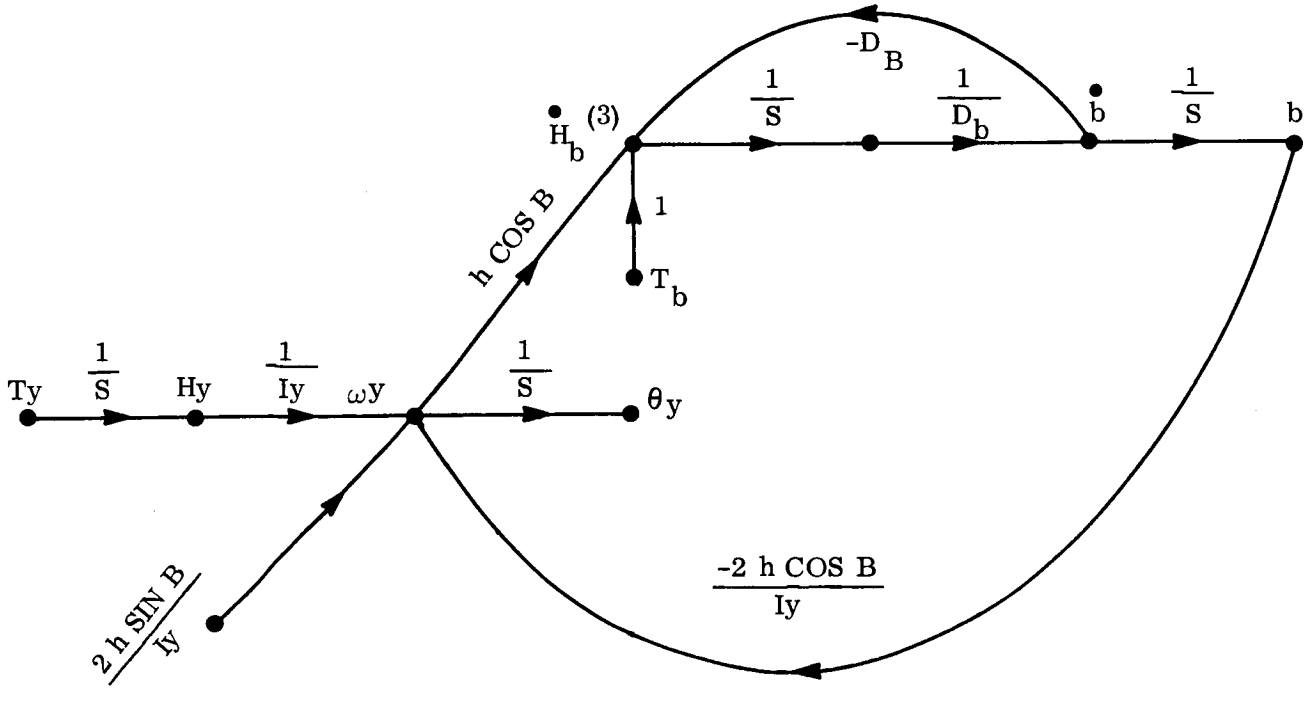

Figure E-7. Y-Axis Signal Flow Graph Using the Pseudo SDF Concept

E.9 THE Z-AXIS UNCOMPENSATED OPEN LOOP EQUATIONS UTILIZING THE TWIN DDF CMG'S IN THE PSEUDO SDF MODE

Using the gyros in the pseudo SDF mode dictates that three equations from the previous z-axis analysis be modified. First, Equation E-15 must show the effect of the constraint.

$$\dot{c}_3 = \frac{H_c^{(3)} - h \sin b_3}{I_c} + \frac{h \sin b_3}{I_c} = \frac{H_c^{(3)}}{I_c} \qquad \text{(E-67)}$$

Finally, a constraint term and a now significant inherent rate feedback term must be introduced into Equation E-18.

Next, the inherent rate feedback term that was negligible in the earlier analysis must be introduced into Equation E-17.

$$\dot{H}_c^{(3)} = T_{c_3} - D_c \dot{c}_3 - w_z h \cos c_3 \cos b_3 \qquad \text{(E-71)}$$

Finally, a constraint term and a now significant inherent rate feedback term must be introduced into Equation E-18.

$$\begin{aligned} H_b^{(3)} &= T_{b_3} - D_b \dot{b}_3 + c_3 h \cos b_3 \\ &\quad - (\dot{c}_3 h \cos b_3) + w_z h \sin b_3 \sin c_3 \\ &= T_{b_3} - D_b \dot{b}_3 + w_z h \sin b_3 \sin c_3 \end{aligned} \qquad \text{(E-72)}$$

The signal flow graph is shown in Figure E-8. Its graph determinant is

$$G_z^{(P)} = \left[2 h \frac{(D_b \cos^2 b \cos^2 C + D_c \sin^2 b \sin^2 C)}{I^2 I_z s^3} \right]$$

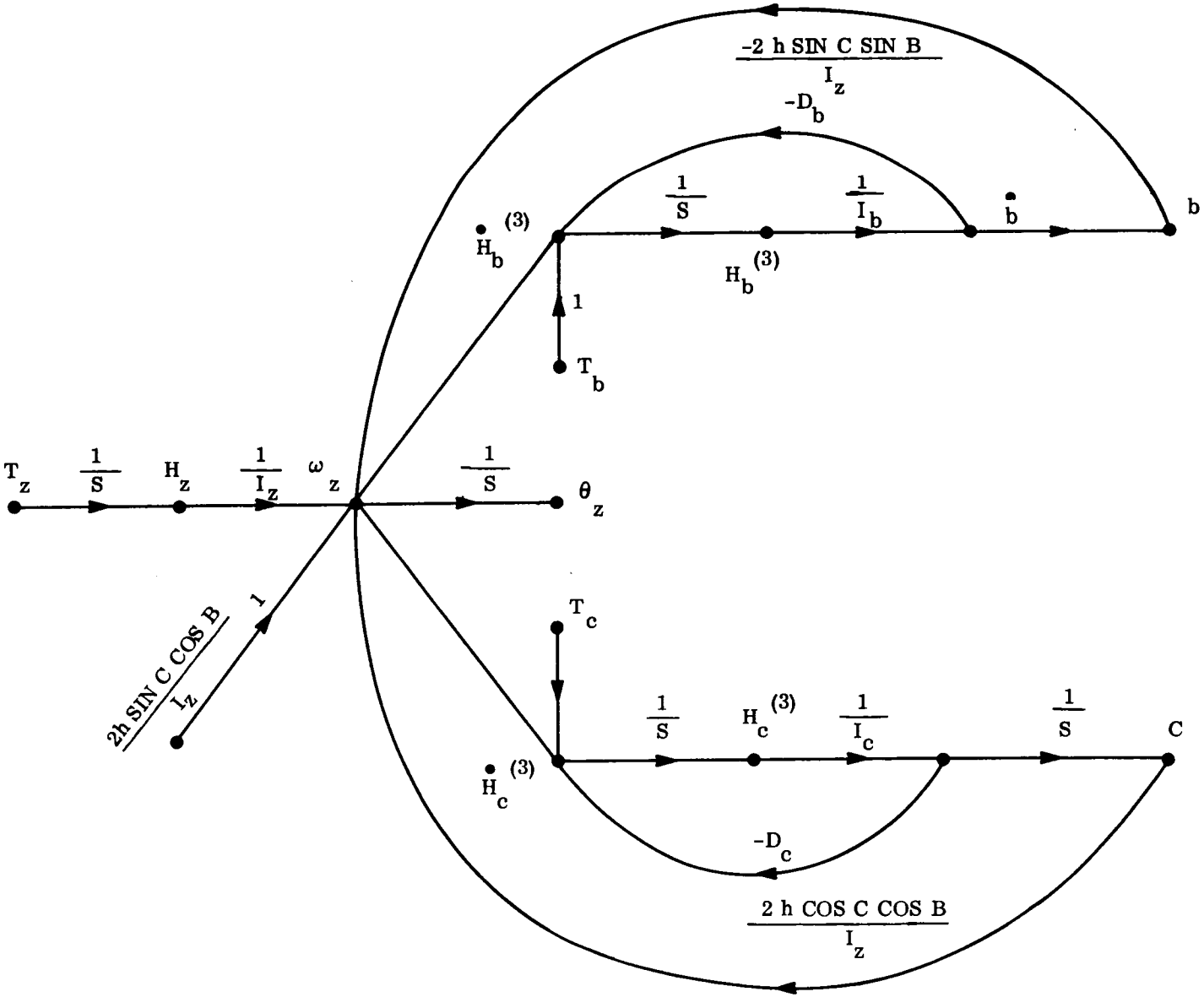

Figure E-8. Z-Axis Signal Flow Graph for DDF CMG's in the Pseudo SDF Mode

$$\left[1+\left(\frac{I_b\cos^2 B\cos^2 C + I_c \sin^2 B \sin^2 C + \frac{I_c D^2}{2h^2}}{D_b\cos^2 B\cos^2 C + D_c \sin^2 B \sin^2 C}\right)s + \frac{2DII_z s^2 + I^2 I_z s^3}{2h^2(D_b\cos^2 B\cos^2 C + D_c \sin^2 B \sin^2 C)}\right] \quad \text{(E-73)}$$

The z-axis response to torque motor excitation is

$$\theta_z = \left(\frac{\theta_z}{T_b}\right) T_b + \left(\frac{\theta_z}{T_c}\right) T_c \quad \text{(E-74)}$$

Putting in the appropriate transfer functions in Equation E-74 yields Equation E-75. Uncoupling it is certainly not an easy task. Note that if either of the gimbal angles is zero that the complete equation does not vanish (because we have a division by zero in the one quadratic).

$$\theta_z = \left\{\frac{2h\cos B\cos C\sin B\sin C}{I_z(D_b\cos^2 B\cos^2 C + D_c\sin^2 B\sin^2 C)}\right\}$$

$$\left\{\frac{-\cos B\cos C\left[1+\frac{D_c I_z s + I_c I_z s^2}{2h^2\cos^2 B\cos^2 C}\right]T_b + \sin B\sin C\left[1+\frac{D_b I_z s + I_b I_z s^3}{2h^2\sin^2 B\sin^2 C}\right]T_c}{1+\left[\frac{I_b\cos^2 B\cos^2 C + I_c\sin^2 B\sin^2 C + \frac{I_c D^2}{2h^2}}{D_b\cos^2 B\cos^2 C + D_c\sin^2 B\sin^2 C}\right]s + \left[\frac{2DII_z s^2 + I_b I_z s^3}{2h^2(D_b\cos^2 B\cos^2 C + D_c\sin^2 B\sin^2 C)}\right]}\right\} \quad \text{(E-75)}$$

Thus, when either gimbal angle is small, Equation E-75 reduces to (B or C small)

$$\vartheta_z \approx \frac{\left[1 + \frac{I_b s}{D_b}\right] T_c}{h \cos B \cos C \left[1 + \frac{(2h^2 I_b \cos^2 B \cos^2 C + I_z D^2)s + 2 D_b I_b I_z s^2 + I^2 I_z s^3}{2 h^2 D_b \cos^2 B \cos^2 C}\right]} \quad \text{(E-76)}$$

which more closely resembles the previously presented SDF forms.

E.10 PRECAUTIONARY REMARK WITH REGARDS TO USE OF ATTITUDE HOLD TRANSFER FUNCTIONS

The transfer functions derived in this Appendix pertain to a single axis of a spacecraft which is operating in an attitude hold mode (which implies that position errors are small and vehicle rates are low). Since even the single axis equations are nonlinear, stability obtained by compensating the given attitude hold transfer functions must be reevaluated when the vehicle is not operating in the attitude hold mode.

For example, consider the x-axis which is controlled by the SDF CMG's. Suppose the torque motors are saturated or at least constant. This may have resulted from a large attitude error or perhaps a slewing command. The governing equation is this case is

$$\dot{H}_y^{(1)} = T_{a_1} - D_a \dot{a}_1 + w_x h \cos a_1 \quad \text{(E-77)}$$

It is convenient to change state variables by time differenting Equation E-13 with w_y eliminated since we are only considering the x-axis. Doing this and rewriting Equation E-77 yields

$$T_{a_1} = I_a \ddot{a}_1 + D_a \dot{a}_1 - w_x h \cos a_1 \quad \text{(E-78)}$$

The variable w_x can be eliminated by substituting in Equation E-4. Thus,

$$T_{a_1} = I_a \ddot{a}_1 + D_a \dot{a}_1 - \frac{(H_x - 2 h \sin a_1) h \cos a_1}{I_x} \qquad \text{(E-79)}$$

This last equation is in the form of a constant input, damped, spring mass system but with a nonlinear spring. The nonlinear restoring force is

$$F(a_1) = - \frac{(H_x - 2 h \sin a_1) h \cos a_1}{I_x} \qquad \text{(E-80)}$$

The derivative of the restoring force with respect to the gimbal angle is

$$\frac{dF(a_1)}{da_1} = \frac{h}{I_x} \left[H_x \sin a_1 + 2 h \cos 2 a_1 \right] \qquad \text{(E-81)}$$

Note that as a function of the total x-axis momentum, the spin vector momentum, and the gimbal angle, Equation E-81 may be either positive or negative. If the constant input torque is of sufficient magnitude to drive the gimbal angle into a region where the slope of the restoring force becomes negative, than the gimbal continues to swing out at an ever increasing rate. This would be true even though the system could perform attitude hold very nicely in the same gimbal angle regions. There are several ways to easily deal with this problem if you do want to slew the vehicle; however, they will not be discussed here. The only reason for presenting this example was to emphasize the point that with CMG's each mode of control should receive its own careful investigation.

E.11 SUMMARY OF CONTROL MOMENT GYRO EQUATIONS

E.11.1 DIFFERENTIAL EQUATIONS FOR THE TOTAL SYSTEM ANGULAR MOMENTUM

$$\dot{H}_x = T_x + w_z H_y - w_y H_z$$

$$\dot{H}_y = T_y - w_z H_x + w_x H_z$$

$$\dot{H}_z = T_z + w_y H_x - w_x H_y$$

E.11.2 VEHICLE ANGULAR VELOCITY EQUATIONS

$$w_x = \frac{H_x - h_x}{I_x}$$

$$w_y = \frac{H_y - h_y}{I_y}$$

$$w_z = \frac{H_z - h_z}{I_z}$$

E.11.3 ANGULAR MOMENTUM STORED BY THE GYROS AS A FUNCTION OF THE GYRO GIMBAL ANGLES AND THEIR TIME DERIVATIVES

$$h_x = h_s (\sin a_1 - \sin a_2) + h (\cos b_3 \cos c_3 - \cos b_4 \cos c_4)$$

$$+ I_b (\dot{b}_3 \sin c_3 + b_4 \sin c_4)$$

$$h_y = I_a (\dot{a}_1 + \dot{a}_2) + h (\sin b_3 - \sin b_4) = I_c (\dot{c}_3 + \dot{c}_4)$$

$$h_z = h_s (\cos a_1 - \cos a_2) - h (\cos b_3 \sin c_3 - \cos b_4 \sin c_4)$$

$$+ I_b (\dot{b}_3 \cos c_3 + \dot{b}_4 \sin b_4)$$

E.11.4 DIFFERENTIAL EQUATIONS FOR THE GYRO GIMBAL ANGLES

$$\dot{a}_1 = \frac{H_y^{(1)}}{I_a} \quad w_y$$

$$\dot{a}_2 = \frac{H_y^{(2)}}{I_a} - w_y$$

$$\dot{c}_3 = \frac{H_c^{(3)} - h \sin b_3}{I_3} - w_y$$

$$\dot{b}_3 = \frac{H_b^{(3)} - I_3 (w_x \sin c_3 + w_z \cos c_3)}{I_b}$$

$$\dot{c}_4 = \frac{H_c^{(4)} + h \sin b_4}{I_4} - w_y$$

$$\dot{b}_4 = \frac{H_b^{(4)} - I_4 (w_x \sin c_4 + w_z \cos c_4)}{I_b}$$

E.11.5 DIFFERENTIAL EQUATIONS FOR THE GYRO ANGULAR MOMENTUM VARIABLES REQUIRED FOR THE GIMBAL ANGLE TIME DERIVATIVES

$$\dot{H}_y^{(1)} = T_{a_1} - D_a \dot{a}_1 + h_s (w_x \cos a_1 - w_z \sin a_1)$$

$$\dot{H}_y^{(2)} = T_{a_2} - D_a \dot{a}_2 - h_s (w_x \cos a_2 - w_z \sin a_2)$$

$$\dot{H}_c^{(3)} = T_{c_3} - D_c \dot{c}_3 + (w_x \cos c_3 - w_z \sin c_3) I_b \dot{b}_3$$

$$- (w_x \sin c_3 + w_z \cos c_3) h \cos b_3$$

$$\dot{H}_b^{(3)} = T_{b_3} - D_b \dot{b}_3 + (w_y + \dot{c}_3) h \cos b_3$$

$$- (w_x \cos c_3 - w_z \sin c_3) h \sin b_3$$

$$\dot{H}_c^{(4)} = T_{c_4} - D_c \dot{c}_4 + (w_x \cos c_4 - w_z \sin c_4) I_b \dot{b}_4$$

$$+ (w_x \sin c_4 + w_z \cos c_4) h \cos b_4$$

$$\dot{H}_b^{(4)} = T_{b_4} - D_b \dot{b}_4 - (w_y + \dot{c}_4) h \cos b_4$$

$$+ (w_x \cos c_4 - w_z \sin c_4) h \sin b_4$$

APPENDIX F

AN INVESTIGATION OF THE USE OF A TILTING PLATE TO IMPLEMENT THE SPACECRAFT POINT-AHEAD ANGLE

APPENDIX F

AN INVESTIGATION OF THE USE OF A TILTING PLATE TO IMPLEMENT THE SPACECRAFT POINT AHEAD ANGLE

F.1 INTRODUCTION

In the Earth-Mars laser communications mission, the spacecraft point ahead angle is introduced by deflecting the laser beam laterally (perpendicular to the optical axis) resulting in an angular rotation of the transmitted beam relative to the optical axis (the point ahead angle). The point ahead is implemented about both axes normal to the optical axis. The study assumed a single axis implementation for simplicity, since the results are directly applicable to the second axis, and because the second point ahead angle is considerably smaller. The use of a tilting plate, a flat plate of glass which operates by refracting the laser beam, was investigated for this application because it possesses the advantage that a large angular rotation of the tilting plate can be used to produce a small lateral deflection of the laser beam, an inherent amplification in resolution that can be used to provide the required accuracy of implementation. The proposed configuration is shown in Figure F-1.

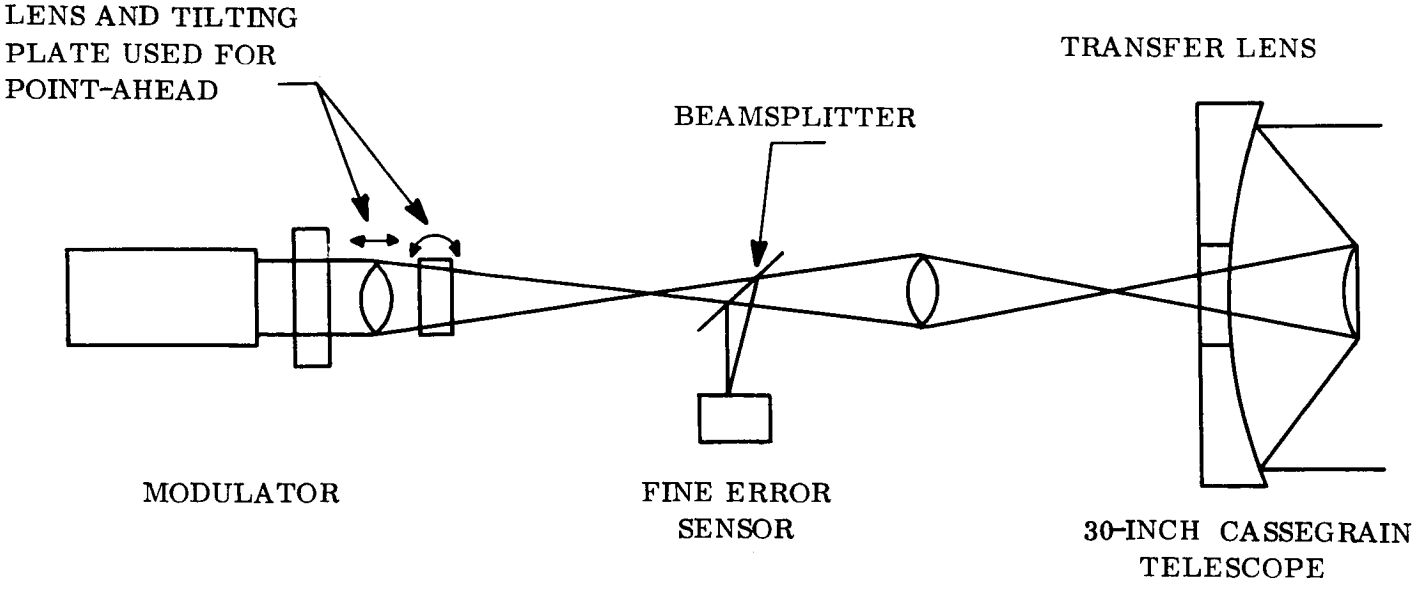

Figure F-1. Optical Configuration

The equations of operation of the tilting plate were generated. Conditions for near optimum operation were defined based upon minimizing the light energy reflected by the tilting plate and maximizing the permitted angular error in tilting plate position for a given system resolution, and a desirable tilting plate size was chosen. The undesirable effect of axial (along the optical axis) movement of the laser beam due to tilting plate rotation was investigated and a means was found to compensate for this effect.

F.2 SUMMARY OF RESULTS

Consideration of light energy losses due to reflection by the tilting plate restricts the maximum rotation of the line normal to the tilting plate to less than on the order of $\pm$ 45 degrees with respect to the optical axis. The resolution required of the system used to drive the tilting plate was found to be much greater if the system were sized so that the tilting plate angle used to accomplish the maximum point ahead angle (75 arc-seconds) is small, and it was found reasonable to consider only sizings of the tilting plate such that the tilting plate angle used to accomplish the maximum point ahead is in excess of 25 degrees. A maximum tilting plate rotation of $\pm$ 40 degrees was chosen, which led to a 0.5 inch thick sizing of the tilting plate and a resolution of 28 arc-seconds required of the control system driving the tilting plate.

For the parameters above, the uncompensated system was found to result in a widening of the laser beam from 0.2 to 1.3 arc-seconds for the beacon tracking mission due to the axial displacement of the beam when tilting plate rotation tending to drive the system out of focus. However, an axial movement of the lens in front of the tilting plate (Figure F-1) can be used to compensate for this effect. The lens needs to be moved axially with a resolution of 0.019 inches, which is well within state of the art.

F.3 EQUATION OF OPERATION

A tilting plate laterally deflects a beam of light through refraction of the beam by the tilting plate. The overall configuration is shown in Figure F-1, and the lateral deflection of a beam of light by a tilting plate is illustrated below:

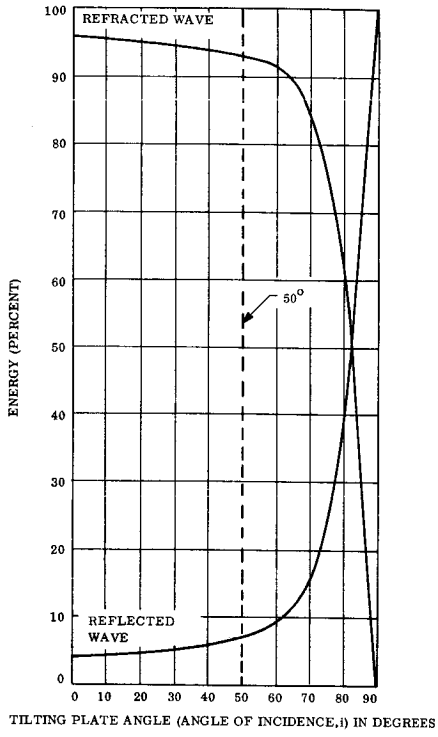

Figure F-2. Energy Distribution of Reflected and Refracted Waves for an Air-Glass Interface

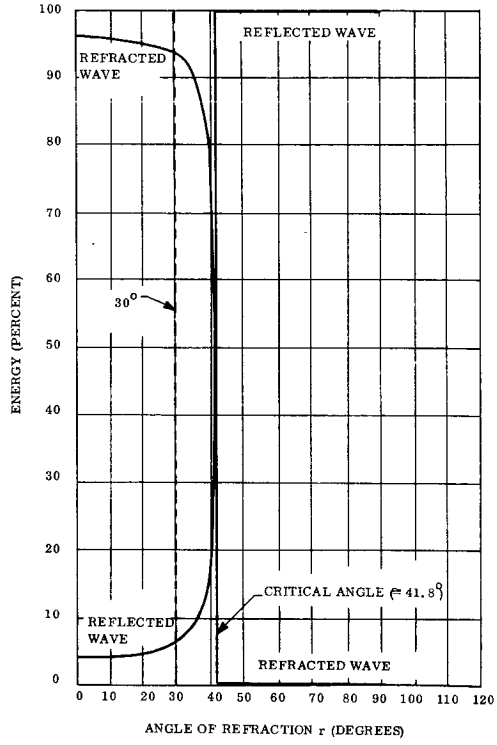

Figure F-3. Energy Distribution of Reflected and Refracted Waves for a Glass-Air Interface

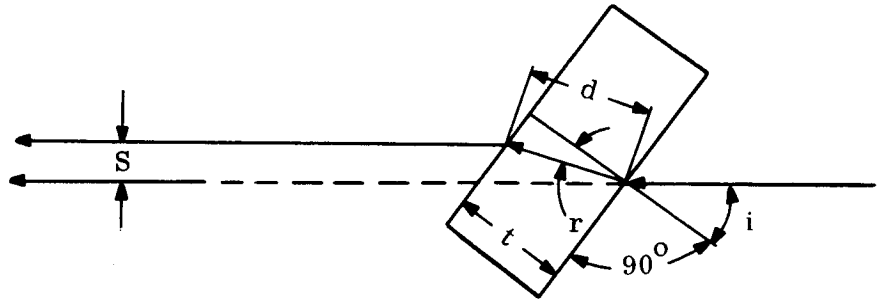

where: i = angle of incidence of the beam

r = angle of refraction of the beam

t = thickness of tilting plate

d = distance travelled through the tilting plate by the refracted beam

s = lateral displacement of the refracted beam

Then $$d = \frac{t}{\cos r} \qquad \text{(F-1)}$$

$$s = d \sin (i - r) \qquad \text{(F-2)}$$

$$= \frac{t \sin (i - r)}{\cos r} \qquad \text{(F-3)}$$

$$\text{Since } \frac{\sin i}{\sin r} = n, \text{ the index of refraction} \qquad \text{(F-4)}$$

(assumed = 1.5 a typical value), and through the use of trigenometric identities the lateral displacement of the refracted beam is given rigorously by

$$s = (t \sin i) \left[1 - \left(\frac{1 - \sin^2 i}{n^2 - \sin^2 i} \right)^{1/2} \right] \qquad \text{(F-5)}$$

F.4 ENERGY CONSIDERATIONS

Not all the light energy incident upon the tilting plate is refracted, but rather some of it is reflected, leading to energy losses. To minimize laser transmitter power, the angular range of operation of the tilting plate must be chosen so as to ensure that the reflected light energy is minimized. Figures F-2 and F-3, from Halliday and Resnick,* show the energy distribution for the reflected and refracted beams for an air-glass and glass-air interface, respectively. The index of refraction for glass is 1.5, and the index of refraction for air is 1.0003 (versus 1.0 for a vacuum) at the wavelength chosen (5890 Angstrons), so the results are directly applicable to the case under study. It can be seen that the glass-air interface imposes the more severe restriction upon the angular range of tilting plate operation, since if the angle between the beam and the normal to the tilting plate surface (angle r by the notation chosen) is greater than approximately 30 degrees, the reflected energe becomes excessive. If r were greater than 41.8 degrees, the "critical angle", total internal reflection would occur. Since $\frac{\sin i}{\sin r} = 1.5$, $i = \sin^{-1} (1.5 \sin r) \cong 50$ degrees for r = 30 degrees. From Figure F-2, i = 50 degrees will not result in excessive reflection at the other interface, and an upper bound of 50 degrees on the tilting plate angle seems reasonable.

* David Halliday and Robert Resnick, "Physics for Students of Science and Engineering," John Wiley and Sons, Inc., 1962, p. 936.

F.5 RESOLUTION CONSIDERATIONS

A lower bound upon the angular range of tilting plate operation can be gained by considering the accuracy with which angular rotations of the tilting plate can be measured. The incremental change in lateral displacement of the beam for a small angular rotation of the tilting plate is found by differentiating the expression for the lateral displacement s with angle i. The result is

$$\frac{ds}{di} = t\left(\cos i - \frac{\sin^4 i + n^2 \cos 2i}{(n^2 - \sin^2 i)^{3/2}}\right) \qquad \text{(F-6)}$$

Given t, the quantity $\frac{ds}{di}/t$ plotted in Figure F-4 will give the sensitivity of beam lateral displacement to error in tilting plate position. It can be seen that the function is monotone increasing, so that the error in lateral displacement introduced by an error in tilting plate position is always a maximum at the maximum tilting plate angle.

However, since

$$t = \left(\frac{\sin i}{s}\right)\left[1 - \left(\frac{1 - \sin^2 i}{n^2 - \sin^2 i}\right)^{1/2}\right] \qquad \text{(F-7)}$$

the tilting plate thickness (t) required to accomplish a given maximum displacement varies with the angular range of tilting plate operation. This variation is plotted in Figure F-5. The value of s assumed is the desired maximum displacement of 0.14 inches from Section 4.5.6 of this report. The assumption is that the zero point ahead angle will be gained by a maximum angular rotation of the tilting plate in one direction, while the maximum point ahead angle will be gained by the maximum rotation of the tilting plate in the other direction from the null ($i = 0^o$). It is possible to make this assumption because the point ahead angle is always in one direction (of one polarity) for the mission under consideration.

Figure F-6 is a plot of the value $\frac{ds}{di} / t$ from Figure F-4 multiplied by the appropriate values of t from Figure F-5. Since, as stated above, the maximum value of $\frac{ds}{di} / t$ occurs at the maximum angular deflection of the tilting plate, the plot is one of maximum sensitivity of beam lateral displacement to tilting plate angular error for different values of tilting plate angle used to accomplish the maximum point ahead (or maximum lateral displacement).

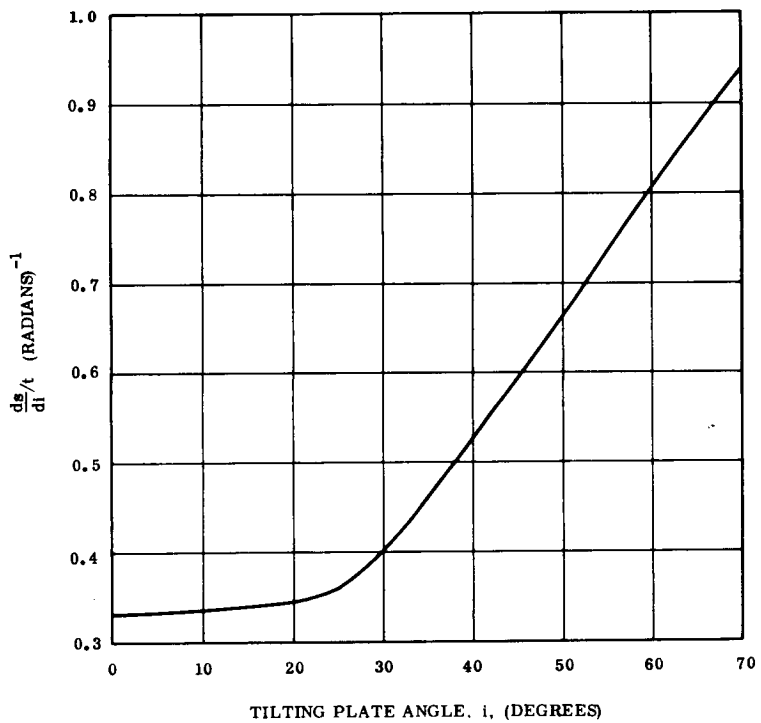

Figure F-4. Sensitivity of Lateral Beam Displacement to Tilting Plate Angular Error Divided by Tilting Plate Thickness Versus Tilting Plate Angle (i)

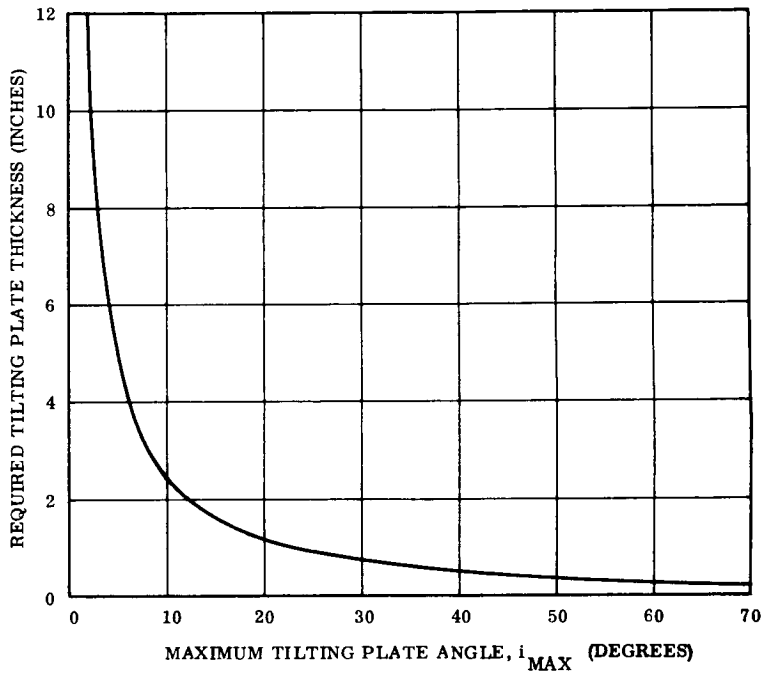

Figure F-5. Required Tilting Plate Thickness Verses Tilting Plate Angle Used to Accomplish the Maximum Point Ahead (Via a Maximum Lateral Displacement, s, of 14 Inches.

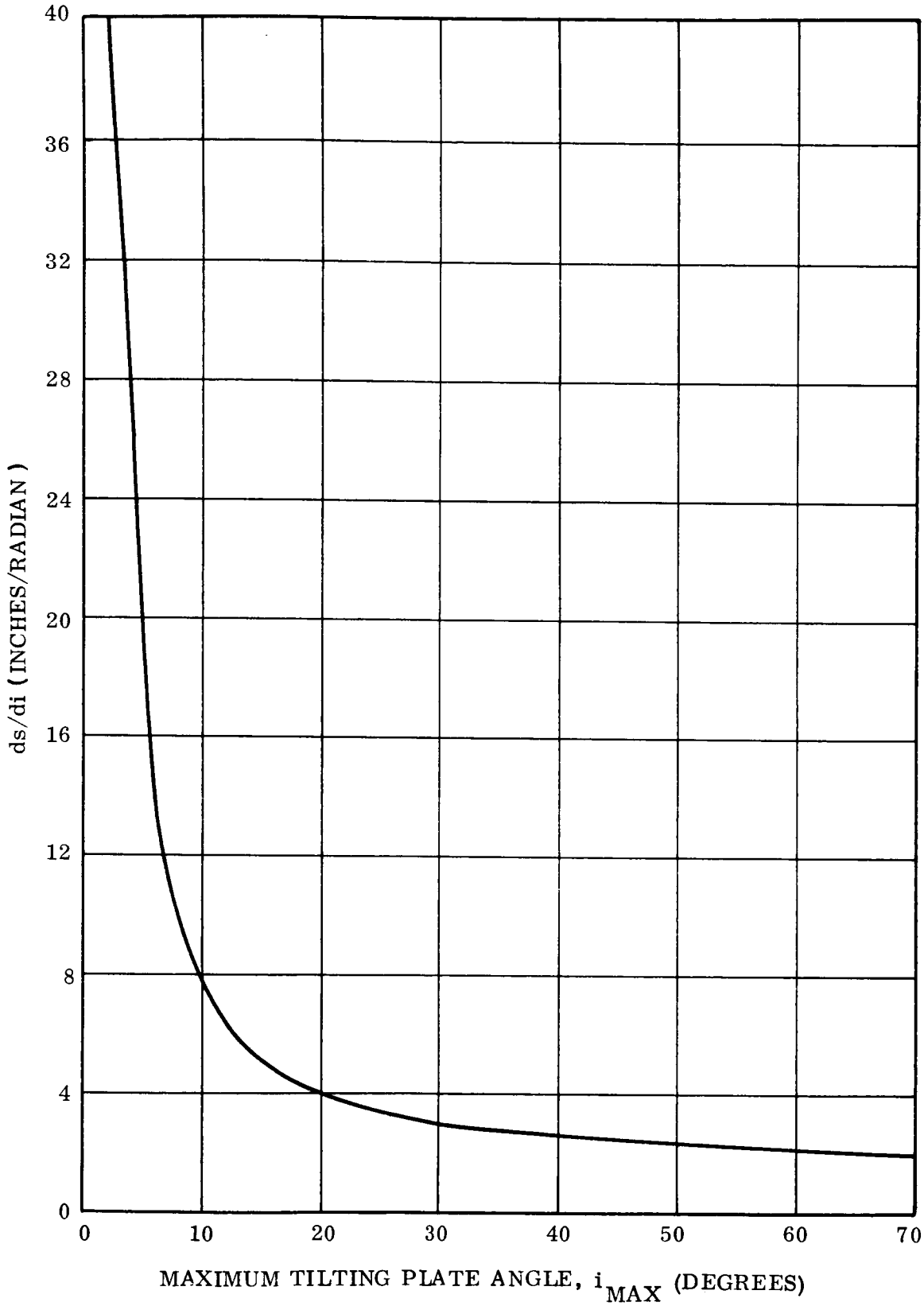

Figure F-6. Sensitivity of Lateral Beam Displacement to Tilting Plate Angular Error as a Function of Maximum Tilting Plate Angle

It can be seen from the plot that the sensitivity of lateral displacement to tilting plate angular error is high if the tilting plate is sized so that the maximum angular rotation of the tilting plate is small. Based upon the plot, it is reasonable to consider only sizings of the tilting plate such that the angular rotation of the tilting plate used to accomplish the maximum point ahead angle is in excess of 25 degrees.

F.6 SIZING THE TILTING PLATE

The analysis summarized thus far was performed for a single ray. However, as the system is sized, the beam going through the tilting plate is neither a single ray nor several parallel rays but rather is converging toward a focus. The parameter of interest is therefore the angle between a ray on the perimeter of the beam and the beam centerline, which is approzimately five degrees for the sizing of the optics chosen. The maximum angle of any ray with a line normal to the tilting plate is therefore five degrees greater than that of the beam centerline.

Therefore, any choice of maximum angular rotation of the tilting plate between 25 degrees and 45 degrees will result in near optimum performance. A value of 40 degrees was chosen, resulting in a tilting plate thickness of 0.5 inches. The tilting plate angular position sensor must be capable of detecting a tilting plate angle which results in a lateral deflection of the laser beam of 37.5 microinches (See Section 4.5.6 of this report). This corresponds to an angular deflection of the tilting plate of

$$\Delta i = \Delta s \Big/ \frac{\Delta s}{\Delta i}\Bigg|_{i = 40^o} = \Delta s \Big/ \frac{ds}{di}\Bigg|_{i = 40^o} = \frac{3.75\ (10\text{-}5)}{2.68\ (10^{-1})}$$

$$= 1.4\ (10^{-4}) \text{ radians} = 28 \text{ arc-seconds} \qquad \text{(F-8)}$$

This resolution is within present day state of the art.

F.7 PROBLEMS INTRODUCED BY THE TILTING PLATE

The use of a tilting plate to deflect the laser beam will tend to drive the system out of focus. This is because the tilting plate deflects the laser image axially (along the optical

axis) as well as laterally, the amount of laser deflection being a function of tilting plate angular rotation.

An expression for the axial deflection of the laser image can be obtained by finding the axial deflection of the laser image caused by introduction of a tilting plate at zero angle and that axial deflection caused by introduction of the tilting plate at an angle i and comparing the two results.

As can be seen from the drawing below, the axial displacement of the laser image with the normal to the tilting plate at zero angle with respect to the beam centerline is given by:

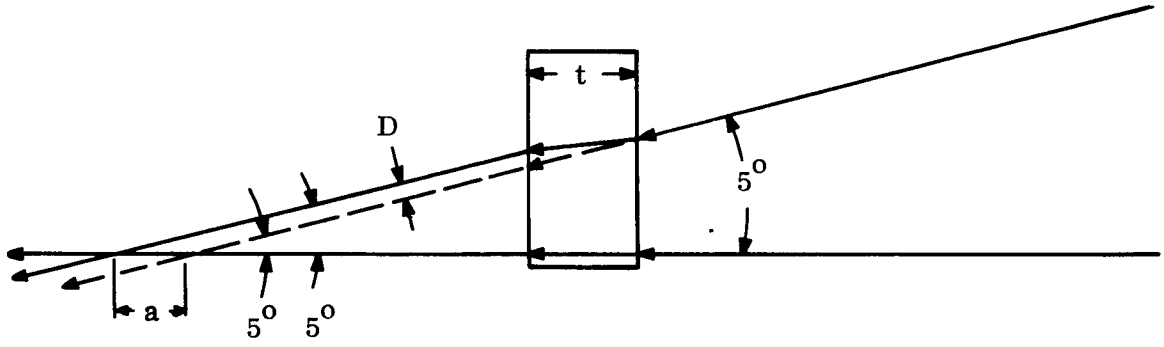

$$a = \frac{D}{\sin 5^{o}} \qquad \text{(F-9)}$$

$$= t\left[1 - \left(\frac{1 - \sin^{2} 5^{o}}{2.25 - \sin^{2} 5^{o}}\right)^{1/2}\right] \qquad \text{(F-10)}$$

The drawing below shows the situation for an arbitrary tilting plate angle i

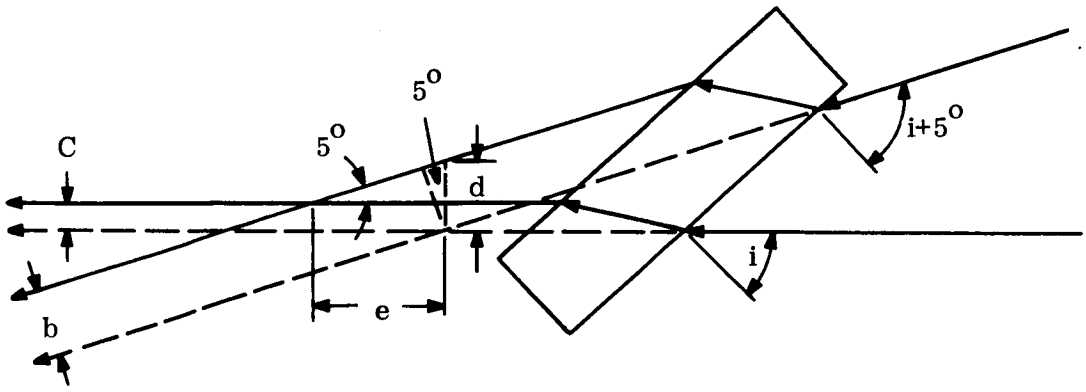

Now $d = \dfrac{b}{\cos 5^{o}}$ and $e = \dfrac{d - c}{\tan 5^{o}}$ (F-11 and F-12)

Since b and c are the lateral deflections,

$$b = \left[t \sin (i + 5^{o})\right] \left[1 - \left(\frac{1 - \sin^{2} (i + 5^{o})}{2.25 - \sin^{2} (i + 5^{o})}\right)^{1/2}\right] \quad \text{(F-13)}$$

$$c = \left[t \sin i\right] \left[1 - \left(\frac{1 - \sin^{2} i}{2.25 - \sin^{2} i}\right)^{1/2}\right] \quad \text{(F-14)}$$

Then the axial deflection e is given by

$$e = \left[\frac{t \sin (i + 5^{o})}{\sin 5^{o}}\right] \left[1 - \left(\frac{1 - \sin^{2} (i + 5^{o})}{2.25 - \sin^{2} (i + 5^{o})}\right)^{1/2}\right] - \left[\frac{t \sin i}{\tan 5^{o}}\right] \left[1 - \left(\frac{1 - \sin^{2} i}{2.25 - \sin^{2} i}\right)^{1/2}\right] \quad \text{(F-15)}$$

Then the expression for the axial deflection, referenced to i = 0 as the null, is given by

$$e - a = \left[\frac{t \sin (i + 5^o)}{\sin 5^o}\right] \left[1 - \left(\frac{1 - \sin^2 (i + 5^o)}{2.25 - \sin^2 (i + 5^o)}\right)^{1/2}\right]$$

$$- \left[\frac{t \sin i}{\tan 5^o}\right] \left[1 - \left(\frac{1 - \sin^2 i}{2.25 - \sin^2 i}\right)^{1/2}\right]$$

$$- t \left[1 - \left(\frac{1 - \sin^2 5^o}{2.25 - \sin^2 5^o}\right)^{1/2}\right] \qquad \text{(F-16)}$$

This expression is plotted in Figure F-7 for t = 0.5 inches (i max = 40 degrees).

Figure F-8 is a plot of (e - a) max as a function of i max, which determines the lens thickness t. Since the plot is nearly linear in the range of interest (25 to 45 degrees), $\frac{d\,(e - a)\,\max}{d\,i\,\max}$ is essentially constant, and the resolution required of any device used to compensate for axial displacement is essentially independent of the maximum rotation of the tilting plate for maximum rotations in the range of 10 to 50 degrees. Thus the choice of i max = 40 degrees and t = 0.5 inches appears to be a good one.

The maximum axial displacement of the laser image is $\pm$ 0.124 inches for the parameters chosen. Using the relationship

$$\frac{1}{f} - \frac{1}{0} = \frac{1}{i} \qquad \text{(F-17)}$$

$$\frac{1}{f} = \frac{1}{f + \Delta} = \frac{1}{i} \qquad \text{(F-18)}$$

$$i = \frac{f\,(f + \Delta)}{\Delta} \cong \frac{f^2}{\Delta} \qquad \text{(F-19)}$$

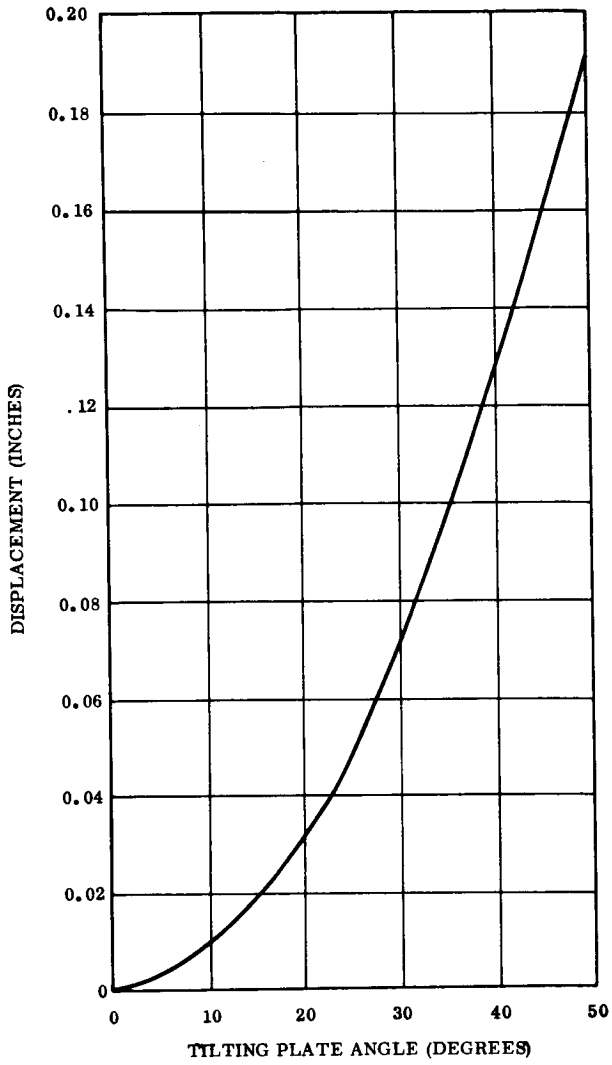

Figure F-7. Axial Displacement of the Laser Image With Tilting Plate Angle

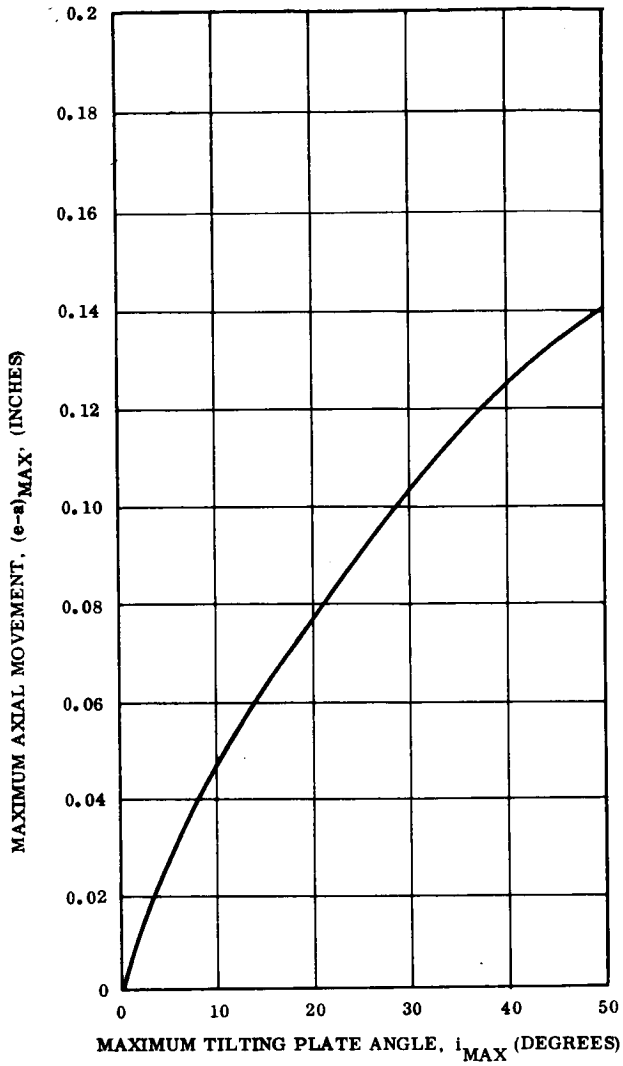

Figure F-8. Maximum Axial Movement of the Laser Image as a Function of Tilting Plate Angle Used to Accomplish the Maximum Point Ahead

From the drawing below,

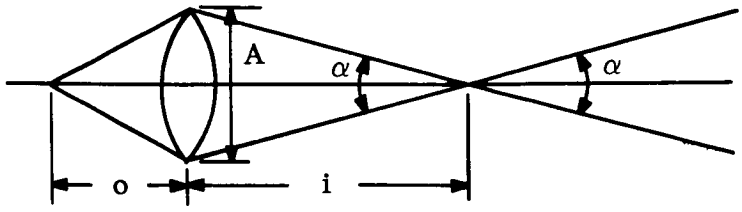

the beamwidth, α , is given by:

$$\alpha = \frac{A}{i} = \frac{A\Delta}{f^2} = \frac{(30)\ (.124)}{5.625\ (105)} = 6.6\ (10^{-6})\ \text{radians} = 1.32\ \text{arc seconds} \qquad \text{(F-20)}$$

for the beacon-tracking mission.

Such a gross widening of the laser beam is clearly intolerable, and corrective steps must be taken to assure diffraction limited operation. The best method of providing the needed compensation appears to be to move the lens in front of the tilting plate along the optical axis. Since the light rays coming into the lens are essentially parallel, a given displacement of the lens will displace the laser image the same amount. The lens must therefore be capable of being displaced through $\pm$ 0.124 inches.

Although the equations developed above are not valid at the diffraction limit of the telescope (0 = f yields i = ∞), they can be used as a first approximation to determine to what value Δ must be held to maintain near normal (diffraction limited) operation. For the beacon-tracking mission

α = 0.2 arc seconds = 10^{-6} radians and

$$\Delta = \frac{f^2\alpha}{A} = \frac{56.25\ (10^4)\ (10^{-6})}{30} = 0.019\ \text{inches} \qquad \text{(F-21)}$$

Tolerances much smaller than this figure are within state of the art. . For instance, if the lens position were controlled by turning a screw with 40 threads to the inch, a tolerance of 0.019 inches linear motion could be maintained if the screw rotation (turning) were held to $\pm$ 135 degrees. It is obvious that even an order of magnitude decreases in the tolerance will result in realizable operation of the corrective lens.

APPENDIX G

TWO-DEGREE-OF-FREEDOM CONTROL MOMENT GYRO EQUATIONS USED IN THE ANALOG COMPUTER SIMULATION

APPENDIX G

TWO-DEGREE-OF-FREEDOM CONTROL MOMENT GYRO EQUATIONS USED IN THE ANALOG COMPUTER SIMULATION

DIFFERENTIAL EQUATIONS FOR THE TOTAL SYSTEM ANGULAR MOMENTUM

$$\dot{H}_y = T_y \tag{G-1}$$

$$\dot{H}_z = T_z \tag{G-2}$$

VEHICLE ANGULAR VELOCITY EQUATIONS

$$w_y = \frac{H_y - 2h \sin b_3}{I_y} \tag{G-3}$$

$$w_z = \frac{H_z + 2h \cos b_3 \sin c_3}{I_z} \tag{G-4}$$

DIFFERENTIAL EQUATIONS FOR THE GYRO GIMBAL ANGLES

$$\dot{b}_3 = \frac{H_b^{(3)}}{I_b} \tag{G-5}$$

$$\dot{b}_4 = \frac{H_b^{(4)}}{I_b} \tag{G-6}$$

$$\dot{c}_3 = \frac{H_c^{(3)}}{I_c} \tag{G-7}$$

$$\dot{c}_4 = \frac{H_c^{(4)}}{I_c} \tag{G-8}$$

DIFFERENTIAL EQUATIONS FOR THE GYRO ANGULAR MOMENTUM VARIABLES

$$\dot{H}_b^{(3)} = T_{b3} - D\dot{b}_3 + \dot{c}_3 \, h \cos b_3 \qquad \text{(G-9)}$$

$$\dot{H}_b^{(4)} = T_{b4} - D\dot{b}_4 - \dot{c}_4 \, h \cos b_3 \qquad \text{(G-10)}$$

$$\dot{H}_c^{(3)} = T_{c3} - D\dot{c}_3 - \dot{b}_3 \, h \cos b_3 \qquad \text{(G-11)}$$

$$\dot{H}_c^{(4)} = T_{c4} - D\dot{c}_4 + \dot{b}_4 \, h \cos b_3 \qquad \text{(G-12)}$$